ARYL-EXTENDED CALIX[4]PYRROLE RECEPTORS WITH METAL CENTERS: ORGANOMETALLIC RECEPTORS AND METALLO-MACROCYCLES BASED ON COORDINATION BONDS

Andrea Rivoli

UNIVERSITAT ROVIRA i VIRGILI

Aryl-extended calix[4]pyrrole receptors with metal centers: organometallic receptors and metallo-macrocycles based on coordination bonds

Andrea Rivoli

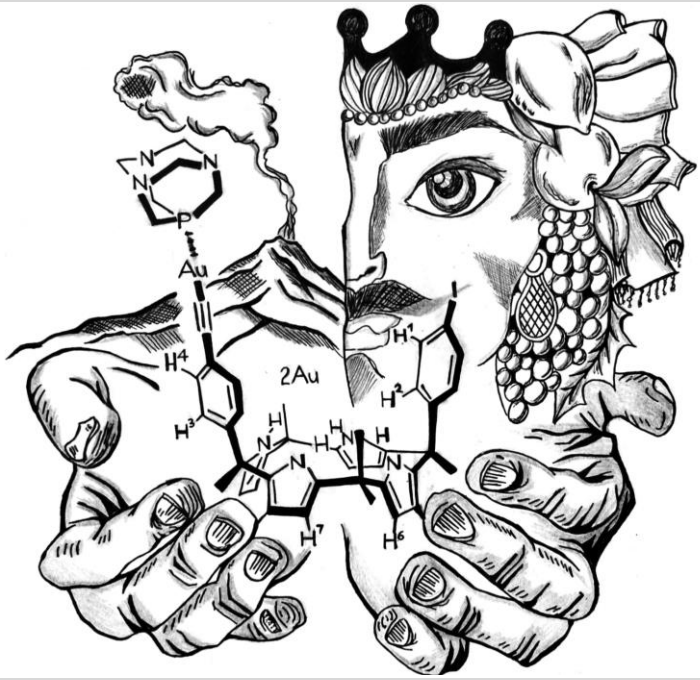

DOCTORAL THESIS
2023

UNIVERSITAT ROVIRA I VIRGILI
ARYL-EXTENDED CALIX[4]PYRROLE RECEPTORS WITH METAL CENTERS: ORGANOMETALLIC RECEPTORS AND METALLO-MACROCYCLES BASED ON COORDINATION BONDS
Andrea Rivoli

UNIVERSITAT ROVIRA I VIRGILI
ARYL-EXTENDED CALIX[4]PYRROLE RECEPTORS WITH METAL CENTERS: ORGANOMETALLIC RECEPTORS AND METALLO-MACROCYCLES BASED ON COORDINATION BONDS
Andrea Rivoli

DOCTORAL THESIS

Andrea Rivoli

ARYL-EXTENDED CALIX[4]PYRROLE RECEPTORS WITH METAL CENTERS: ORGANOMETALLIC RECEPTORS AND METALLO-MACROCYCLES BASED ON COORDINATION CHEMISTRY

Supervised by Prof. Pablo Ballester Balaguer

UNIVERSITAT
ROVIRA i VIRGILI

Tarragona

2023

UNIVERSITAT ROVIRA I VIRGILI
ARYL-EXTENDED CALIX[4]PYRROLE RECEPTORS WITH METAL CENTERS: ORGANOMETALLIC RECEPTORS AND METALLO-MACROCYCLES BASED ON COORDINATION BONDS
Andrea Rivoli

ICIQ
Institut Català d'Investigació Química

Av. Països Catalans, 16
43007 Tarragona, Spain
Tel. (+34) 977 920 200
email: iciq@iciq.es

UNIVERSITAT ROVIRA i VIRGILI
Dept. de Química Analítica i Química Orgànica

Carrer de Marcel·lí Domingo, 1
43007 Tarragona, Spain
Tel. (+34) 977 55 97 69
email: sdn4@urv.cat

I STATE that the present study, entitled "Aryl-extended calix[4]pyrrole receptors with metal centers: organometallic receptors and metallo-macrocycles based on coordination bonds", presented by Andrea Rivoli for the award of the degree of Doctor, has been carried out under my supervision at the Institute of Chemical Research of Catalonia (ICIQ).

Tarragona, September 2023

Doctoral Thesis Supervisor

Prof. Pablo Ballester Balaguer

UNIVERSITAT ROVIRA I VIRGILI
ARYL-EXTENDED CALIX[4]PYRROLE RECEPTORS WITH METAL CENTERS: ORGANOMETALLIC RECEPTORS AND METALLO-MACROCYCLES BASED ON COORDINATION BONDS
Andrea Rivoli

Calati juncu ca passa la china"

Bend over rush that passes the flood Proverbio siciliano

Sicilian proverb

Non est ad astra mollis e terries via

There is no easy way from the earth to the stars

Lucio Anneo Seneca

UNIVERSITAT ROVIRA I VIRGILI
ARYL-EXTENDED CALIX[4]PYRROLE RECEPTORS WITH METAL CENTERS: ORGANOMETALLIC RECEPTORS AND METALLO-MACROCYCLES BASED ON COORDINATION BONDS
Andrea Rivoli

Acknowledgements

The work contained in this thesis has been made possible thanks to the financial support from the Ministerio de Ciencia y with the grant CTQ2017-84319-9.

UNIVERSITAT ROVIRA I VIRGILI
ARYL-EXTENDED CALIX[4]PYRROLE RECEPTORS WITH METAL CENTERS: ORGANOMETALLIC RECEPTORS AND METALLO-MACROCYCLES BASED ON COORDINATION BONDS
Andrea Rivoli

A Dora, Nicolina, Maria e i Filippi

UNIVERSITAT ROVIRA I VIRGILI
ARYL-EXTENDED CALIX[4]PYRROLE RECEPTORS WITH METAL CENTERS: ORGANOMETALLIC RECEPTORS AND METALLO-MACROCYCLES BASED ON COORDINATION BONDS
Andrea Rivoli

Table of Contents

UNIVERSITAT ROVIRA I VIRGILI
ARYL-EXTENDED CALIX[4]PYRROLE RECEPTORS WITH METAL CENTERS: ORGANOMETALLIC RECEPTORS AND METALLO-MACROCYCLES BASED ON COORDINATION BONDS
Andrea Rivoli

Chapter 1

Introduction

1.1. Introduction

Since the end of the last century, many efforts of chemistry research have been oriented towards the study of non-covalent (supramolecular) interactions. The importance of the supramolecular forces, such as offset and stacked π-π[1], cation-π[2,3], anion-π[4,5] interactions, chalcogen[6], halogen[7], hydrogen bonding[8], as well as dispersive interactions, lies in their weak and reversible nature in comparison to the strong and irreversible covalent bonds. Reversible intermolecular forces are the basis of the hydrophobic effect phenomenon[9] and multiple molecular dynamic systems (i.e. host-guest), in which bound and unbound species are in chemical equilibrium[10]. The possibility to modulate the equilibrium (e.g. bound vs unbound or folded vs unfolded species) through external stimuli lies on the presence of supramolecular interactions. Supramolecular interactions are extremely versatile and can be found in many biological processes. The importance of non-covalent interactions in natural system can be exemplified with the functioning of the adrenergic receptors. These membrane receptors, which are highly specific for the binding of certain molecules, are coupled to different "G proteins" (**Figure 1**). When

[1] Salonen, L. M.; Ellermann, M.; Diederich, F., Aromatic Rings in Chemical and Biological Recognition: Energetics and Structures. *Angew. Chem. Int. Ed.* **2011,** *50*, 4808-4842.

[2] Huo, H.; Xiao, X.; Chang, L.; Xiong, X.; Shi, M.; Wang, J.; Tian, W., Cation-π and electrostatic interactions co-driven assembly of two-dimensional heteropore supramolecular polymers with rapid iodine capture capability. *Science China Chemistry* **2023,** *66*, 2070-2082.

[3] Liu, C.; Li, M.; Sun, J.; Li, P.; Bai, Y.; Zhang, J.; Qian, Y.; Shi, M.; He, J.; Huo, H.; Pang, J.; Fan, L.; Tian, W., Cation-π Interaction-Mediated Tumour Drug Delivery for Deep Intratumoral Penetration and Treatment. *Adv. Funct. Mater.* **2022,** *32*, 2205043.

[4] Garain, S.; Wagalgave, S. M.; Kongasseri, A. A.; Garain, B. C.; Ansari, S. N.; Sardar, G.; Kabra, D.; Pati, S. K.; George, S. J., Anion−π-Induced Room Temperature Phosphorescence from Emissive Charge-Transfer States. *J. Am. Chem. Soc.* **2022,** *144*, 10854-10861.

[5] Plais, R.; Clavier, G.; Salpin, J.-Y.; Gaucher, A.; Prim, D., Anion-π Interaction for Molecular Recognition of Anions: Focus on Cooperativity with Hydrogen Bonding. *Eur. J. Org. Chem.* **2023,** *26*, e202201281.

[6] Mahmudov, K. T.; Gurbanov, A. V.; Aliyeva, V. A.; Guedes da Silva, M. F. C.; Resnati, G.; Pombeiro, A. J. L., Chalcogen bonding in coordination chemistry. *Coord. Chem. Rev.* **2022,** *464*, 214556.

[7] Kanao, E.; Osaki, H.; Tanigawa, T.; Takaya, H.; Sano, T.; Adachi, J.; Otsuka, K.; Ishihama, Y.; Kubo, T., Rational Supramolecular Strategy via Halogen Bonding for Effective Halogen Recognition in Molecular Imprinting. *Anal. Chem.* **2023,** *95*, 9304-9313.

[8] Böhm, H. J.; Schneider, G.; Mannhold, R.; Kubinyi, H.; Folkers, G., *Protein-Ligand Interactions: From Molecular Recognition to Drug Design, Volume 19*. Wiley: 2003.

[9] Li, X.; Zhou, Y.; Lu, Z.; Shan, R.; Sun, D.; Li, J.; Li, P., Switchable enzyme mimics based on self-assembled peptides for polyethylene terephthalate degradation. *J. Colloid Interface Sci.* **2023,** *646*, 198-208.

[10] Meyer, E. A.; Castellano, R. K.; Diederich, F., Interactions with Aromatic Rings in Chemical and Biological Recognition. *Angew. Chem. Int. Ed.* **2003,** *42*, 1210-1250.

the substrate or an agonist binds to the receptor it experiences a significant conformational change. Next, the conformational change is transmitted to the coupled G protein causing its activation. [11] The transfer of the chemical information is exclusively based on non-covalent interactions, these include from the agonist-receptor binding and the subsequent conformational change of the receptor to the connection between the receptor's conformation and the quaternary structure[12,13] of the G protein. [14] In the last decades, the study of the binding properties of synthetic receptors[15] and molecular containers was key in gaining further knowledge and understanding on how complex biological systems work. Despite this, it is necessary to continue investigating the nature and properties of supramolecular interactions[16] using simple synthetic systems (vide infra).

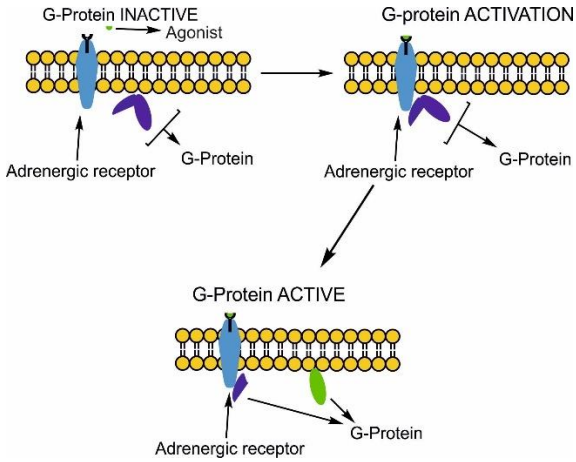

***Figure 1**: Scheme of the activation of the G-Protein.*

[11] Cooper, G. M., *The Cell: A molecular approach 2nd ed*. Sunderland, MA: Sinauer Associates: **2000**.

[12] Hughes, R. M.; Waters, M. L., Model systems for β-hairpins and β-sheets. *Curr. Opin. Struct. Biol.* **2006,** *16*, 514-524

[13] Deechongkit, S.; Nguyen, H.; Powers, E. T.; Dawson, P. E.; Gruebele, M.; Kelly, J. W., Context-dependent contributions of backbone hydrogen bonding to β-sheet folding energetics. *Nature* **2004,** *430*, 101-105.

[14] Fersht, A., *structure and mechanism in protein science*. Freeman, WH, 1999.

[15] Persch, E.; Dumele, O.; Diederich, F., Molecular Recognition in Chemical and Biological Systems. *Angew. Chem. Int. Ed.* **2015,** *54*, 3290-3327.

[16] Krueger, A. T.; Kool, E. T., Model systems for understanding DNA base pairing. *Curr. Opin. Chem. Biol.* **2007,** *11*, 588-594.

Supramolecular interactions[17,18] have been successfully applied in organic synthesis[19], in the transmission of stereochemical information[20], as well as in controlling the structure and properties of molecular materials[21]. In these examples, multiple, different non-covalent interactions operate simultaneously. The quantification of a particular non-covalent interaction amidst other interactions that contribute to the overall binding[22] is challenging. Several strategies were designed to dissect and quantify, either experimentally or theoretically, the strength of selected non-covalent interactions.
Among these strategies it is worth citing:

- Double Mutant Cycle (DMC) analyses are referred to as such since they were originally developed for analysing supramolecular interactions in proteins by amino-acid residues mutagenesis.[23] However, the same conceptual framework can be used for probing non-covalent interactions using synthetic systems by replacing the interacting functional groups using chemical synthesis. The approach involves experimentally determined binding free energies of at least four supramolecular complexes that are involved in a thermodynamic cycle (**Figure 2**). The cycle comprises a supramolecular complex containing the interaction of interest, two others in which one of the two interacting residues were omitted (mutated) and a double-mutant lacking the two interacting residues. The quantification of a specific interaction in a supramolecular complex is challenging owing to the fact that it occurs in combination with others (secondary interactions)

[17] Geng, W.-C.; Sessler, J. L.; Guo, D.-S., Supramolecular prodrugs based on host–guest interactions. *Chem. Soc. Rev.* **2020,** *49*, 2303-2315.

[18] Biedermann, F.; Nau, W. M.; Schneider, H.-J., The Hydrophobic Effect Revisited—Studies with Supramolecular Complexes Imply High-Energy Water as a Noncovalent Driving Force. *Angew. Chem. Int. Ed.* **2014,** *53*, 11158-11171.

[19] Amabilino, D. B.; Stoddart, J. F., Interlocked and Intertwined Structures and Superstructures. *Chem. Rev.* **1995,** *95*, 2725-2828.

[20] Clayden, J., Transmission of stereochemical information over nanometre distances in chemical reactions. *Chem. Soc. Rev.* **2009,** *38*, 817-829.

[21] Lehn, J.-M., Toward Self-Organization and Complex Matter. *Science* **2002,** *295*, 2400-2403.

[22] Biedermann, F.; Schneider, H.-J., Experimental Binding Energies in Supramolecular Complexes. *Chem. Rev.* **2016,** *116*, 5216-5300.
Carter, P. J.; Winter, G.; Wilkinson, A. J.; Fersht, A. R., The use of double mutants to detect structural changes in the active site of the tyrosyl-tRNA synthetase (Bacillus stearothermophilus). *Cell* **1984,** *38*, 835-40.

affecting it [24,25]. The DMC approach has proven effective in cancelling the effects caused by the mutations not being independent of each other. [26].

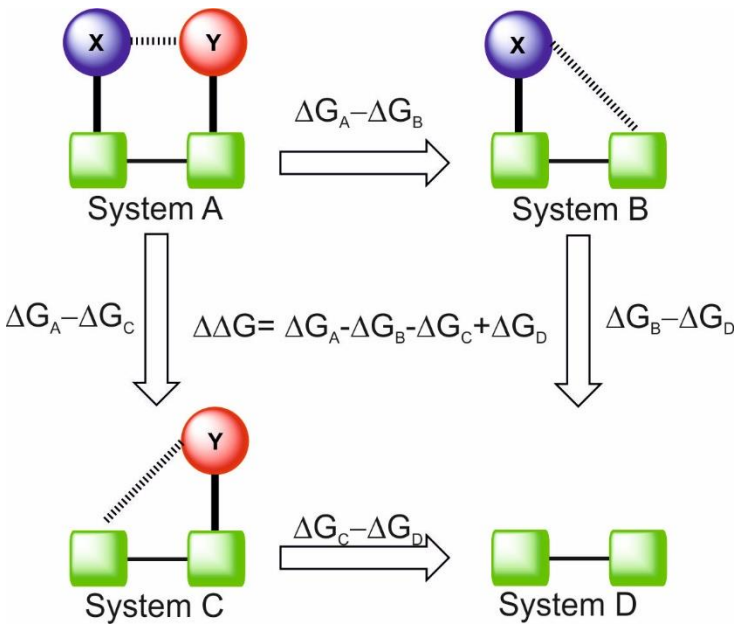

Figure 2: *Schematic representation of the double-mutant cycle.*

By calculating the difference in the free binding energies for the entire thermodynamic cycle (ΔΔG), it is possible to determine the interaction energy of the targeted non-covalent interaction.

- Molecular torsion balances (MTB) are rotameric folding molecules.[27] They are associated with the study of a rotation around a covalent bond. MTB exhibit two distinct conformational states: folded and unfolded. In the folded state, the MTB adopts a conformation in which the investigated non-covalent interaction is present. On the other hand, in the unfolded state the adopted conformation is characterized by the absence of the non-covalent

[24] von Krbek, L. K. S.; Schalley, C. A.; Thordarson, P., Assessing cooperativity in supramolecular systems. *Chem. Soc. Rev.* **2017,** *46*, 2622-2637.
[25] Hunter, C. A., Quantifying Intermolecular Interactions: Guidelines for the Molecular Recognition Toolbox. *Angew. Chem. Int. Ed.* **2004,** *43*, 5310-5324.
[26] Cockroft, S. L.; Hunter, C. A., Chemical double-mutant cycles: dissecting non-covalent interactions. *Chem. Soc. Rev.* **2007,** *36*, 172-188.
[27] Paliwal, S.; Geib, S.; Wilcox, C. S., Molecular Torsion Balance for Weak Molecular Recognition Forces. Effects of "Tilted-T" Edge-to-Face Aromatic Interactions on Conformational Selection and Solid-State Structure. *J. Am. Chem. Soc.* **1994,** *116*, 4497-4498.

interaction (**Figure 3**). MTB experiments measure the equilibrium between the two conformational states. Moreover, MTBs represent a unimolecular approach to quantify the free energy of interacting functional groups. They provide an enhanced control of the geometry of the investigated interaction compared to related intermolecular approaches. This characteristic is a significant and valuable advantage because even slight alterations in the interaction geometry can have a profound impact on its strength. MTBs can accurately measure extremely weak interactions that are unable to overcome the entropic penalty linked to intermolecular association or would otherwise have a negligible impact on the overall stability of the intermolecular complex. MTBs have been employed in the design of thermodynamic DMCs (**Figure 2**).

1.2. How do molecular torsion balances work?

MTBs are molecules that rotate one part of it with respect to another around a covalent bond (molecular torsion). In doing so, they switch between two states i.e. from a folded to an unfolded conformation. By studying the kinetic or thermodynamic properties of the conformational switch, it is possible to obtain valuable information about the free energy barrier of the process ($\Delta G^{\ddagger}$, difference between a ground state and the transition state) or the free energy difference between the two states at equilibrium (ΔG, difference between ground-state conformers), respectively. From the determined values, it is possible to derive the strength of the involved non-covalent interactions. Rotational energy barriers are experimentally determined through variable temperature NMR experiments. The interpretation of the measurements is not straightforward because the nature of the transition state (TS) can be hard to define. The TS cannot be observed directly and the energetic effects of the substituents might be difficult to predict. On the other hand, the relative populations of the two conformational states of the MTB, ΔG, is more easily interpreted and can also be quantified using NMR spectroscopy when the molecular flexibility process is slow on the chemical shift timescale[28,29]. The assignment of the interactions present in the two conformational states are based on a combination of i) X-ray crystal structures, ii) NMR solution studies and

[28] Mati, I. K.; Cockroft, S. L., Molecular balances for quantifying non-covalent interactions. *Chem. Soc. Rev.* **2010,** *39*, 4195-4205.
[29] Nakamura, K.; Houk, K. N., Theoretical Studies of the Wilcox Molecular Torsion Balance. Is the Edge-to-Face Aromatic Interaction Important? *Org. Lett.* **1999,** *1*, 2049-2051.

iii) electronic structure computational methods[30, 31]. Interactions energies must be interpreted with care and the role of the solvent in determining molecular conformations always considered.

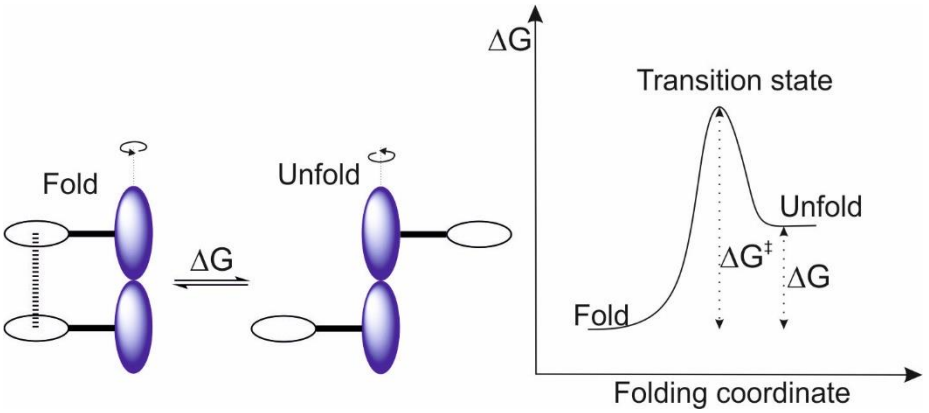

Figure 3: *Simplified folding equilibrium for a molecular torsion balance including the corresponding energy profile showing the energy barrier to rotation, ΔG‡, and the free energy of folding, ΔG.*

As already mentioned above, NMR spectroscopy is a valuable technique for evaluating conformational equilibrium of small molecules, despite all the associated challenges.[32]. Sometimes, the equilibrium between to two conformers displays a fast exchange on the NMR chemical shift time scale leading to averaged chemical shift signals, making their interpretation difficult or even sometimes impossible. To overcome this limitation, molecules that possess a single restricted bond rotation are often used. The bond rotation should be slow enough enabling the direct quantification of distinct conformational populations using NMR spectroscopy, and rapid enough to warrant reaching equilibrium within a reasonable time scale (i.e. human time scale).

[30] Bhayana, B.; Dickie, D. A., Intramolecular Nitro-Aromatic Interactions Within a Molecular Torsion Balance: A Quantitative Assessment. *Cryst. Growth Des.* **2018,** *18*, 6404-6410.
[31] Gardner, R. R.; McKay, S. L.; Gellman, S. H., Solvent-Dependent Stabilization of the E Configuration of Propargylic Secondary Amides. *Org. Lett.* **2000,** *2*, 2335-2338.
[32] Sankararaman, S.; Venkataramana, G.; Varghese, B., Conformational Isomers from Rotation of Diacetylenic Bond in an Ethynylpyrene-Substituted Molecular Hinge. *J. Org. Chem.* **2008,** *73*, 2404-2407.

1.3. Different classes of scaffolds used in the design of MTBs.

Aromatic interactions play a crucial role in molecular recognition being largely expressed in chemical and biological systems[10]. This fact makes that the study of interactions between aromatic systems became highly significant in the recent years. The study of interactions involving π systems is also of particularly interest due to their contribution in rational drug design strategies[33]. The scientific literature offers a diverse array of molecular scaffolds used in the design of molecular torsion balances (MTBs) to quantify different interactions involving aromatic π-systems. The selection of a particular scaffold depends on the nature and geometry of the aromatic interaction under investigation, for example aromatic "edge-to-face" interactions, or heteroatom-π interactions. Likewise, the selected scaffold of the MTB will have a profound impact on the energy barrier of the rotational bond and the interactions with the solvent. In the next section, we summarize selected examples of relevant scaffolds used in the design and study of MTBs.

1.3.1 Tröger base scaffold

In 1994, Wilcox and co-workers[34] were the first in coining the term ”molecular torsion balance” in the study of the conformational equilibria experienced by a series of aryl esters incorporating the Tröger base scaffold[35,36] (**Figure 4**). The designed MTBs were used to probe and quantify aromatic edge-to-face CH-π interactions[37]. In the two conformational states of the balance, only one (folded) exhibited a well-defined edge-to-face CH-π interaction. The other conformer (unfolded) did not display this interaction owing to the remote placement of the interacting groups. Nevertheless, both conformations included an interaction between the aryl substituent of the ester and one of the aromatic rings of the Tröger’s base that should not perturb the relative populations. The obtained results

[33] Li, S.; Xu, Y.; Shen, Q.; Liu, X.; Lu, J.; Chen, Y.; Lu, T.; Luo, C.; Luo, X.; Zheng, M.; Jiang, H., Non-Covalent Interactions with Aromatic Rings: Current Understanding and Implications for Rational Drug Design. *Current Pharmaceutical Design* **2013,** *19*, 6522-6533.

[34] Paliwal, S.; Geib, S.; Wilcox, C. S., Molecular Torsion Balance for Weak Molecular Recognition Forces. Effects of "Tilted-T" Edge-to-Face Aromatic Interactions on Conformational Selection and Solid-State Structure. *J. Am. Chem. Soc.* **1994,** *116*, 4497-4498.

[35] Tröger, J., Ueber einige mittelst nascirenden Formaldehydes entstehende Basen. *J. Prakt. Chem.* **1887,** *36*, 225-245.

[36] Spielman, M. A., The Structure of Troeger's Base. *J. Am. Chem. Soc.* **1935,** *57*, 583-585.

[37] Fleischhacker, W.; Schönfeld, T., *Pioneering Ideas for the Physical and Chemical Sciences: Josef Loschmidt’s Contributions and Modern Developments in Structural Organic Chemistry, Atomistics, and Statistical Mechanics*. Springer US: 2013.

showed that the interactions were weak (0.5 kcal·mol^{-1} conformational preference) and that cyclohexyl and phenyl esters had similar affinities for the face on an aryl-ring.

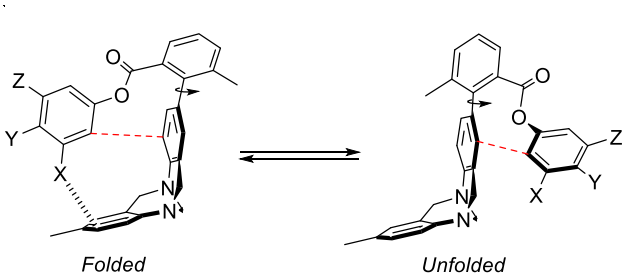

X= H, Me
Y= H, OMe, NO_2, Me, CN,nBu
Z= H, Me

Figure 4: *Conformational states of the equilibrium for the aryl ester torsion molecular balances (MTBs) of Wilcox incorporating Tröger's base scaffold.*

Similarly, in 2004 Diederich[38] *et al.* used MTBs incorporating a modified Tröger's base scaffold in an attempt to quantify the interaction between an organic fluorine atom (CF_3) and the π-face of the carbonyl of an amide group. In this report, the authors used a double-mutant thermodynamic cycle in order to dissect the interaction of interest from secondary background effects. They also performed a linear free energy relationship using a series of MTBs. The study led to the quantification of the Ar-F···C=O interaction as an attractive force with a value ranging from 0.8 to 1.5 kJ·mol^{-1} in non-polar solvents (benzene and chloroform).

[38] Hof, F.; Scofield, D. M.; Schweizer, W. B.; Diederich, F., A Weak Attractive Interaction between Organic Fluorine and an Amide Group. *Angew. Chem. Int. Ed.* **2004,** *43*, 5056-5059.

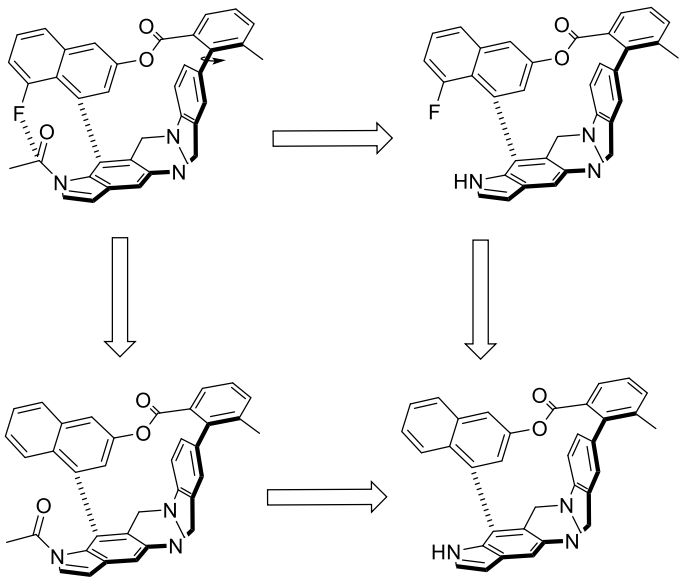

Figure 5: *Indole-extended Tröger-based torsion molecular balance used by Diederich et al. combined with a double mutant cycle analysis to determine the C_{sp2}-F bond and the amide carbonyl group.*

Few years later, the same group synthetized several MTBs having an indole-extended Tröger's base scaffold[39] (**Figure 5**). They reported the quantification of attractive orthogonal dipolar interactions between the fluorine attached to C_{sp3}-and C_{sp2} atoms and the carbonyl group of acetamide in nonpolar solvents using a DMC.
In 2008, Diederich[40] and co-workers studied the impact of polar substituents on the edge-to-face interaction of phenyl groups (**Figure 6**). Not surprisingly, the relative populations of the conformers involved in the equilibria were determined using ^{1}H NMR spectroscopy. The determined free energies (ΔG) of the investigated folding equilibria were directly related to the strength of the C–H---π interactions. In benzene and chloroform solutions, the folding free energies of the balances having a *p*-trifluoromethyl substituent in the edge aromatic ring followed a linear relationship with the σ_{meta} values of the substituent of the face aromatic ring. The slope of the line was steep, which is consistent with the expected behavior for an interaction strongly modulated by the electrostatic effect. The sole significant deviation from linearity was observed for balances having an acetamide substituent

[39] Fischer, F. R.; Schweizer, W. B.; Diederich, F., Molecular Torsion Balances: Evidence for Favorable Orthogonal Dipolar Interactions Between Organic Fluorine and Amide Groups. *Angew. Chem. Int. Ed.* **2007,** *46*, 8270-8273.

[40] Fischer, F. R.; Schweizer, W. B.; Diederich, F., Substituent effects on the aromatic edge-to-face interaction. *Chem. Commun.* **2008**, 4031-4033.

on the face aromatic ring. Most likely, the orthogonal dipole C-F···C=O interaction between the appended groups shifted the equilibria towards the folded conformation. In contrast, an analogous plot for the torsion balances bearing a non-substituted phenyl in the edge aromatic ring displayed a line with a slope close to zero indicating that the interaction was independent of the substituent in the face aromatic ring. The discrepancy regarding the magnitude of substituents effect on the folding equilibria cannot be rationalized invoking solvent-solute effects.[41]

High level computational analyses indicated that dispersion energy provided the largest contribution to *edge-to-face* CH-π interactions. While substituent effects may be attributed to a modulation of the electrostatic contributions.

Considering that the total energy of *edge*-to-*face* CH-π interactions (E_{tot}) can be estimated as a sum of electrostatic (E_{es}) and exchange repulsion (E_{exch}) terms in combination with other energy increments that are not affected by the *p*-substituent in the *edge* aromatic (E_{ind}, E_{disp} and δ_{int}),[42] Diederich concluded that the electrostatic term E_{es} increased upon increasing the electron-donating character of the functional group appended to the *face* aromatic ring for the MTBs having an electron-poor *edge*-aromatic (*p*-R = CF_3). Contrarily, for MTBs bearing an electron rich *edge*-aromatic (p-R = H), the change in the electrostatic term E_{es} was counterbalanced by an increase in the exchange repulsion term E_{exch} resulting in the small slope in the corresponding LFERs. The final revelation of the study is that even though dispersion interactions dominated the total energy of the interaction, the substituents effects in the folding equilibria of the MTBs were modulated by the level of the counterbalancing of electrostatic and exchange repulsion terms.[42, 43, ,44]

[41] Cockroft, S. L.; Hunter, C. A., Desolvation tips the balance: solvent effects on aromatic interactions. *Chem. Commun.* **2006**, 3806-3808.

[42] Lee, E. C.; Hong, B. H.; Lee, J. Y.; Kim, J. C.; Kim, D.; Kim, Y.; Tarakeshwar, P.; Kim, K. S., Substituent Effects on the Edge-to-Face Aromatic Interactions. *J. Am. Chem. Soc.* **2005,** *127*, 4530-4537.

[43] Sinnokrot, M. O.; Sherrill, C. D., Substituent Effects in π–π Interactions: Sandwich and T-Shaped Configurations. *J. Am. Chem. Soc.* **2004,** *126*, 7690-7697.

[44] Ringer, A. L.; Sinnokrot, M. O.; Lively, R. P.; Sherrill, C. D., The Effect of Multiple Substituents on Sandwich and T-Shaped π–π Interactions. *Chem. Eur. J.* **2006,** *12*, 3821-3828.

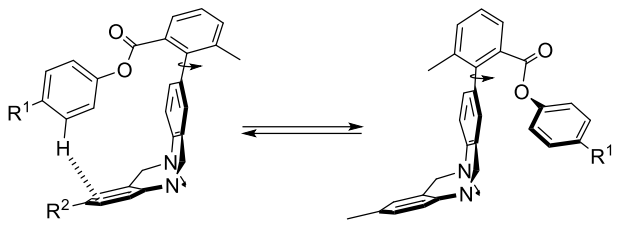

R^1= H, CF_3

R^2= H, Me, NH_2, OH, NHAc, I, Br, NO_2

Figure 6: *Conformational states of the equilibrium for the aryl ester incorporating Tröger's base torsion molecular balances (MTBs) used by Diederich et al.*

1.3.2 Bicyclic N-arylimide scaffold

In addition to the molecular torsion balances incluiding a Tröger base scaffold, molecular balances containing a bicyclic N-arylimide unit were reported for the quantification of non-covalent interactions involving aromatic rings.[45] In particular, they were used to investigate: i) aromatic slipped or offset stacked π-π interaction,[46] ii) interactions between solvent molecules an aromatic rings[47] and iii) the influence of the solventon the susbtituents effect in CH-π interactions. In this vein, Yoo et al.[48] investigated the correlation between the substituents effect (ρ values from Hammett plots) in CH-π interactions and the hydrogen-bond acceptor properties of the solvent. To this end, the authors measured CH-π interaction energies using a series of aryl-substituted molecular balances (**Figure 7**) in which the conformational

[45] Emenike, B. U.; Farshadmand, A.; Zeller, M.; Roman, A. J.; Sevimler, A.; Shinn, D. W., Electrostatic CH−π Interactions Can Override Fluorine Gauche Effects To Exert Conformational Control. *Chem. Eur. J.* **2023,** *29*, e202203139.

[46] Carroll, W. R.; Pellechia, P.; Shimizu, K. D., A Rigid Molecular Balance for Measuring Face-to-Face Arene−Arene Interactions. *Org. Lett.* **2008,** *10*, 3547-3550.

[47] Maier, J. M.; Li, P.; Vik, E. C.; Yehl, C. J.; Strickland, S. M. S.; Shimizu, K. D., Measurement of Solvent OH−π Interactions Using a Molecular Balance. *J. Am. Chem. Soc.* **2017,** *139*, 6550-6553.

[48] Emenike, B. U.; Spinelle, R. A.; Rosario, A.; Shinn, D. W.; Yoo, B., Solvent Modulation of Aromatic Substituent Effects in Molecular Balances Controlled by CH−π Interactions. *J. Phys. Chem. A* **2018,** *122*, 909-915.

preferences depended on the relative strength of methyl- and aryl CH-π interactions in the folded and unfolded states, respectively.

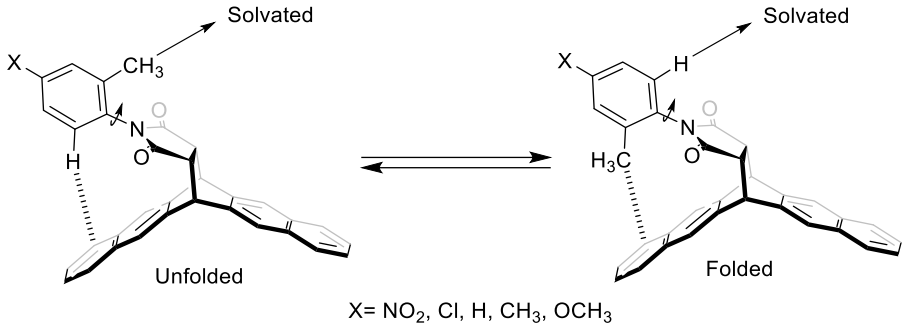

Figure 7: *Folded-Unfolded equilibrium of the Bicyclic N-arylimide used by Yoo et al. to investigate the correlation of the substituents effect (X) in CH-π interactions with the hydrogen-bond acceptor properties of the solvent.*

The interpretation/explanation of the conformational free energy as a function of substituents and the hydrogen-bond acceptor nature of the solvent reported in Yoo's work made extensive use of Hunter's solvation model[41,49,50]. This model considers that solvation can be modelled as the collection of explicit electrostatic interactions between solute electron-rich and electron-poor sites (MTB) and molecules of solvent (αβ parameters). This involves establishing pairs of hydrogen bond donors (α) and acceptors (β). Only four electron-donor sites of the MTB were considered to undergo changes between the folded and unfolded states. These were the three -$C_{sp3}H_3$ benzylic hydrogen atoms and the *ortho*-C_{sp2}-H, hydrogen atom, having α_1 and α_2 hydrogen-donor properties, respectively. The hydrogen-bond donor properties are dependent on the X-substituent. In contrast, the electron-donor properties (β) of the naphthalene π-face were considered to be constant independently of the X-substituent. Thus the energetics of the aromatic substituent effect can be calculated as $\Delta\Delta G = \Delta G_X - \Delta G_H = (\Delta 2\alpha_1 - \Delta\alpha_2)(\beta_s - \beta)$. Experimentally, the quantitative assessment of substituent effects in CH-π interactions is usually assessed through linear free-energy (LFE) relationships or Hammett plots following the equation $\Delta\Delta G = \Delta G_X - \Delta G_H = \rho\sigma_m$. The ρ value (slope of the plot) describes the susceptibility of the balance's conformational preferences to

[49] Cockroft, S. L.; Hunter, C. A., Desolvation and substituent effects in edge-to-face aromatic interactions. *Chem. Commun.* **2009**, 3961-3963.

[50] Hunter, C. A., Quantifying Intermolecular Interactions: Guidelines for the Molecular Recognition Toolbox. *Angew. Chem. Int. Ed.* **2004,** *43*, 5310-5324.

the changes of the aromatic substituents. A large value of ρ indicates a strong substituent effect and the importance of the electrostatic term in the interaction energy. The experimental Hammett plots in different solvents showed steeper slopes for polar solvents (i.e. DMSO, THF) than non-polar counterparts (i.e. benzene, chloroform). As mentioned above, these results could be explained by the dominance of dispersion interactions in non-polar solvents, which is also a way to account for poor Hammett correlations. However, comparing the equations of the Hammett plots with that of Hunter's model, it turned out that $\Delta\Delta G$ is directly proportional to solvent dependent properties: ρ and β_s-β, respectively. In other words, it should exist a linear relationship between ρ and β_s if Hunter's solvation model is valid for the system under investigation. Indeed, the authors showed a beautiful linear correlation between the two parameters. In short, the aromatic substituents effect (ρ) increased with the increasing hydrogen-bond acceptor properties of the solvent (β_s). It was suggested that the folding of the balance was driven mainly by the favorable solvation of the exposed *ortho*-C_{sp2}-H having a larger α value. Conversely, for non-polar solvents the β_s-β becomes almost zero explaining the apparent lack of substituent effect for the interaction under study. This and other related studies[41,49,51] demonstrated the delicate balance between solvation/desolvation and functional group interactions in explaining the different behaviour of a molecular system in different solvents.

In 2011, Shimizu *et al.* reported another series of conformationally flexible bicyclic N-arylimides[52] (**Figure 8**) to study weak aliphatic CH-π interactions between alkyl and aryl groups. The authors placed particular interest on studying the influence of the length and width/size of the alkoxy groups in the CH-π interactions.

[51] Li, P.; Vik, E. C.; Shimizu, K. D., N-Arylimide Molecular Balances: A Comprehensive Platform for Studying Aromatic Interactions in Solution. *Acc. Chem. Res.* **2020,** *53*, 2705-2714.

[52] Carroll, W. R.; Zhao, C.; Smith, M. D.; Pellechia, P. J.; Shimizu, K. D., A Molecular Balance for Measuring Aliphatic CH−π Interactions. *Org. Lett.* **2011,** *13*, 4320-4323.

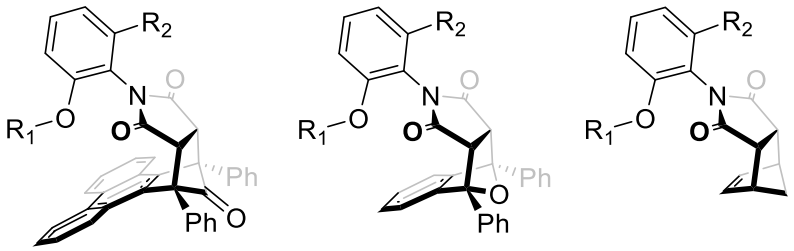

R_1= Me, Et, *i*-Pr, *n*-Bu,*c*-Hex
R_2= OMe, OEt, H

Figure 8: *Molecular torsion balances containing bicyclic N-arylimides formwork used by the Shimizu group to investigate and determine the strength of CH–π interactions between alkyl and arene groups.*

The folding properties of the benzene and ethylene balances were used as control in the study of those of the phenanthrene derivative. It is worth mentioning, that the benzene balance does not form CH-π interactions owing to geometrical restrictions, however, it retains the lone-pair-π interaction between the oxygen of the ether linker and the arene shelf that is also present in the phenanthrene analog. Branched alkoxy arms (O*i*-Pr and O*c*-Hex) were found to weaken the intramolecular CH-π interactions with the phenanthrene surface. Molecular modelling showed that these secondary alkyl groups created steric strain in the folded-conformation. Additionally, the balances with longer alkyl chains (OEt and O*n*-Bu) showed a destabilization of the folded conformer. This result was difficult to explain because the longer alkoxy group can establish up to two CH-π interaction and are conformationally flexible to minimize any steric strain. The authors suggested that differences in conformational entropy of the chains could be responsible for this destabilization (**Figure 8**). To test this theory, they evaluated the entropic and enthalpic terms for the folding equilibria of the phenanthrene and benzene-shelved balances having a single OMe and OEt substituent. The obtained data confirmed that the apparent differences in CH-π interactions derived from conformational entropy costs. They also validated the possibility to quantify the enthalpic differences associated with the CH-π interactions via differences in free folding free energies of the corresponding phenanthrene and benzene-shelved balances. The Shimizu group quantified the CH-π interaction to be of the order of ∼1.0 kcal/mol. They also showed that due to the weakness of the interaction and the sensitivity of the balances any stability trend can be masked by other effects. However, by using carefully designed control balances they were able to isolate the relative contribution of the CH-π interaction to the ΔG_{fold}. In addition, they dissected the

measured apparent repulsive value (0.45 kcal·mol^{-1}) for the interaction in the phenanthrene balance having one OMe substituent as a sum of three terms: i) the attractive CH-π interaction (- 0.95 kcal·mol^{-1}), ii) the oxygen lone pair-π repulsion (1.23 kcal·mol^{-1}), and iii) the slight preference of the balances for the unfolded conformer (0.17 kcal·mol^{-1}).

Another example reported by Shimizu[53] *et al.* showcased the synthesis and experimental survey of a library of molecular balances to compare pairs (**Figure 9**) of S-π versus O-π interactions over a wide range of structural, geometric and solvent parameters (chloroform and dimethyl sulfoxide).

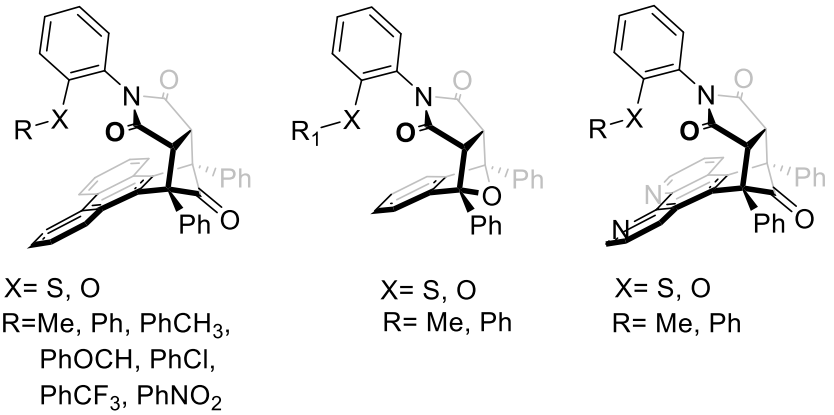

Figure 9: Three examples of *N-aryl imide based molecular torsion balances used by the Shimizu group to investigate and determine the strength of the S–π and O–π interactions*

To identify differences in the S-π and O-π interactions, the experimental folding energies of the sulfur (ΔG_S) and oxygen (ΔG_O) balances of each pair were plotted against each other in a correlation plot. In each balance pair, the scaffold, R substituent and aromatic shelf were identical. The only difference was the chalcogen atom. The authors observed a good linear correlation between the folding energies of the sulphur and oxygen balances across the balance pair series in the two solvents (chloroform and dimethyl sulfoxide). The observed strong linear correlation confirmed the similarity in structures, interactions and conformations biases between the sulfur and oxygen balances. It also supported the ability of the

[53] Hwang, J.; Li, P.; Smith, M. D.; Warden, C. E.; Sirianni, D. A.; Vik, E. C.; Maier, J. M.; Yehl, C. J.; Sherrill, C. D.; Shimizu, K. D., Tipping the Balance between S-π and O-π Interactions. *J. Am. Chem. Soc.* **2018,** *140,* 13301-13307.

balances for the accurate isolation and comparison of the S-π and O-π interaction energies. Interestingly, the linear correlations displayed a slope larger than 1. The experimental line crossed the hypothetical line of slope 1 ($\Delta G_S = \Delta G_O$). Data points above the hypothetical line were balance pairs in which the oxygen balances have higher folded/unfolded ratios. Those pairs of balances below the hypothetical line corresponded to sulfur balances with a more favorable folded/unfolded ratio. This systematic switch in folding preferences provide an explanation to previous conflicting results. In short, the more stable chalcogen interaction (O-π vs S-π) is structure, geometry and solvent dependent. The results from a single pairwise comparison can vary depending of where the O sv S pair falls.

Balance pairs favoring O-π interaction show the lowest folded ratio. This bias can be explained using steric repulsion arguments. The rigid scaffold of these balances is slightly too short, positioning the chalcogen atom close to the aromatic surface in the folded conformer. Those with the oxygen atom experienced weaker repulsive interactions than those with the larger sulfur atom. Despite this explanation, most balance pairs have higher folding ratios for the sulfur balance. However, we are forced to conclude that, in many cases, the preferred stabilizing effect of the sulfur atom can be outweighed by steric repulsive interactions.

To further investigate the origins of the observed experimental trends, the Shimizu group conducted computational studies involving simple bimolecular complexes between a phenyl-chalcogen (S or O)-methyl ether and a benzene ring. The energy surfaces of the complexes were explored by varying the chalcogen-to-arene distance. On the one hand, the linear correlation between chalcogen-π interactions is probably due to the similar shape of the two potential curves. The switch in preference of the chalcogen-π is due to the larger energy of the S-π interaction at optimal distances. Nevertheless, the S-π interaction displayed a stronger exchange repulsion energy at short distances making the O-π interaction more favourable. The examination of the components of the interaction energies (SAPT calculations) confirmed the interplay between the greater stabilizing dispersion and destabilizing exchange-repulsion interactions of the larger and more polarizable sulfur atom varies with the distance to the arene surface.

1.3.3 Dibenzobicyclo[3.2.2]nonane scaffold

The dibenzobicyclo[3.2.2]nonane (BCN) framework provides a lower degree of conformational freedom for the carbon chain than previous scaffolds used in the

design of MTBs i.e. Tröger's base. Nevertheless, there is sufficient freedom in BCN to allow for the formation of X-H···π interactions (X = C, N, O) with the substituents of the central bridge carbon atom. [54] In addition, heteroatoms directly connected to the central carbon atom of the bridge are also brought in close proximity to the centers of the BCN aromatic rings in a well-defined trajectory and the interaction energies are large enough to be measured experimentally using BCN as a molecular conformational balance (MCB). Notably, the conformational equilibrium of propane bridged anthracenes display a rather low energy barrier and the approach of reaching slow-exchange at low temperatures failed.[55] An alternative method was developed relying of the fact that the equilibrium constants can be determined using the experimentally determined average coupling constants if the *J* coupling are known for both conformers. Motherwell[56] and co-workers determined the conformational preferences of an spiro-oxathiolane inserted in a dibenzobicyclo[3.2.2]nonane architecture (**Figure 10**). Not surprisingly and based on the previous results of the Shimizu group, the authors determined that there was a preference in this molecule and in multiple solvents for placing the S atom over the π-system with respect to the counterbalancing oxygen atom.

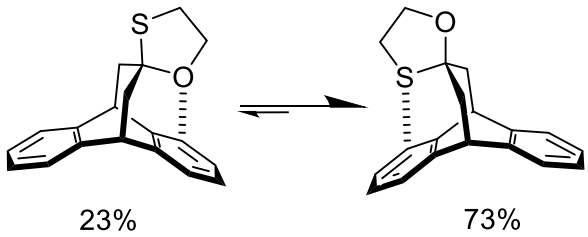

Figure 10: *Conformational equilibrium of* a molecular balance containing a *dibenzobicyclo[3.2.2]nonane framework equipped with an spiro-oxathiolane unit to quantify S···arene versus O···arene interaction.*

[54] Aliev, A. E.; Moïse, J.; Motherwell, W. B.; Nič, M.; Courtier-Murias, D.; Tocher, D. A., Probing weak non-covalent interactions in solution and solid states with designed molecules. *Phys. Chem. Chem. Phys.* **2009,** *11*, 97-100.

[55] Motherwell, W. B.; Moïse, J.; Aliev, A. E.; Nič, M.; Coles, S. J.; Horton, P. N.; Hursthouse, M. B.; Chessari, G.; Hunter, C. A.; Vinter, J. G., Noncovalent Functional-Group–Arene Interactions. *Angew. Chem. Int. Ed.* **2007,** *46*, 7823-7826.

[56] Motherwell, W. B.; Moreno, R. B.; Pavlakos, I.; Arendorf, J. R. T.; Arif, T.; Tizzard, G. J.; Coles, S. J.; Aliev, A. E., Noncovalent Interactions of π Systems with Sulfur: The Atomic Chameleon of Molecular Recognition. *Angew. Chem. Int. Ed.* **2018,** *57*, 1193-1198.

In 2020, Jian[57] *et al.* reported a closely related conformational equilibrium study to probe the competition between halogen–π and CH–π interactions (**Figure 11**) by means of NMR spectroscopy.

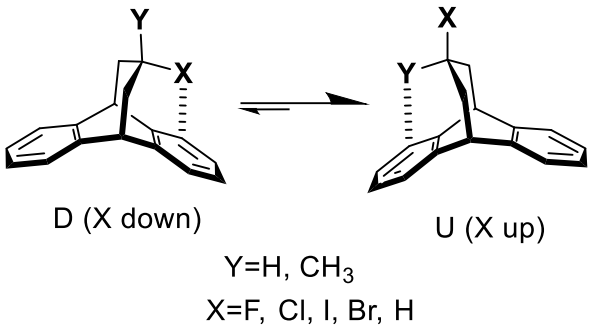

Figure 11: *Dibenzobicyclo[3.2.2]nonane based molecular torsion balance used to probe the competition between halogen-π and CH-π interactions by Jia et al. The U and D nomenclature refers to the position of the halogen in relation to the aromatic rings.*[57]

All halogen atoms seemed to establish weaker interactions with the aromatic surface when a hydrogen atom was the counterbalancing. This was demonstrated by the predominant formation of the U conformer (halogen up, H down) (**Figure 11**). Among the series of halogens, the fluorine (-F) substituent was the only one partially competing with -H (U:D = 83:17). In contrast to this U conformational preference, F seemed to form stronger intramolecular interactions when competing with -CH for the interaction with the aromatic ring (U:D = 13:87). This result suggested that the competition between halogens and hydrogen for the adoption of the preferred conformer (interaction with an electron-rich aromatic ring) was mainly driven by steric effects [52]. Indeed, the competition between Cl and CH_3, having similar volumes, showed that Cl–π interactions are slightly stronger than CH_3–π interactions, leading to observe a conformer ratio U:D = 40:60.

1.3.4 C60-fulleropyrrolidine scaffold

It is well known that nanostructures, such as carbon nanotubes and fullerenes, possessing curved π-electron systems[58] were used in a wide range of applications

[57] Jian, J.; Poater, J.; White, P. B.; McKenzie, C. J.; Bickelhaupt, F. M.; Mecinović, J., Probing Halogen–π versus CH–π Interactions in Molecular Balance. *Org. Lett.* **2020,** *22*, 7870-7873.

[58] Kawase, T.; Kurata, H., Ball-, Bowl-, and Belt-Shaped Conjugated Systems and Their Complexing Abilities: Exploration of the Concave–Convex π–π Interaction. *Chem. Rev.* **2006,** *106*, 5250-5273.

such as organic photovoltaics[59,60], photoluminescent probes and sensors[61,62], and medical science[63,64,65,66]. Consequently, there has been a significant research interest in quantifying non-covalent interactions with curved π-electronic systems.[67]

For instance, Yamada et al. [68,69] conducted two studies on the quantification and nature of arene-fullerene interactions. The authors prepared fullerene-based molecular torsion balances (**Figure 12**) and evaluated the effect of the arene substituents and its size on the strength of the interaction. They found that the face-to-face stacked π-π interaction established with the fullerene surface in the folded conformer became stronger with the increase in the electron-donating properties of the *p*-arene substituent. They observed a good linear correlation between ΔG_{fold} and the Hammett parameters of the substituents. Contrary to the results obtained by Diederich in quantifying edge-to-face π-π interactions, the slope of the line was steeper in C_6D_6 than in $CDCl_3$. These results implied that electrostatic interactions

[59] Scharber, M. C.; Mühlbacher, D.; Koppe, M.; Denk, P.; Waldauf, C.; Heeger, A. J.; Brabec, C. J., Design Rules for Donors in Bulk-Heterojunction Solar Cells—Towards 10 % Energy-Conversion Efficiency. *Adv. Mater.* **2006,** *18*, 789-794.

[60] Carati, C.; Gasparini, N.; Righi, S.; Tinti, F.; Fattori, V.; Savoini, A.; Cominetti, A.; Po, R.; Bonoldi, L.; Camaioni, N., Pyrene–Fullerene Interaction and Its Effect on the Behavior of Photovoltaic Blends. *The Journal of Physical Chemistry C* **2016,** *120*, 6909-6919.

[61] Langenbacher, R.; Budhathoki-Uprety, J.; Jena, P. V.; Roxbury, D.; Streit, J.; Zheng, M.; Heller, D. A., Single-Chirality Near-Infrared Carbon Nanotube Sub-Cellular Imaging and FRET Probes. *Nano Lett.* **2021,** *21*, 6441-6448.

[62] Ackermann, J.; Metternich, J. T.; Herbertz, S.; Kruss, S., Biosensing with Fluorescent Carbon Nanotubes. *Angew. Chem. Int. Ed.* **2022,** *61*, e202112372.

[63] Friedman, S. H.; DeCamp, D. L.; Sijbesma, R. P.; Srdanov, G.; Wudl, F.; Kenyon, G. L., Inhibition of the HIV-1 protease by fullerene derivatives: model building studies and experimental verification. *J. Am. Chem. Soc.* **1993,** *115*, 6506-6509.

[64] Martinez, Z. S.; Castro, E.; Seong, C.-S.; Cerón, M. R.; Echegoyen, L.; Llano, M., Fullerene Derivatives Strongly Inhibit HIV-1 Replication by Affecting Virus Maturation without Impairing Protease Activity. *Antimicrob. Agents Chemother.* **2016,** *60*, 5731-5741.

[65] Ghiassi, K. B.; Olmstead, M. M.; Balch, A. L., Gadolinium-containing endohedral fullerenes: structures and function as magnetic resonance imaging (MRI) agents. *Dalton Trans.* **2014,** *43*, 7346-7358.

[66] Ashcroft, J. M.; Tsyboulski, D. A.; Hartman, K. B.; Zakharian, T. Y.; Marks, J. W.; Weisman, R. B.; Rosenblum, M. G.; Wilson, L. J., Fullerene (C60) immunoconjugates: interaction of water-soluble C60 derivatives with the murine anti-gp240 melanoma antibody. *Chem. Commun.* **2006**, 3004-3006.

[67] Yamada, M., Unraveling the Nature and Strength of Non-Covalent Interactions on the Surface of Fullerenes. *ChemPlusChem* **2023,** *88*, e202300062.

[68] Yamada, M.; Narita, H.; Maeda, Y., A Fullerene-Based Molecular Torsion Balance for Investigating Noncovalent Interactions at the C60 Surface. *Angew. Chem. Int. Ed.* **2020,** *59*, 16133-16140.

[69] Yamada, M.; Kurihara, Y.; Koizumi, M.; Tsuji, K.; Maeda, Y.; Suzuki, M., Understanding the Nature and Strength of Noncovalent Face-to-Face Arene–Fullerene Interactions. *Angew. Chem. Int. Ed.* **2022,** *61*, e202212279.

were important in the stabilization of the conformers. Conversely, the correlation of ΔG_{fold} and the polarizability of the arenes revealed a significant fluctuation even for aromatic rings with the same level of polarizability. This finding indicated that other factors different from dispersion forces, such as electrostatic interactions, influenced the folding. Nevertheless, ΔG_{fold} was negative for arenes having a particularly large polarizability and turned positive for those with small polarizability, indicating the contribution of the dispersion term.

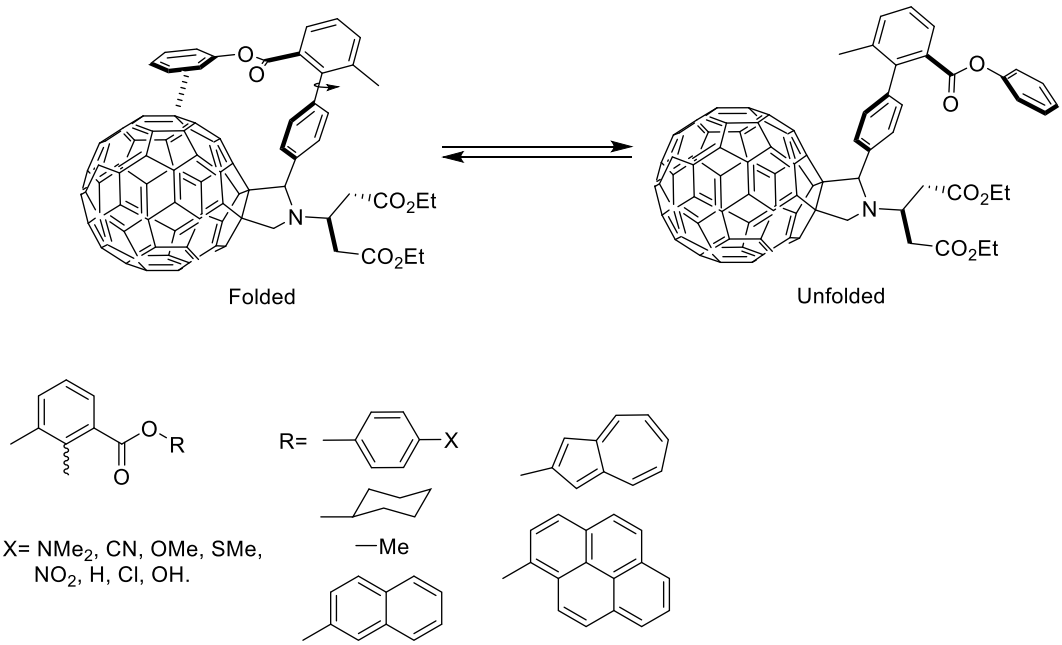

Figure 12: *a) Structure of the C_{60}-fulleropyrrolidine molecular torsion balance used by Yamada et al. for quantifying arene-fullerene interactions.*

Furthermore, the change in the interaction of the arene with fullerene was also investigated by adding DIEA (diisopropylethylamine) to the phenol substituted balance. The ΔG_{fold} became slightly more positive for the anionic phenolate residue suggesting that anion-fullerene interactions were almost insignificant for this model compound.

They also observed that for polyaromatic substituents the ΔG_{fold} was more negative as the number of aromatics rings increased. Generally, the polarizability of the polyarenes showed a good correlation with ΔG_{fold}, indicating that dispersion forces played a major role in polyarene-fullerene interactions.

1.4. Conclusions and limitations of the MTBs as physical organic chemistry tools

In the introduction we presented how molecular torsion and conformational balances have emerged as valuable physical organic tools for the study and quantification of non-covalent interactions. Their ability to offer an enhanced control over the geometry of the non-covalent interactions allowed the accurate measurement of even very weak forces. Different scaffolds, such as the Tröger-base, bicyclic N-arylimides, dibenzobicyclo[3.2.2]nonanes, and C60-fulleropyrrolidines, were employed in the construction of MTBs. We showed that each scaffold can be used for specific objectives allowing the investigation of different types of non-covalent interactions.

We discussed how different research groups used the molecular balances to study interactions mainly with aromatic systems. These involved π-π interactions, CH-π and chalcogen-π interactions. The selected examples explored the influence of the substituents in the aromatic components, as well as the solvent effect on the folding energies, that is the interaction preferences. The use of control compounds, thermodynamic double-mutant cycles, and solvation models assisted the accurate quantification and comparison of the strengths of the interactions.

The selected examples discussed in the introduction served to highlight the strong points for the use of molecular balances in quantifying non-covalent interactions. For example, the geometry of the non-covalent intramolecular interaction is precisely defined and fixed by the scaffold of the balance. This is really helpful in determining the distance between the interacting units and the energies of weak non-covalent interactions. However, this strength represents at the same time a weakness in the use of molecular balances as model systems for quantifying non-covalent interactions. Indeed, if the scaffold of the molecular balance is not well designed or selected with respect to the geometry of the targeted non-covalent interaction, it could lead to problems in the interpretation of the results. Theoretically, a good molecular balance must be designed in a way that allows the optimization of the binding geometry between the two interacting partners of the non-covalent intramolecular interaction by emulating that of the intermolecular non-covalent interaction version. It is possible to distinguish two cases of a not well-designed molecular balance:

1) A rigid molecular torsion or conformational balance displaying a scaffold determining the interaction distance and the angle between the functional groups

that does not coincide with that of the "real" equilibrium state. Such a balance will probe a "forced" interacting geometry providing an energy that is markedly different from that of the constraint-free ideal case.

2) A too flexible molecular balance could build up some torsional or entropic strain, resulting in a smaller apparent binding energy for the non-covalent interaction.

A final caveat is that the interplay of numerous factors contributing to non-covalent interactions probably limits the direct transferability of the absolute energies measured using molecular balances. Nevertheless, this limitation is common to all model systems employed in the quantification of intermolecular forces.

1.5. Aims of the thesis

The general aim of the thesis is to design, prepare and characterize "two-wall" aryl-extended calix[4]pyrrole receptors containing metal centers in their structure (organometallic or coordination complexes). More precisely, we based our designs on "two wall" aryl-extended calix[4]pyrroles featuring a metallo-ethynyl (metal-acetylide) unit connected to the *para*-position of its *meso*-phenyl substituents.

We expect that the unique structural features of the calix[4]pyrrole receptors combined with the presence of a metal center close to the cavity will provide a series of compounds with interesting properties. We are interested in studying the molecular recognition and binding properties of the prepared receptors for small polar molecules in organic solvents (e.g. tetraalkylammonium chloride salts (as a source of chloride) and pyridine N-oxide derivatives).

In order to achieve the main aim, we pursued the following objectives:

O.1) Incorporation of metal centers into "two wall" aryl-extended calix[4]pyrroles.

We propose the synthesis of symmetric and non-symmetric α,α and α,β "two wall" calix[4]pyrrole receptors. We will incorporate one or two metal centers (e.g. Au(I), Pt(II) at the upper rim). More in detail, we plan to synthetize and characterize a mono-nuclear gold(I) phosphine complex based on a 'two-wall' aryl-ethynyl extended calix[4]pyrrole. We want to evaluate the binding properties of mono-Au(I) aryl-ethynyl extended calix[4]pyrrole with tetraalkylammonium chloride salts using ^{1}H NMR titration experiments and compare it with the non-metallated counterpart. Moreover, we also plan to synthesize and characterize a symmetric di-nuclear "two-wall" aryl-extended calix[4]pyrroles containing platinum(II)–ethynyl substituents at their upper rim.

O.2) Self-assembly and characterization of di-nuclear metallo-macrocycles based on an organometallic bis-Pt(II)-ethynyl "two wall" calix[4]pyrrole and di-pyridine derivatives as bis-strap ligands.

We will use a symmetric bis-Pt(II)-ethynyl "two wall" calix[4]pyrrole described in objective O.1, to study the self-assembly of different di-nuclear Pt(II) metallo-macrocycles in organic solvents using various di(pyridinyl)pyridine-2,6-dicarboxamides as strap ligands. We will investigate the binding properties of the self-assembled metallo-macrocycles, the bis-Pt(II)-ethynyl "two wall"

calix[4]pyrrole, and its synthetic "two wall" calix[4]pyrrole precursor with pyridine N-oxide and 4,4'-bipyridine N,N'-dioxide using NMR spectroscopic titrations (^{1}H and ^{31}P NMR). We are interested in evaluating the influence of the metals and the strap ligands in the binding properties of the receptors for the selected guests.

O.3) Design and synthesis of a supramolecular conformational balance based on an α,β-isomer of a "two-wall" mono-nuclear Au(I)-acetylide calix[4]pyrrole.

We propose the synthesis and characterization of a non-symmetric mono-nuclear organometallic α,β-calix[4]pyrrole bearing one Au(I)-acetylide unit in the *para*-position of one of the *meso*-phenyl substituents. We aim at using the mono-nuclear Au(I) compound as a supramolecular conformational balance to quantify chloride-π interactions. We plan to characterize thermodynamically the complexes of the mono-nuclear Au(I)-acetylide α,β-calix[4]pyrrole receptor with tetraalkylammonium chloride salts using NMR spectroscopic titrations (^{1}H NMR). We propose to use computational methods to investigate the electronic properties of the receptor (i.e. electrostatic surface protential (ESP) of the *meso*-aromatic ring), as well as the structure and energy of its complexes. We envisaged that theoretical studies would help us in supporting the experimental results. We expect that the presence of different chloride-π interactions in the two possible conformers (folded and unfolded) of the complexes of the Au(I)-acetylide calix[4]pyrrole and its synthetic precursor will translate into changes in their equilibrium populations. We aimed at quantifying the strength of the chloride-π interaction in the complexes.

Finally, we plan to use the non-metallated α,β-"two wall" calix[4]pyrrole receptors equipped with iodine and ethynyl *para*-substituents to study the interchangeability of the isoelectronic iodo- and ethynyl substituents and disorder in the solid state structures. .

1.6. Outline of the thesis.

The present doctoral thesis is divided into six chapters, as follows: an introduction on molecular torsion balances (**Chapter 1**), and five chapters (**Chapter 2-6**) including the results of this Thesis. Each chapter includes a more specific introduction, results and discussion, and the corresponding experimental section. We also include a final section summarizing the conclusions of the performed research.

In **Chapter 2**, we report the synthesis and characterization of a mono-nuclear "two wall" aryl-extended calix[4]pyrrole receptor decorated with an acetylide-gold(I)-PTA complex at its upper rim. We describe the ^{1}H NMR titration experiments of the calix[4]pyrrole acetylide-gold(I)-PTA complex and its non-metallated synthetic precursors (i.e. the non-symmetric mono-iodo-mono-ethynyl and the symmetric bis-iodo aryl extended calix[4]pyrrole) with TBACl in dichloromethane and acetone solution. In acetone solution, we use isothermal titration calorimetry (ITC) experiments to thermodynamically characterize the formed 1:1 chloride complexes and perform pair-wise competitive binding experiments. In both solvents, we measured a decrease in the binding constant of the mono-nuclear acetylide-Au(I)-PTA complex for chloride compared to the parent mono-iodo-mono-ethynyl. In turn, mono-iodo-mono-ethynyl calix[4]pyrrole receptor also shows a reduction in binding affinity for chloride compared to its precursor bis-iodo calix[4]pyrrole. The free energy differences (ΔG) of the 1:1 chloride complexes cannot be exclusively attributed to their dissimilar electrostatic surface potential values either at the center of the *meso*-phenyl wall or its *para*-substituent. We conclude that solvation/desolvation processes play an important role in the stabilization of the chloride complexes. In acetone solution and in the presence of TBACl, a reference compound for the acetylide Au(I)•PTA unit, produces a bis(alkynyl)gold(I) anionic complex. Thus, the observation of two separate sets of signals in the ^{1}H NMR spectra for the bound aromatic calix[4]pyrrole protons, when more than 1 equiv. of the salt is added, is assigned to the formation of the chloride complexes of the calix[4]pyrrole acetylide-gold(I)-PTA complex and of the "in situ" formed corresponding calix[4]pyrrole anionic dimer. Finally, preliminary data obtained in cell viability assays of the calix[4]pyrrole acetylide-gold(I)-PTA complex and the reference acetylide Au(I)•PTA compound with human cancer cells lines assign them with moderate activities showing that the calix[4]pyrrole unit is not relevant.

In **Chapter 3**, we present our results concerning the self-assembly of metal-mediated macrocycles, which consist on a di-platinum(II)ethynyl-organometallic

"two-wall" calix[4]pyrrole and a series of bis-pyridine ligands. Furthermore, we report the results of the ^{1}H NMR titration experiments performed with the self-assembled metallocycles and pyridine N-oxide derivatives. We describe our studies on the binding properties of the prepared metallocycles and compared them with those of its synthetic precursors.

In **Chapter 4**, we synthesized a mono-nuclear Au(I)-acetylide of a non-symmetrically substituted α,β-isomer "two-wall" calix[4]pyrrole and employed it as a supramolecular conformational balance. We hypothesized that the chloride complex of the non-symmetrically substituted mono-nuclear "two-wall" α,β calix[4]pyrrole, in cone conformation, would position only one of its two *meso*-phenyl substituents axially while the other would remain equatorially oriented. This would produce two distinct cone conformers for the complex that are in equilibrium. Significantly, in both conformers, only the axially oriented *meso*-phenyl substituent can engage in anion-π interactions with the bound chloride ion. We hypothesized that the potential presence of different attractive/repulsive chloride-π interactions in the two conformers of the complex would modify the equilibrium population between the folded and unfolded states compared to that of an analogous calix[4]pyrrole (synthetic precursor) lacking the Au(I) atom. To investigate this putative behaviour, we examined the binding of chloride ions to symmetrically, non-symmetrically substituted and mono-nuclear "two-wall" α,β calix[4]pyrrole receptors in various solvents using ^{1}H NMR spectroscopic titrations, variable temperature NMR experiments (VT-NMR), and isothermal titration calorimetry (ITC) experiments. Alkylammonium salts such as tetra-butyl ammonium chloride (TBACl) and methyl trioctyl ammonium chloride (MTOACl) were employed as chloride sources. Additionally, we performed theoretical calculations to validate and support the experimental findings.

Chapter 5 deals with the synthesis and X-ray characterization of three α,β “two wall” aryl-extended calix[4]pyrroles having either identical (symmetrically substituted) or different (non-symmetrically substituted) *meso*-aryl substituents (aryl=4-ethynylphenyl and 4-iodophenyl). The X-ray structures of the co-crystals formed by the two symmetrically substituted calix[4]pyrroles is also described. In the solid state, all studied α,β-calix[4]pyrroles exhibit a 1,3-alternate conformation with two co-crystallized acetonitrile solvent molecules H-bonded to adjacent *cis*-pyrrole rings. Remarkably, the 1,3-conformer of the non-symmetrically substituted iodophenyl/ethynylphenyl compound is intrinsically chiral. The two enantiomers are present in the average asymmetric unit in a 65 : 35 occupancy ratio displaying a

head-to-tail directional disorder. This is due to the functional complementarity and the isosteric and isoelectronic properties of the *para*-substituents: iodo and ethynyl. That is, the negative belt of iodine is similar to the negative π-system of the C≡C triple bond and the σ-hole in the iodine atom is similar to the positive proton at the C≡C−H group.

UNIVERSITAT ROVIRA I VIRGILI
ARYL-EXTENDED CALIX[4]PYRROLE RECEPTORS WITH METAL CENTERS: ORGANOMETALLIC RECEPTORS AND METALLO-MACROCYCLES BASED ON COORDINATION BONDS
Andrea Rivoli

Chapter 2

Chloride Binding Properties of a Macrocyclic Receptor Equipped with an Acetylide Gold(I) Complex

Chloride Binding Properties of a Macrocyclic Receptor Equipped with an Acetylide Gold(I) Complex

Chloride Binding Properties of a Macrocyclic Receptor Equipped with an Acetylide Gold(I) Complex

2.1 Introduction

Alkynyl gold(I) complexes play a significant role in the construction of molecular receptors and metal ligands[1,2] . Notably, arylacetylide gold(I) units have interesting emissive properties deriving from the intraligand 3(ππ*) state owing to the introduction of spin-orbit coupling with the heavy metal. The emissive properties inherent in arylacetylide gold(I) units render them a potent choice for receptor functionalization. For example, to create multi-nuclear luminescent probes suitable for cation binding, the Yam's group utilized arylalkynyl gold(I) complexes to decorate calix[4]arene scaffolds[3,4,5]. In these receptors, the observed emission changes were also assigned to modulations of the existent Au(I)···Au(I) aurophilic interactions upon cation binding. By incorporating mono-nuclear arylacetylide gold(I) complexes into hydrogen-bonding donor functional groups, such as urea and amide, selective anion-binding chemosensors were obtained [6,7]. Calix[4]pyrroles are macrocyclic hosts with interesting binding properties for the recognition of anions, ion-pairs, and electron-rich substrates *via* hydrogen-bonding interactions[8,9,10]. However, examples of the incorporation of metal centers in the calix[4]pyrrole scaffold are scarce in the literature. Cafeo *et al.* reported the incorporation of a Pt(II) metal

[1] Herrera, R. P.; Gimeno, M. C., Main Avenues in Gold Coordination Chemistry. *Chem. Rev. (Washington, DC, U. S.)* **2021,** *121* , 8311-8363.

[2] Gil-Rubio, J.; Vicente, J., The Coordination and Supramolecular Chemistry of Gold Metalloligands. *Chem.--Eur. J.* **2018,** *24*, 32-46.

[3] Hau, F. K.-W.; Yam, V. W.-W., Synthesis and cation-binding studies of gold(i) complexes bearing oligoether isocyanide ligands with ester and amide as linkers. *Dalton Trans.* **2016,** *45* , 300-306.

[4] He, X.; Lam, W. H.; Zhu, N.; Yam, V. W.-W., Design and Synthesis of Calixarene-Based Bis-alkynyl-Bridged Dinuclear AuI Isonitrile Complexes as Luminescent Ion Probes by the Modulation of Au···Au Interactions. *Chem.--Eur. J.* **2009,** *15*, 8842-8851.

[5] Yam, V. W.-W.; Cheung, K.-L.; Yuan, L.-H.; Wong, K. M.-C.; Cheung, K.-K., Synthesis, structural characterization and binding studies of a novel dinuclear gold(I) calix[4]crown acetylide complex. *Chem. Commun.* **2000,** 1513-1514.

[6] Zhou, Y.-P.; Zhang, M.; Li, Y.-H.; Guan, Q.-R.; Wang, F.; Lin, Z.-J.; Lam, C.-K.; Feng, X.-L.; Chao, H.-Y., Mononuclear Gold(I) Acetylide Complexes with Urea Group: Synthesis, Characterization, Photophysics, and Anion Sensing Properties. *Inorg. Chem.* **2012,** *51*, 5099-5109.

[7] Shi, H.-Y.; Qi, J.; Zhao, Z.-Z.; Feng, W.-J.; Li, Y.-H.; Sun, L.; Lin, Z.-J.; Chao, H.-Y., Synthesis, characterization, photophysics, and anion binding properties of gold(I) acetylide complexes with amide groups. *New J. Chem.* **2014,** *38*, 6168-6175.

[8] Gale, P. A.; Sessler, J. L.; Král, V.; Lynch, V., Calix[4]pyrroles: Old Yet New Anion-Binding Agents. *J. Am. Chem. Soc.* **1996,** *118*, 5140-5141.

[9] Rather, I. A.; Wagay, S. A.; Hasnain, M. S.; Ali, R., New dimensions in calix[4]pyrrole: the land of opportunity in supramolecular chemistry. RSC Advances 2019, 9, 38309-38344.

[10] Kim, S. K.; Sessler, J. L., Calix[4]pyrrole-Based Ion Pair Receptors. *Acc. Chem. Res.* **2014,** *47*, 2525-2536.

center by trans-coordination with the amino group at the upper rim of the "mono wall" *meso*-p-aminophenyl-calix[4]pyrrole[11]. The authors demonstrated the cytotoxic activity of compounds by conducting in vitro studies on various cancer cell lines. They showed that the cytotoxic activity derived from the presence of both the calix[4]pyrrole element and the bound Pt(II) metal center. Recently, our group described the synthesis and characterization of the anion receptor **1Au** based on a mono-nuclear gold(I) acetylide complex containing a "two wall" calix[4]pyrrole as recognition element for anions[12]. The acetylide gold(I) complex was installed as a *para*-substituent of one of the *meso*-aryl groups of the "two-wall" aryl-extended calix[4]pyrrole **1Au**. 1,3,5-triaza-7-phosphaadamantane (PTA) was used as an ancillary ligand to stabilize the acetylide gold(I) complex. Compared to the 10α,20α-bis-*p*-ethynylaryl-calix[4]pyrrole parent compound **1** that did not show any emission properties, the mono-nuclear gold(I) derivative **1Au** displayed weak emission upon excitation at 300 nm. A five-fold decrease in the binding affinity of chloride was measured for the mono-nuclear gold(I) calix[4]pyrrole derivative **1Au** compared to its parent di-alkynyl compound **1** in dichloromethane solution. The observed difference was attributed to the repulsive chloride-π interactions between the bound anion and the *meso*-phenyl group decorated with para-acetylide gold(I). During the ^{1}H NMR titrations, two distinct sets of signals for the aromatic protons of the calix[4]pyrrole bound in the **Cl$^-$●1Au** complex were detected. One set of signals had a significantly lower intensity than the other. We hypothesized that receptor **1Au** coordinated the chloride by adopting cone and partial-cone conformations[13,14] (**Figure 1**). Unexpectedly, the two hypothesized isomers of the **Cl$^-$●1Au** complex underwent a chemical exchange process with slow dynamics on the chemical shift time scale.

[11] Cafeo, G.; Carbotti, G.; Cuzzola, A.; Fabbi, M.; Ferrini, S.; Kohnke, F. H.; Papanikolaou, G.; Plutino, M. R.; Rosano, C.; White, A. J. P., Drug Delivery with a Calixpyrrole–trans-Pt(II) Complex. *J. Am. Chem. Soc.* **2013,** *135*, 2544-2551.

[12] Sun, Q.; Aragay, G.; Pinto, A.; Aguiló, E.; Rodríguez, L.; Ballester, P., Influence of the Attachment of a Gold(I) Phosphine Moiety at the Upper Rim of a Calix[4]pyrrole on the Binding of Tetraalkylammonium Chloride Salts. *Chem.--Eur. J.* **2020,** *26*, 3348-3357.

[13] Wu, Y.-D.; Wang, D.-F.; Sessler, J. L., Conformational Features and Anion-Binding Properties of Calix[4]pyrrole: A Theoretical Study. *J. Org. Chem.* **2001,** *66*, 3739-3746.

[14] Blas, J. R.; López-Bes, J. M.; Márquez, M.; Sessler, J. L.; Luque, F. J.; Orozco, M., Exploring the Dynamics of Calix[4]pyrrole: Effect of Solvent and Fluorine Substitution. *Chem.--Eur. J.* **2007,** *13*, 1108-1116.

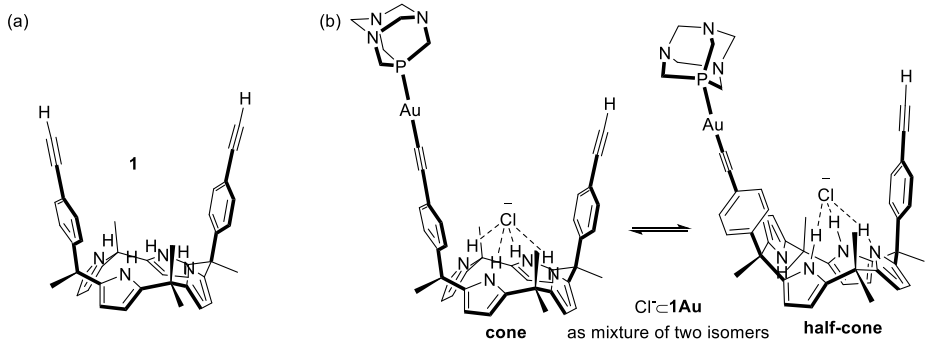

Figure 1: *(a) Line-drawing structure of the bis-alkynyl calix[4]pyrrole **1**; (b) equilibrium between the two putative conformers of the 1:1 complexes of the mono-nuclear calix[4]pyrrole receptor **1Au** with chloride, Cl^-⊂**1Au**, hypothesized in our previous work[12].*

In this thesis chapter, we describe the synthesis and characterization of a mono-nuclear gold(I) calix[4]pyrrole receptor **2Au** (***Scheme 1***), analogue to **1Au**. We also aim to study the binding properties of **2Au** and its synthetic precursor **2**. Moreover, the present study was conducted to assess the validity of the aforementioned observations in a more generalized context. We aim to confirm that the low-intensity proton signals observed during the titration of **1Au** with TBACl were not due to the formation of a new species induced by the excessive addition of the salt. We briefly describe the increase of antitumoral activity of the arylacetylide phosphine gold(I) units when incorporated into a calix[4]pyrrole scaffold. We also report and discuss the results of the ^{1}H NMR titration experiments of receptor **2Au** and its synthetic precursors, **2** and **3**, with TBACl in dichloromethane and acetone solution. We perform ITC experiments and pair-wise competitive experiments for the accurate thermodynamic characterization of the 1:1 chloride complexes formed in acetone solution. We measured a decrease in the binding stability of the 1:1 complex of **2Au** with chloride compared to the parent *meso*-10α,20α-*p*-ethynylphenyl-*p*-iodophenyl receptor **2**, and the C_{2v} symmetrical *p*-iodophenyl precursor **3**. We performed DFT calculations and computed the ESP values at the center of the aromatic ring and at the *para*-substituent to support the trend in binding affinities experimentally measured.

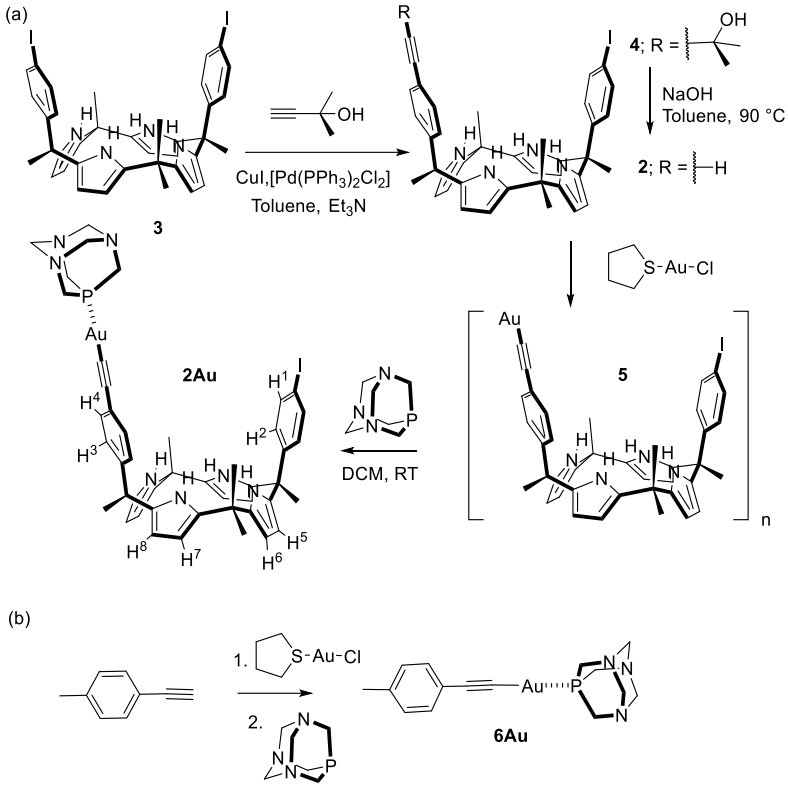

Scheme 1: *Synthetic schemes for the preparation of (**a**) the calix[4]pyrrole mono-nuclear gold(I) acetylide complex **2Au** and (**b**) the reference mono-nuclear gold(I) acetylide **6Au.***

In analogy to the observations previously made for **1Au**[12], the titrations of **2Au** with incremental amounts of TBACl, either in dichloromethane-d_2 or acetone-d_6 solutions, produced the appearance of two separate sets of aromatic signals for the bound receptor. Previously, we ascribed the two sets of signals to existence of the "bound" receptor as a mixture of two conformers (**Figure 1**b). We use the reference compound **6Au**, lacking the calix[4]pyrrole unit, to evidence the lability of the acetylide-Au(I)-PTA unit in the presence of chloride.

2.2 Results and Discussion

2.2.1 Synthesis

The mono-nuclear acetylide gold(I) complex **2Au** possesses a para-iodo substituent in the non-metalated *meso*-phenyl instead of the para-ethynyl present in **1Au**. This alteration in structure was expected to enhance the stability of **2Au** and simplify its

synthesis. Compound **2Au** contains an α,α-"two wall" calix[4]pyrrole binding site and is prepared in four synthetic steps from the well-known *meso*-hexamethyl-10α,20α-bis-p-iodophenyl-calix[4]pyrrole **3**[15] (***Scheme 1***a). Firstly, following described synthetic methodology [15,16], the statistical Sonogashira reaction of the C2v symmetric bis-iodo 3 with 2-methyl-3-butyn-2-ol (5 equiv.), at r.t in dry toluene and triethylamine amine as base, allowed the isolation of the unprecedented mono-substituted iodo-ethynyl protected calix[4]pyrrole **4**. Compound **4** was obtained in 33 % yield after column chromatography purification of the reaction crude. Next, the treatment of **4** with sodium hydroxide in toluene at 90 °C for 12 h yielded the mono-iodo-mono-ethynyl calix[4]pyrrole **2** in 70% yield following a simple reaction work-up[15,16]. We treated mono-iodo-mono-ethynyl **2** with freshly prepared chloro(tetrahydrothiophene)gold(I)[17], **(tht)AuCl**, to obtain the corresponding oligomeric gold(I) acetylide **5**, probably having both σ and π bonds to the alkynyl group. Compound **5** was used immediately and without further purification. Finally, **5** was reacted with 1,3,5-triaza-7-phosphaadamantane (**PTA**)[18] to yield the mono-nuclear gold(I) complex **2Au** in 40% yield, through the replacement of the gold–alkyne bonds with the stronger phosphine donor[19]. All compounds, except **5**, were fully characterized by a complete set of high-resolution spectra (see SI). By applying the synthetic methodology employed to convert **2** into **2Au**, we synthesized the mono-nuclear gold(I) acetylide complex **6Au** using *p*-ethynyl-toluene as starting material. (***Scheme 1***b). **6Au** was used as a reference compound to investigate the stability of the phenyl-ethynyl- Au(I)●PTA unit of **2Au** upon incremental additions of **TBACl**.

---

[15] Valderrey, V.; Escudero-Adán, E. C.; Ballester, P., Polyatomic Anion Assistance in the Assembly of [2]Pseudorotaxanes. *J. Am. Chem. Soc.* **2012,** *134*, 10733-10736.

[16] Valderrey, V.; Escudero-Adán, E. C.; Ballester, P., Highly Cooperative Binding of Ion-Pair Dimers and Ion Quartets by a Bis(calix[4]pyrrole) Macrotricyclic Receptor. *Angew. Chem., Int. Ed.* **2013,** *52*, 6898-6902.

[17] Kemper, B.; Hristova, Y. R.; Tacke, S.; Stegemann, L.; van Bezouwen, L. S.; Stuart, M. C. A.; Klingauf, J.; Strassert, C. A.; Besenius, P., Facile synthesis of a peptidic Au(I)-metalloamphiphile and its self-assembly into luminescent micelles in water. *Chem. Commun.* **2015,** *51*, 5253-5256.

[18] Aguiló, E.; Gavara, R.; Baucells, C.; Guitart, M.; Lima, J. C.; Llorca, J.; Rodríguez, L., Tuning supramolecular aurophilic structures: the effect of counterion, positive charge and solvent. *Dalton Trans.* **2016,** *45*, 7328-7339.

[19] McArdle, C. P.; Van, S.; Jennings, M. C.; Puddephatt, R. J., Gold(I) Macrocycles and Topologically Chiral [2]Catenanes. *J. Am. Chem. Soc.* **2002,** *124*, 3959-3965.

2.2.2 Binding Studies

Dichloromethane

The interaction of the mono-nuclear calix[4]pyrrole **2Au** with chloride in dichloromethane-d_2 solution was probed using 1H NMR spectroscopy and tetrabutylammonium chloride (TBACl) as the chloride precursor. The ^{1}H NMR spectrum of **2Au** exhibited features consistent with C_s symmetry: four doublets for its aromatic protons ($H_{1\text{-}4}$), four overlapping double doublets for the β-pyrrole ($H_{5\text{-}8}$) protons and four singlets for its methyl groups. The two pairs of diastereotopic pyrrole NHs resonated as a broad singlet centered at δ = 7.3 ppm (**Figure 2a**).

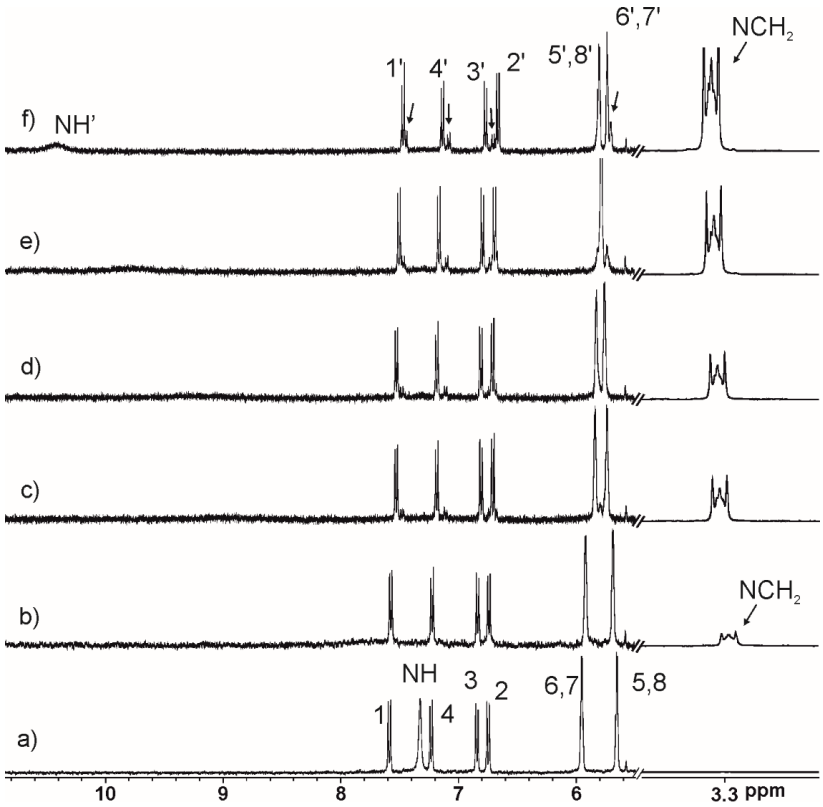

***Figure 2**: Selected downfield and upfield regions (aromatic and TBA regions, respectively) of the ^{1}H NMR spectra (400 MHz, CD_2Cl_2, 298 K) acquired during the titration of the mono-nuclear **2Au** calix[4]pyrrole receptor ([**2Au**] = 1.9 mM) with TBACl: (**a**) 0 (**b**) 1 (**c**) 4.5 (**d**) 10.5 (**e**) 21 and (**f**) 27 equiv. added. See Scheme 1a for proton assignment. The scale of the aromatic region is increased 16 times with respect to the upfield TBA region in order to show the presence of the second set of aromatic proton signals.*

Chloride Binding Properties of a Macrocyclic Receptor Equipped with an Acetylide Gold(I) Complex

The addition of incremental amount of TBACl to the 1.9 mM solution of **2Au** produced noticeable changes in the chemical shift of most proton signals of the mono-nuclear receptor. In particular, all aromatic doublets shifted upfield, supporting the existence of chloride–π interactions[20]. The doublets of the β-pyrrole protons moved in opposite direction in response to the conformational change experienced by the receptor. That is, from alternate in the free state to cone in the bound counterpart. In the presence of ~20 equiv. of TBACl, the pyrrole NHs were visible in the downfield region of the spectrum as a broadened signal centered at δ = 9.7 ppm. This signal shifted even further downfield as the concentration of the salt was increased from 20 to 27 equiv. (**Figure 2**e and f). The downfield shifts experienced by the NH protons indicated their involvement in hydrogen bonding interactions with the bound chloride. In fact, it is well known, that "two wall" calix[4]pyrroles bind the chloride anion by establishing four convergent hydrogen bonds with the pyrrole NHs[20]. Notably, in the initial phase of the titration, the multiplet assigned to the methylene protons alpha to the nitrogen atom of the TBA^+ cation (**Figure 2**, aliphatic region) appeared upfield shifted with respect to the same protons in the free TBACl salt. However, as the concentration of the TBACl increased the triplet moved downfield towards the chemical shift value of free TBACl. Ion-pairs such as TBACl are not significantly dissociated in chlorinated non-polar solvents such as dichloromethane-d_2. Likewise, the interaction of TBACl with the mono-nuclear calix[4]pyrrole **2Au** is expected to produce an ion-paired complex. The initial upfield shifts observed for the TBA^+ alpha methylene protons, located the TBA^+ cation of the 1:1:1 ion-paired complex, Cl^-●**2Au**●TBA^+, in the shallow and electron rich cavity defined by the pyrrole rings of the receptor's cone conformation. This cavity is opposite to the binding site of the chloride resulting in a receptor separated binding geometry for the ion paired complex, Cl^-●**2Au**●TBA^+ [10,21,22]. During the titration, the overall concentration of TBACl is increased favoring the relative amount of free salt. Because the TBA^+ cation of the free salt is involved in a chemical exchange equilibrium with the bound counterpart displaying fast dynamics on the chemical

[20] Adriaenssens, L.; Gil-Ramírez, G.; Frontera, A.; Quiñonero, D.; Escudero-Adán, E. C.; Ballester, P., Thermodynamic Characterization of Halide–π Interactions in Solution Using "Two-Wall" Aryl Extended Calix[4]pyrroles as Model System. *J. Am. Chem. Soc.* **2014,** *136*, 3208-3218.

[21] Kim, S. K.; Sessler, J. L., Ion pair receptors. *Chem. Soc. Rev.* **2010,** *39*, 3784-3809.

[22] Ciardi, M.; Tancini, F.; Gil-Ramírez, G.; Escudero Adán, E. C.; Massera, C.; Dalcanale, E.; Ballester, P., Switching from Separated to Contact Ion-Pair Binding Modes with Diastereomeric Calix[4]pyrrole Bis-phosphonate Receptors. *J. Am. Chem. Soc.* **2012,** *134*, 13121-13132.

shift timescale, the increase of the relative concentration of the free TBACl provokes that the alpha methylene proton signal move downfield, approaching the chemical shift value of the free salt. We performed analogous titrations of the synthetic precursors of the mono-nuclear calix[4]pyrrole **2Au**, bis-iodo **3** and the mono-iodo-mono-ethynyl parent **2**, obtaining very similar results. The most relevant difference between the three titrations was the appearance of a second set of aromatic signals in the case of **2Au**. This second set of signals had a reduced intensity and was initially detected when 4.5 equiv. of TBACl were added. The two sets of aromatic signals moved upfield as the concentration of TBACl was increased. The intensity of the second set of signals was also slightly increased upon the incremental addition of TBACl. The chemical shift changes experienced by selected proton signals[23] of the calix[4]pyrroles **2Au**, **2,** and **3,** and the TBA^+ cation during the titrations were mathematically analyzed (non-linear regression) using the HypNMR2008[24,25] software version 4.0.66, Leeds, England, UK and a 1:1 binding theoretical model. The fit of the data was good (sigma < 2.8), supporting the formation of the 1:1:1 ion-paired ternary complex. The determined apparent binding constants are summarized in **Table 1**.

[23] The second set of proton signal showing a reduced intensity were not considered for the fit.

[24] Frassineti, C.; Ghelli, S.; Gans, P.; Sabatini, A.; Moruzzi, M. S.; Vacca, A., Nuclear Magnetic Resonance as a Tool for Determining Protonation Constants of Natural Polyprotic Bases in Solution. *Anal. Biochem.* **1995,** *231*, 374-382.

[25] Frassineti, C.; Alderighi, L.; Gans, P.; Sabatini, A.; Vacca, A.; Ghelli, S., Determination of protonation constants of some fluorinated polyamines by means of 13C NMR data processed by the new computer program HypNMR2000. Protonation sequence in polyamines. *Anal. Bioanal. Chem.* **2003,** *376*, 1041-1052.

Chloride Binding Properties of a Macrocyclic Receptor Equipped with an Acetylide Gold(I) Complex

Table 1: *Apparent binding constants (K_a, M^{-1}) of the ion-paired complexes of receptors **2**, **3**, and **2Au** with TBACl in dichloromethane. The value of the binding constants ratio using K(TBA●**3**●Cl^-) as reference and the corresponding **ΔΔG** are also listed. ESP values at the center of the phenyl ring and at the para-substituent (ESP_1; ESP_2) are also indicated.*

Receptor	$K_a \times 10^{-2}$ CD_2Cl_2 [a]	K(TBA●3●Cl^-) /K(TBA●n●Cl^-)	**ΔΔG** kcal/mol	**ESP (Ar;Subst)** kcal/mol [b]
Bis-iodo **3**	2.54 ± 0.1	1	0	−13.1; −13.7
Mono-iodo-mono-ethynyl **2**	1.11 ± 0.02	2.28 ± 0.10	0.49 ± 0.03	−14.8; −18.7
Mono-nuclear **2Au**	0.76 ± 0.1	3.3 ± 0.14	0.71 ± 0.03	−30.3; −41.1

[a] The titration experiments were performed in dichloromethane-d_2 solution at 298 K and monitored using ^{1}H NMR spectroscopy. The titration data were fit to a 1:1 theoretical binding model. [b] The reported ESP values correspond to the center of the phenyl group and the center of the *para*-substituent, respectively, in the used model systems (see text for details).

From the data listed in **Table 1**, we draw the following conclusions: (a) the substitution of one *p*-iodo substituent by one *p*-gold(I)acetylide in the scaffold of a "two wall" calix[4]pyrrole receptor (i.e., **3** vs. **2Au**) produced a drop in binding energy for TBACl of 0.71 kcal/mol; (b) the drop in binding affinity can be dissected into 0.49 Kcal/mol produced by the substitution of the iodo group by the ethynyl counterpart (i.e., **3** vs. **2**) and the 0.22 Kcal/mol caused by the incorporation of a gold(I) phosphine moiety (i.e., **2** vs. **2Au**). Notably, these structural modifications are associated with changes in the electron surface potential (ESP) values of the *meso*-substituent. We used *p*-iodotoluene, *p*-ethynyltoluene and *p*-gold(I)acetylidetoluene as model systems of the *meso*-phenyl substituent in **3**, **2** and **2Au**, respectively, to compute the ESP values at the center of the phenyl ring and at the *para*-substituent (ESP_1; ESP_2). Although the larger change in ESP values was caused by the introduction of the gold(I) phosphine moiety, **2** (−14.8; −18.7) *vs.* **2Au** (−30.3; −41.1), it did not translate into the most significant component of the dissected reduction of binding affinity (only 0.22 Kcal/mol of the total 0.71 Kcal/mol). Conversely, the substitution of the *p*-iodo substituent by the *p*-ethynyl counterpart having a reduced impact on ESP values (−13.1; −13.7 Kcal/mol for **3** vs. −14.8; −18.7 Kcal/mol for **2**) contributed more significantly to the energy difference

of the corresponding chloride complexes (0.49 Kcal/mol). These results suggested that the increase in electrostatic repulsive chloride-π interactions caused by changing the *para*-substituent of one of the "walls" in calix[4]pyrrole complexes is not enough to explain the differences in measured binding affinities between the complexes. We concluded that solvation/desolvation processes are also important in accounting for these differences.

Acetone

Aiming at studying the differences in chloride binding energies for the series of "two wall" calix[4]pyrroles in a more polar solvent, we switched to acetone. In our previous study with the mono-nuclear **1Au**, we observed two sets of aromatic proton signals in the ^{1}H NMR spectra of the titration with TBACl in acetone-d_6 solution which were attributed to a mixture of two conformers in solution. Because acetone is polar in nature, ion-pair salts dissociate significantly. The TBA^+ cation is well-solvated by acetone molecules. In contrast, the reduced solvation of the chloride anions results in larger binding constants for the anionic calix[4]pyrrole complexes formed in acetone compared to dichloromethane. We monitored the interaction of receptor **2Au** with chloride using ^{1}H NMR spectroscopy and TBACl as anion precursor. The ^{1}H NMR spectra acquired during the titration of **2Au** with incremental amounts of TBACl in acetone-d_6 solution are depicted in **Figure 3**.

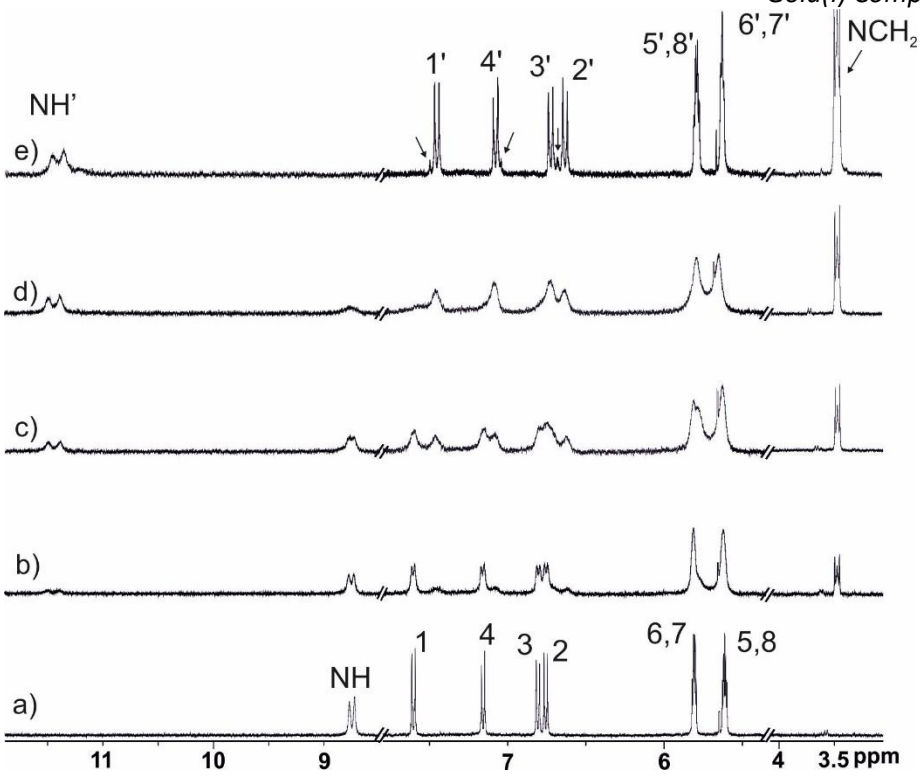

Figure 3: *Selected regions of the ^{1}H NMR spectra (400 MHz, acetone-d_6, 298 K) acquired during the titration of receptor* ***2Au*** *(2.2 mM) with incremental amounts of TBACl: (**a**) 0 (**b**) 0.25 (**c**) 0.5 (**d**) 0.75 and (**e**) 1.2 equiv. Black arrows indicate the presence of a second set of proton signals.*

The incremental addition of TBACl produced the observation of two separate sets of broadened signals for the protons of **2Au**. This result is in contrast with the steady downfield/upfield shifts observed in dicloromethane-d_2. The observation of separate proton signals for the free and bound **2Au** indicated that the chemical exchange of the binding process displayed slow kinetics on the chemical shift timescale. The doublet emerging at δ = 11.4 ppm was assigned to the hydrogen-bonded pyrrole NHs in the Cl^-●**2Au** complex. All proton signals of bound **2Au** became sharp and well-defined in the presence of 1 equiv. of TBACl and did not experience changes when more salt was added. This result served to estimate the binding constant of the Cl^-●**2Au** complex as larger than 10^4 M^{-1}. Throughout the titration, the signal of the methylene protons *alpha* to the nitrogen atom of the TBA^+ cation did not experience chemical shift changes. This behavior supported the non-involvement of the TBA^+ cation in the formation of the complex of chloride with **2Au** in this solvent, which as mentioned above existed mainly as anionic Cl^-●**2Au** species.

We also performed ^{1}H NMR titrations of **2** and **3** in acetone-d_6 with TBACl obtaining identical results. As mentioned above for the titrations in dichloromethane-d_2, only in the titration of **2Au** with TBACl in acetone-d_6 solution we observed two sets of signals with different intensity for the aromatic protons of the bound calix[4]pyrrole unit. Taken together, the obtained results showed that the used solvent impacted on the kinetics of the binding equilibrium of the calix[4]pyrroles with TBACl (fast in dichloromethane-d_2 and slow in acetone-d_6). However, in both solvents, the excess of TBACl produced the observation of two separate sets of signals for the aromatic protons of the calix[4]pyrrole. We raised some doubts on our previous assignment of the two sets of separate signals to the conformational isomers of the bound calix[4]pyrrole, cone and half-cone, in the ion-paired Cl^-●**2Au**●TBA and anionic Cl^-●**2Au** complexes[12] (**Figure 1**b). To address the issue at hand, we decided to investigate the effect caused by the addition of TBACl to an acetone solution of the model compound **6Au**. This compound lacking the calix[4]pyrrole unit was investigated as reference for the lability of the phenyl-ethynyl-Au(I)●PTA unit of **2Au** in the presence of chloride.

2.2.3 ^{1}H NMR spectroscopy analysis of the addition of incremental amounts of TBACl to an acetone solution of 6Au

The ^{1}H NMR spectrum of a 5 mM solution of **6Au** shows sharp and well-defined proton signals (**Figure 4**a). The addition of 2 equiv. of TBACl provoked the appearance of a new set of signals for the aromatic protons and the methyl group (**Figure 4**b). The protons of the PTA ligand did not split, however, they experienced chemical shift changes. Remarkably, the intensity of the new set of signals grew over time while those of **6Au** decreased correspondingly (**Figure 4**c). After several hours, the intensity changes reached a plateau. At this point, we added two additional equivalents of TBACl. The ^{1}H NMR spectrum of the mixture acquired immediately after the addition of the salt revealed that the new proton signals were the most intense ones (**Figure 4**d). At this point, the intensity increase of the new signals over time was not substantial. Nevertheless, incremental additions of TBACl caused further increases in their intensity. It is worthy to note that we also observed the formation of a precipitate following each addition of TBACl. In the presence of 10 equiv. of TBACl and after several hours, the proton signals of the new species were almost exclusively observed in the ^{1}H NMR spectrum of the mixture (**Figure 4**e).

Taken together, these observations indicated that **6Au** reacted with TBACl to produce other species of unknown structure. We searched for prior examples of this transformation in the literature and discovered a report by Abu-Salah[26] describing the transformation of Ph_3P●Au(I)ethynyl-toluene into the corresponding anionic bis-(alkynyl)gold(I)complex and Ph_3P●Au(I)-I by addition of TBAI in acetone solution at r.t. Likewise, in the case at hand, the anionic bis-alkynyl-gold(I) complex [**7Au**]$^-$ should be obtained from **6Au** by treatment with TBACl (**Scheme 2**). In any case, this is not the most common synthetic methodology used for the preparation of anionic bis-(alkynyl)gold(I) complexes. Using other synthetic methodologies, [**7Au**]$^-$ and other bis-(alkynyl)gold(I) anionic complexes have already been reported in literature[27,28,29]. We compared the ^{1}H and ^{13}C NMR spectroscopic features of the new species in the reaction mixture of **6Au** with excess TBACl with those reported for compound [**7Au**]$^-$. Based on the agreement of spectroscopic data, we concluded that the new species was indeed the anionic bis-(alkynyl)gold(I) complex [**7Au**]$^-$. The ESI—MS spectrum of the solution showed an ion peak at m/z 427 with 10% relative intensity corresponding to [**7Au**]$^-$ (SI). The precipitate was also isolated and analyzed using ^{1}H and ^{31}P NMR spectroscopy. We observed the diagnostic signals for PTA●Au(I)-Cl in the acquired NMR spectra. Finally, we performed a DOSY experiment of the acetone solution containing a mixture of **6Au**, [**7Au**]$^-$, free PTA and partially solubilized PTA●Au(I)-Cl. As expected, the diffusion constant assigned to the signals related to [**7Au**]$^-$ was smaller than that of any other species in solution. Moreover, the signals of the PTA ligand showed a larger diffusion constant suggesting that it was involved in other species with reduced hydrodynamic radii compared to [**7Au**]$^-$ (i.e. free PTA and PTA●Au(I)-Cl) (See SI). Based on the results obtained for the alkynyl gold(I) model compound **6Au** in the presence of chloride, we assigned the set of proton signals of low intensity observed in the ^{1}H NMR titrations of **2Au** with TBACl to the corresponding bis(alkynyl)gold(I)anionic dimer [**8Au**]$^-$ (**Scheme 2**). The calix[4]pyrrole anionic dimer was formed to a reduced extent

[26] Abu-salah, O. M., A novel method for the preparation of two bis(arylethynyl)-aurate(I) complex anions. *J. Chem. Res., Synop.* **1984**, 187.

[27] Vicente, J.; Chicote, M.-T.; Alvarez-Falcon, M. M.; Jones, P. G., Gold(I) Complexes Derived from C6Me3(C⁝CH)3-1,3,5, C6Me4(C⁝CH)2-1,4, and MeC6H4C⁝CH-4. *Organometallics* **2005,** *24*, 5956-5963.

[28] Liu, Q.; Xie, M.; Chang, X.; Cao, S.; Zou, C.; Fu, W.-F.; Che, C.-M.; Chen, Y.; Lu, W., Tunable Multicolor Phosphorescence of Crystalline Polymeric Complex Salts with Metallophilic Backbones. *Angew. Chem., Int. Ed.* **2018,** *57*, 6279-6283.

[29] Abu-Salah, O. M.; Al-Ohaly, A. R. A.; Al-Showiman, S. S.; Al-Najjar, I. M., A13C nuclear magnetic resonance study of some linear alkynyl gold(I) and silver(I) complexes. *Transition Met. Chem.* (London) **1985**, *10*, 207-210.

during the titration experiments because the amount of free chloride in solution was small. In fact, only when an excess of chloride was present in solution (> 4.5 equiv. in dichloromethane-d_2 and > 1.2 equiv. in acetone-d_6) we detected the signals of the anionic complex [**8Au**]$^-$.

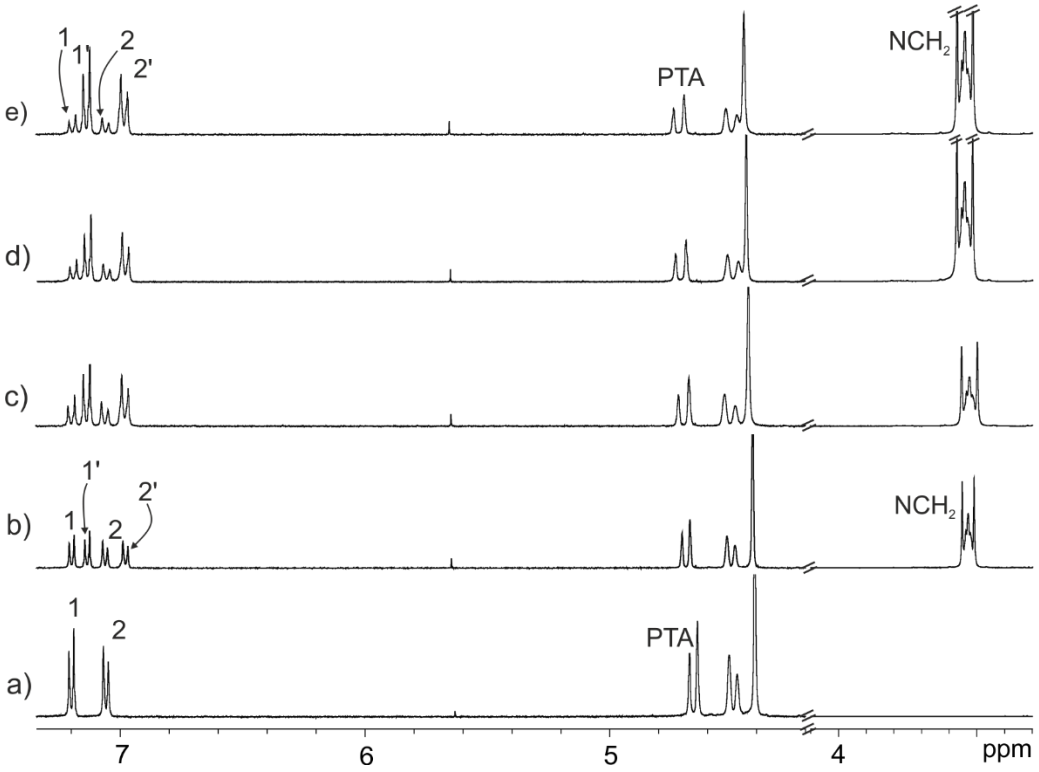

Figure 4:*Selected regions of the ^{1}H NMR spectra (400 MHz, acetone-d_6, 298 K) acquired during the titration of the model compound* ***6Au*** *(5 mM) (a) with incremental amounts of TBACl: (b) 2 equiv. of TBACl after 10 min; c) 1.30 h and 2 equiv. of TBACl; d) 4h and 4 equiv. of* ***2a*** *and e) 13 h and 4 equiv. of TBACl. See top panel for proton assignment.*

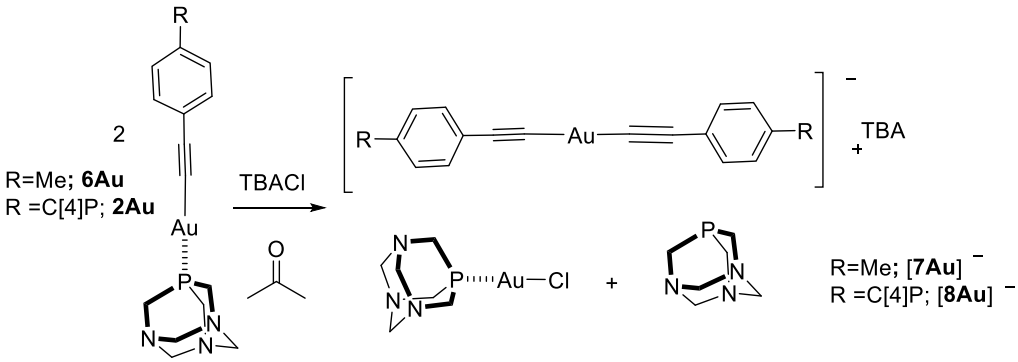

***Scheme 2**: Synthetic scheme for the formation of the anionic-bis(alkynyl)gold(I) complexes [**7Au**]$^-$ and [**8Au**]$^-$.*

We also performed a DOSY experiment to a mixture of **2Au** containing a large excess of TBACl (i.e. 9 equiv.). The pseudo 2D plot of the DOSY (Figure S47) revealed that the two sets of signals related to the calix[4]pyrrole scaffold displayed different diffusion constants. The less intense set of signals, attributed to the chloride complex of the [**8Au**]$^-$ dimer, displayed a smaller diffusion coefficient ($D = 1.1 \times 10^{-9}$ $m^2 \cdot s^{-1}$) compared to the one assigned to the set of signals of the 1:1 anionic Cl^-●**2Au** complex ($D = 1.6 \times 10^{-9}$ $m^2 \cdot s^{-1}$). This result agrees with the larger size of the chloride complex of the [**8Au**]$^-$ dimer compared to that of the Cl^-●**2Au** counterpart. The proton signals of the PTA ligand displayed a diffusion coefficient constant that did not coincide with any of the previous ones. Most likely, the PTA is experiencing a chemical exchange that is fast on the DOSY time scale between different species present in solution (**2Au**, Cl^-●**2Au**, PTA and PTA●Au(I)-Cl).

2.3 Isothermal titration calorimetry (ITC) experiments

We deemed it necessary to employ isothermal titration calorimetry (ITC) experiments to accurately determine the large binding constants of receptor **2Au** and its synthetic precursors **2** and **3** with chloride in acetone solution. During these experiments, the concentration of free chloride in solution at the end of the titration is nearly 1 equivalent. For this reason, we expected that in the ITC experiments of **2Au**, the anionic dimer [**8Au**]$^-$ would be formed to reduced extent. The computer-controlled injection of incremental amounts of TBACl, dissolved in acetone, to a solution of **2Au** in the same solvent 7-10 fold more diluted and placed in the

calorimeter's cell produced the release of heat peaks. The binding isotherm obtained from the plot of the normalized integration of the heat peaks had the shape of a single sigmoidal curve with an inflexion point at a molar ratio [TBACl]/[**2Au**] close to 1. This is the expected result for the formation of a 1:1 complex. The titration data beautifully fit the one set of sites model implemented in the Microcal ITC Data Analysis software. The fitting procedure returned the values of the binding constant and the enthalpy of binding of the Cl^-●**2Au** complex. We performed similar ITC experiments with receptors **2** and **3**. The determined thermodynamic constants (K_{app}, ΔH and $T\Delta S$) are summarized in Table 2. We refer to the binding constants as apparent owing to the simplification of the used binding model, which neither considers the association/dissociation of the ion-pairs (i.e. TBACl and TBACl●**2Au**) nor the contribution to the measured heat of the reaction yielding [**8Au**]$^-$ and its putative binding to chloride. Notably, all binding processes are enthalpy and entropy favored. The large and favorable entropy term supports that solvation/desolvation processes are highly relevant in all binding processes. Surprisingly to us, the values of the free energy differences between the chloride complexes of **2Au** and the calix[4]pyrrole receptors used as synthetic precursors, **2** and **3**, calculated in acetone are in reasonable agreement with those determined in dichloro-methane solution for the ion-paired counterparts.

Table 2. Apparent binding constants (K_a, M^{-1}) and thermodynamic constants (Kcal mol^{-1}) of the binding equilibria of receptors **3**, **2**, and **2Au** with TBACl salt in acetone solution at 288 K determined by ITC experiments. The value of the binding constants ratio using K(TBA●**3**●Cl^-) as reference and the corresponding ΔG and ΔΔG are also listed.

	$K_a \times 10^{-4}$ (M^{-1}) $(CH_3)_2CO$[a]	ΔH	-TΔS	K(3●Cl^-) /K(n●Cl^-)	ΔG	ΔΔG
Bis-iodo **3**	15.1±0.1	3.70±0.04	3.13±0.04	1.0	6.83±0.01	0.0
Mono-iodo-mono-ethynyl **2**	9.2±0.6	3.29±0.08	3.25±0.09	1.6±0.1	6.54±0.04	0.29±0.04
Mono-nuclear **2Au**	5.5±0.1	2.83±0.01	3.43±0.01	2.7±0.1	6.25±0.01	0.58±0.01

[a] The titration data were fit to a 1:1 theoretical binding model

2.4 Competitive pair-wise binding experiments

Due to the side reaction induced by the excessive addition of TBACl to **2Au** and the similarity of the binding constant values of chloride and the receptor series (**2Au**, **2** and **3**) obtained *via* ITC experiments, we opted to conduct NMR pair-wise competitive binding assays. The results of these experiments are expected to produce a better assessment of the ratios of the binding constant values. Moreover, in these experiments the TBACl is used in a sub-stoichiometric amount with respect to the competing calix[4]pyrroles (i.e. 1:2 molar ratio). Under these conditions, the concentration of unbound chloride in solution was kept to a minimum during the experiment, preventing the conversion of **2Au** into the bis(alkynyl)gold(I) anionic dimer [**8Au**]$^-$.

We analyzed different acetone-d_6 solutions containing an equimolar mixture of two receptors and the TBACl salt using ^{1}H NMR spectroscopy. At 213 K, the chemical exchange between the free and bound receptors was slow on the chemical shift timescale. This permitted the observation of separate proton signals for the free and bound receptors, especially in the aromatic region of the ^{1}H NMR spectra. In this region we observed multiple sets of doublets. Moreover, some of the doublets assigned to different species were overlapped. Nevertheless, the careful and detailed analyses of the ^{1}H NMR spectra allowed the quantification of the concentrations of the different species involved in the equilibria. We used the integral values to determine relative concentrations and derive the ratio of the complexes' binding constants (see SI). We calculated two binding constant ratios by performing direct pairwise competitive experiments: ***K***(**3**●Cl$^-$)/***K***(**2**●Cl$^-$) and ***K***(**2Au**●Cl$^-$)/***K***(**2**●Cl$^-$). The obtained values were used to derive the ***K***(**3**●Cl$^-$)/ *K*(**2Au**●Cl$^-$) binding constant ratio without having to experimentally perform the direct pairwise competitive experiment which was expected to be complex due to extensive signal overlapping.

Table 3

	K(3●Cl-)/***K***(n●Cl-)[a]	***K***(3●Cl-)/***K***(n●Cl-)[b]
Bis-iodo **3**	1.00	1.00
Mono-iodo-mono-ethynyl **2**	1.6±0.1	1.4
Mono-nuclear **2Au**	2.7±0.1	3.8

presents the ratios of binding constant values calculated using the bis-iodo receptor **3** as a reference and compares them with those obtained from the ITC experiments. The agreement between them was very good for ***K*(3●Cl$^-$)/*K*(2●Cl$^-$)** but the ***K*(3●Cl$^-$)/*K*(2Au●Cl$^-$)** ratio determined by ITC and pair-wise competitive experiments was slightly different. This suggested that the effect caused by the reaction of **2Au→[8Au]$^-$** during the determination of the binding constants using ITC experiments is not completely negligible. In any case, the obtained results supported previous findings. In dichloromethane and acetone solution, the substitution of one iodo group at the upper rim of "two wall" calix[4]pyrrole **3** by an ethynyl-gold(I)PTA unit in **2Au** produced a destabilizing effect of the 1:1 complex with chloride that can be quantified in 0.6-0.7 kcal/mol. The existence of stronger repulsive chloride-π interactions in the **2Au●**Cl$^-$ compared to the **2●**Cl$^-$ counterparts is supported by ESP calculations. However, the observed drop in binding energy cannot be exclusively ascribed to electrostatic factors. This is because the comparison of the binding energies of complexes **3●**Cl$^-$ (R=R'=I) and **2●**Cl$^-$ (R=I; R= ethynyl) assigned an energetic advantage around - 0.4 kcal/mol to the former (∼-0.5 kcal/mol in dichloromethane-d_2 and ∼-0.3 kcal/mol in acetone-d_6). In this case, however, the change in ESP value produced by the modification of the upper rim substituent is small. Here, we are forced to consider solvation effects as the main responsible for the differences observed in binding. We already noticed important solvation/desolvation effects in the anion binding of other "two wall" aryl-extended calix[4]pyrrole in polar solvents reflecting that the entropic term was mainly responsible for the measured free energy differences[20].

Table 3. Values of the binding constants' ratios determined using the results of ITC experiments and pairwise-competitive binding experiments.

	***K*(3●Cl$^-$)/*K*(n●Cl$^-$)[a]**	***K*(3●Cl$^-$)/*K*(n●Cl$^-$)[b]**
Bis-iodo **3**	1.00	1.00
Mono-iodo-mono-ethynyl **2**	1.6±0.1	1.4
Mono-nuclear **2Au**	2.7±0.1	3.8

[a] ITC experiments. [b] Pair-wise competitive experiments.

2.5 Theoretical Calculations

In order to gain some insights on the structures of the chloride complexes formed by the "two wall" calix[4]pyrrole receptors, as well as its electronic binding energies, we decided to undertake DFT calculations. Calculations, including geometry optimization, were performed in the gas phase using Turbomole[30,31] , at the RI[32,33,34]-BP86[35] -D3BJ[36,37]-def2-TZVP[38] (C, H, N, P, O, Au)(def2-ECP(Au)) level of theory. We derived theoretical binding energies based on a 1:1 binding equilibrium (Figure 5).

[30] TURBOMOLE V7.0 2015, a development of University of Karlsruhe and Forschungszentrum Karlsruhe GmbH, 1989-2007, TURBOMOLE GmbH, since 2007; available from http://www.turbomole.com.

[31] Ahlrichs, R.; Bär, M.; Häser, M.; Horn, H.; Kölmel, C., Electronic structure calculations on workstation computers: The program system turbomole. *Chem. Phys. Lett.* **1989,** *162*, 165-169.

[32] Eichkorn, K.; Treutler, O.; Ohm, H.; Haser, M.; Ahlrichs, R., AUXILIARY BASIS-SETS TO APPROXIMATE COULOMB POTENTIALS (VOL 240, PG 283, 1995). *Chem. Phys. Lett.* **1995,** *242*, 652-660.

[33] Eichkorn, K.; Weigend, F.; Treutler, O.; Ahlrichs, R., Auxiliary basis sets for main row atoms and transition metals and their use to approximate Coulomb potentials. *Theor. Chem. Acc.* **1997,** *97*, 119-124.

[34] Sierka, M.; Hogekamp, A.; Ahlrichs, R., Fast evaluation of the Coulomb potential for electron densities using multipole accelerated resolution of identity approximation. *J. Chem. Phys.* **2003,** *118*, 9136-9148.

[35] Perdew, J. P., Density-functional approximation for the correlation energy of the inhomogeneous electron gas. *Phys. Rev. B* **1986,** *33*, 8822-8824

[36] Grimme, S.; Antony, J.; Ehrlich, S.; Krieg, H., A consistent and accurate ab initio parametrization of density functional dispersion correction (DFT-D) for the 94 elements H-Pu. *J. Chem. Phys.* **2010,** *132*, 154104.

[37] Grimme, S.; Ehrlich, S.; Goerigk, L., Effect of the Damping Function in Dispersion Corrected Density Functional Theory. *J. Comput. Chem.* **2011,** *32*, 1456-1465.

[38] Weigend, F.; Ahlrichs, R., Balanced basis sets of split valence, triple zeta valence and quadruple zeta valence quality for H to Rn: Design and assessment of accuracy. *Phys. Chem. Chem. Phys.* **2005,** *7*, 3297-3305.

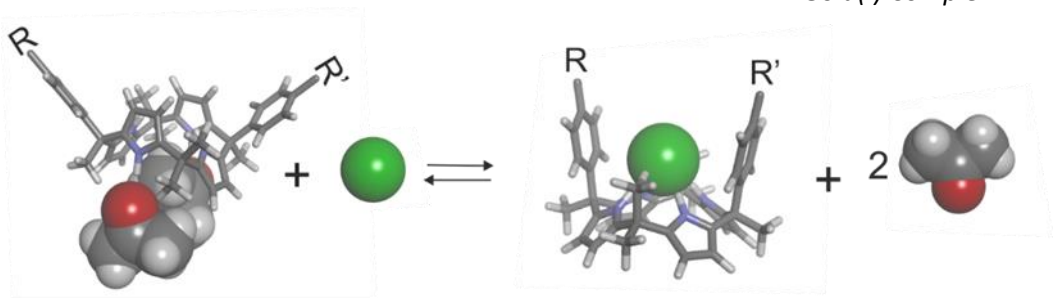

***Figure 5**. Molecular structures of the species involved in the 1:1 binding equilibrium used to calculate the electronic interaction energies of chloride binding to the receptors' series: ΔE = [E(chloride_complex)+ **2** × E(acetone)]-[E(acetone solvated 1,3-alternate receptor) + E(chloride)]. The receptor is displayed in stick representation. The chloride and the acetone molecules are shown as CPK models.*

We evaluated the solvent effect in the binding of chloride by assuming the displacement of two molecules of acetone that originally were bound to the "free" receptor in 1,3-alternate-conformation[39]. The optimized geometry of the 2:1 complexes formed between acetone and the "free" calix[4]pyrrole revealed a single hydrogen-bonding interaction between two pyrrole NHs and the oxygen atoms of distinct acetone molecules. The structure of the acetone solvate was inspired by the solid state structure observed in the X-ray diffraction study of a single crystal of *meso*-hexamethyl-10α,20α-diphenyl calix[4]pyrrole grown from acetone solution.[Errore. Il segnalibro non è definito.,40] Upon binding of the chloride, the receptor underwent a conformational change to adopt the cone conformation, leading to the release of two acetone molecules to the bulk solution and the formation of the corresponding 1:1 chloride complex. The chloride is sandwiched between the *meso*-phenyl substituents and established four convergent hydrogen bonds with the pyrrole NHs.

In the energy minimized structure of the chloride complexes (**Figure 6**), the distance between the centroid of the *meso*-*p*-iodophenyl ring and the chloride anion decreased from 4.021 Å in the **3**●Cl^- complex to 3.961 Å in the **2Au**●Cl^- analogue. Conversely, the distance between the chloride and the differently substituted phenyl ring changed from 4.018 Å for R'=I, 4.040 Å for R'= ethynyl, and 4.076 Å when

[39] Other considerations of the theoretical equilibrium i.e. use of implicit solvation or explicit solvation of the complexes with one or two molecules of acetone produced results that were in contrast with the experimental ones.
[40] CCDC 1002710 contains the crystallographic data. Refcode: BOGWIF

R'= ethynyl-gold(I)PTA. These results indicated that at the used level of theory, the repulsive nature of the chloride-π interactions can be deduced from the latter geometrical parameter.

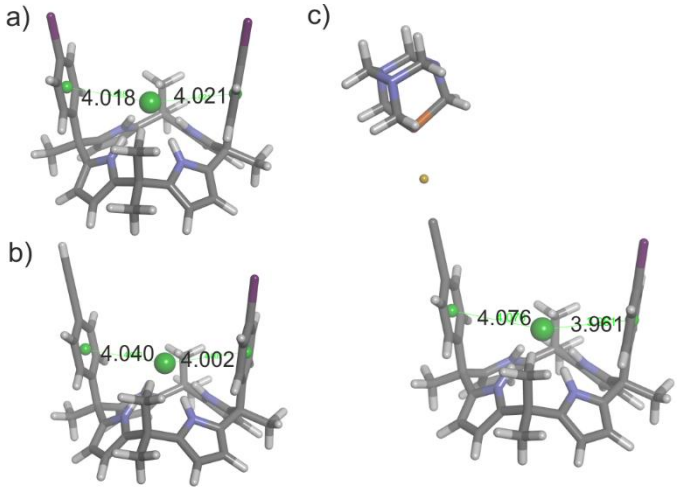

***Figure 6**:. Energy minimized structures at the DFT level of theory of the chloride complexes of the receptor series: a) **3**●Cl^-; **2**●Cl^-; c) **2Au**●Cl^-. The distances between the chloride anion and the centroids of the two aromatic rings are shown in Å. The receptors are depicted in stick representation and the chloride as scaled ball.*

The magnitudes of the calculated electronic interaction energies are enormous. Most likely, this is due to theoretical equilibrium used to estimate them and that the used energies for the species were calculated in the gas phase. The data obtained from computational calculations were consistent with the trend observed in the experimentally measured free energies and binding enthalpies. Using the Cl^-●**3** complex as reference, the differences between the calculated electronic energies of the complex are of the same order than the experimentally measured differences for their free energies of binding. It is worth noting that the consideration of other equilibria to compute the electronic energies of the complexes i.e. reorganization of one or two solvent molecules from the free receptor to the complex, and/or the use of implicit solvation models produced a larger discrepancy with respect to the experimental results. The obtained results showed the importance of adequately modeling the solvent effect in calculations trying to reproduce the trend of experimentally determined free energies of binding in solution and the difficulties of doing it using calculations at the DFT level.

Table 4. Theoretically calculated binding energies for the chloride complexes of the series of "two wall" calix[4]pyrrole receptors

Complex (n●Cl^-)	ΔE in Kcal/mol	ΔΔE in Kcal/mol
n = Bis-iodo **3**	-32.8502	0
n = Mono-iodo-mono-ethynyl **2**	-32.5431	0.3
n = Mono-nuclear **2Au**	-31.8133	1.0

2.6 Studies of the cytotoxicity of 2Au and the reference compound 6Au using human cancer cell lines

Various types of organo-gold and gold coordination-based complexes have been reported to exhibit potential cytotoxic activities[41,42]. Among these, alkynyl gold complexes, which feature strong Au-C bonds, have been identified as particularly promising agents for use as anticancer drugs[43]. We became interested in testing **2Au** for its cytotoxicity towards different human cancer cell lines (HeLa, MIA PaCa-2 and A549) using a cell viability assay based on tetrazolium reduction. We also tested the reference compound **6Au** in order to identify the role played by the calix[4]pyrrole unit in the cytotoxic activity of **2Au**. As summarized in Table 5, the IC_{50} values determined from the assays of **2Au** in the three cell lines are very similar. We observed an increase in the cytotoxic activity of **2Au** with MIA PaCa-2 cell line. Moreover, **2Au** shows only small differences in activity in A549 cell line compared to the reference compound **6Au**. This result suggested that the calix[4]pyrrole unit does not have a major effect in the cytotoxic activity of **2Au**. However, we cannot exclude that the presence of the calix[4]pyrrole scaffold endows **2Au** with different properties leading to a different cellular uptake, interaction with biological targets and/or different cell death mechanisms compared to the reference compound **6Au**.

[41] Montanel-Pérez, S.; Elizalde, R.; Laguna, A.; Villacampa, M. D.; Gimeno, M. C., Synthesis of Bioactive N-Acyclic Gold(I) and Gold(III) Diamino Carbenes with Different Ancillary Ligands. European Journal of Inorganic Chemistry 2019, 2019, 4273-4281

[42] Quero, J.; Ruighi, F.; Osada, J.; Gimeno, M. C.; Cerrada, E.; Rodriguez-Yoldi, M. J., Gold(I) Complexes Bearing Alkylated 1,3,5-Triaza-7-phosphaadamantane Ligands as Thermoresponsive Anticancer Agents in Human Colon Cells. Biomedicines 2021, 9, 1848

[43] Cerrada, E.; Fernández Moreira, V.; Gimeno, M. C., *Gold and platinum alkynyl complexes for biomedical applications*. Elsevier: 2019; Vol. 71.

Table 5. IC_{50} (μM) of **2Au** and **6Au** with HeLa, A549, and MIA PaCa-2 cell lines after 72h of incubation.

Cell line	IC_{50} 2Au (μM)	IC_{50} 6Au (μM)
MIA PaCa-2	0.78 ± 0.15	-
A549	0.90 ± 0.26	2.69±0.19
HeLa	1.09 ± 0.71	-

2.7 Conclusions

We report the synthesis and characterization of the mono-nuclear organo-gold(I)-PTA "two wall" aryl extended calix[4]pyrrole receptor **2Au**. We performed ^{1}H NMR titration experiments in dichloromethane-d_2 and acetone-d_6 of **2Au** and their precursors, the mono-iodo mono-ethynyl **2** and the reference bis-iodo **3**, with TBACl. We also performed ITC and pair-wise competitive ^{1}H NMR experiments in acetone to accurately determine the differences in binding. Taken together, the titration data reveal a ~2 and ~3-fold decrease in the binding constant of mono-iodo mono-ethynyl **2** and mono-nuclear **2Au**, respectively, compared to the reference receptor bis-iodo **3**. The calculated ΔG of the complexes allow us to dissect the binding energies of **2Au** vs **3** for TBACl into ~0.4 kcal/mol produced by the substitution of one iodo substituent by an ethynyl group and ~0.3 kcal/mol caused by the incorporation of a gold(I)-PTA moiety in the terminal ethynyl. DFT calculations were also in agreement with the experimental results and nicely reproduced the trend observed in the determined free energy values. However, the differences in the calculated ESP values at the centers of the aromatic ring and at the para-substituent of the differently-substituted aromatic walls was not enough to explain the dissimilar binding free energies of the 1:1 chloride complexes exclusively in terms of repulsive anion-π interactions. Therefore, we conclude that solvation/desolvation processes have a strong contribution to the measured differences.

In agreement with previous findings,[12] the addition of more than 1 equiv. of TBACl to dichloromethane and acetone solution of **2Au** provoked the appearance of two set of aromatic signals for the bound calix[4]pyrrole units. The model compound **6Au**, lacking the calix[4]pyrrole unit, transformed into the gold(I)-anionic dimer [**7Au**]$^-$ upon addition of TBACl. This finding led us to conclude that in the titrations of **2Au** with the salt an analogous calix[4]pyrrole gold(I)anionic dimer [**8Au**]$^-$ is

produced with the concomitant appearance of free PTA and the PTA-**Au**(I)Cl complex. We assigned the two sets of signals observed for the aromatic protons of the bound calix[4]pyrrole unit in the ^{1}H NMR spectra of the titrations of **2Au** with TBACl to the formation of the corresponding chloride complexes of **2A**u and [**8Au**]$^{-}$. We also are forced to disregard our previous hypothesis[12] suggesting that the mono-nuclear gold(I) calix[4]pyrrole receptor **1Au** adopted cone and half-cone conformations in the 1:1 complex with chloride. The results of the cytotoxicity studies of **2Au** using different human cancer cell lines assigned IC_{50} values close to 1 µM. The cytotoxic activity of **2Au** is comparable to that of **6Au** (2.7 µM) suggesting that the role of calix[4]pyrrole moiety has a reduced effect. Nevertheless, we cannot rule out the possibility that the calix[4]pyrrole unit endows the compound with different biological properties (cellular uptake, biological target and cell death mechanisms).

2.8 Experimental section

2.8.1 General methods and instrumentation

Reagents were obtained from commercial suppliers and used without further purification unless otherwise stated. All solvents were commercially obtained and used without further purification except pyrrole which was distilled and freshly used. Dry solvents were taken from a solvent system MB SPS 800. Et_3N was dried, distilled and degassed by three freeze-pump-thaw cycles before used in the cross-coupling reactions. Routine ^{1}H NMR and ^{13}C{1H} NMR spectra were recorded on a Bruker Avance 300 (300 MHz for ^{1}H NMR and 75 MHz for ^{13}C NMR), Bruker Avance 400 (400 MHz for ^{1}H NMR and 100 MHz for ^{13}C NMR), Bruker Avance 500 (500 MHz for ^{1}H NMR and 125 MHz for ^{13}C NMR) or Bruker Avance 500 with cryoprobe (500 MHz for ^{1}H NMR and 125 MHz for ^{13}C NMR). Deuterated solvents used are indicated in the characterization and chemical shifts are given in ppm. Residual solvent peaks were used as reference[44]. All NMR J values are given in Hz. COSY, NOESY, HMQC and HMBC experiments were recorded to help with the assignment of ^{1}H and ^{13}C signals. High Resolution Mass Spectra (HRMS) were obtained on a Bruker HPLC-TOF (MicroTOF Focus) with ESI as ionization mode and Bruker HPLC-QqTOF (MaXis

[44] Fulmer, G. R.; Miller, A. J. M.; Sherden, N. H.; Gottlieb, H. E.; Nudelman, A.; Stoltz, B. M.; Bercaw, J. E.; Goldberg, K. I., NMR Chemical Shifts of Trace Impurities: Common Laboratory Solvents, Organics, and Gases in Deuterated Solvents Relevant to the Organometallic Chemist. *Organometallics* **2010,** *29* (9), 2176-2179.

Impact) with ESI as ionization mode. Nominal mass spectra were obtained by direct injection on an Agilent 1200 HPLC and using as detection unit an Agilent 6130 quadrupole. IR spectra were recorded on a Bruker Optics FTIR Alpha spectrometer equipped with a DTGS detector, KBr beamsplitter at 4 cm^{-1} resolution using a one bounce ATR accessory with diamond windows. Melting points were measured on a MP70 Melting Point System Mettler Toledo. Column chromatography was performed with silica gel technical grade (Sigma-Aldrich), pore size 60 Å, 230-400 mesh particle size, 40-63 µm particle size and Thin Layer Chromatography (TLC) analysis on silica gel 60 F254. ITC experiments were performed using a MicroCal VP-ITC MicroCalorimeter with the VP Viewer 2000 software.

2.8.2 Synthesis and characterization data

Mono-alcohol-mono-iodo calix[4]pyrrole 4

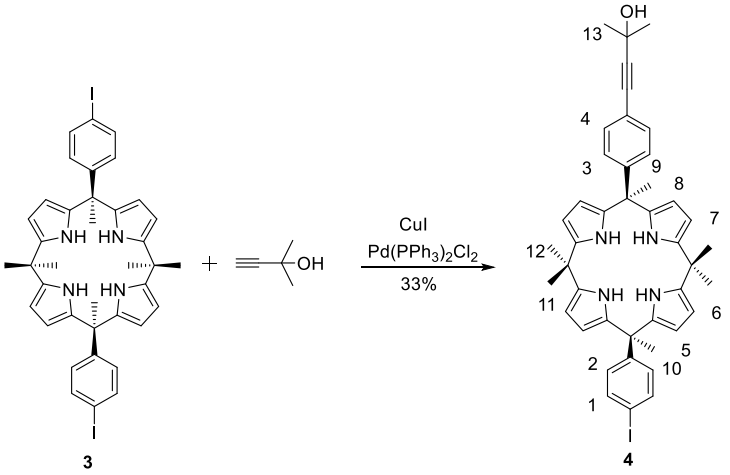

Scheme S 1. *Synthesis of compound **4**.*

In a 10 mL Schlenk flask, 10α,20α-bis(4-iodophenyl)calix[4]pyrrole (**3**) (50 mg, 0.062 mmol, 1 equiv.), CuI (0.6 mg, 0.003 mmol, 0.05 equiv.) and $Pd(PPh_3)_2Cl_2$ (2.2 mg, 0.003 mmol, 0.05 equiv.) were dissolved in 5 mL of toluene under Ar atmosphere. Afterwards, triethylamine (0.82 mL, 0.31 mmol, 5 equiv.) and 2-methyl-3-butyn-2-ol (0.03 mL, 0.311 mmol, 5 equiv.) were added. The reaction mixture was stirred for 6 hours at room temperature. Then DCM (5 mL) was added to the reaction mixture and was washed with 0.5 M HCl (10 mL×1) and water (10 mL×2). The collected organic layer was dried with sodium sulfate, filtered and concentrated under vacuum to obtain a brown solid. The product was purified through silica column chromatography using a 9:1 DCM:Hexane mixture as eluent (Rf = 0.25). The product was obtained as a dark orange solid (yield = 33%).

^{1}H NMR (500 MHz, $CDCl_3$, 298 K) δ (ppm) H1 (d, 7.54 ppm, 2H, *J*= 8.79 Hz), H4 (d, 7.28 ppm, 2H, *J*= 8.45 Hz), NH (br, 7.20 ppm 4H), H3 (d, 6.90 ppm, 2H, *J*= 8.45 Hz), H2 (d, 6.72 ppm, 2H, *J*= 8.79 Hz), H6; H7 (t, 5.92 ppm, 4H), H5; H8 (m, 5.61 ppm, 4H), H10 (s, 1.87 ppm, 3H), H9 (s, 1.85 ppm,3H), H11 (s, 1.61 ppm, 6H), H13 (s, 1.59 ppm,6H), H12 (s, 1.52 ppm,6H). ^{13}C NMR (125 MHz, $CDCl_3$, 298 K) δ (ppm) 148.36, 147.97, 138.69 (d, *J*= 14.79 Hz), 136.86, 136.19 (d, *J*= 39.63), 131.12, 129.71, 127.50, 120.89, 106.23, 106.17, 103.44, 103.41, 93.70, 92.09, 82.18, 65.78, 44.79, 44.64,

35.27, 31.66, 30.14, 27.97, 27.81, 27.71. M.p. = 170 ºC. FTIR (ATR): $\bar{\upsilon}_{max}$ (cm^{-1}) = 3419 (s), 2969 (s), 2924 (m), 1573 (m), 1218 (m), 766 (m). HRMS (ESI/ TOF) m/z: $[M-H]^-$ = $[C43H44IN4O]^-$ Calcd 759.2565; Found 759.2564.

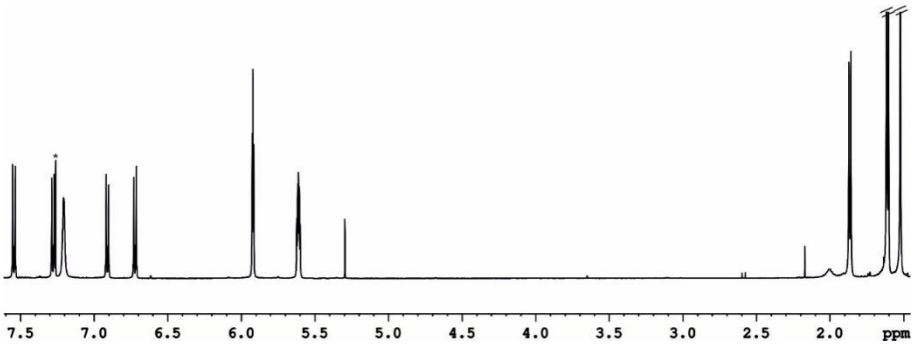

***Figure S 1**: [1]H NMR (500 MHz, $CDCl_3$, 298 K) spectrum of **4**.*

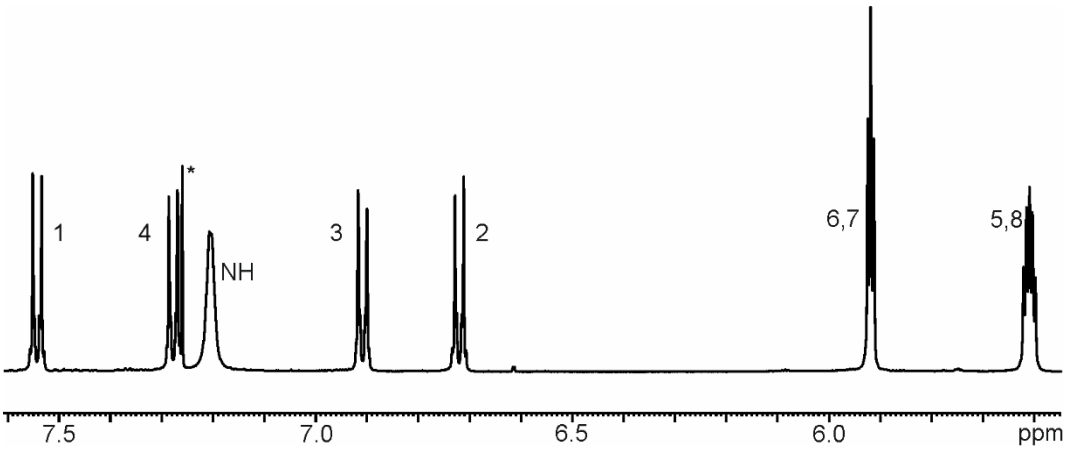

***Figure S 2:** Selected downfield region of the [1]H NMR (500 MHz, $CDCl_3$, 298 K) spectrum of **4**. See scheme S1 for proton assignment. *Solvent residual peak.*

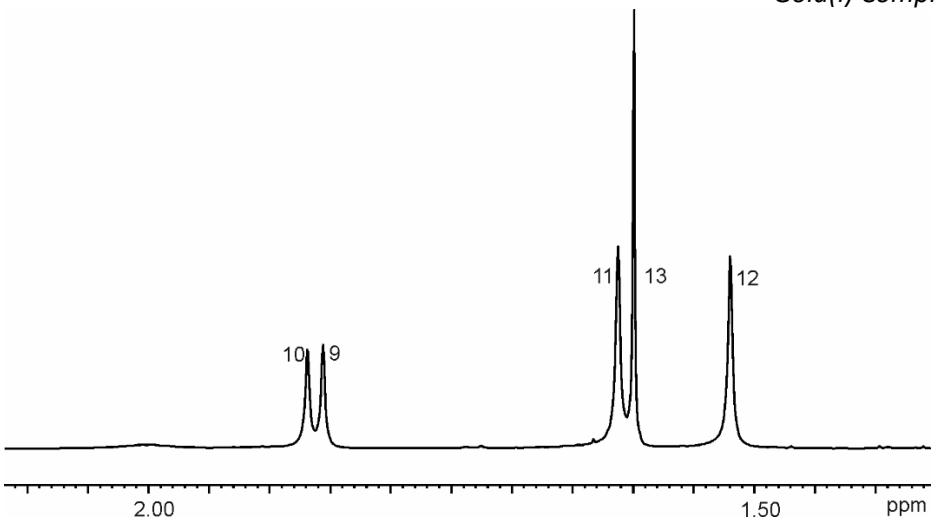

***Figure S 3**: Selected upfield region of the ^{1}H NMR (500 MHz, $CDCl_3$, 298 K) spectrum of **4**. See scheme S1 for proton assignment. *Solvent residual peak.*

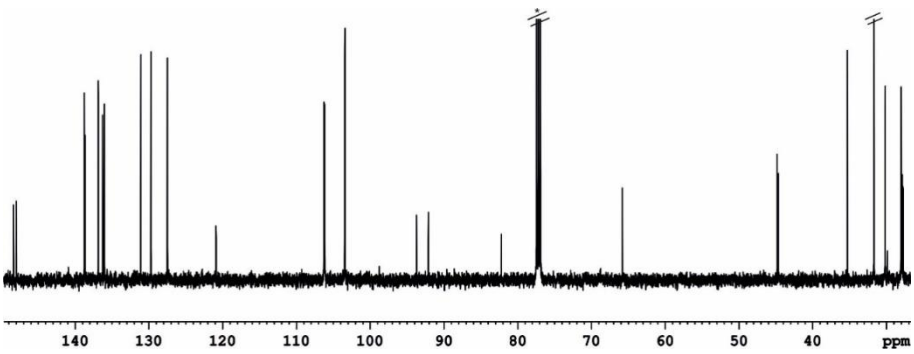

***Figure S 4:** ^{13}C NMR (125 MHz, $CDCl_3$, 298 K) spectrum of **4**.*

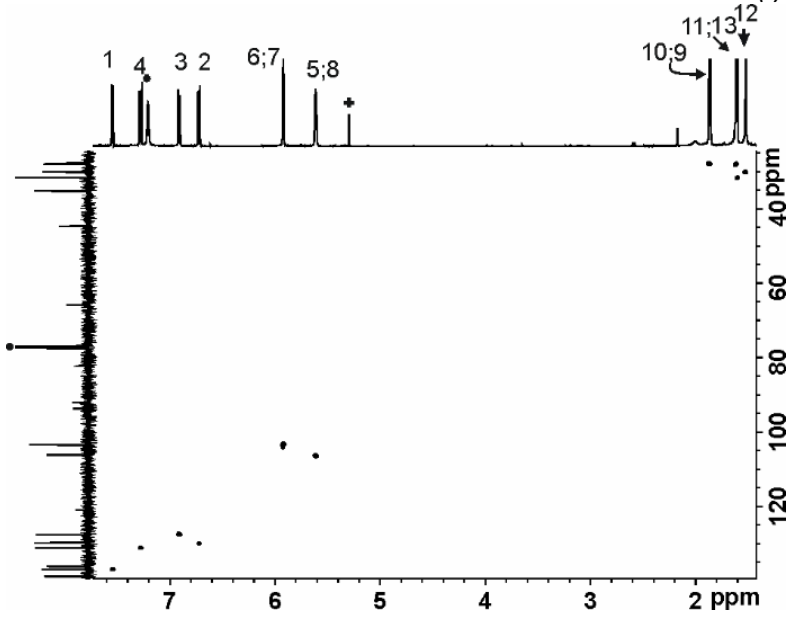

Figure S 5: *2D ^{1}H-^{13}C HSQC NMR ($CDCl_3$, 298 K) spectrum of* ***4.*** *See scheme S1 for proton assignment. *Solvent residual peak.*

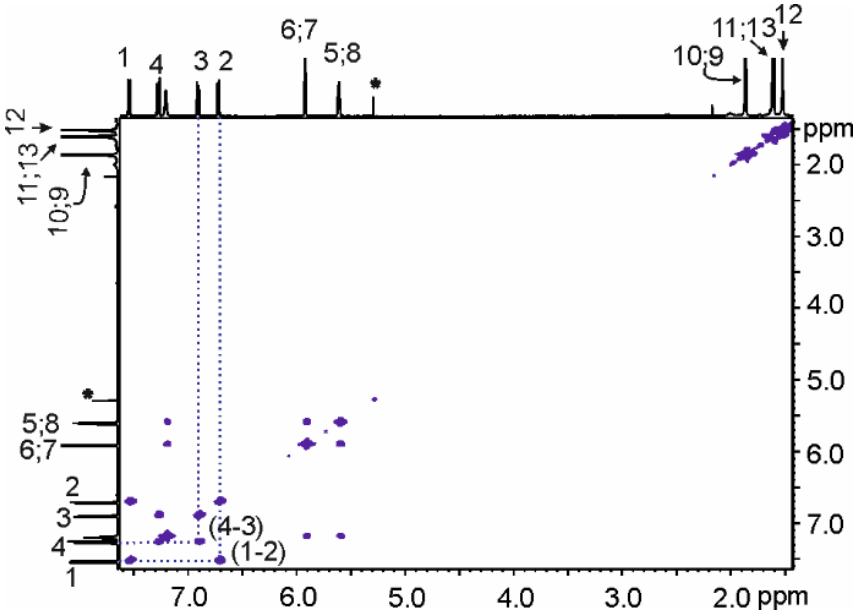

Figure S 6: *2D 1H-1H COSY NMR (500 MHz, $CDCl_3$, 298 K) spectrum of* ***4.*** *See scheme S1 for proton assignment. *Solvent residual peak.*

meso-10α,20α-_p_-ethynylphenyl-_p_-iodophenyl calix[4]pyrrole 2

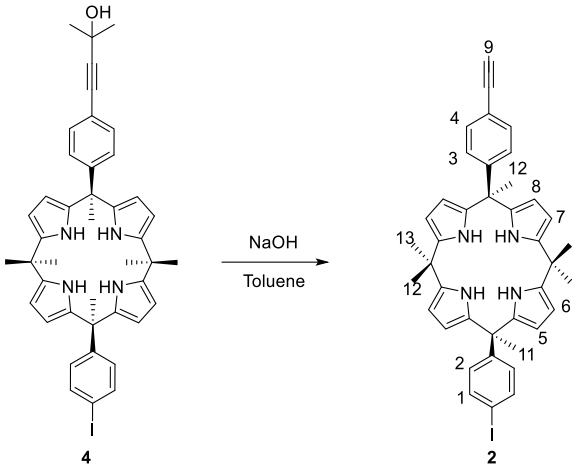

Scheme S 2. *Synthesis of compound* ***2.***

Compound **4** (52 mg, 0.07 mmol, 1 equiv.) was dissolved in 6.5 mL of dry toluene in a 10 mL round bottom flask. Then, powdered sodium hydroxide (56 mg, 1.2 mmol, 20 equiv.) was added to the solution. The orange mixture was stirred at 90 ºC for 12 h under Ar atmosphere. The reaction mixture was concentrated and washed with DCM (5mL×2). The combined organic phase was washed with 0.5 M HCl (5mL×1) and water (10 mL×2). The collected organic phase was dried with Na_2SO_4, filtered and concentrated under vacuum to give a brown solid as the pure product (34 mg) (70% yield).

^{1}H NMR (500 MHz, CD_2Cl_2, 298 K) δ (ppm) H1 (d, 7.55 ppm, 2H, *J*= 8.48 Hz), H4 (d, 7.35 ppm, 2H, *J*= 8.44 Hz,), NH (br, 7.27 ppm, 4H), H3 (d, 6.92 ppm, 2H, *J*= 8.44 Hz), H2 (d, 6.71 ppm, 2H, *J*= 8.48 Hz), H6; H7 (t, 5.92 ppm, 4H), H5; H8 (q, 5.62 ppm, 4H), H9 (s, 3.08 ppm, 1H), H10 (s, 1.86 ppm, 3H), H11 (s, 1.85 ppm, 3H), H12 (s, 1.62 ppm, 6H), H13 (s, 1.51 ppm, 6H). ^{13}C NMR (125 MHz, CD_2Cl_2, 298 K) δ (ppm) 149.49, 148.48, 139.12 (d, *J*= 6.50 Hz), 137.09, 136.33 (d, *J*= 12 Hz), 131.78, 130.04, 127.89, 120.44, 106.47, 103.65, 92.09, 83.83, 77.17, 45.10, 44.92, 35.40, 30.39, 27.63, 27.54, 27.23. M.P. =273.3 ºC. FTIR (ATR): $\bar{\upsilon}_{max}$ (cm^{-1}) = 3419 (s), 3282 (m), 2967 (m), 2924 (m),1573 (m), 2119 (m), 769 (m). HRMS (ESI/ TOF) m/z: $[M-H]^-$= $[C_{40}H_{38}IN_4]^-$ Calcd 701.2146; Found 701.2153.

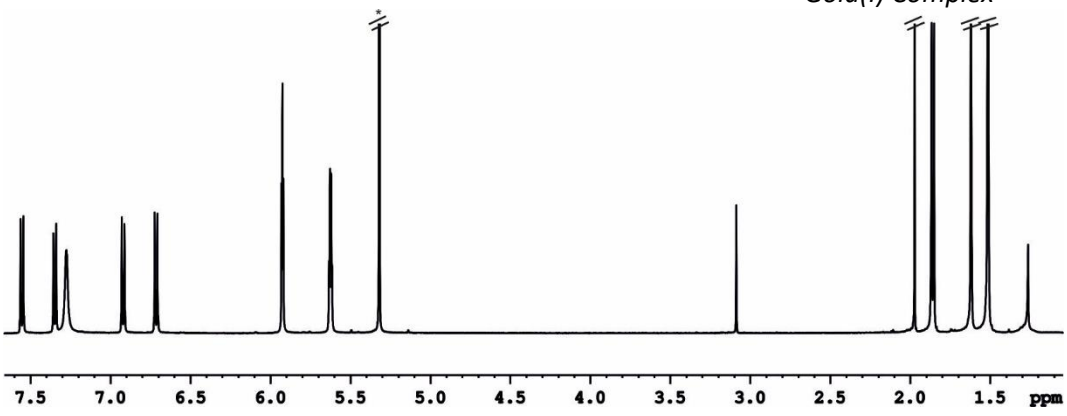

Figure S 7: *^{1}H NMR (500 MHz, CD_2Cl_2, 298 K) spectrum of **2**. *Solvent residual peak.*

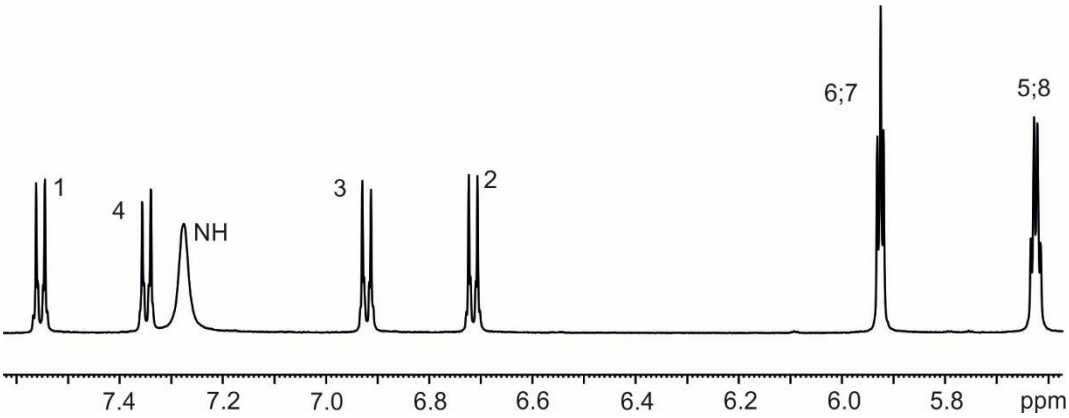

Figure S 8: *Selected downfield region of the ^{1}H NMR (500 MHz, CD_2Cl_2, 298 K) spectrum of **2**. See scheme S2 for proton assignment. *Solvent residual peak.*

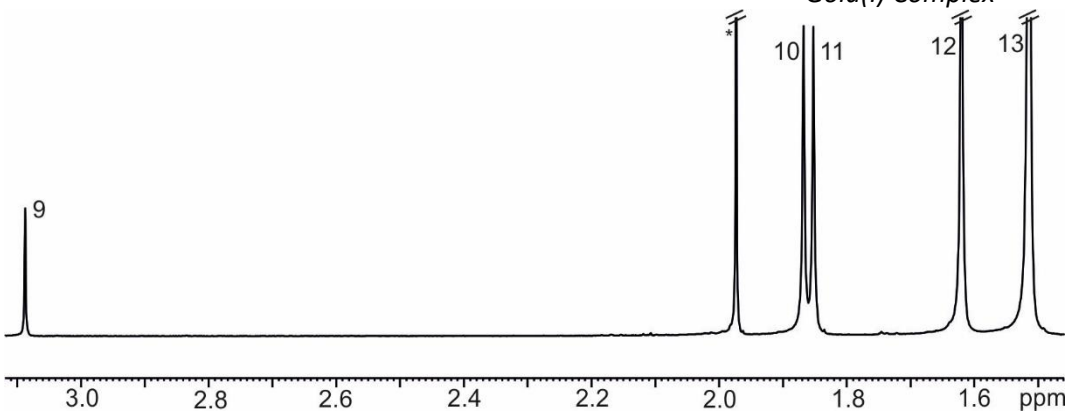

Figure S 9: *Selected upfield region of the ^{1}H NMR (500 MHz, CD_2Cl_2, 298 K) spectrum of* ***2****. See scheme S2 for proton assignment. *Solvent residual peak*

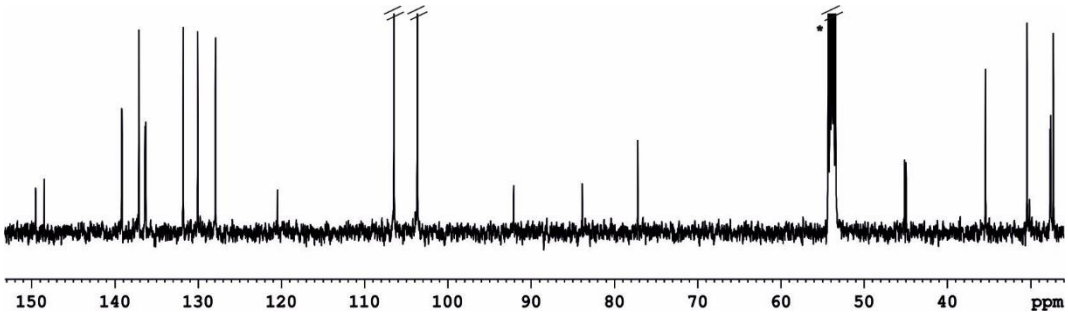

Figure S 10: *^{13}C NMR (125 MHz, CD_2Cl_2, 298 K) spectrum of* ***2****. *Solvent residual peak.*

Chloride Binding Properties of a Macrocyclic Receptor Equipped with an Acetylide Gold(I) Complex

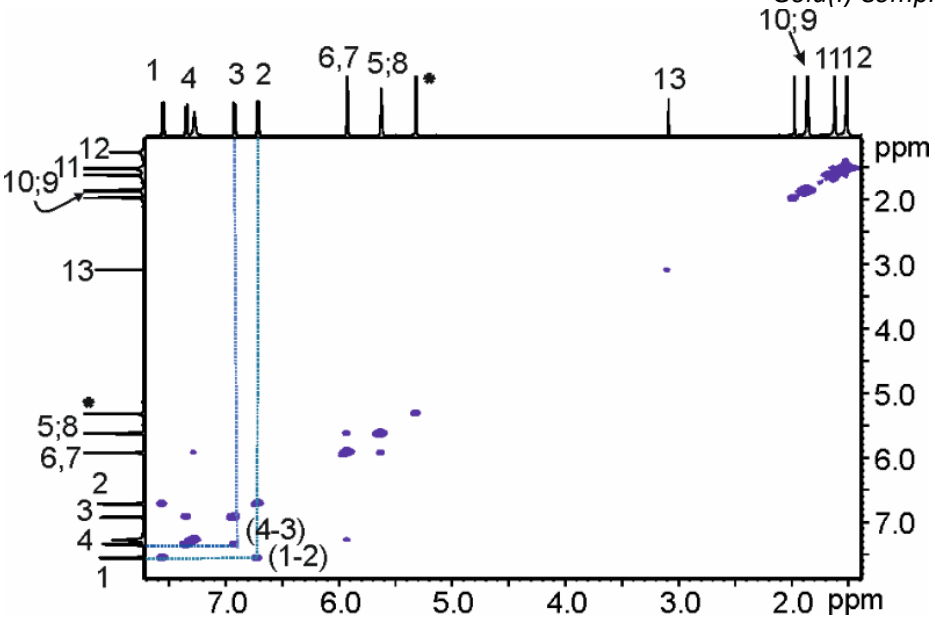

Figure S 11: *2D ^{1}H-^{1}H COSY NMR (500 MHz, CD_2Cl_2, 298 K) spectrum of **2**. Some selected COSY cross-peaks are indicated. See scheme S2 for proton assignment. *Solvent residual peak*

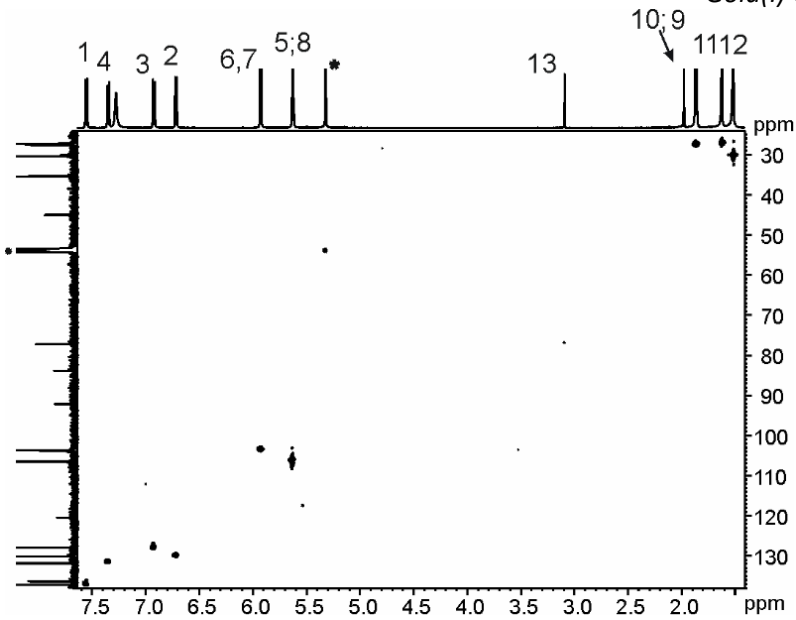

Figure S 12: *2D ^{1}H-^{13}C HSQC NMR (CD_2Cl_2, 298 K) spectrum of* ***2.*** *See scheme S2 for proton assignment. *Solvent residual peak.*

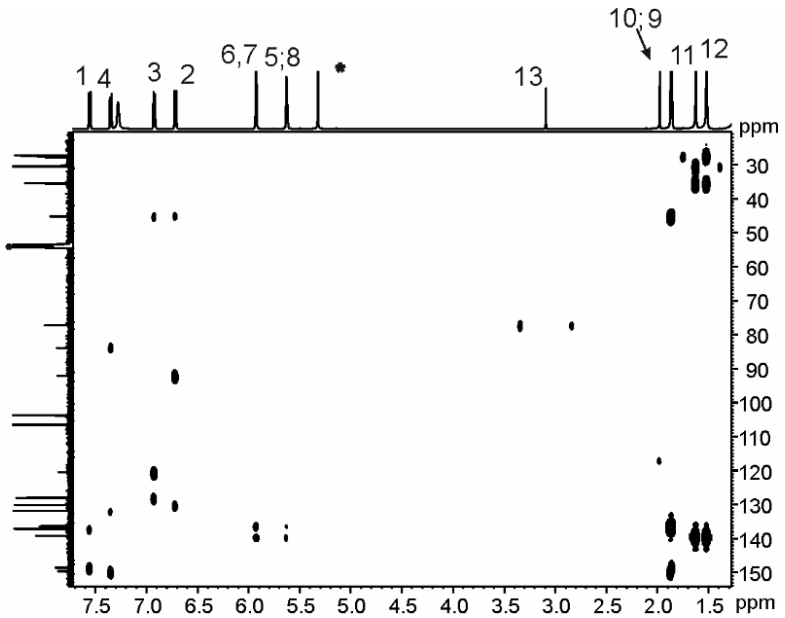

Figure S 13: *2D ^{1}H-^{13}C HMBC NMR (CD_2Cl_2, 298 K) of* ***2.*** *See scheme S3 for proton assignment. *Solvent residual peak.*

Gold(I)-phosphine substituted "two-wall" calix[4]pyrrole (2Au)

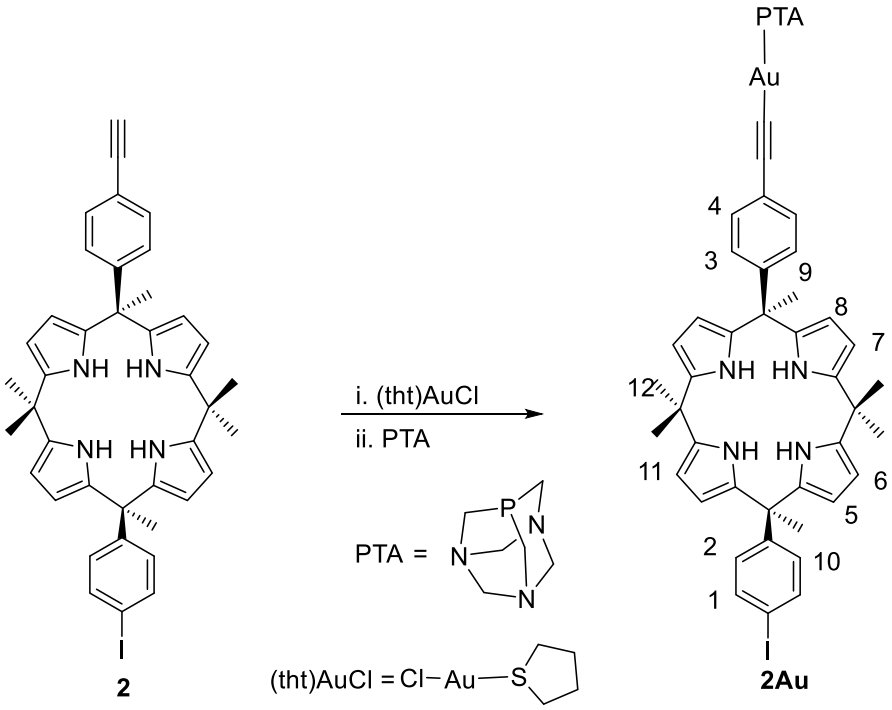

Scheme S 3. *Synthesis of compound* ***2Au***.

In a 2 mL solution of **2** (50 mg, 0.071 mmol, 1 equiv.) in DCM, we added (tht)AuCl (25 mg, 0.078 mmol, 1.1 equiv.) dissolved in 1 mL of DCM and triethylamine (TEA) (0.028ml, 0.210 mmol, 3 equiv.). The reaction mixture was stirred under Ar atmosphere for 2 h protected from light. With time it shows the formation of a black precipitate. The suspension was centrifuged and the supernatant was separated from the black solid. The supernatant solution was reduced to ~1 mL under vacuum. Next, we added 2 mL of MeOH to induce the precipitation of the oligomeric gold(I) acetylide **5** as a yellow solid. The yellow solid was washed with a small amount of diethyl ether (10 mL) (35.4 mg of **5**). This solid was used immediately without purification. The oligomeric gold(I) acetylide **5** (35.4 mg, 1 equiv.) was suspended in 5 mL of DCM and we added 6.2 mg of 1,3,5-triaza-7-phosphaadamantane (PTA). The suspension (with black solid) was stirred for 5h under Ar atmosphere and protected

from the light. After 5h the suspension was centrifuged and the supernatant was reduced to ~2 ml under vacuum. Finally, the addition of MeOH (7 mL) yields the pure mono-nuclear gold(I) complex **2Au** in 58% yield.

^{1}H NMR (500 MHz, CD_2Cl_2, 298 K) δ (ppm) H^1 (d, 7.55 ppm, 2H, *J*= 8.58 Hz), NH (br, 7.36 ppm, 4H), H^4 (d, 7.19 ppm, 2H, *J*= 8.44 Hz,), H^3 (d, 6.8 ppm, 2H, *J*= 8.44 Hz), H^2 (d, 6.71 ppm, 2H, *J*= 8.85 Hz), H^6; H^7 (m, 5.92 ppm, 4H), H^5; H^8 (q, 5.62 ppm, 4H), PTA region (d, 4.54 ppm, 6H, J= 13.13 Hz, d, 4.46 ppm, 6H, J= 13.13 Hz, s, 4.24 ppm, 10 H), H^9 (s, 1.85 ppm, 3H), H^{10} (s, 1.84 ppm, 3H), H^{11} (s, 1.61 ppm, 6H), H^{12} (s, 1.50 ppm, 6H). ^{13}C NMR (125 MHz, CD_2Cl_2, 298 K) δ (ppm) 148.18, 146.84, 138.84, 138.53, 136.31, 165.84, 131.16, 129.60, 127.19, 105.94, 130.13, 91.65, 73.12, 73.20, 52.37, 44.5, 34.96, 30.17, 27.23, 27.17, 26.73. ^{31}P NMR (161 MHz, CD_2Cl_2, 298 K) δ (ppm) -46.77 ppm. M.p> 240 ºC (decompose). FTIR (ATR): $\bar{\upsilon}_{max}$ (cm^{-1}) 2110 cm^{-1} (C≡C) (w). HRMS (ESI/TOF) m/z: 1056.2649 Calcd for $[C_{46}H_{50}AuIN_7P + H]^+$; Found 1056.2635.

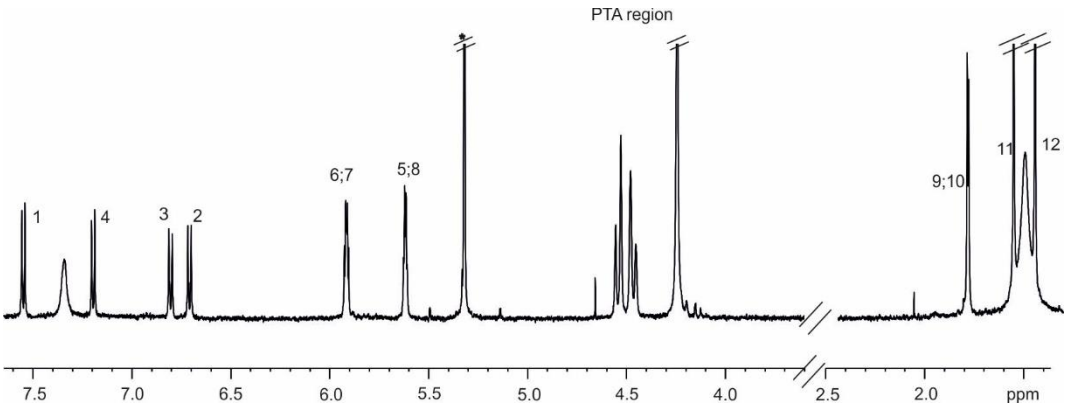

***Figure S 14**: ^{1}H NMR (500 MHz, CD_2Cl_2, 298 K) spectrum of **2Au.** See scheme S3 for proton assignment. *residual solvent peak.*

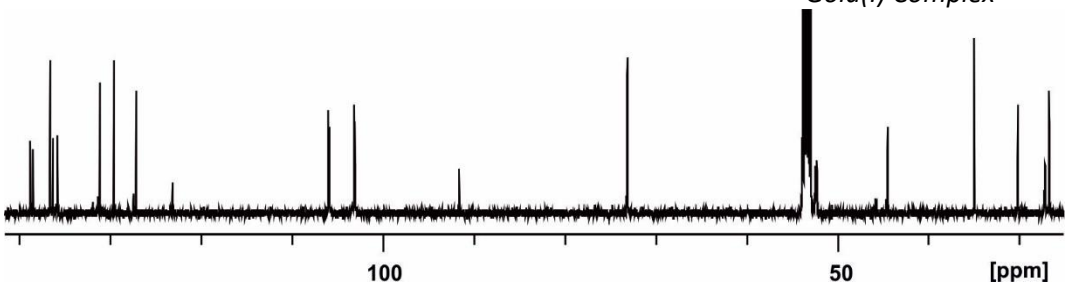

***Figure S 15**: ^{13}C NMR (125 MHz, CD_2Cl_2, 298 K) spectrum of **2Au**.*

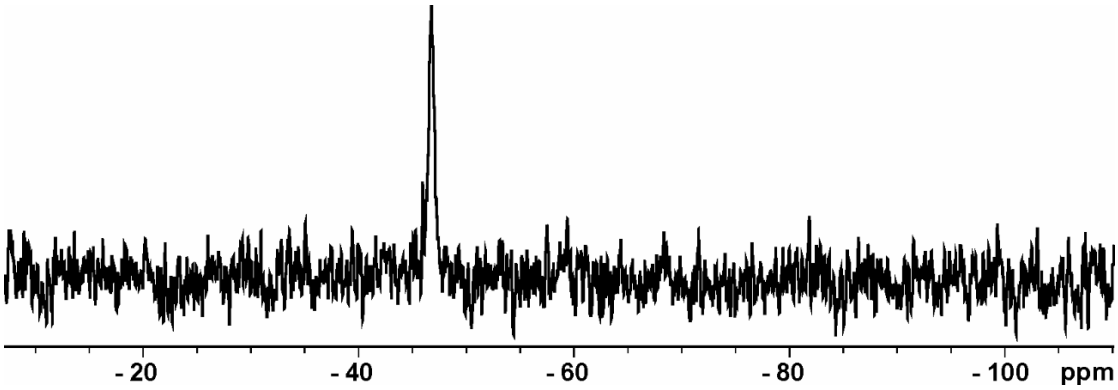

***Figure S16**: ^{31}P NMR (161 MHz, CD_2Cl_2, 298 K) spectrum of **2Au**.*

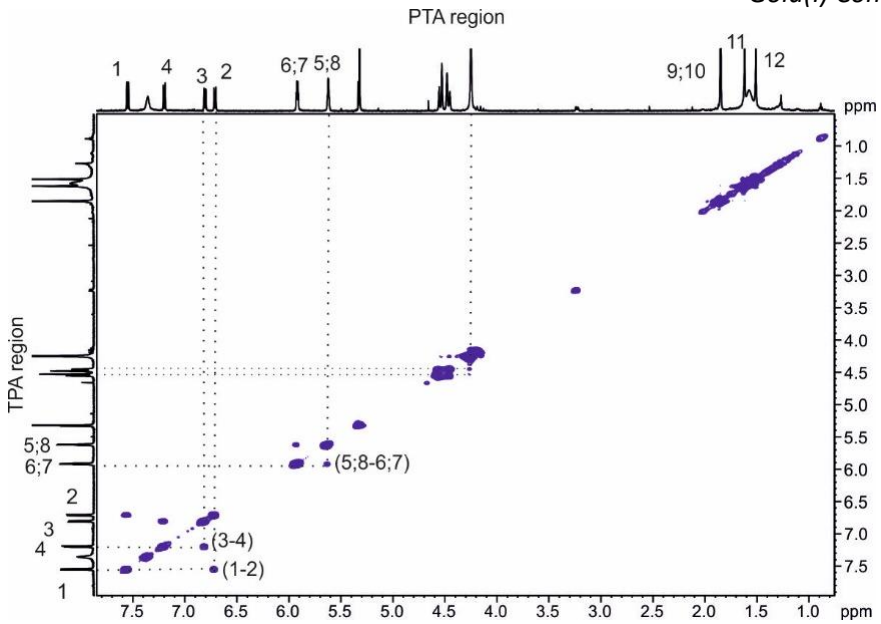

Figure S 17: *2D ^{1}H-^{1}H COSY NMR (500 MHz, CD_2Cl_2, 298 K) spectrum of* ***2Au****. Some selected COSY cross-peaks are indicated. See scheme S3 for proton assignment.*

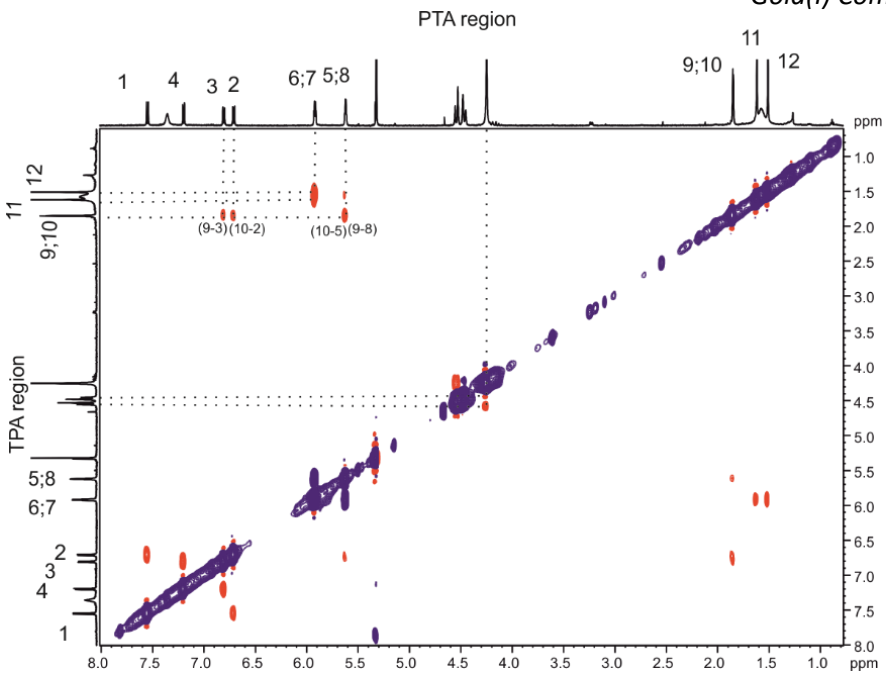

Figure S 18: 2D ^{1}H-^{1}H ROESY NMR (500 MHz, CD_2Cl_2, 298 K, mixing time = 0.3 s) spectrum of **2Au.** Some selected ROESY cross-peaks are indicated. See scheme S3 for proton assignment.

Preparation of (tht)AuCl

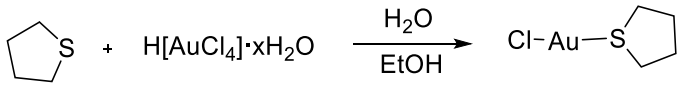

Scheme S 4. Synthesis of **(tht)AuCl**.

To a solution of hydrogen tetracloroaurate (III) (50.9 mg; 0.150 mmol; 1 equiv.) in 0.7 mL of a 5:1 mixture of water:ethanol we added dropwise tetrahydrothiophene (0.022 mL; 0.385 mmol; 2.6 equiv.). We observed the formation of a white precipitate. After the addition, 0.46 mL of ethanol were added and the mixture was stirred to 20 min. The white solid was filtered under vacuum and washed with ethanol. The ^{1}H NMR spectrum was in complete agreement with the one described in the literature[45].

[45] B. Kemper, Y. R. Hristova, S. Tacke, L. Stegemann, L. S. van Bezouwen, M. C. A. Stuart, J. Klingauf, C. A. Strassert, P. Besenius, Facile synthesis of a peptidic Au(i)-metalloamphiphile and its self-assembly into luminescent micelles in water, *Chemical Communications* **2015**, *51*, 5253-5256.

Preparation of *p*-ethynyl-toluene gold PTA complex 6Au

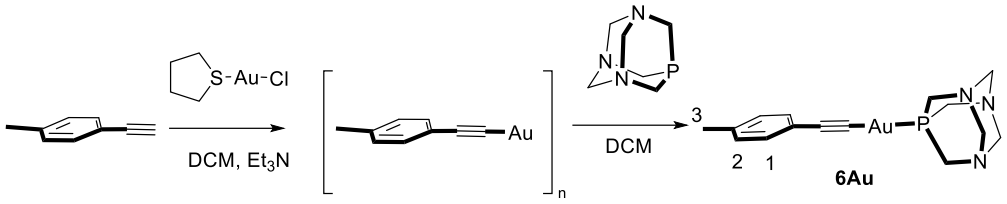

Scheme S 5. *Synthetic scheme for the preparation of the model p-ethynyl-toluene gold(I) PTA complex **6Au**.*

In a 4 mL solution of 4-ethynyl toluene (15 µL, 0.12 mmol, 1 equiv.) in DCM, we added 2 mL of a solution containing (tht)AuCl (38 mg, 0.12 mmol, 1 equiv.) in the same solvent and TEA (47 µL, 0.36 mmol, 3 equiv.). The mixture was stirred for 2 h under Ar atmosphere and protected from the light. Afterwards, the brown suspension was centrifuged to remove a black solid. The supernatant solution was reduced to ~1 ml and 2 mL of MeOH were added to induce the precipitation of a yellowish solid, the oligomeric gold(I) acetylide (21 mg).

The oligomeric gold(I) acetylide was suspended in 4 mL of DCM (21mg) and we added 5.3 mg of PTA (0.067 mmol, 1 equiv.) to the suspension. The suspension was stirred for 5h under Ar atmosphere and protected from the light. After 5h the suspension was centrifuged, and the supernatant was concentrated to a volume of ~2.5 mL. Next, MeOH (7 mL) was added to induce the precipitation of compound **6Au** as a yellow solid. ^{1}H NMR (500 MHz, acetone-d_6, 298 K) δ (ppm) H^1 (d, 7.21 ppm, 2H, *J*= 8.2 Hz), H^2 (d, 7.06 ppm, 2H, *J*= 8.2 Hz), TPA region (d, 4.66 ppm, 3H, J= 12.8 Hz, d, 4.5 ppm, 3H, J= 12.8 Hz, s, 4.42 ppm, 6 H), H^3 (s, 2.29 ppm, 3H). ^{13}C NMR (125 MHz, acetone-d_6, 298 K) δ (ppm) 135.87, 131.49, 128.69, 123.30, 102.43, 72.62 ($J_{C\text{-}N}$= 7.32 Hz), 51.54 ($J_{C\text{-}P}$= 19.43 Hz), 20,41. ^{31}P NMR (161 MHz, acetone-d_6, 298 K) δ (ppm) -46.26 ppm. FTIR (ATR): $\bar{\upsilon}_{max}$ (cm^{-1}) 2111 cm^{-1} (C≡C) (w). HRMS (ESI/TOF) m/z: 470.1075 Calcd for $[C_{15}H_{19}AuN_3P + H]^+$; Found 470.1053.

Chloride Binding Properties of a Macrocyclic Receptor Equipped with an Acetylide Gold(I) Complex

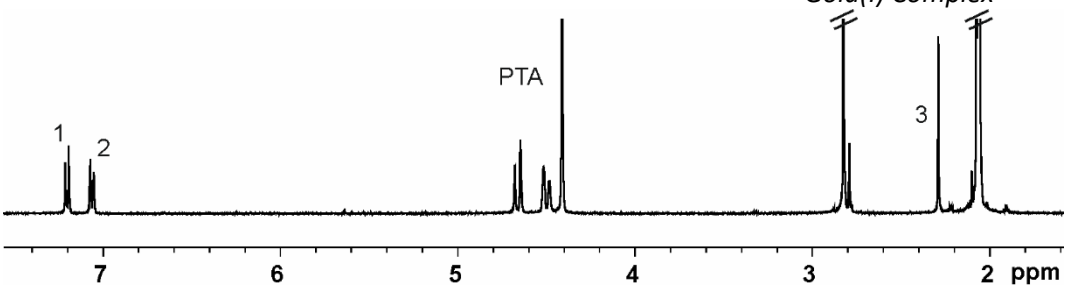

Figure S 19: *^{1}H NMR (500 MHz, acetone-d_6, 298 K) spectrum of* ***6Au.***

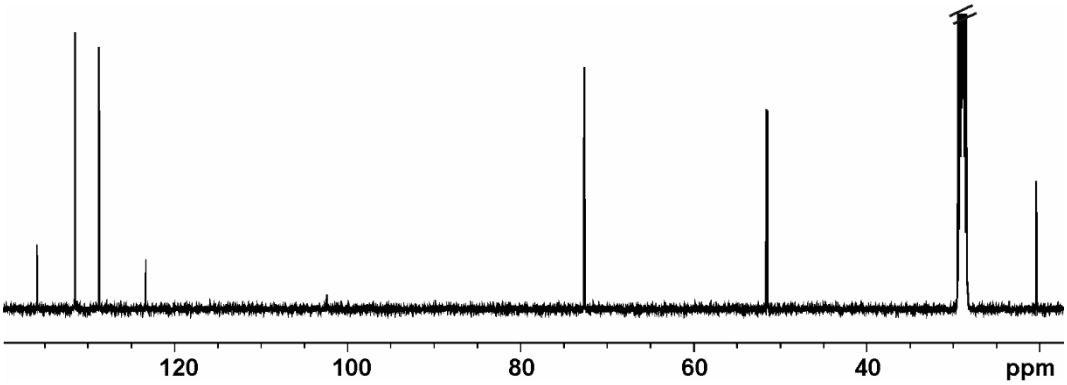

Figure S 20: *^{13}C NMR (125 MHz, acetone-d_6, 298 K) spectrum of* ***6Au****.*

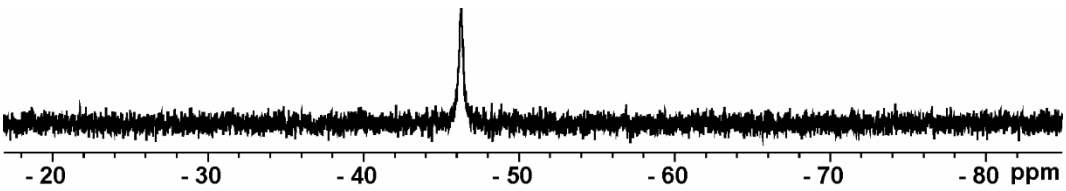

Figure S 21: *^{31}P NMR (161 MHz, acetone-d_6, 298 K) spectrum of* ***6Au****.*

2.8.3 ^{1}H NMR binding studies

^{1}H NMR titrations in DCM

A solution of host (2-5 mM), 3, 2 or 2Au, was prepared in dichloromethane-d_2 or acetone-d_6. Subsequently, 0.5 mL of the solution were transferred to an NMR tube. The remaining solution of the host was used to prepare the titrant's solution, which contained TBACl at 20-fold higher concentration ([TBACl] = 40 mM and [H] = 2-5 mM). In this manner, the concentration of the host was maintained constant throughout the titration. Immediately, the 0.5 mL of the host solution was titrated by manually injecting incremental amounts of the titrant's solution using a micro syringe. A ^{1}H NMR spectrum of the mixture was acquired after each injection and vigorous hand shaking of the NMR tube for few seconds. The apparent binding constants were derived from the fit of the chemical shift changes of the titration data to a 1 : 1 theoretical binding model and using the HypNMR2008[24,25]software.

2Au vs ***TBACl***

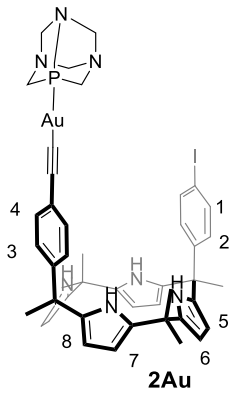

2Au

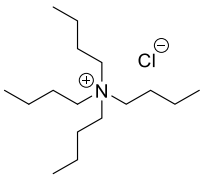

Chloride Binding Properties of a Macrocyclic Receptor Equipped with an Acetylide Gold(I) Complex

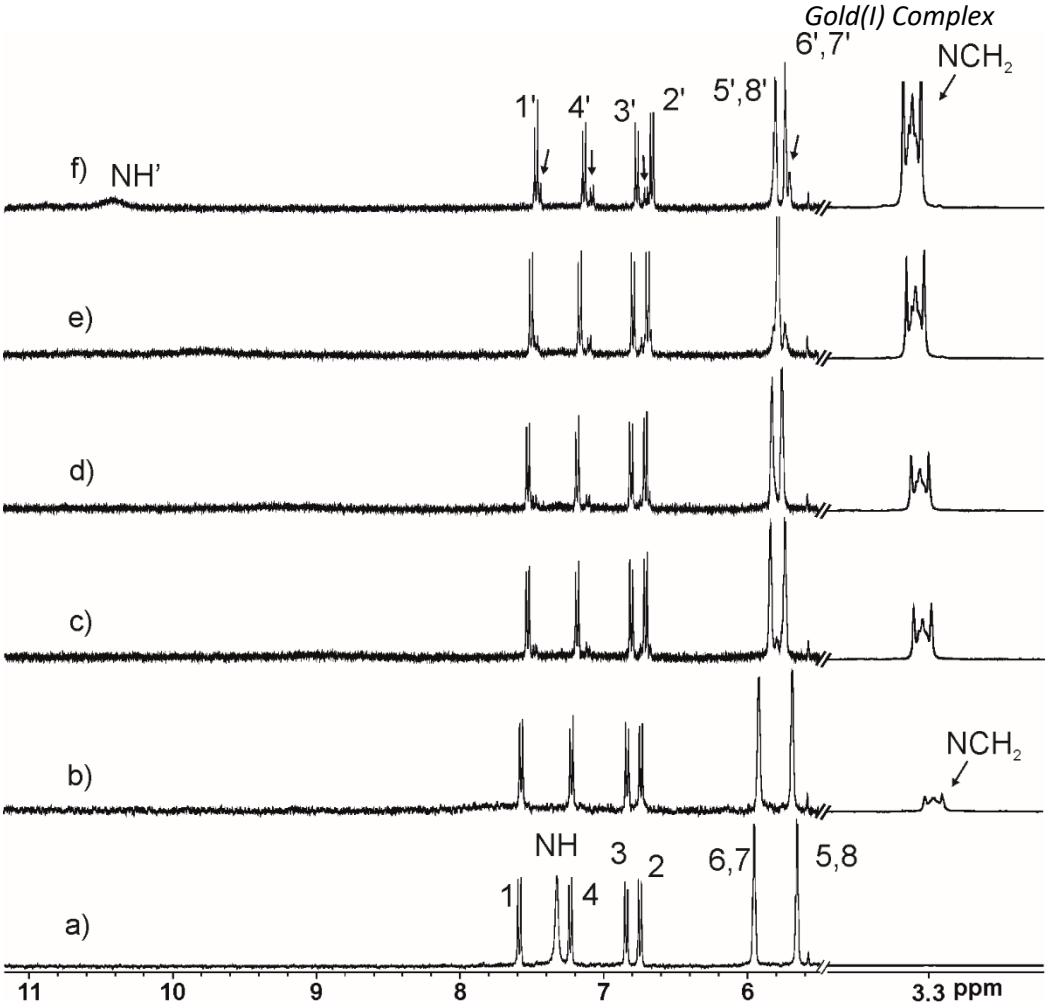

Figure S 22: *Selected regions of the ^{1}H NMR spectra (400 MHz, CD_2Cl_2, 298 K) acquired during the titration of the mono-nuclear* ***2Au*** *calix[4]pyrrole receptor ([**2Au**]=1.9 mM) with* ***TBACl****: a) 0 b) 1 c) 5.4 d) 10.5 e) 21 and f) 27 equiv. added. See top panel for proton assignment. The scale of the downfield region is increased 16 times with respect to the upfield one in order to show the presence of the second set of aromatic proton signals.*

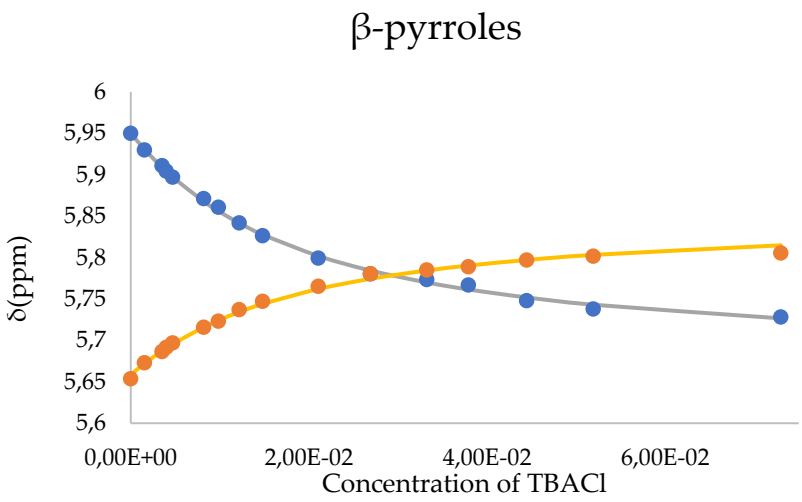

Figure S 23: *Chemical shifts of the β-pyrroles protons of* ***2Au*** *upon incremental amounts of* ***TBACl*** *and fit of the NMR titration data to a theoretical 1:1 binding model.*

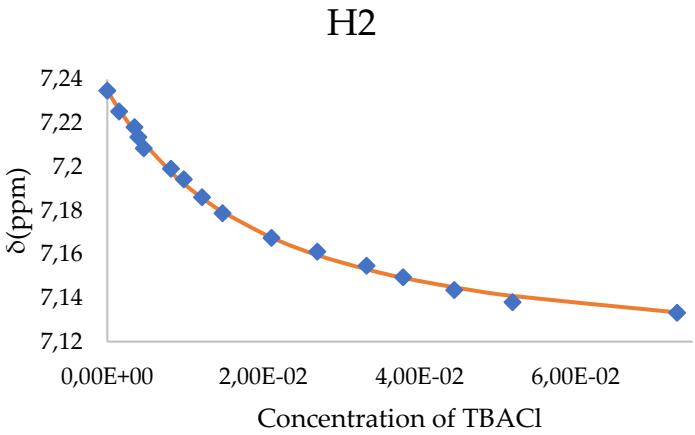

Figure S 24: *Chemical shifts of aromatic protons H2 of* ***2Au*** *upon incremental amounts of* ***TBACl*** *and fit of the NMR titration data to a theoretical 1:1 binding model.*

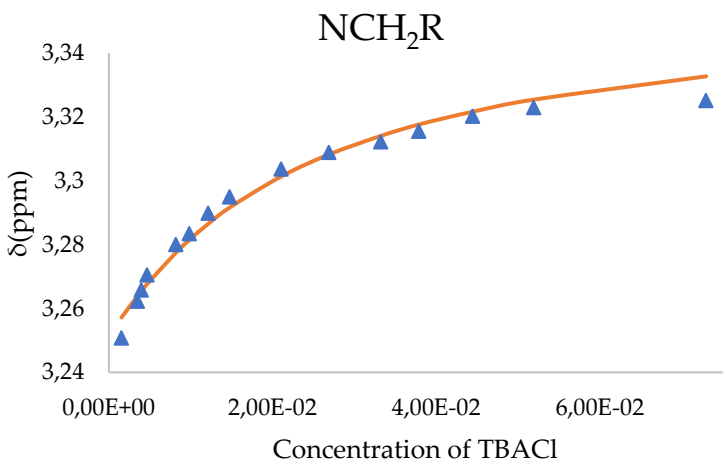

Figure S 25: *Chemical shifts of the CH_2 protons α to the nitrogen of* ***TBA+*** *cation upon incremental amounts of* ***TBACl*** *and fit of the NMR titration data to a theoretical 1:1 binding model.*

Table S 1: *Table of induced chemical shifts of the titration of* ***2Au*** *with* ***TBACl****.*

	H1	**H2**	**β-pyrroles H6 and H7**	**β-pyrroles H5 and H8**	**NCH_2**	**NH**
δ_{free}	7.58	7.23	5.96	5.66	2.91	7.42
δ_{bound}	7.44	7.11	5.67	5.85	3.36	10.52
Δδ	-0.14	-0.12	-0.29	+0.19	-0.45	3.1

2 vs **TBA·Cl**

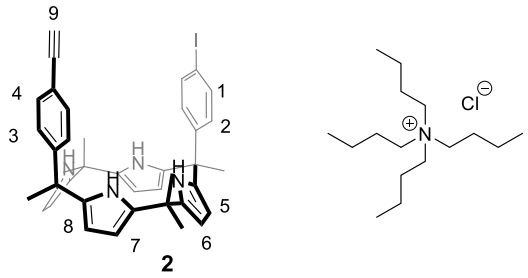

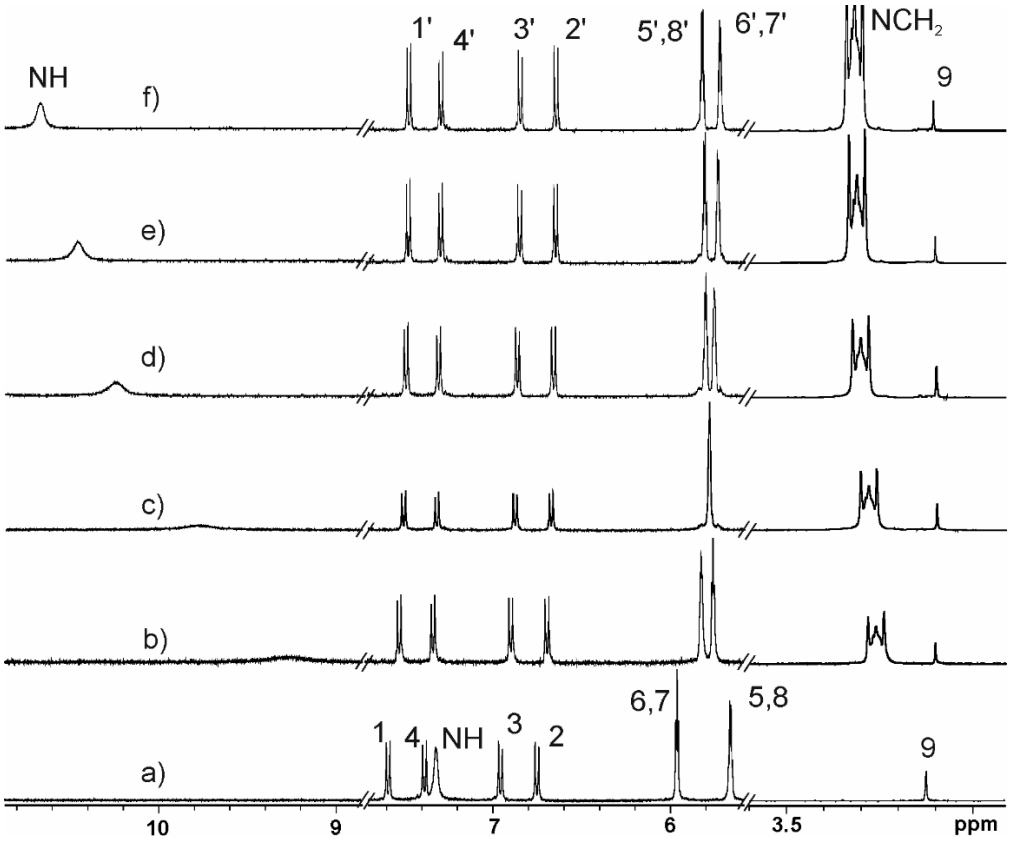

Figure S 26: *Selected regions of the ^{1}H NMR spectra (400 MHz, CD_2Cl_2, 298 K) of* ***2*** *(5 mM) (a) with incremental amounts of* ***TBACl*** *b) 2 equiv.; c) 3 equiv.; d) 5 equiv.; e) 7.5 equiv. and f) 11.5 equiv. See top panel for proton assignment.*

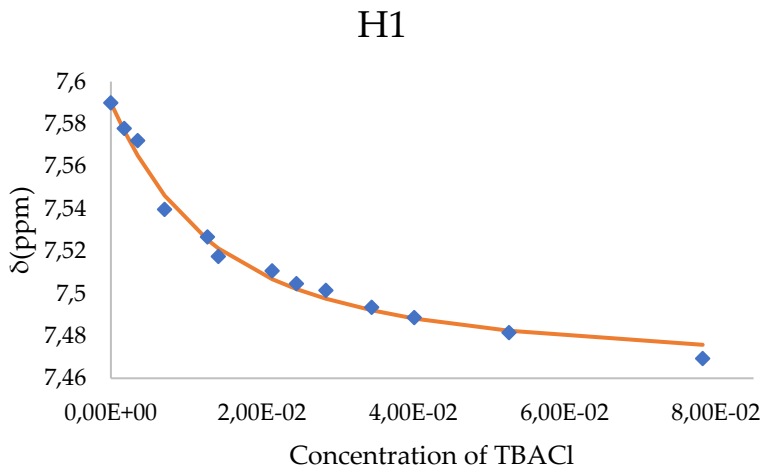

Figure S 27: *Chemical shifts of aromatic protons H1 of* ***2*** *upon incremental amounts of* ***TBACl*** *and fit of the NMR titration data to a theoretical 1:1 binding model.*

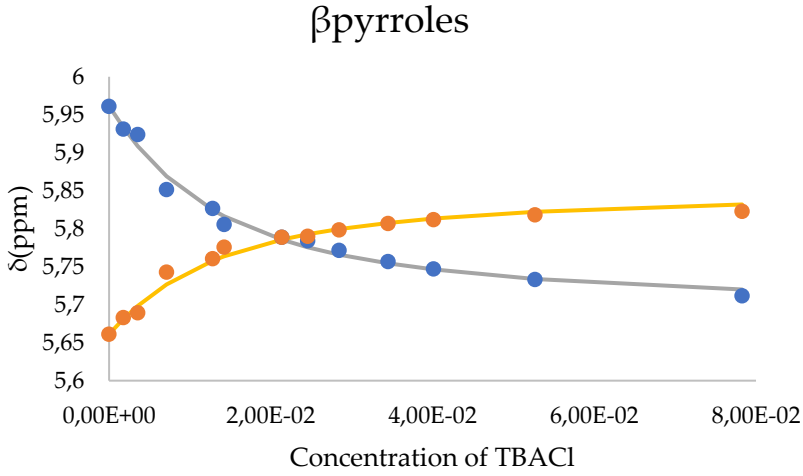

Figure S 28: *Chemical shifts of β- pyrroles protons of* ***2*** *upon incremental amounts of* ***TBACl*** *and fit of the NMR titration data to a theoretical 1:1 binding model.*

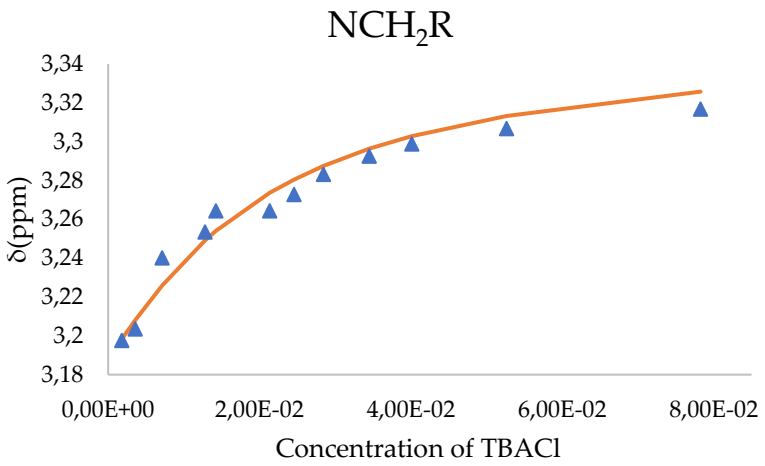

Figure S 29: *Chemical shifts of CH_2 protons α to the nitrogen atom of **TBA⁺** cation upon incremental amounts of **TBACl** and fit of the NMR titration data to a theoretical 1:1 binding model.*

	H1	**H4**	**β-pyrroles H6, H7**	**β-pyrroles H5, H8**	**NCH_2**	**NH**
δ_{free}	7.59	7.38	5.96	5.66	2.97	7.33
δ_{bound}	7.46	7.28	5.69	5.85	3.36	10.75
Δδ	-0.13	-0.10	-0.3	+0.19	-0.39	3.42

Table S 2: *Table of induced chemical shifts of **2** upon addition of **TBACl**.*

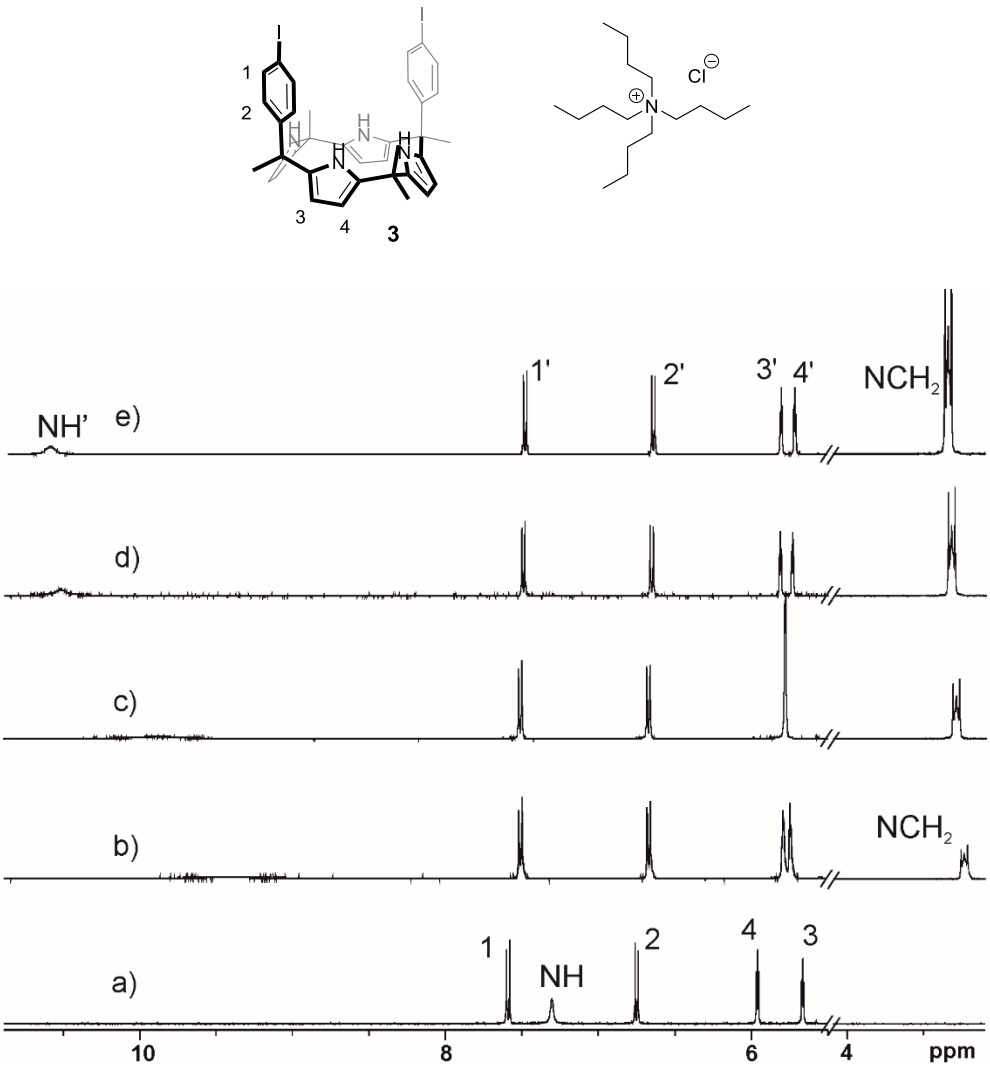

Figure S 30: Selected regions *the ^{1}H NMR spectra (400 MHz, CD_2Cl_2, 298 K) of **3** (5 mM) (a) with incremental amounts of **TBACl** b) 2 equiv.; c) 3 equiv.; d) 5 equiv. and e) 9 equiv. See top panel for proton assignment.*

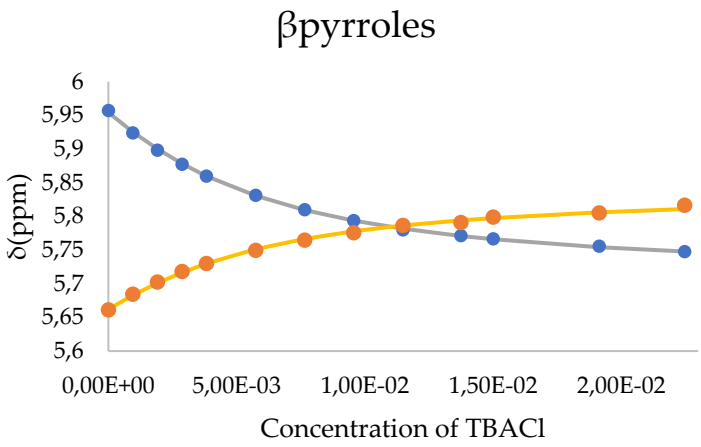

Figure S 31: *Chemical shifts of β- pyrroles protons of* ***3*** *upon incremental amounts of* ***TBACl*** *and fit of the NMR titration data into a theoretical 1:1 binding model.*

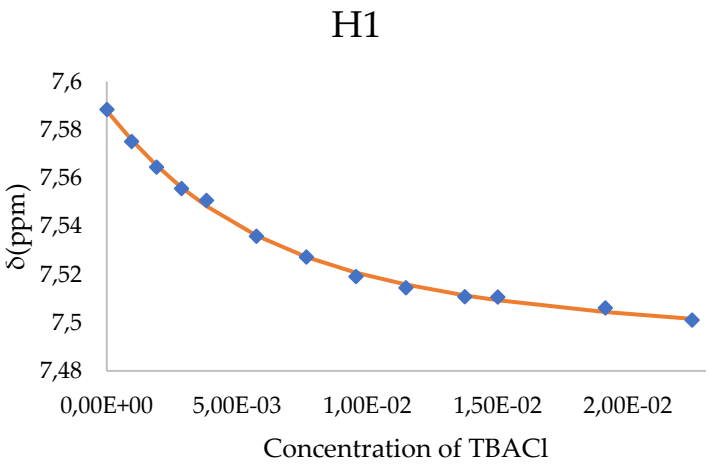

Figure S 32: *Chemical shifts of aromatic protons H1 of* ***3*** *upon incremental amounts of* ***TBACl*** *and fit of the NMR titration data to a theoretical 1:1 binding model.*

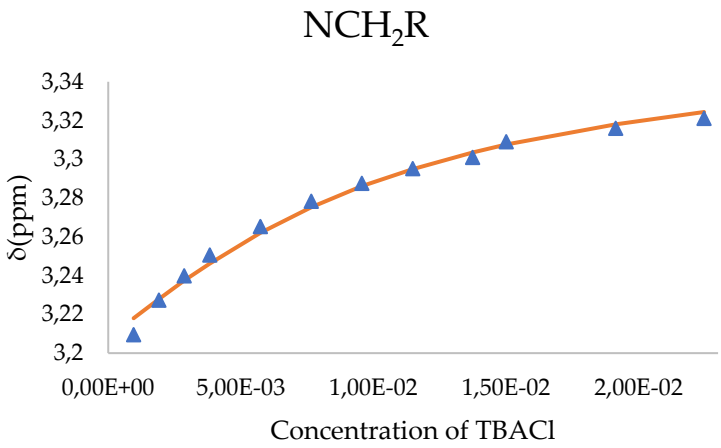

Figure S 33: *Chemical shifts of the CH_2 protons α to the nitrogen atom of* ***TBA***$^+$ *cation· upon incremental amount of* ***TBACl*** *and fit of the NMR titration data to a theoretical 1:1 binding model.*

Table S 3: *Table of induced chemical shifts of* ***3*** *upon addition of* ***TBACl****.*

	H1	**H2**	**β-pyrroles H4**	**β-pyrroles H3**	**NCH_2**	**NH**
δ_{free}	7.59	6.75	5.96	5.66	3.20	7.30
δ_{bound}	7.49	6.65	5.73	5.81	3.32	10.60
Δδ	-0.1	-0.1	-0.23	+0.15	-0.12	3.3

^{1}H NMR titration in Acetone

2 vs TBA·Cl

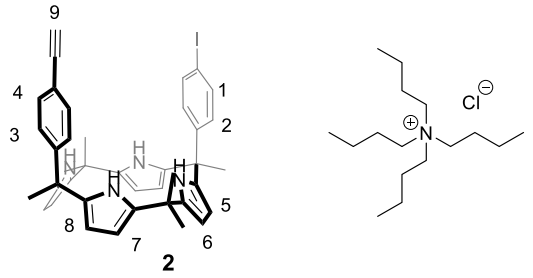

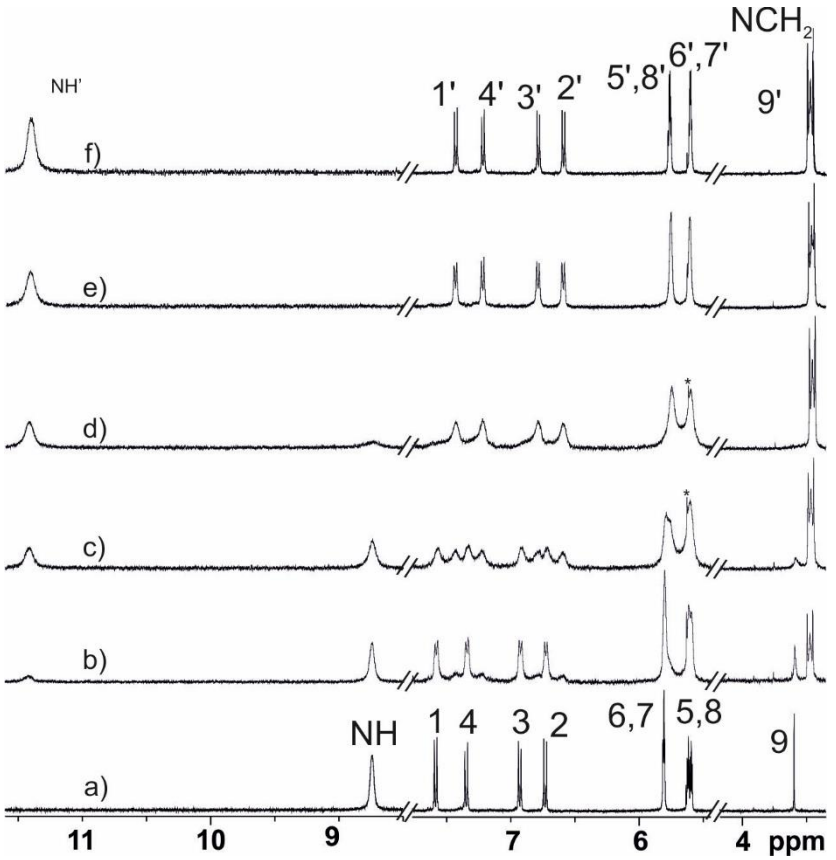

Figure S 34: Selected regions of*the ^{1}H NMR spectra (400 MHz, acetone-d_6, 298 K) of **2** (5 mM) (a) with incremental amounts of TBACl b) 0.25 equiv.; c) 0.5 equiv.; d) 0.75 equiv.; e) 1 equiv. and f) 1.2 equiv. See top panel for proton assignment. *Solvent residual peak.*

Chloride Binding Properties of a Macrocyclic Receptor Equipped with an Acetylide Gold(I) Complex

3 vs **TBA·Cl**

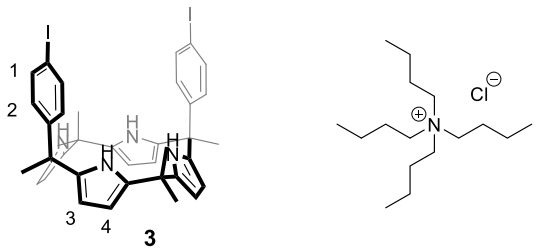

3

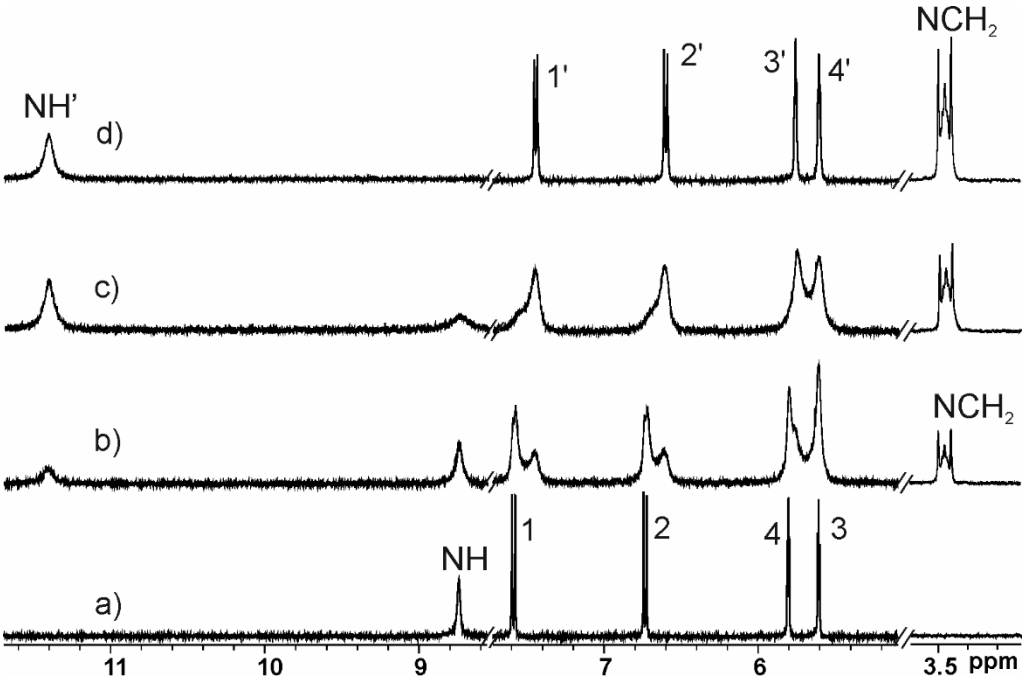

Figure S 35: Selected regions *of the ^{1}H NMR spectra (400 MHz, acetone-d_6, 298 K) of **3** (4.3 mM) (a) with incremental amounts of **TBACl** b) 0.25 equiv.; c) 0.5 equiv. and d) 1 equiv. See top panel for proton assignment*.

2.8.4 ITC binding studies

All titrations were performed by injecting small aliquots (8 µL, 16 s) of acetone solution of the TBACl from a computer controlled micro syringe into the solution of the hosts (3, 2 and 2Au, 0.6-0.8 mM) in the same solvent placed in the cell. The concentration of the TBACl solutions were approximately ten times more concentrated than the receptor ones (6.5-7.7 mM). The temperature was set to 288 K. The apparent association constants and enthalpy values were derived from the fit of the titration data to a 1:1 binding model using the Microcal ITC Data Analysis module.

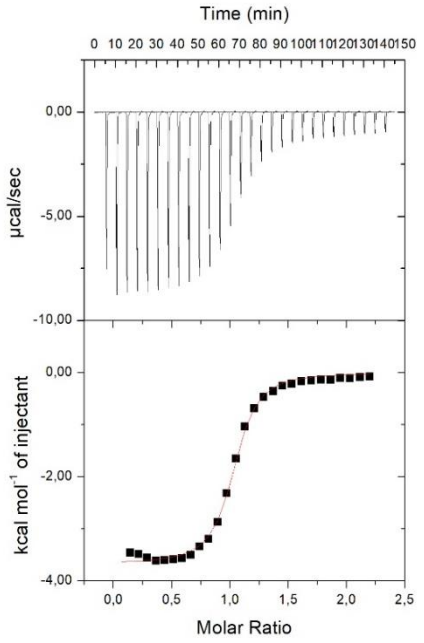

Figure S 36: *(Top) Raw data for the ITC titrations of receptor **3** with **TBACl** at 288K in acetone. Bottom) Normalized integration of heat vs **TBACl** / **3** molar ratio; the fit of the experimental data to the one set of sites binding isotherm (red line) is also shown. [**TBACl**] = 6.56 mM and [**3**] = 0.64 mM.*

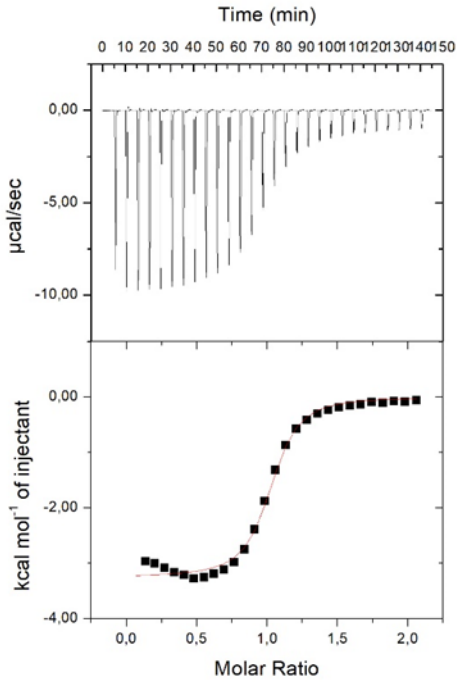

Figure S 37: *(Top) Raw data for the ITC titrations of receptor **2** with **TBACl** at 288K in acetone. Bottom) Normalized integration of heat vs **TBACl** / **2** molar ratio; the fit of the experimental data to the one set of sites binding isotherm (red line) is also shown. [**TBACl**] = 7.72 mM and [**2**] = 0.8 mM.*

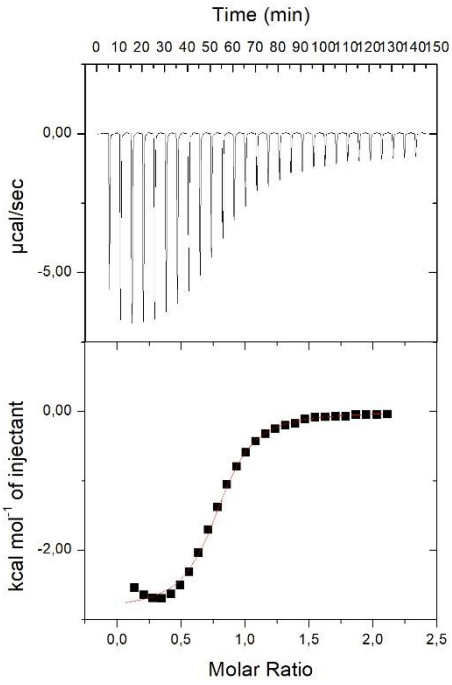

Figure S 38: *(Top) Raw data for the ITC titrations of receptor* ***2Au*** *with* ***TBA·Cl*** *at 288 K in acetone. Bottom) Normalized integration of heat vs* ***TBACl*** */1 molar ratio; the fit of the experimental data to the one set of sites binding isotherm (red line) is also shown. [****TBACl****] = 6.56 mM and [****2Au****] = 0.66 mM.*

Table S 4: *Binding constants (K) and the thermodynamic parameters (ΔH, TΔS and ΔG in Kcal·mol^{-1}) obtained from the ITC titration experiments of* ***TBACl*** *and* ***2, 3*** *and* ***2Au*** *at 288 K in acetone.*

Receptor	**2Au**	**2**	**3**
ΔH	-2.83±0.01	-3.29±0.08	-3.70±0.04
TΔS	3.43±0.03	3.25±0.09	3.13±0.04
ΔG	-6.25±0.09	-6.54±0.05	-6.83±0.05
$K_a \times 10^{-4}$	5.54±0.13	9.17±0.628	15.1±0.1

Chloride Binding Properties of a Macrocyclic Receptor Equipped with an Acetylide Gold(I) Complex

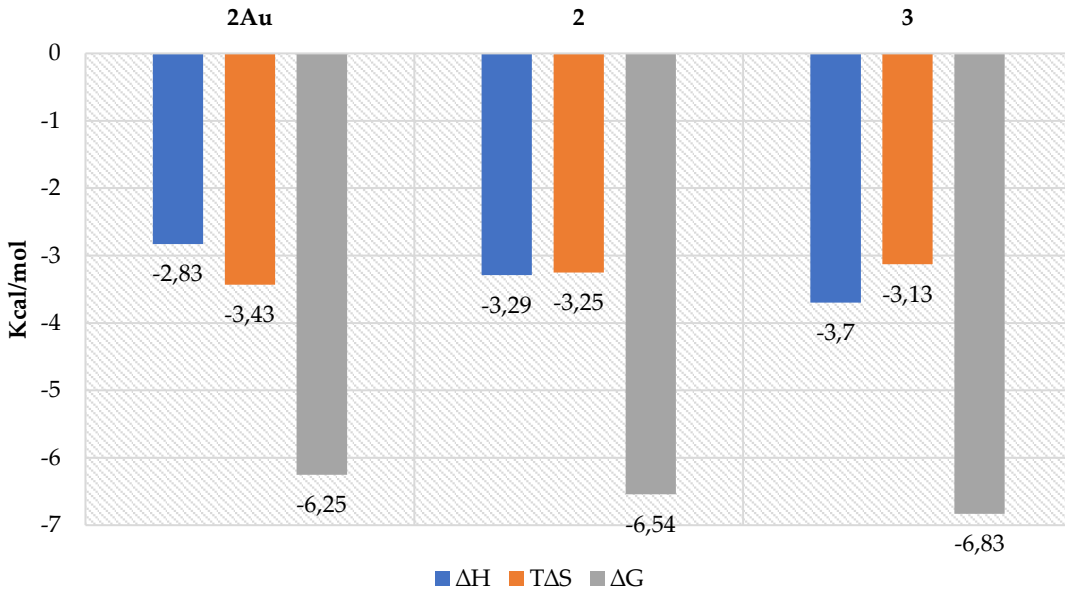

Figure S 39: *Thermodynamic parameters (ΔH, TΔS and ΔG in Kcal·mol^{-1}) of the 1:1 complexes of* ***2Au***, ***2*** *and* ***3*** *with TBACl in acetone*

2.8.5 Study of the formation of the anionic-bis(alkynyl)gold(I) complexes $[7Au]^-$ and $[8Au]^-$

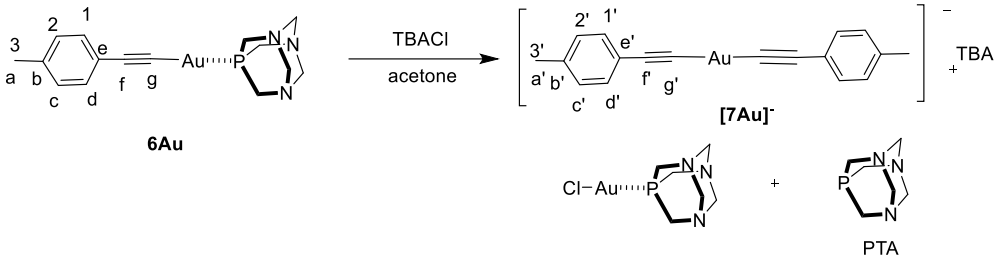

Scheme S 6. *Reaction of **6Au** with an excess of TBACl to produce the dimeric anionic species [**7Au**]-*

Chloride Binding Properties of a Macrocyclic Receptor Equipped with an Acetylide Gold(I) Complex

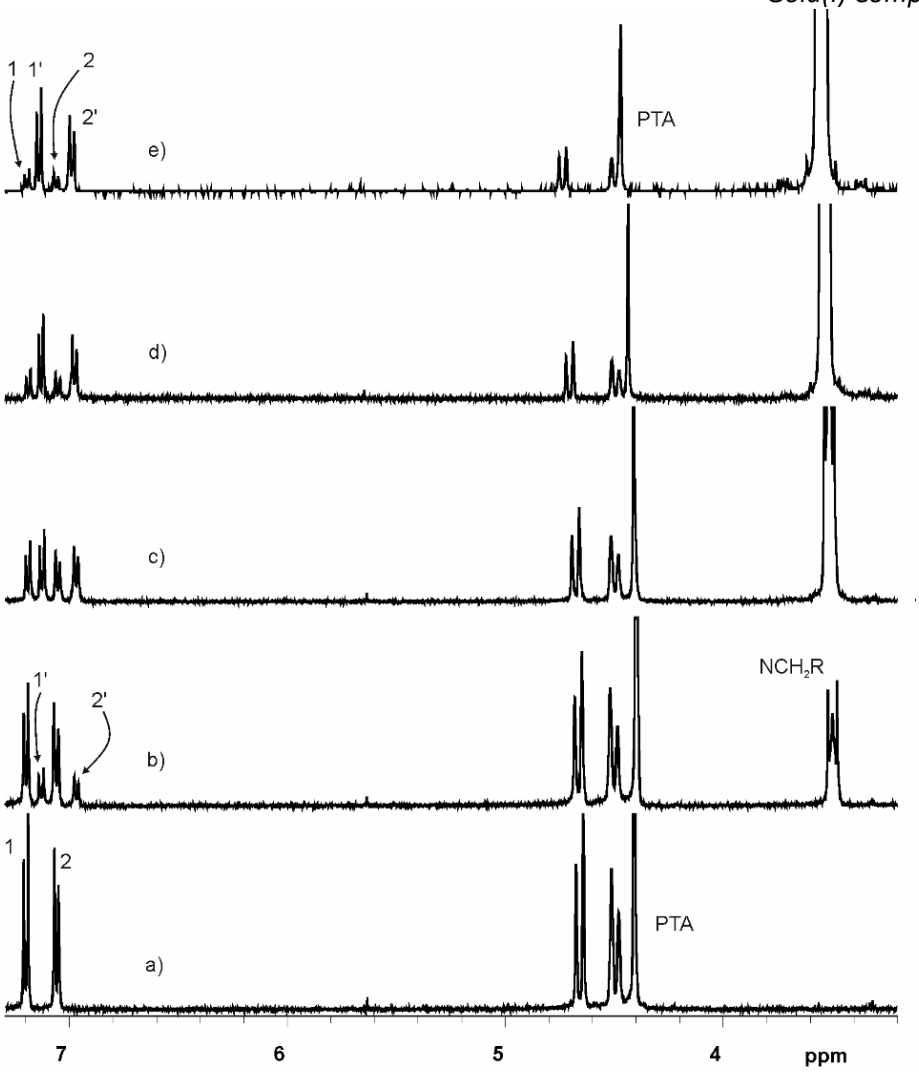

Figure S 40: *Selected region of the ^{1}H NMR spectra (400 MHz, acetone-d_6, 298 K) of the model compound* ***6Au*** *(5 mM) (a) with incremental amounts of TBACl b) 0.5 equiv.; c) 1.7 equiv.; d) 5 equiv. and e) 9 equiv. See scheme S6 for proton assignment.*

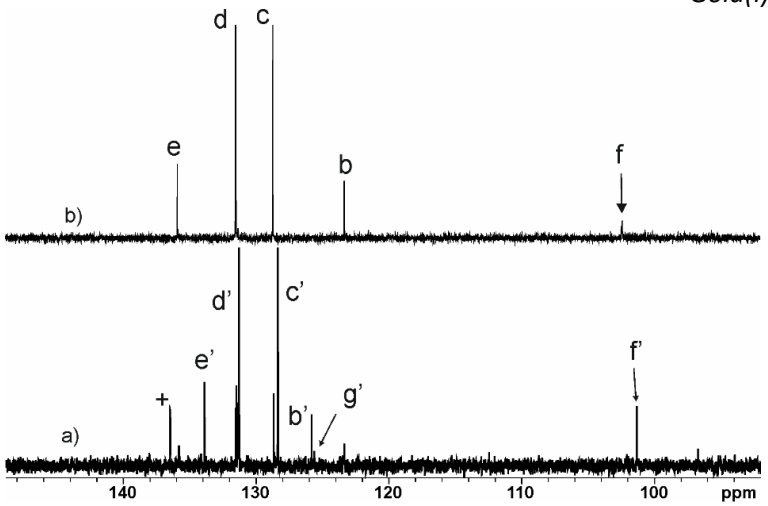

Figure S 41: *Selected region of the ^{13}C NMR (125 MHz, acetone-d_6, 298 K) spectra of the model compound* ***6Au*** *(5 mM) after the addition of 9 equiv. of TBACl (producing the anionic complex [****7Au****]$^-$) and b) the model compound* ***6Au*** *(5 mM). See scheme S6 for proton assignment.*

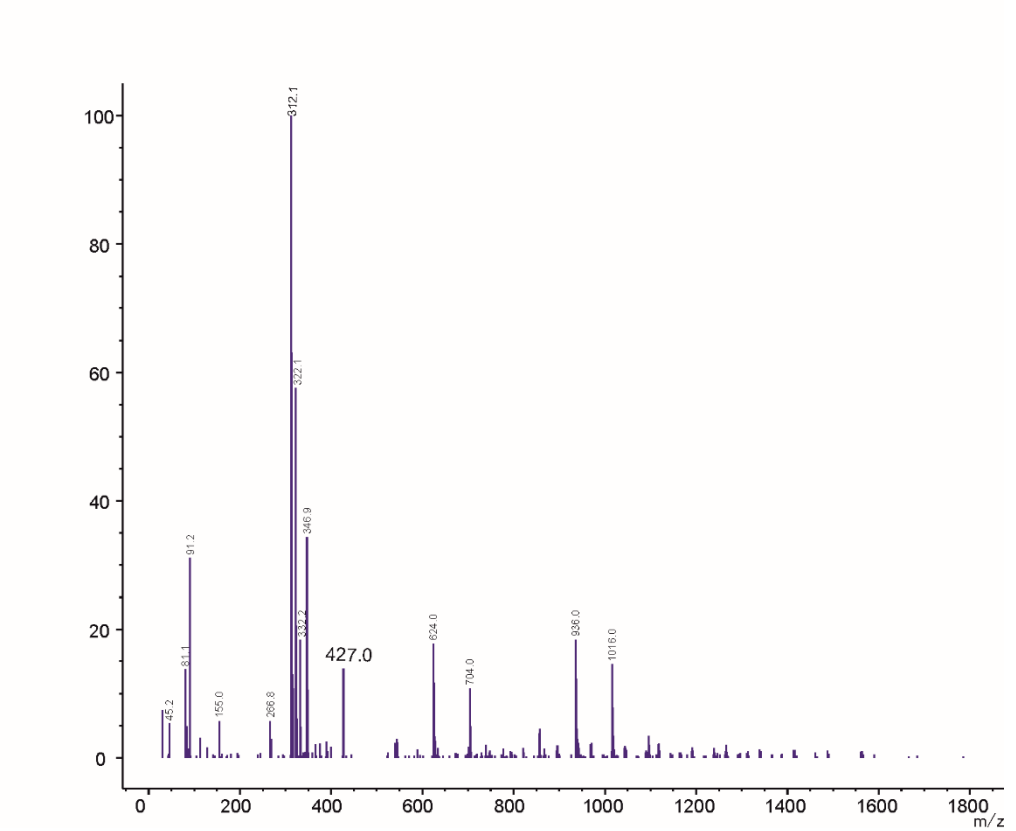

Figure S 42: MS (*I ESI/q; negative mode) of* ***[7Au]***$^{-}$.

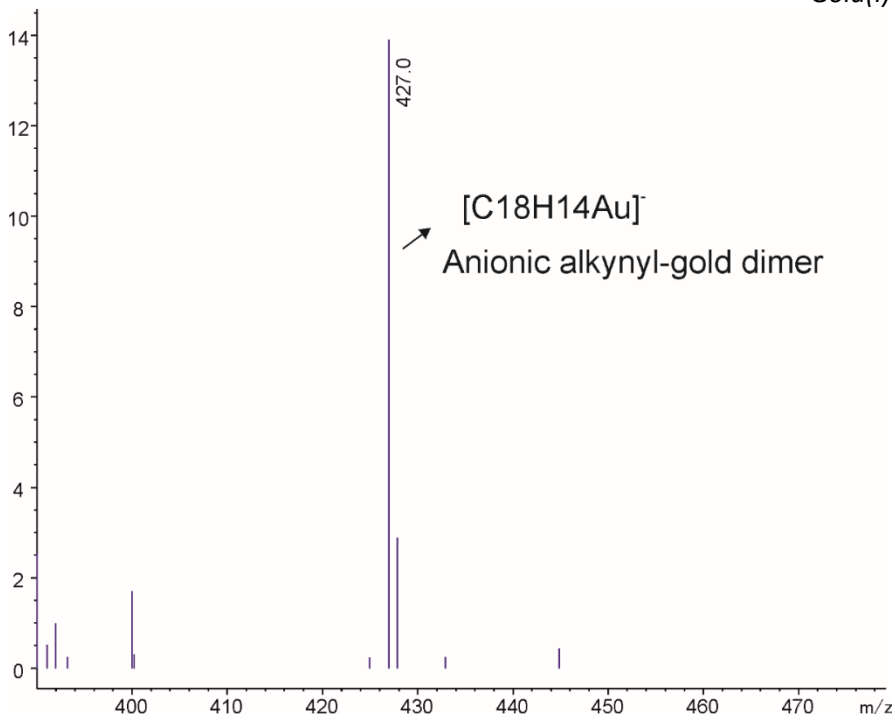

Figure S 43: *Selected region of the MS (ESI/q; negative mode) of [**7Au**]-. The peak at m/z = 427.0 corresponds to the molecular ion of the anionic bis(alkynyl)gold(I) complex [**7Au**]-.*

Chloride Binding Properties of a Macrocyclic Receptor Equipped with an Acetylide Gold(I) Complex

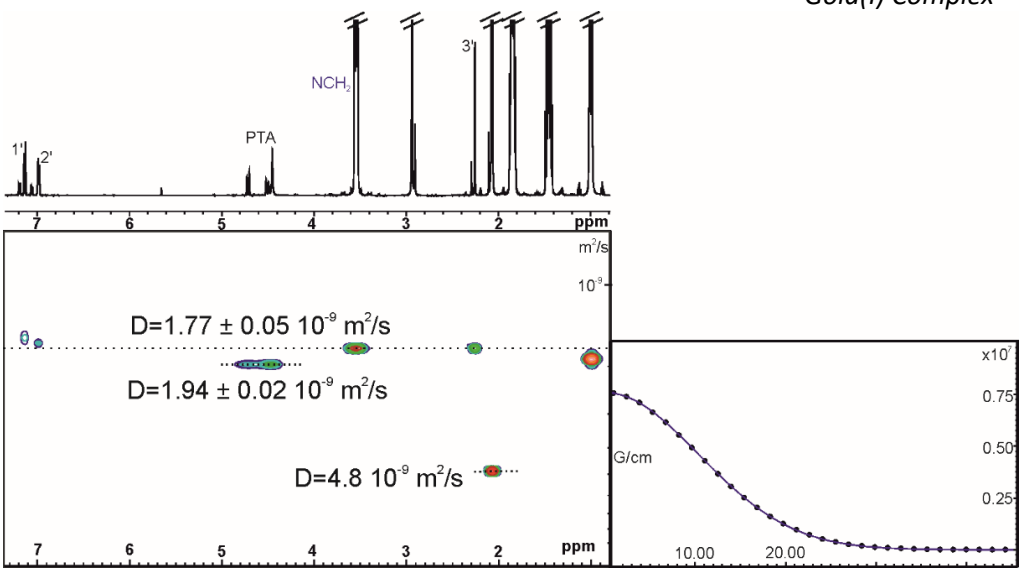

Figure S 44: *Left) ^{1}H Pseudo 2D plot of DOSY NMR (500 MHz, acetone-d_6, 298 K, d20=0.15 s; p30 = 750 ms) of a solution mixture of **6Au** and [**7Au**]$^-$. Right) Fit of the decay of the signal 2' to a mono-exponential function. Primed letters correspond to the protons of the anionic bis(alkynyl)gold(I) complex [**7Au**]$^-$. See scheme S 6 for proton assignment. Errors are indicated as standard deviations.*

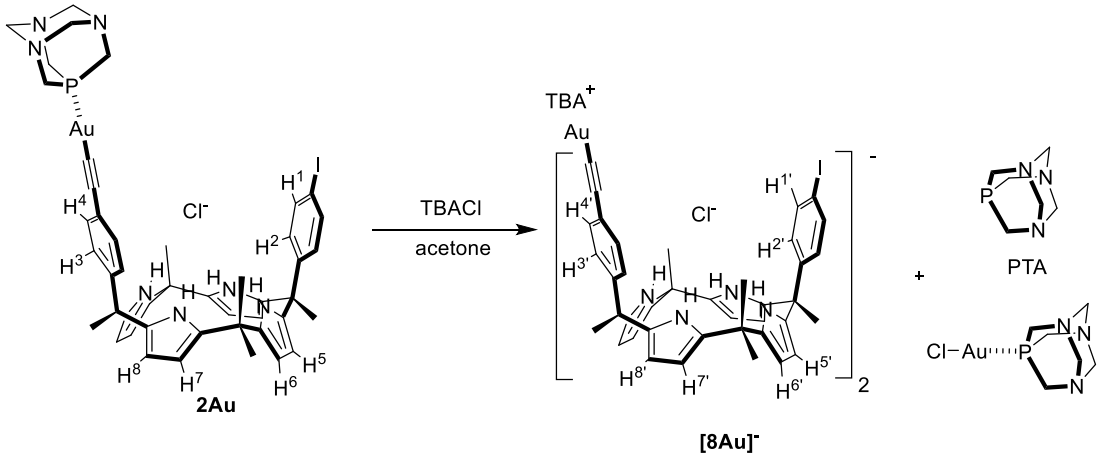

Scheme S 7. *Scheme of the side reaction of the chloride complex of **2Au** with and excess of TBACl to produce chloride complexes of the anionic dimer [**8Au**]$^-$.*

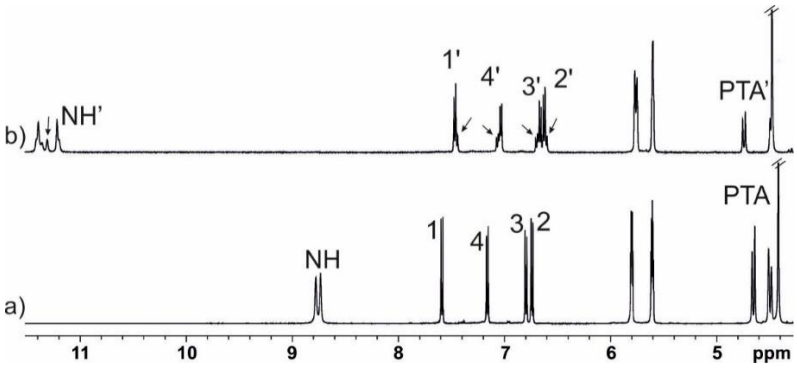

Figure S 45: *Selected region of the ^{13}C NMR (500 MHz, acetone-d_6, 298 K) spectra of the model compound **2Au** (5 mM) after the addition of 9 equiv. of TBACl (producing the anionic complex [**8Au**]$^-$) and b) the model compound **2Au** (Black arrows indicate the presence of Cl$^-$●**2Au**). Primed letters correspond to the protons of the anionic bis(alkynyl)gold(I) complex [**8Au**]$^-$. See scheme S7 for proton assignment.*

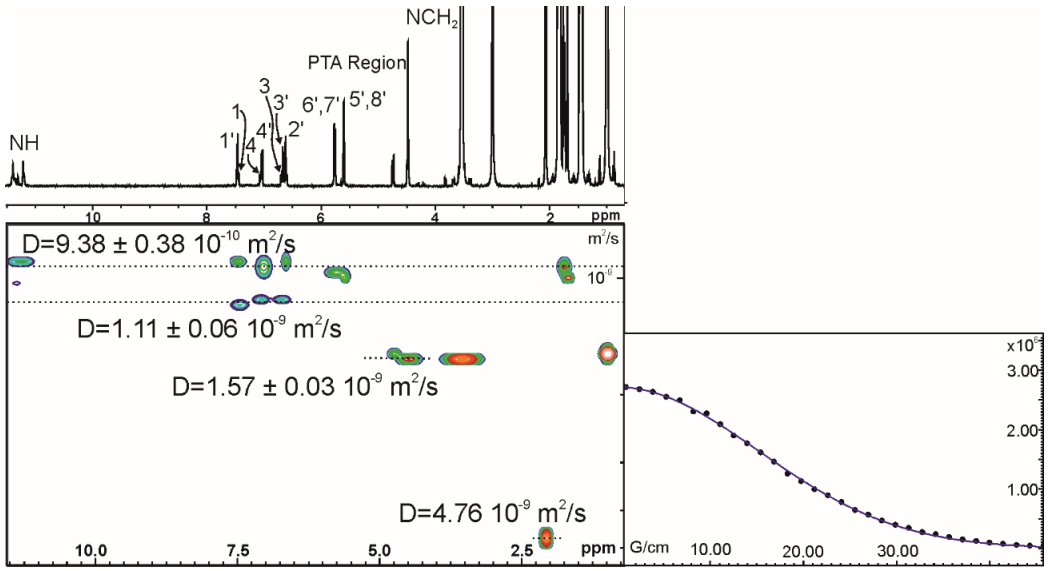

Figure S 46: *Left) ^1H Pseudo 2D plot of DOSY NMR (500 MHz, acetone-d_6, 298 K, d20=0.15s; p30 = 750 ms) of a solution of **2Au** with 9 equiv. of TBACl (producing anionic complex [**8Au**]$^-$). Right) Fit of the decay of the signal 4' to a mono-exponential function. Primed letters correspond to the protons of the anionic bis(alkynyl)gold(I) dimer [**8Au**]$^-$. See Scheme S 7 for proton assignment. Errors are indicated as standard deviations.*

2.8.6 ^{1}H NMR Pair-wise competitive experiments

A series of pair-wise NMR competitive titration experiments were performed using receptors **3, 2** and **2Au** (hosts A, B and C), and the TBACl (guest G) in acetone-d_6. Stock solutions of the hosts in acetone-d_6 were prerared. Equimolar 1:1:1 mixtures of two receptors and TBACl were prepared in independent NMR tubes by adding the appropiate amount of each stock solution in acetone-d_6 to reach a final concentration 4-5 mM (final volume: 500 µL). The ^{1}H NMR spectra were acquired at 213 K in order to observe separate signals for the bound and free species. The binding constant ratio between the two competing complexes (i.e. AG and BG) was determined by integration of selected proton signals in the acquired ^{1}H NMR spectra

In a general pair-wise experiment:

$$A + B + 2G \leftrightarrows AG + BG$$

the following equation was used to calculate the binding constant ratios using the NMR peak integrals:

$$K_{AG} = \frac{[AG]}{[A] * [G]} \; ; \; K_{BG} = \frac{[BG]}{[B] * [G]} \; ;$$

$$\frac{K_{AG}}{K_{BG}} = \frac{[AG] * [B]}{[BG] * [A]} \qquad (1)$$

Equation (1) can be presented as:

$$\frac{K_A}{K_B} = \frac{IntA_{bound} * IntB_{free}}{IntB_{bound} * IntA_{free}} \qquad (2)$$

Where $IntX_{status}$ is the value of the normalized *integral* of proton *X* of the free or bound hosts.

2Au vs 2

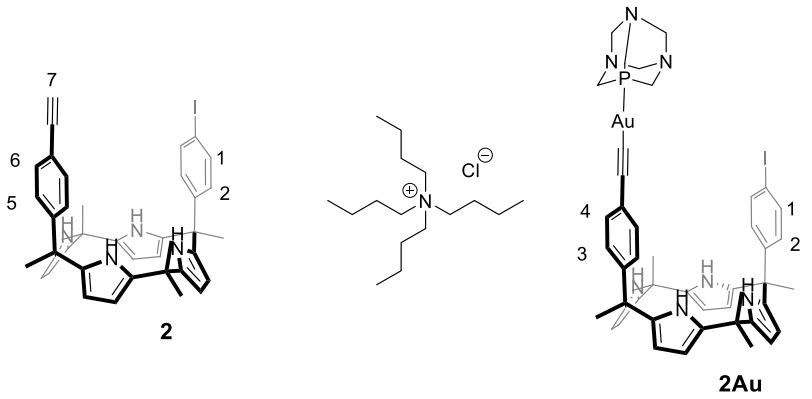

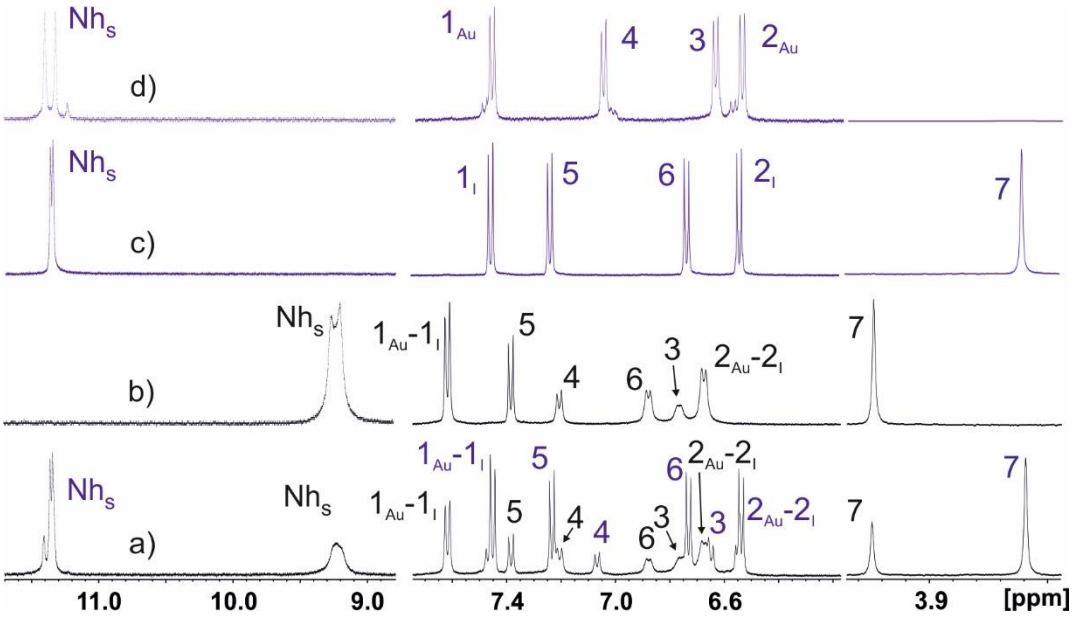

***Figure S 47**: Selected region of the ^{1}H NMR (500 MHz, acetone-d_6, 213 K) spectra of the pair-wise competitive experiment of **2Au, 2** and **TBA·Cl**: a) mixture of **2Au, 2** and **TBA·Cl** in a 1:1:1 molar ratio (4.3 mM); b) mixture of **2Au** and **2** in a 1:1 molar ratio (4.6 mM); c) mixture of **2** and **TBACl** in a 1:1 molar ratio (4.9 mM) (in blue); d) mixture of **2Au** and **TBA·Cl** in a 1:1 molar ratio (4.7 mM) (in blue). The scales of the regions are different in order to show the presence and/or the absence of the second set of signals. Black numbers and letters indicate the proton signals of free hosts; Blue numbers and letters indicate the proton signals of the complexes. See top panel for proton assignment.*

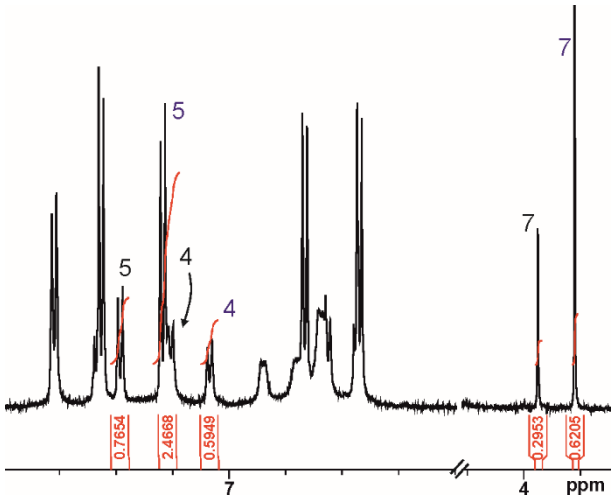

Figure S 48: *Selected regions of the ^{1}H spectrum of the mixture of* ***2Au, 2*** *and* ***TBA·Cl*** *in a 1:1:1 molar ratio (4.3 mM) showed in Figure S 48a displaying the values of the integrals used to calculate the binding constants ratio. Black numbers indicate the proton signals of free hosts; Blue numbers indicate the proton signals of the complexes. See top panel for the proton assignment.*

2 vs 3

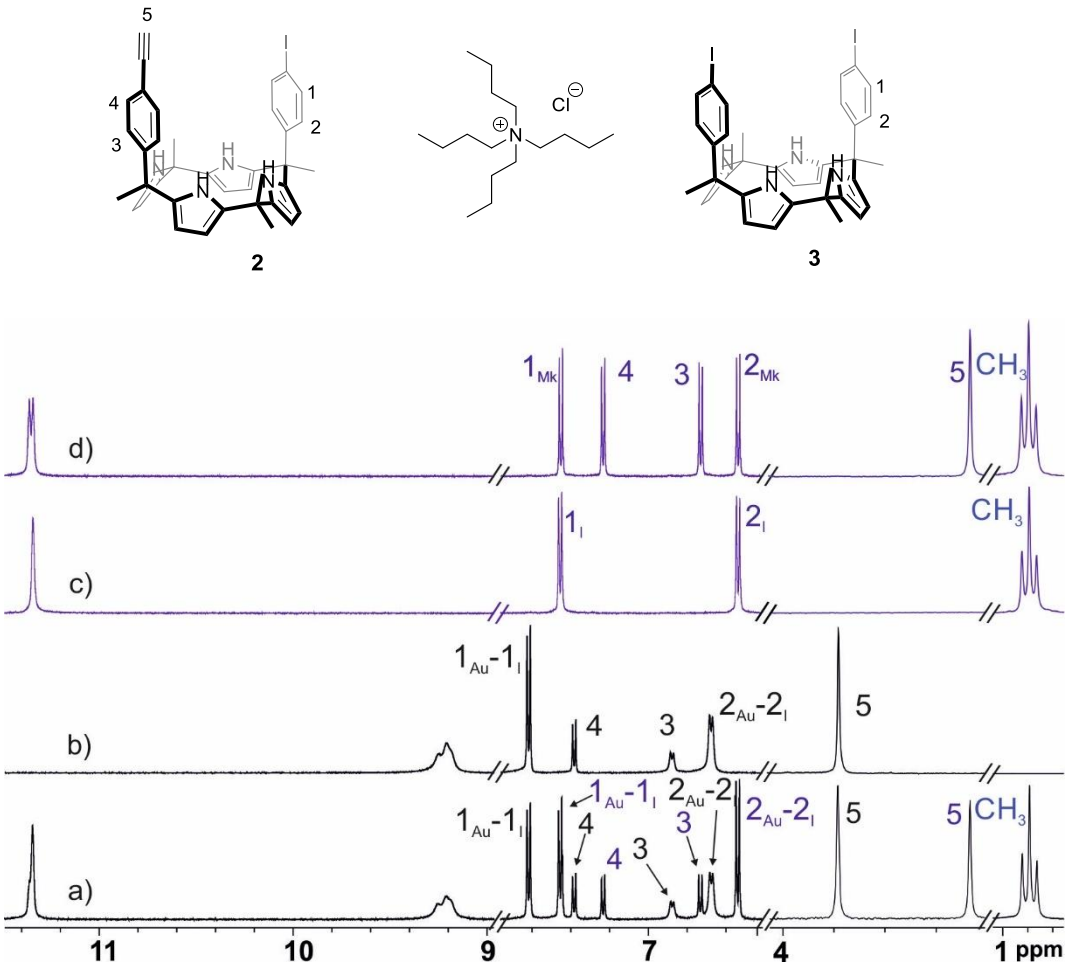

Figure S 49: *Selected region of the ^{1}H NMR (500 MHz, acetone-d_6, 213 K) spectra of the pair-wise competitive experiment of **2, 3** and **TBACl**: a) mixture of **2, 3** and **TBACl** in a 1:1:1 molar ratio (4.3 mM); b) mixture of **3** and **2** in a 1:1 molar ratio (4.6 mM); c) mixture of **3** and **TBACl** in a 1:1 molar ratio (4.9 mM) (in blue); d) mixture of **2** and **TBACl** in a 1:1 molar ratio (4.7 mM) (in blue). The scales of the regions are different. Black numbers and letters indicate the proton signals of free hosts; Blue numbers and letters indicate the proton signals of the complexes. See top panel for proton assignment*

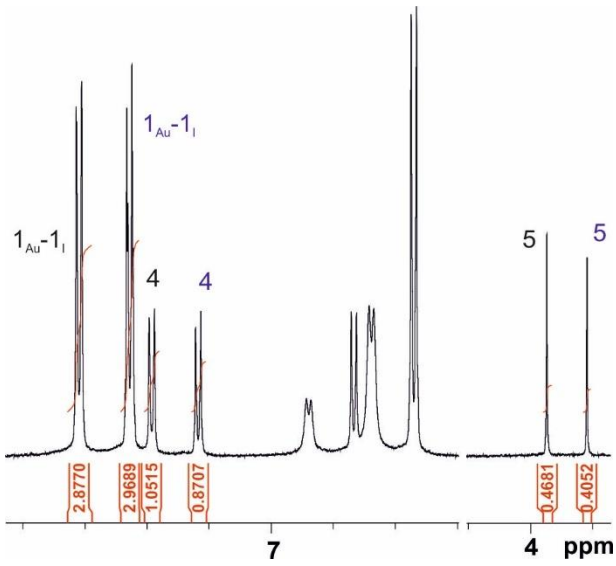

Figure S 50: *Selected regions of the ^{1}H spectrum of the mixture of **3, 2** and **TBA·Cl** in a 1:1:1 molar ratio (4.3 mM) showed in Figure S 50a displaying the values of the integrals used to calculate the binding constants ratio. Black numbers indicate the proton signals of free hosts; Blue numbers indicate the proton signals of the complexes*

UNIVERSITAT ROVIRA I VIRGILI
ARYL-EXTENDED CALIX[4]PYRROLE RECEPTORS WITH METAL CENTERS: ORGANOMETALLIC RECEPTORS AND METALLO-MACROCYCLES BASED ON COORDINATION BONDS
Andrea Rivoli

Chapter 3

Self-assembly of Metallocycles based on a *p*,*p*'-diethynyl "two wall" Calix[4]pyrrole diplatinum(II) complex.

Self-assembly of Metallocycles based on a-β,β'-diethynyl "two wall" Calix[4]pyrrole diplatinum(II) complex.

3.1 Introduction

Over the past decades, the use of supramolecular architectures for sensing and recognition of biologically relevant species has attracted considerable attention.[1,2,34,5] The binding properties (affinity and selectivity) of the most efficient supramolecular synthetic receptors derive from a three-dimensional architecture containing a polar cavity that mimics the binding pocket of proteins and enzymes.[6,7,8,9,10]

On the other hand, metal-mediated self-assembly is a well-known strategy for the spontaneous construction of discrete supramolecular architectures possessing

[1] . Kolesnichenko, I. V.; Anslyn, E. V., Practical applications of supramolecular chemistry. *Chem. Soc. Rev.* **2017,** *46*, 2385-2390.

[2] L.; Zha, D.; Anslyn, E. V., Recent Advances in Supramolecular Analytical Chemistry Using Optical Sensing. *Chem. Rev.* **2015,** *115*, 7840-7892.

[3] Beer, P. D.; Gale, P. A., Anion Recognition and Sensing: The State of the Art and Future Perspectives. *Angew. Chem. Int. Ed.* **2001,** *40*, 486-516.

[4] Moreno-Alcántar, G.; Casini, A., Bioinorganic supramolecular coordination complexes and their biomedical applications. *FEBS Lett.* **2023,** *597*, 191-202.

[5] Tao, Y.; Zhou, X.; Sun, L.; Lin, D.; Cai, H.; Chen, X.; Zhou, W.; Yang, B.; Hu, Z.; Yu, J.; Zhang, J.; Yang, X.; Yang, F.; Shen, B.; Qi, W.; Fu, Z.; Dai, J.; Cao, G., Highly efficient and robust π-FISH rainbow for multiplexed in situ detection of diverse biomolecules. *Nat. Commun.* **2023,** *14*, 443.

[6] Persch, E.; Dumele, O.; Diederich, F., Molecular Recognition in Chemical and Biological Systems. *Angew. Chem. Int. Ed.* **2015,** *54*, 3290-3327.

[7] Meyer, E. A.; Castellano, R. K.; Diederich, F., Interactions with Aromatic Rings in Chemical and Biological Recognition. *Angew. Chem. Int. Ed.* **2003,** *42*, 1210-1250..

[8] Krämer, J.; Grimm, L. M.; Zhong, C.; Hirtz, M.; Biedermann, F., A supramolecular cucurbit[8]uril-based rotaxane chemosensor for the optical tryptophan detection in human serum and urine. *Nat. Commun.* **2023,** *14*, 518.

[9] Geng, W.; Zheng, Z.; Jiang, H.; Guo, D., Nucleotide Recognition by a Guanidinocalixarene Receptor in Aqueous Solution. *Chem. Res. Chin. Univ.* **2023,** *39*, 144-150.

[10] Sierra, A. F.; Hernández-Alonso, D.; Romero, M. A.; González-Delgado, J. A.; Pischel, U.; Ballester, P., Optical Supramolecular Sensing of Creatinine. *J. Am. Chem. Soc.* **2020,** *142*, 4276-4284.

sizeable cavities able to include one or multiple copies of complementary guest molecules.[11,12,1314]

The rational design and synthesis of metal-mediated assemblies possessing defined shapes, sizes and functionalized interiors is based on the well-known coordination geometry, directionality and often-dynamic nature of the metal–ligand interactions. The combination of metal centers with multi-topic ligands leads to the formation of metal–mediated assemblies with cyclic, cage and polyhedron structures.[15,16,17]

The final structure of a metal-mediated assembly is instructed not only by the constrains of the ligands' covalent connectivity but also by those of the coordination geometry of the selected metal. For example, as shown in **Figure 1:** Change in the coordination geometry for quaterpyridine ligand depending on the specific interaction with different metals. (Left) mono-helicate arranged in square-planar metal Pd(II). (Right) double-helicate on tethraedric Cu(I) depending on the coordination geometry of the metal, the quaterpyridine can assume an helicate or double-helicate structure.

[11] Chen, B.; Holstein, J. J.; Platzek, A.; Schneider, L.; Wu, K.; Clever, G. H., Cooperativity of steric bulk and H-bonding in coordination sphere engineering: heteroleptic PdII cages and bowls by design. *Chem. Sci.* **2022,** *13* (6), 1829-1834.

[12] Sun, Y.; Chen, C.; Liu, J.; Stang, P. J., Recent developments in the construction and applications of platinum-based metallacycles and metallacages via coordination. *Chem. Soc. Rev.* **2020,** *49*, 3889-3919.

[13] Zheng, Y.-R.; Suntharalingam, K.; Johnstone, T. C.; Lippard, S. J., Encapsulation of Pt(IV) prodrugs within a Pt(II) cage for drug delivery. *Chem. Sci.* **2015,** *6*, 1189-1193.

[14] Benchimol, E.; Nguyen, B.-N. T.; Ronson, T. K.; Nitschke, J. R., Transformation networks of metal–organic cages controlled by chemical stimuli. *Chem. Soc. Rev.* **2022,** *51*, 5101-5135.

[15] Wu, K.; Tessarolo, J.; Baksi, A.; Clever, G. H., Guest-Modulated Circularly Polarized Luminescence by Ligand-to-Ligand Chirality Transfer in Heteroleptic PdII Coordination Cages. . *Angew. Chem., Int. Edition* **2022,** *61*, e202205725.

[16] Lescop, C., Coordination-Driven Syntheses of Compact Supramolecular Metallacycles toward Extended Metallo-organic Stacked Supramolecular Assemblies. *Acc. Chem. Res.***2017,** *50*, 885-894.

[17]Sepehrpour, H.; Fu, W.; Sun, Y.; Stang, P. J., Biomedically Relevant Self-Assembled Metallacycles and Metallacages. *J. Am. Chem. Soc.* **2019,** *141*, 14005-14020.

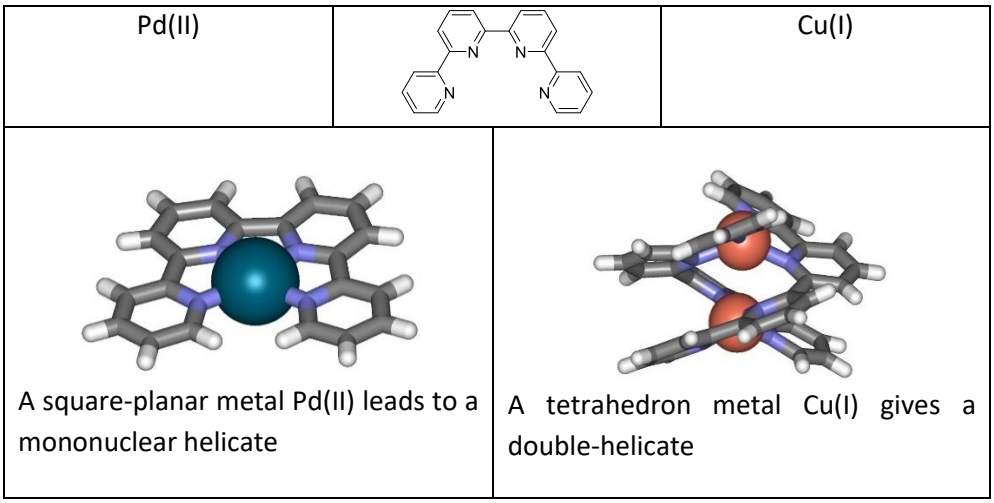

Figure 1: *Change in the coordination geometry for quaterpyridine ligand depending on the specific interaction with different metals. (Left) mono-helicate arranged in square-planar metal Pd(II). (Right) double-helicate on tethraedric Cu(I)*

In this context, the square-planar coordination geometry of Pt(II) and Pd(II) metal centers was used in conjunction with multi-topic nitrogenated ligands, such as pyridine derivatives, for the construction of a wide variety of metal mediated assemblies.[18,19,20] In short, metal-mediated self-assembly is a dynamic process, normally occurring under thermodynamic control and leading to the thermodynamically most stable supramolecular cyclic or oligo-cyclic aggregates.[21,22] Metal-mediated self-assembly can be considered as an algorithm translating covalent and coordination connectivity into tertiary structure.

In 2016, Miyaji an co-workers reported a di-nuclear cyclic-dimer of an α,α-dipyridyl-calix[4]pyrrole (C[4]P) derivative that was assembled via coordination with two *trans*-bis(triethylphosphine) palladium(II) metal centers (**Figure 2**). The

[18] Zheng, Y.-R.; Suntharalingam, K.; Johnstone, T. C.; Lippard, S. J., Encapsulation of Pt(IV) prodrugs within a Pt(II) cage for drug delivery. *Chem. Sci.* **2015,** *6*, 1189-1193.

[19] Y. Li, S. S. Rajasree, G. Y. Lee, J. Yu, J.-H. Tang, R. Ni, G. Li, K. N. Houk, P. Deria, P. J. Stang, *J. Am. Chem. Soc.* **2021**, *143*, 2908-2919.

[20]Sun, Q.; Escobar, L.; Ballester, P., A Dinuclear Metallobridged Super Aryl-Extended Calix[4]pyrrole Cavitand. *Angew. Chem. Int. Ed.* **2022,** *61*, e202202140.

[21] Northrop, B. H.; Yang, H.-B.; Stang, P. J., Coordination-driven self-assembly of functionalized supramolecular metallacycles. *Chem. Commun.* **2008**, 5896-5908.

[22] Wu K, Benchimol E, Baksi A, Clever G. Evolution of Multicomponent [Pd2ABCD] Cages. *ChemRxiv*. Cambridge: Cambridge Open Engage; 2023; This content is a preprint and has not been peer-reviewed.

supramolecular receptor was shown to selectively recognize tetrabutylammonium di-carboxylates like azelate and suberate by hydrogen bonding to the two C[4]Ps .[23]

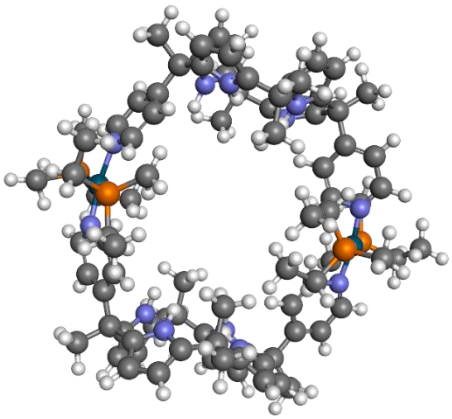

***Figure 2**:Molecular modeling of Miyaji's C[4]P-based Pd(II) cage.*

The possibility to mold as the architectures of the metal-mediated assemblies expanded their applications in multiple areas that include their use as alternative material to conventional biomedical counterparts[24] and in advanced photophysical studies of opening and closing dynamics in coordination cages.[25] As mentioned above, many metal-mediated assemblies possess sizable well-defined cavities suitable to encapsulate small molecules (guests) by establishing multiple intermolecular interactions.[26] This feature makes that metal-mediated assemblies can also be used as synthetic receptors in selective molecular recognition processes. [27] However, the achievement of selective and high-affinity molecular recognition using synthetic metallo-cycles is not trivial. Multiple factors influence the binding properties (selectivity and affinity) of the metallomacrocyles. These include the

[23] Kiriyama, N.; Ebihara, M.; Udagawa, T.; Miyaji, H., Self-organization of dipyridylcalix[4]pyrrole into a supramolecular cage for dicarboxylates. *RSC Advances* **2016,** *6* , 19794-19796.
[24] Sepehrpour, H.; Fu, W.; Sun, Y.; Stang, P. J., Biomedically Relevant Self-Assembled Metallacycles and Metallacages. *J. Am. Chem. Soc.* **2019,** *141*, 14005-14020.
[25] Artmann, K.; Li, R.-J.; Juber, S.; Benchimol, E.; Schäfer, L. V.; Clever, G. H.; Nuernberger, P., Steering the Ultrafast Opening and Closure Dynamics of a Photochromic Coordination Cage by Guest Molecules. *Angew. Chem. Int. Ed.* **2022,** *61*, e202212112.
[26] Cai, L.-X.; Li, S.-C.; Yan, D.-N.; Zhou, L.-P.; Guo, F.; Sun, Q.-F., Water-Soluble Redox-Active Cage Hosting Polyoxometalates for Selective Desulfurization Catalysis. *J. Am. Chem. Soc.* **2018,** *140*, 4869-4876.
[27] Tamura, Y.; Takezawa, H.; Fujita, M., A Double-Walled Knotted Cage for Guest-Adaptive Molecular Recognition. *J. Am. Chem. Soc.* **2020,** *142*, 5504-5508.

intermolecular forces involved and the shape, size and function complementarity that exist between the metallocycle binding site and the targeted guest. In 2020, Barbour *et al.* assembled a copper based metallocycle ($Cu_2L_2Cl_4$) able to discriminate between the three xylene isomers over a wide concentration range. The order of the binding selectivity displayed by the receptors was *p*-xylene ≫ *m*-xylene ≫ *o*-xylene (**Figure 3**).[28]

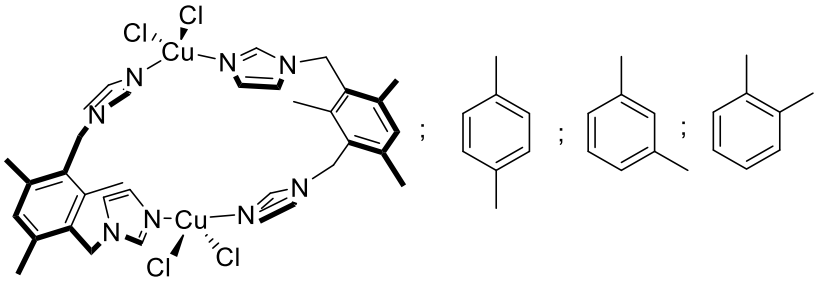

Figure 3: *Line drawing of the Cu-based metallocycle ($Cu_2L_2Cl_4$) Barbours' cages with the guest in order of selectivity;*

In 2020 Stang *et al*. reported the incorporation of pillar[5]arene units into a hexagonal Pt(II) metallacycle. The binding of the guest to the metallacycle in solvent mixtures (water/acetone) caused its co-aggregation inducing an increase in fluorescence intensity (**Figure 4**).[29]

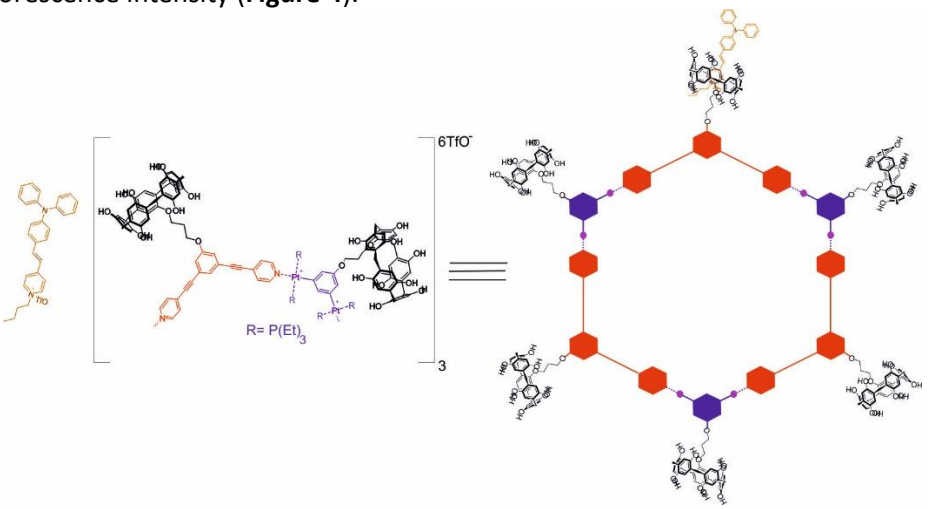

Figure 4: *Stang's hexagonal Pt(II) metallacycle with the fluorescent guest.*

[28] du Plessis, M.; Nikolayenko, V. I.; Barbour, L. J., Record-Setting Selectivity for p-Xylene by an Intrinsically Porous Zero-Dimensional Metallocycle. *J. Am. Chem. Soc.* **2020,** *142*, 4529-4533.

[29] Tuo, W.; Sun, Y.; Lu, S.; Li, X.; Sun, Y.; Stang, P. J., Pillar[5]arene-Containing Metallacycles and Host–Guest Interaction Caused Aggregation-Induced Emission Enhancement Platforms. *J. Am. Chem. Soc.* **2020,** *142*, 16930-16934.

In this chapter, we describe our results on the self-assembly of metal-mediated oligo-macrocycles consisting on a di-ethynyl-"two-wall" calix[4]pyrrole di-platinum(II)-organometallic complex and a series of bis-pyridine ligands (***Figure 5***).[30] We also report ^{1}H NMR titration experiments of the self-assembled metallocycles with pyridine *N*-oxide derivatives. We undertook these experiments with the aim to evaluate the binding properties of the prepared metallocycles.

3.2 Results and discussion

3.2.1 Synthesis

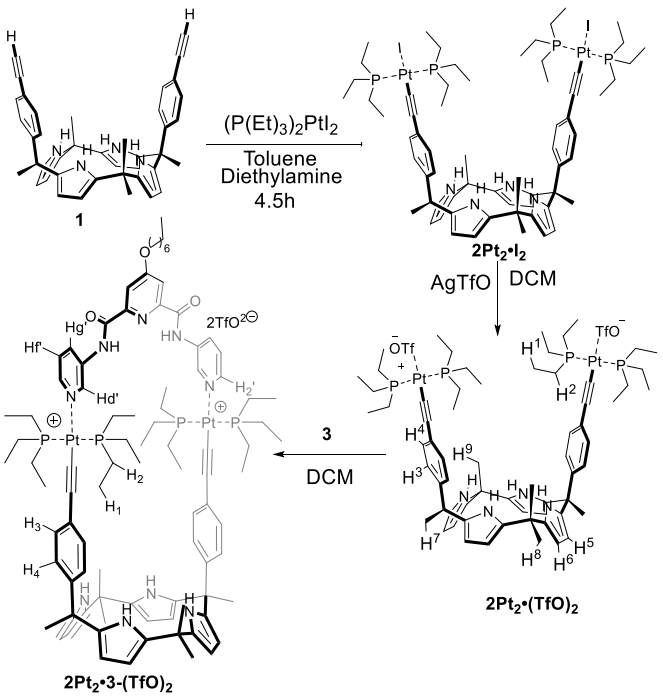

Scheme 1: *Synthetic scheme for the preparation of the "two wall" di-ethynyl calix[4]pyrrole di-platinum complexes* **$2Pt_2$ •I_2** *and* •OTf_2 *and the self-assembly of the metal-mediated macrocycle* **$2Pt_2$•3-$(TfO)_2$** *Proton assignment is included for* **$2Pt_2$•3-$(TfO)_2$** and **$2Pt_2$•$(TfO)_2$**

[30] Shanmugaraju, S.; Joshi, S. A.; Mukherjee, P. S., Self-Assembly of Metallamacrocycles Using a Dinuclear Organometallic Acceptor: Synthesis, Characterization, and Sensing Study. *Inorg. Chem.* **2011**, *50*, 11736-11745.

The calix[4]pyrrole bis-nuclear Pt(II) acetylide complex ***2*Pt$_2$•*(TfO)$_2$*** contains a *p,p*'-diethynyl α,α-"two wall" calix[4]pyrrole ligand. We prepared the organometallic complex ***2*Pt$_2$•*(TfO)$_2$*** in two synthetic steps starting from the *meso*-hexamethyl-10α,20α-bis-*p*-ethynylphenyl-calix[4]pyrrole ligand **1**[31] (***Scheme 1***).

Metalation of ligand **1** with $(P(Et)_3)_2PtI_2$ in dry toluene using dry diethylamine as base allowed the isolation of the unprecedented di-ethynyl-di-nuclear Pt(II) calix[4]pyrrole ***2*Pt$_2$•I$_2$*** in 45% yield after purification by column chromatography. We performed the iodine metathesis of ***2*Pt$_2$•I$_2$*** by adding an equimolar amount of AgTfO in dry dichloromethane (DCM) solution under Ar atmosphere. The resulting suspension was transferred through a cannula and filtered using celite. The desired triflate salt ***2*Pt$_2$•(TfO)$_2$** was isolated as a brownish solid in 75% yield after removing the solvent under reduced pressure.

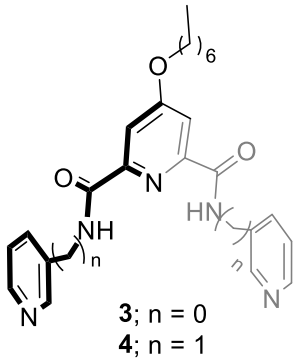

***Figure 5**:Line-drawing structures of the bis-pyridine ligands **3**-**4** used in this study.*

The amount of silver triflate used in the halogen metathesis reaction of ***2*Pt$_2$•I$_2$** producing ***2*Pt$_2$•(TfO)$_2$** (see **Scheme 1**) played a crucial role in the isolation of pure metallo-macrocycle ***2*Pt$_2$•(TfO)$_2$** (*vide infra*).

Self-assembly of the metallo-macrocycles

The metallo-macrocycles ***2*Pt$_2$•*3*-(TfO)$_2$** and ***2*Pt$_2$•*4*-(TfO)$_2$** were obtained via coordination driven self-assembly by mixing equimolar amounts of the ditopic-bipyridyl ligand **3** or **4** and the calix[4]pyrrole bis-nuclear Pt(II) acetylide complex ***2*Pt$_2$•(TfO)$_2$** (**Scheme 1**).

[31] Valderrey, V.; Escudero-Adán, E. C.; Ballester, P., Polyatomic Anion Assistance in the Assembly of [2]Pseudorotaxanes. *J. Am. Chem. Soc.* **2012,** *134* , 10733-10736.

In the initial self-assembly experiments of the metallo-macrocyle ***2***Pt_2•***3*****-(TfO)**$_2$ we used a solution of ***2*****Pt$_2$•(TfO)$_2$** containing unreacted AgTfO. This was due to the use of the silver salt in excess for the iodide metathesis reaction of the parent di-nuclear Pt(II) ***2*****Pt$_2$•I$_2$** complex.

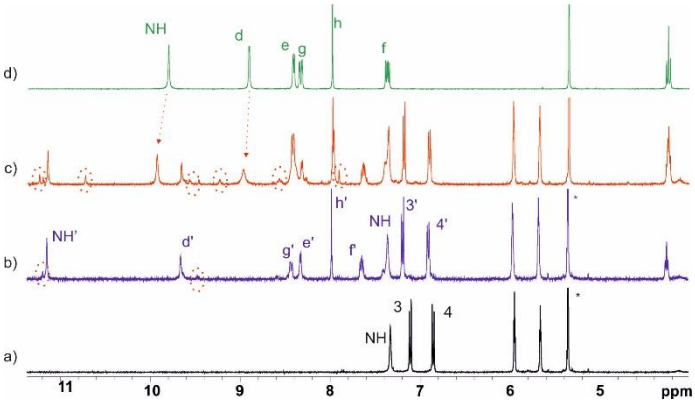

Figure 6*: ^{1}H NMR spectra (400 MHz, CH_2Cl_2, 298 K) of (a) calix[4]pyrrole **3**; b) the assembled macrocycle **2Pt$_2$•3-(TfO)$_2$**.; c) the assembled macrocycle **2Pt$_2$•3-(TfO)$_2$** with an excess of 1 equiv. of bis amide ligand **1**; d) bis amide ligand **1**. For proton assignments see **Scheme 1.***

Calix[4]pyrroles are known to act as heteroditopic receptor in the binding of ion-pairs.[32,33,34] At first, we hypothesized that to some extent the unreacted AgTfO might be bound to the calix[4]pyrrole unit of ***2*****Pt$_2$•(TfO)$_2$** yielding a 1:1 complex featuring receptor-separated binding mode. However, owing to the soft and non-coordinating character of the triflate anion we discarded this possibility as relevant. On the other hand, literature reports demonstrate that the mono-charged Ag^+ cation coordinates to pyridine derivatives producing linear Py•Ag^+•Py coordination complexes.[35,36] In our case, we anticipated that the bis-pyridine ligands **3** and **4** possessing a ditopic nature (***Figure 5***) might coordinate to the Ag^+ cation leading to the formation of aggregates in solution.

[32] Romero, J. R.; Aragay, G.; Ballester, P., Ion-pair recognition by a neutral [2]rotaxane based on a bis-calix[4]pyrrole cyclic component. *Chem. Sci.* **2017,** *8*, 491-498.
[33]Kim, S. K.; Sessler, J. L., Calix[4]pyrrole-Based Ion Pair Receptors. *Acc. Chem. Res.* **2014,** *47*, 2525-2536.
[34] Ciardi, M.; Galán, A.; Ballester, P., Tetra-phosphonate Calix[4]pyrrole Cavitands as Multitopic Receptors for the Recognition of Ion Pairs. *J. Am. Chem. Soc.* **2015,** *137*, 2047-2055.
[35] Kleinmaier, R.; Arenz, S.; Karim, A.; Carlsson, A.-C. C.; Erdélyi, M., Solvent effects on ^{15}N NMR coordination shifts. *Magn. Reson. Chem.* **2013,** *51*, 46-53.
[36] Wong, V. H. L.; White, A. J. P.; Hor, T. S. A.; Hii, K. K., Ligand Effect and Control of E- and Z-Selectivity in the Silver-Catalyzed Synthesis of 4-Bromooxazolines. *Adv. Synth. Catal.* **2015,** *357*, 2485-2491.

We monitored the self-assembly of the metallo-macrocycle ***2*Pt$_2$•*3*-(TfO)$_2$** using ^{1}H NMR spectroscopy. To a mM DCM solution of the di-nuclear C[4]P precursor ***2*Pt$_2$•(TfO)$_2$** containing residual AgTfO, we added incremental amounts of the di-pyridyl ligand **3**. In the presence of 1 equiv. of **3**, we exclusively observed the diagnostic proton signals of the quantitatively self-assembled metallo-macrocye ***2*Pt$_2$•*3*-(TfO)$_2$** (**Figure 6b** and **6c**). The addition of ligand **3** in excess produced the observation of a new set of proton signals that we assigned to the protons of ligand **3**. However, the chemical shifts of the observed proton signals did not coincide with those in the free ligand. We concluded that **3** in excess coordinated to the Ag^+ cation in solution producing oligomeric aggregates of unknown structures. We also detected a series of small signals. The small signals grew in intensity on addition of **3** in excess (more than 1 equiv.) (**Figure 6**). We assigned the new signals to the formation of the acyclic 2:1 complexes **2Pt$_2$•3$_2$-(TfO)$_2$**. Most likely, the effective molarity of the metallocycle is small and in the presence of excess ligand at mM concentration it opened up and produced the high stoichiometry acyclic complex. The metallo-cycle **2**Pt$_2$**•3-(TfO)$_2$** was characterized by a set of high-resolution spectra including multinuclear NMR spectroscopy ((^{1}H NMR and ^{31}P {^{1}H} NMR, COSY, ROESY) and mass spectrometry (ESI-TOF).

***Figure 7*b** depicts the ^{1}H NMR spectrum of the metallo-macrocycle **2Pt$_2$•3-(TfO)$_2$** assembled from an equimolar DCM solution of its two components. The precursor di-nuclear ***2*Pt$_2$•(TfO)$_2$** complex was obtained using a strict stoichiometric control of the AgTfO salt. The formation of the metallo-macrocycle **2Pt$_2$•3-(TfO)$_2$** was evidenced by the reduced downfield shifts experienced by the protons of the *meso*-aromatic substituent of the C[4]P unit ($\Delta\delta(H_3)$= 0.08 ppm and $\Delta\delta(H_4)$= 0.05 ppm, see Scheme 1 for assignments). In contrast, the signals of the protons of the triethyl phosphine ligands moved upfield ($\Delta\delta(H_2)$= -0.19 ppm and $\Delta\delta(H1)$= -0.02 ppm)).

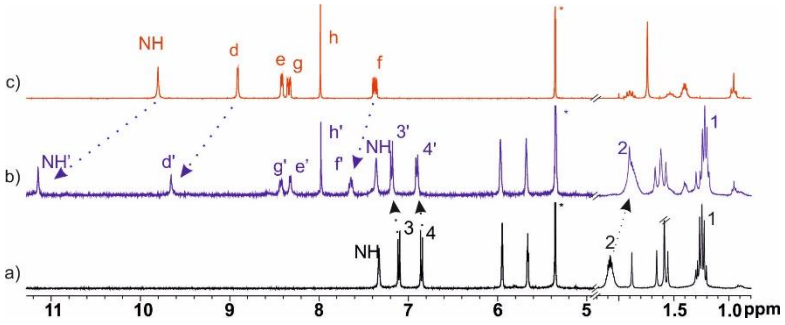

Figure 7: ^{1}H NMR spectra (400 MHz, CD_2Cl_2, 298 K) of (a) calix[4]pyrrole ***2*Pt$_2$•(TFO)$_2$** b) the assembled macrocycle **2**Pt$_2$**•3-(TfO)$_2$** ; c) bis amide ligand **3**. For proton assignments see **Scheme 1**.

The self-assembly of the metallocycle **2**Pt_2**•3-(TfO)**$_2$ implied the formation of two Pt-N coordination bonds. Upon coordination, the proton signals of the pyridyl unit shifted downfield ($\Delta\delta(H_1)$ = 0.75 ppm $\Delta\delta(H_4)$ = 0.09 ppm, $\Delta\delta(H_3)$= 0.27 ppm), in agreement with a reduction in the electron density of the aromatic ring. In addition, the amide protons of the bound di-pyridyl ligand **3** moved significantly downfield ($\Delta\delta$(NH) = 1.35 ppm).

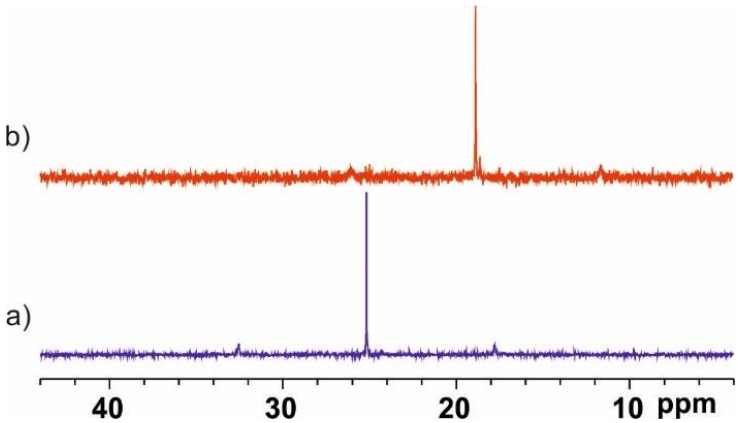

***Figure 8**:[31]P NMR spectra (202 MHz, CD_2Cl_2, 298 K) of (a) di-nuclear calix[4]pyrrole **2**Pt_2**•(TfO)$_2$** b) and the self-assembled metallo-macrocycle **2**Pt_2**•3$_2$-(TfO)$_2$**.*

The proton-decoupled ^{31}P NMR spectrum of the self-assembled macrocycle **2**Pt_2**•3-(TfO)**$_2$ showed a sharp singlet resonating at 25.19 ppm, along with two small satellites resulting from the coupling to the ^{195}Pt metal center. Compared to the chemical shift of the phosphorus atoms in the precursor dinuclear acetylide, ***2***Pt_2**•(TfO)$_2$**, the self-assembly of the metallo-cycle caused a downfield shift of 18.8 ppm to the phosphorous signal.[37] (***Figure 8***).

Finally, Diffusion-Ordered Spectroscopy (DOSY) experiments were used to support the self-assembly of the metallo-macrocycle. The calculated diffusion coefficient (D=2.62 10^{-10} ± 0.11 m^2/s) (D) was used in combination to the Stokes–Einstein equation ($D = k_BT/6\pi\eta r$, k_B: Boltzmann constant, T: temperature, η: dynamic viscosity, r: hydrodynamic radius) to derive the radius of a putative spherical object for the diffusing metallo-cycle (r= 11.6 Å) (***Figure 9*****, Figure 10**). Notably, the energy

[37] Li, R.-H.; Feng, X.-Y.; Zhou, J.; Yi, F.; Zhou, Z.-Q.; Men, D.; Sun, Y., Rhomboidal Pt(II) Metallacycle-Based Hybrid Viral Nanoparticles for Cell Imaging. *Inorg. Chem.* **2021,** *60*, 431-437.

minimized structure of the metallo-cycle [**2**Pt_2•**3**$_2$]$^{2+}$ fits nicely in the volume of the calculated sphere supporting its self-assembly in solution.

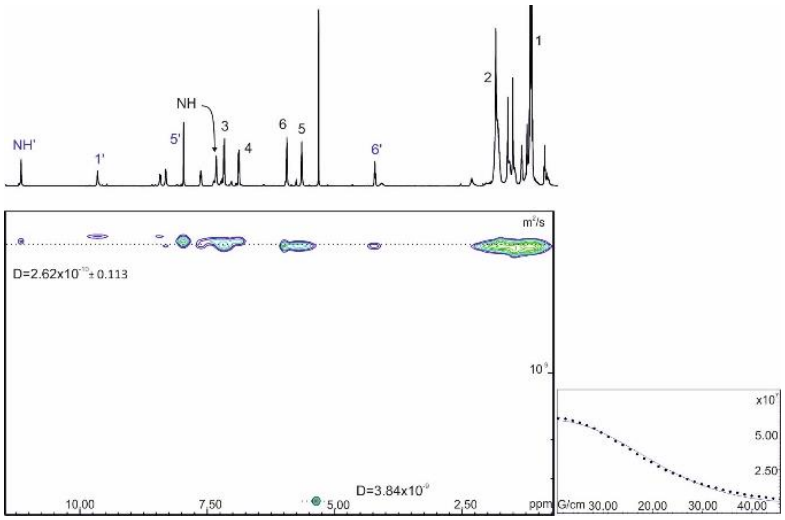

***Figure 9**: DOSY experiment (500 MHz, CD_2Cl_2, 298 K) for **2**Pt_2•**3**-**(TfO)**$_2$, with the assignments.*

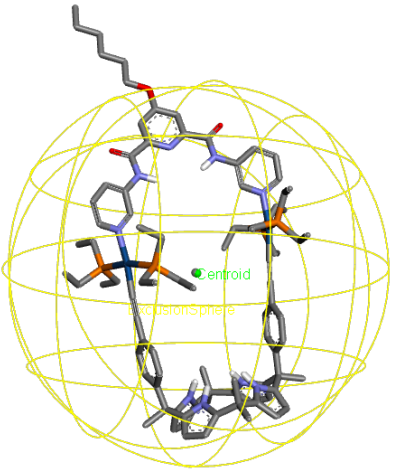

Figure 10:** Energy minimized structure of **2**Pt_2•**3**-(TfO)***$_2$ inscribed in a sphere with radius (r= 11.6 Å)*

3.2.2 Binding studies

In order to investigate the binding properties of the metallocycle **$2Pt_2$•3-$(TfO)_2$,** we performed ^{1}H NMR titration experiments using pyridine *N*-oxide **5** and bis-pyridine bis-*N*,*N*'-oxide **6** as guests. We demonstrated previously that pyridine *N*-oxides are outstanding guests for binding with two- and four-wall C[4]P receptors both in water and organic solvents[38,39,40].

We selected pyridine-*N*-oxide **5** in order to test the putative formation of 2:1 complexes with **$2Pt_2$•3-$(TfO)_2$**. The metallo-macrocyle possesses two endohedral polar binding sites equipped with hydrogen-bond donors. One is defined by the four converging pyrrole NH of the C[4]P core in cone conformation.

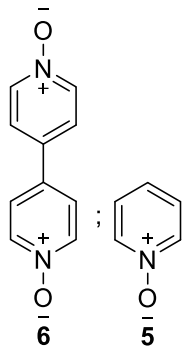

Figure 11**: Structure of the selected guests **5** and **6.

The other contains the two amide NHs of the 1,5-bis-carboxamidepyridine spacer in *cis*-conformation. On the other hand, bis-*N*-oxide **6** represents a good match in length and size for a ditopic interaction with **$2Pt_2$•3-$(TfO)_2$** yielding a ditopically bound 1:1 complex. Before performing the titrations with the **$2Pt_2$•3-$(TfO)_2$** metallo-cycle, we studied the interaction of the two guests with the precursor C[4]P compound **$2Pt_2$•I_2** as binding-model systems.

[38] Adriaenssens, L.; Acero Sánchez, J. L.; Barril, X.; O'Sullivan, C. K.; Ballester, P., Binding of calix[4]pyrroles to pyridine N-oxides probed with surface plasmon resonance. *Chem. Sci.* **2014,** *5*, 4210-4215.

[39] Escobar, L.; Aragay, G.; Ballester, P., Super Aryl-Extended Calix[4]pyrroles: Synthesis, Binding Studies, and Attempts To Gain Water Solubility. *Chemistry – A European Journal* **2016,** *22*, 13682-13689.

[40] R. Muriel, Calix[4]pyrrole Based Receptors of the Recognition of Ion Pairs, *Doctoral Thesis,* 147.

^{1}H NMR titration of $2Pt_2 \bullet I_2$ *with pyridine N-oxide 5*

We monitored the titration of the di-nuclear C[4]P $\mathbf{2Pt_2 \bullet I_2}$ with pyridine *N*-oxide **5** in d_2-DCM solution using ^{1}H NMR spectroscopy. In agreement with C_{2v} symmetry, the ^{1}H NMR spectrum of $\mathbf{2Pt_2 \bullet I_2}$ displayed four separate doublets, corresponding to the aromatic protons and the β-pyrrole protons, and three singlets for the methyl groups (***Figure 13*a**). The four pyrrole NHs resonated as a broad singlet centered at δ = 7.3 ppm (***Figure 13*a**). The incremental addition of **5** produced substantial chemical shift changes to the proton signals of $\mathbf{2Pt_2 \bullet I_2}$ (***Figure 13***). The pyrrole NHs of the C[4]P moved downfield (complexation induced shift (CIS) = 2.9 ppm) indicating their involvement in hydrogen bonding interactions with the oxygen atom of the *N*-oxide. The aromatic protons of $\mathbf{2Pt_2 \bullet I_2}$ were slightly shifted in opposed directions (CIS = 0.02 and - 0.05 ppm for H_4 and H_3, respectively). The two signals of the β-pyrrole protons also experienced opposed chemical shift changes but of larger magnitude (CIS = - 0.17 and 0.3 ppm). This observation suggested a change in the receptor's conformation from 1,3-alternate in the free state to the cone conformation in the complex. We obtained a good fit of the titration data to a 1:1 theoretical binding model. From the data fitting, we derived that the binding constant of the $\mathbf{5 \subset 2Pt_2 \bullet I_2}$ was $K_a(\mathbf{5 \subset 2Pt_2 \bullet I_2}) = 63 \pm 12\ M^{-1}$. The magnitude of the binding constant is in line with those reported for similar complexes of "two wall" C[4]Ps having triazole substituents at the upper rim.[40] The observation of a single set of signals for both the host and the guest throughout the titration demonstrated that the binding equilibrium was fast on the chemical shift timescale.

The extrapolation of the chemical shift changes experienced by the proton *alpha* to the nitrogen atom of **5** (H_a) was used to determine that its chemical shift in the $\mathbf{5 \subset 2Pt_2 \bullet I_2}$ complex was δ = 5.1 ppm. The significant upfield (CIS = -3 ppm) experienced by this proton supported the inclusion of **5** in the polar aromatic cavity of $\mathbf{2Pt_2 \bullet I_2}$. The included **5** formed four converging hydrogen-bonds with the pyrrole NHs of $\mathbf{2Pt_2 \bullet I_2}$. In the $\mathbf{5 \subset 2Pt_2 \bullet I_2}$ complex, the pyridine N-oxide is sandwiched between the two *meso*-phenyl substituents of the receptor. In this binding geometry, the H_a proton of the bound N-oxide is highly shielded owing to the magnetic anisotropy of the two phenyl rings. The signals of the H_b and H_c protons of bound **5** are less affected because they protruded out of the receptor's aromatic cleft. We concluded that bis-triethylphosphine ligand of the *para*-acetylide $\mathbf{2Pt_2 \bullet I_2}$ complex did not represent noticeable steric problems for the binding of the pyridine-*N*-oxide **5**.

Self-assembly of Metallocycles based on a-β,β'-diethynyl "two wall" Calix[4]pyrrole diplatinum(II) complex.

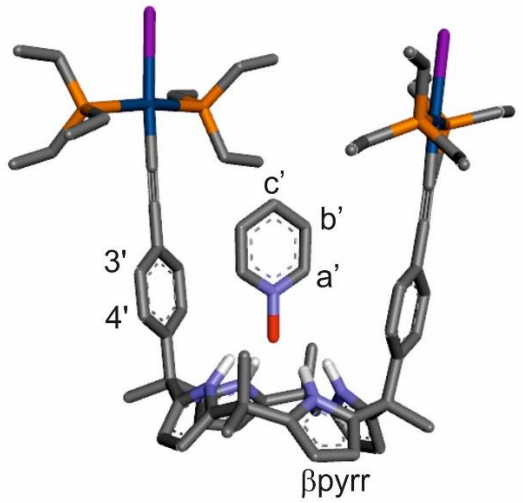

Figure 12**: Energy minimized structure (MM3)* of the **5⊂*2Pt₂•I₂ complex with proton assignment

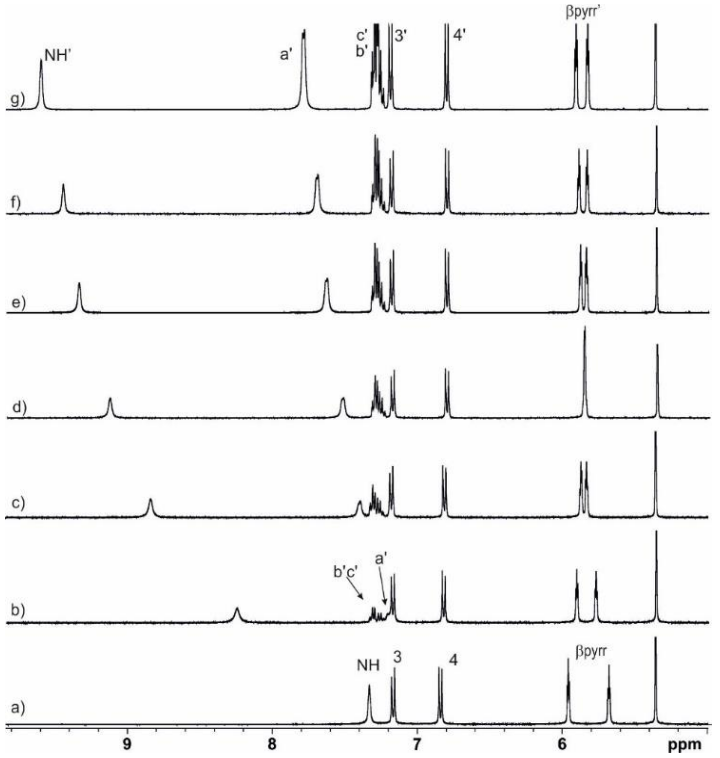

***Figure 13:** Selected regions of the ^{1}H NMR spectra (400 MHz, CH_2Cl_2, 298 K) of **$2Pt_2•I_2$** (4.6 mM) with incremental amounts of pyridine N-oxide **5:** a) 0 equiv. b) 1 equiv.; c) 2 equiv.; d) 3 equiv.; e) 4 equiv.; f) 5 equiv. and g) 6 equiv. See Figure 10 for proton assignment.*

^{1}H NMR titration of $2Pt_2\bullet I_2$ *with 4,4'-bipyridine N,N'-dioxide 6*

The cone conformation of the di-nuclear **2**$Pt_2\bullet I_2$ C[4]P receptor displays a polar aromatic cleft with a wide opening. For this reason, we did not expect significant changes (affinity, stoichiometry and binding geometry) in the interaction with the longer bipyridine-*N*,*N*'-dioxide **6** compared to pyridine N-oxide **5.** We probed the interaction of **$2Pt_2\bullet I_2$** with the bipyridine *N*,*N*'-dioxide **6** in d_2-DCM solution by means of ^{1}H NMR spectroscopic titrations. Owing to the reduced solubility of **6** in CD_2Cl_2, we decided to perform an inverse titration placing the bis-*N*-oxide **6** in the NMR tube and adding incremental amounts of the C[4]P **$2Pt_2\bullet I_2$.**

The incremental addition of **$2Pt_2\bullet I_2$** (52.1 mM) to a 4.1 mM solution of bis-pyridine *N*-oxide **6** produced noticeable chemical shift changes to all the protons signals of the *N*-oxide. In particular, the doublet appearing more downfield-shifted and corresponding to the *ortho*-proton *alpha* to the nitrogen atom (H_a) moved upfield experiencing a CIS = - 1.08 ppm and significant broadening. In contrast, the *meta*-aromatic proton of **6** (H_b) moved slightly downfield (CIS + 0.3 ppm; see **Figure 15**) and did not broaden. In analogy to the changes observed for the binding of **5,** the β-pyrrole proton signals of **$2Pt_2\bullet I_2$** shifted in different directions. Taken together, these results suggested that *N*-oxide **6** was interacting with the C[4]P **$2Pt_2\bullet I_2$** and that the binding equilibrium was fast on the chemical shift timescale. It is worth noting here that the quantitative formation of a 1:1 **6⊂$2Pt_2\bullet I_2$** complex (i.e. by adding a large excess of **$2Pt_2\bullet I_2$**) should cause the loss of symmetry of the bound *N*-oxide if it was not involved in a chemical exchange process or this was slow on the chemical shift timescale. However, we observed only two signals instead of the four expected for the protons of bound **6** in the **6⊂$2Pt_2\bullet I_2$** complex. The observation of broadening exclusively for the signal assigned to the aromatic *ortho*-protons, *alpha* to the nitrogen atom of **6**, was also remarkable. This fact indicated that the bound guest in the **6⊂$2Pt_2\bullet I_2$** complex experiences a spinning/pirouetting motion that is fast on the chemical shift timescale. This motion will produce the existence of a chemical exchange between the two *N*-oxide ends of bound **6** in the **6⊂$2Pt_2\bullet I_2$** complex. Alternatively, the dissociation of bound guest **6** and its re-complexation through the opposite terminal end would produce a similar result.

The *ortho*-aromatic proton of the *terminal* end of **6** that is sandwiched between the aromatic walls of the C[4]P suffers noticeable shielding (H_{a1}). We estimated a CIS of -3 ppm for the analogous H_a proton in the bound pyridine-*N*-oxide **5**. On the contrary, the distal *ortho*-proton, *alpha* to the nitrogen atom at the other end of the bound *N*-oxide **6**, feels a reduced shielding effect caused by the acetylide Pt(II) units.

We determined an upfield CIS for H_a of just -1.08 ppm in the **6⊂2Pt₂•I₂**. This value represents the average CIS of the two signals H_{a1} and H_{a2}. Previously, we measured a CIS of -3 ppm for the analogous H_a proton in the **5⊂2Pt₂•I₂** complex. Consequently, we estimated that H_{a2} in the **6⊂2Pt₂•I₂** complex featured a downfield CIS = 0.9 ppm, that is a deshielding effect caused by the Pt(II) acetylide groups.

In short, the binding geometry of the **6⊂2Pt₂•I₂** complex produced significantly different chemical shift values for the two *ortho*-protons (H_{a1} and H_{a2}, CIS of -3 ppm and 0.9 ppm, respectively) at the distal terminal ends of bound **6**. Conversely, the two *meta*-counterparts (H_b) displayed similar complexation induced chemical shifts. This phenomenon served to explain the selective broadening observed for the *alpha*- or *ortho*- (H_a) proton of bound **6** in the **6⊂2Pt₂•I₂** complex.

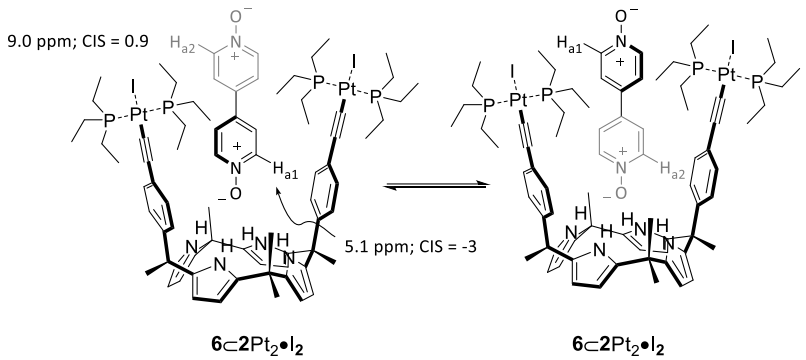

6⊂2Pt₂•I₂ **6⊂2Pt₂•I₂**

***Scheme 1**. Equilibrium of the pirouetting process of the bis-N-oxide **6** in the **6⊂2Pt₂•I₂** complex resulting in a chemical exchange between the two terminal N-oxide groups of the bound guest. The motion is fast on the chemical shift timescale producing the exclusive broadening of the signal of ortho-proton (H_a).*

The two double doublets of the β-pyrrole protons ($H_{\beta pyrr}$) shifted respectively downfield and upfield (calculated CIS -0.15 ppm and 0.28, respectively) ($H_{\beta pyrr}$ **Figure 15b-h**) in response to the conformational change experienced by the calix[4]pyrrole **2Pt₂•I₂** upon binding **6**. Indeed, the cone conformation of calix[4]pyrroles is stabilized in the presence of suitable guests i.e. *N*-oxides, while the 1,3-alternate conformation is preferred when free in chlorinated organic solvents i.e. DCM and $CHCl_3$.

When 0.2 equiv. of **2Pt₂•I₂** were added to the solution of **6**, the pyrrole NHs signals were detected in the downfield region of the ^{1}H NMR spectrum as a broad signal centered at δ = 8.4 ppm. The downfield shift (calculated CIS 2.65 ppm) experienced by the C[4]P NH protons in the **6⊂2Pt₂•I₂** complex indicated their involvement in hydrogen bonding interactions with bound **6**.

As extensively reported in literature, *N*-oxide derivatives show high affinity for calix[4]pyrroles, leading to the formation of four convergent hydrogen bonds.[41]

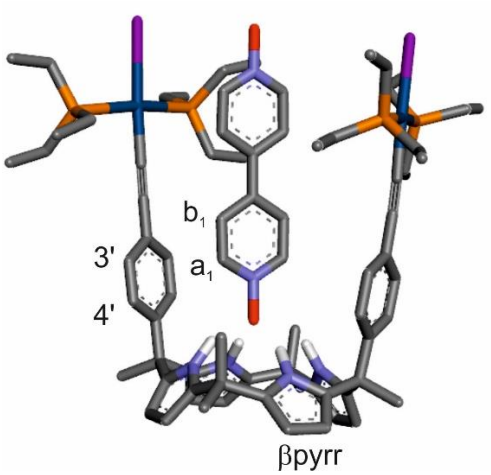

Figure 14: *Energy minimized structure (MM3) of the* ***6⊂2Pt₂•I₂*** complex. The proton assignment is also indicated.

[41] Escobar, L.; Ballester, P., Quantification of the hydrophobic effect using water-soluble super aryl-extended calix[4]pyrroles. *Org. Chem. Front.* **2019,** *6*, 1738-1748.

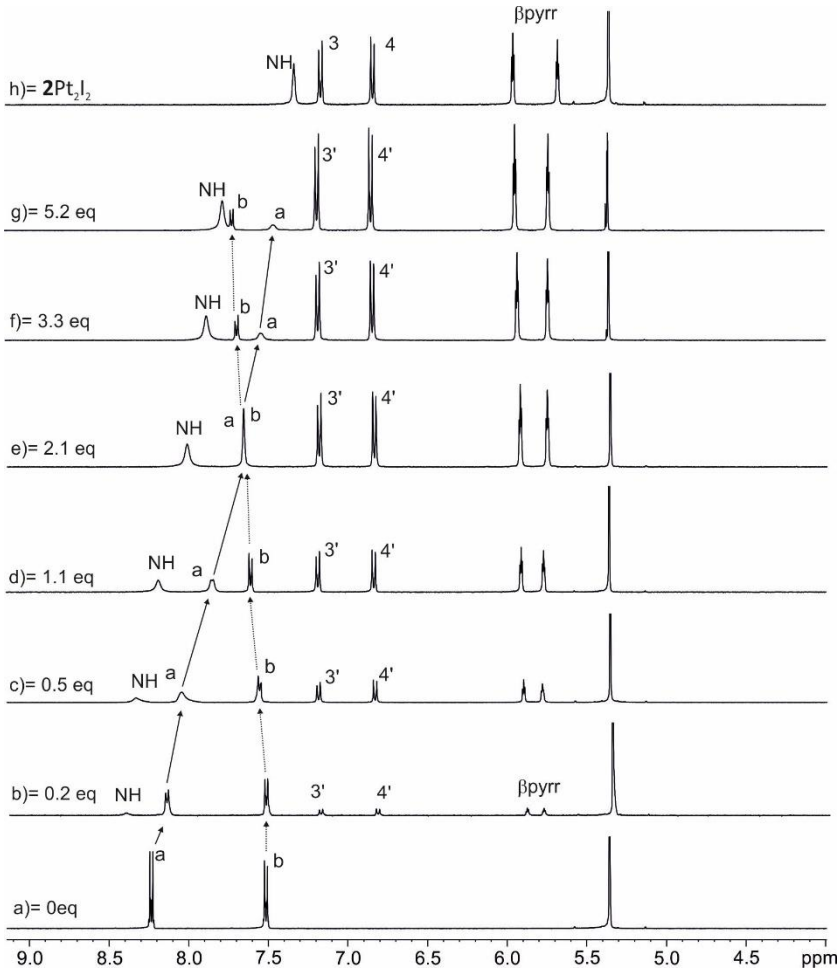

***Figure 15**: Selected region of the ^{1}H NMR spectra acquired during the titration of the bis-pyridiine-bis-N-oxide **6** (a) with incremental amounts of **2 Pt_2•I_2** (h) in CD_2Cl_2 solution: a) 0 equiv; b) 0.2 equiv; c) 0.5 equiv; d) 1.1 equiv; e) 2.1 equiv; f) 3.3 equiv and g) 5.2 equiv.*

The fit of the chemical shift changes experienced by the aromatic protons of **6** to a theoretical 1:1 binding model was good. This observation supported the 1:1 stoichiometry assigned to the **6⊂2Pt_2•I_2** complex. We calculated a macroscopic binding constant for the complex of K(**6⊂2Pt_2•I_2**) = $2 \times 10^2 \pm 50$ M^{-1}. Notably, the value of the statistically corrected binding constant (K(**6⊂2Pt_2•I_2**)/2) is in line with the stability constant calculated for the **5⊂2Pt_2•I_2** complex and other complexes previously reported in binding studies of pyridine-*N*-oxides with "two wall" calix[4]pyrroles in chlorinated organic solvent.[40] Again, we must conclude that the open cleft defined by the cone conformation of **2Pt_2•I_2** does not impose significant steric constrains to the inclusion of **6**.

Binding studies of the metallo-macrocycle $2Pt_2$•3-(TfO)$_2$** with pyridine *N*-oxide 5**

Having established the binding properties of the di-nuclear C[4]P macrocyclic precursor, **$2Pt_2$•I_2**, toward the pyridine *N*-oxide derivatives, we undertook the binding studies with the metallo-macrocyle **$2Pt_2$•3-(TfO)$_2$**. As mentioned above, the metallo-macrocycle possesses two endohedral polar binding sites: one defined by four converging pyrrole NH of the C[4]P core in cone conformation and the other by two amide NHs of the 1,5-bis-carboxamide pyridine spacer in *cis*-conformation. However, the cavity of the metallo-macrocycle **$2Pt_2$•3-(TfO)$_2$** has fixed dimensions and reduced flexibility owing to the bis-pyridine ligand **3** acting as a molecular clip. The ^{1}H NMR spectrum of **$2Pt_2$•3-(TfO)$_2$** displayed a number of signals in agreement with C_{2v} symmetry.

The incremental addition of a pyridine *N*-oxide **5** to a 4.6 mM solution of **$2Pt_2$•3-(TfO)$_2$** in dichlorometane-d_2 produced noticeable chemical shift changes in some of the proton signals of the metallocycle. The most affected signal was the one of the pyrrole NHs. It moved downfield (CIS = 2.3 ppm) indicating their involvement in hydrogen bonding interaction with the oxygen atom of the *N*-oxide **5**. The aromatic and β-pyrrole protons of the C[4]P scaffold experienced similar chemical shift changes to those observed in the titration of the parent cleft receptor **$2Pt_2$•I_2**. In addition, the aromatic and amide proton signals of the metallocycle clip, bis-amide **3**, showed reduced chemical shift changes. These observations suggested that the pyridine N-oxide **5** was selectively bound by the C[4]P unit. The fit of the titration data to a 1:1 theoretical binding model was good and returned a binding constant of K_a(**5**⊂**$2Pt_2$•3-(TfO)$_2$**) = 40 $\pm$ 8 M^{-1}. This constant value is slightly smaller than the one observed for the complex of **5** with the di-nuclear cleft **2**Pt_2•I_2. Most likely, the fixed dimensions of the aromatic cavity of the metallo-macrocyclic receptor **$2Pt_2$•3-(TfO)$_2$** imposed reduced constrains to the inclusion of **5**.

Notably, we determined that the upfield CIS for the H_a proton of **5** in the **5⊂$2Pt_2$•3-(TfO)$_2$** complex was only -2.2 ppm. This is almost 1 ppm less than in the **5⊂$2Pt_2$•I_2** complex counterpart. We surmised that due to the reduction in flexibility imposed by the bis-amide clip **3**, the inclusion of the *N*-oxide **5** in the metallo-macrocycle **$2Pt_2$•3-(TfO)$_2$** produced almost exclusively an offset π-stacked binding geometry (7 Å distance between meso-phenyls). The alternative edge-to-face binding mode of the complex based on CH-π interactions demanded a larger distance between the two aromatic *meso*-phenyl substituents (> 10 Å) that is unattainable in the case of the metallo-macrocyle **$2Pt_2$•3-(TfO)$_2$** owing to the ditopic interaction with clip **3**.

Self-assembly of Metallocycles based on a p,p'-diethynyl "two wall" Calix[4]pyrrole diplatinum(II) complex.

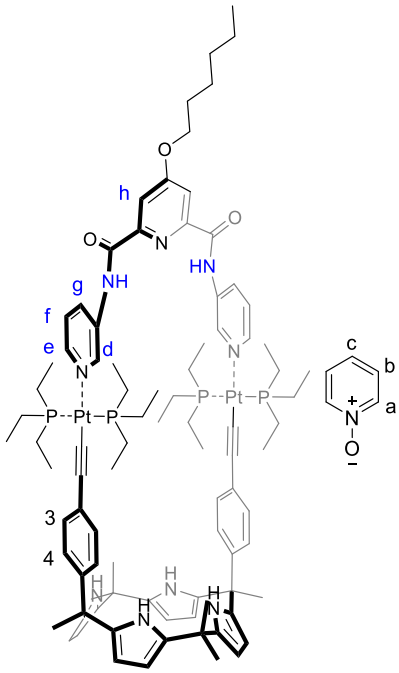

***Figure 16**: Line-drawing structures of the metallo-macrocycle **2Pt$_2$•3-(TfO)$_2$** and the pyridine-N-oxide **5**. The proton assignments are also indicated.*

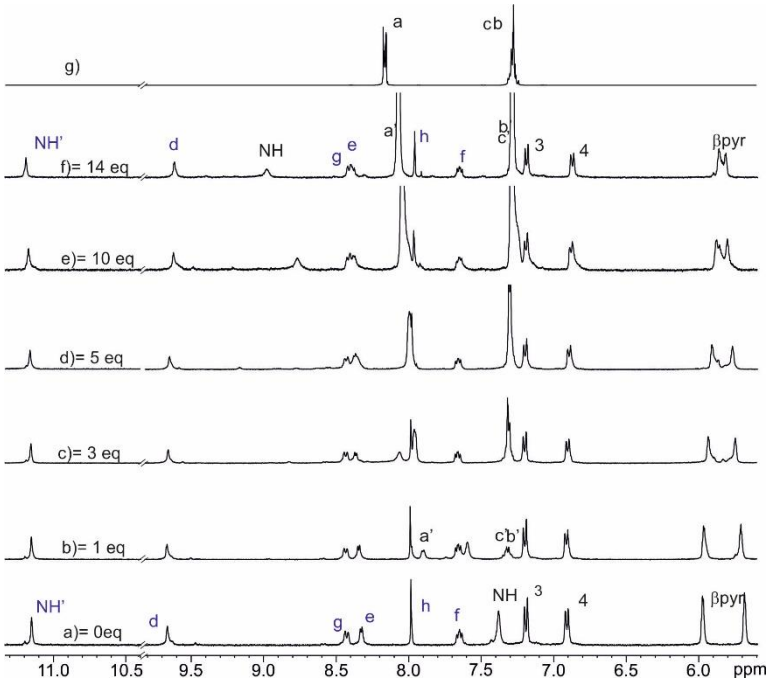

***Figure 17**: Selected regions of the ^{1}H NMR spectra (400 MHz, CH_2Cl_2, 298 K) of **2Pt$_2$•3-(TfO)$_2$** (4.6 mM) (a) with incremental amounts of pyridine N-oxide **5** (g) b) 1 equiv.; c) 3 equiv.; d) 5 equiv.; e) 10 equiv. f) 14 equiv. and g) free pyridine N-oxide **5**. See **Figure 16**for proton assignment.*

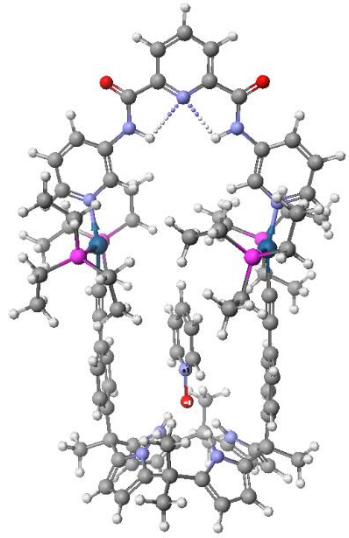

***Figure 18**: Energy minimized structure (MM3) of the **5⊂2Pt$_2$•3-(TfO)$_2$** complex highlighting the offset π-stacked binding geometry.*

Binding studies of the metallo-macrocycle $2Pt_2$•3-**$(TfO)_2$ with bis-pyridine-*N*-*N*'-bis-oxide 6**

Molecular modelling studies (MM3) of **5⊂$2Pt_2$•3-$(TfO)_2$** complex suggested that the binding site of the metallo-macrocycle defined by the bis-carboxamide pyridine unit was very crowded by the ethyl substituents of the phosphines to allow the inclusion of an additional pyridine-*N*-oxide **5**. The exclusive formation of the 1:1 complex, **5⊂$2Pt_2$•3-$(TfO)_2$,** in the previous section supported this hypothesis. For this reason, we anticipated that a ditopic interaction of **6** with the metallo-macrocycle **$2Pt_2$•3-$(TfO)_2$** was not likely.

As shown in **Figure 20** the incremental addition of bis-pyridine N,N'-oxide **6**, up to 4 equiv., to a solution of **$2Pt_2$•3-$(TfO)_2$** induced small chemical shift changes. The diagnostic pyrrole NH protons of the metallo-macrocycle shifted downfield approximately ~ 0.2 ppm in the presence of 4 equiv. of **6**. In contrast, in the titration of **$2Pt_2$•3-$(TfO)_2$** with **5** the addition of 3 equiv. produced a downfield shift of the NHs of more than 0.6 ppm. This observation suggested that the hydrogen bonding interaction of the metallo-macrocycle **$2Pt_2$•3-$(TfO)_2$** with the bis-N-oxide **6** was weaker. Most likely, the larger size of **6** does not allow for an ideal binding geometry with the C[4]P binding site. Clearly, a ditopic interaction is not established between the two binding partners.

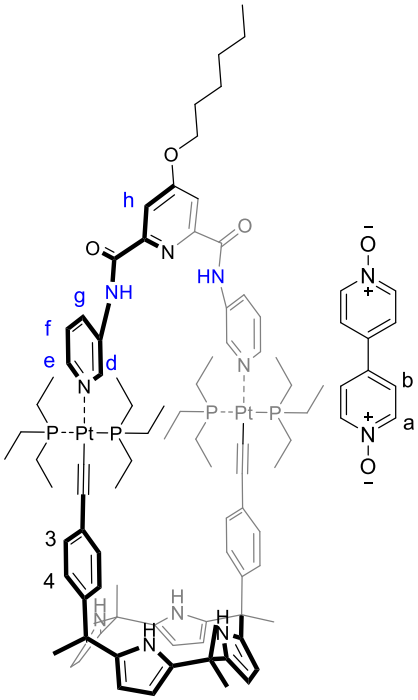

***Figure 19**: Line drawing structures of the metallo-macrocycle **2Pt$_2$•3-(TfO)$_2$** and the bis-pyridine-N,N'-oxide **6**. The proton assignment used in **Figure 20** is included.*

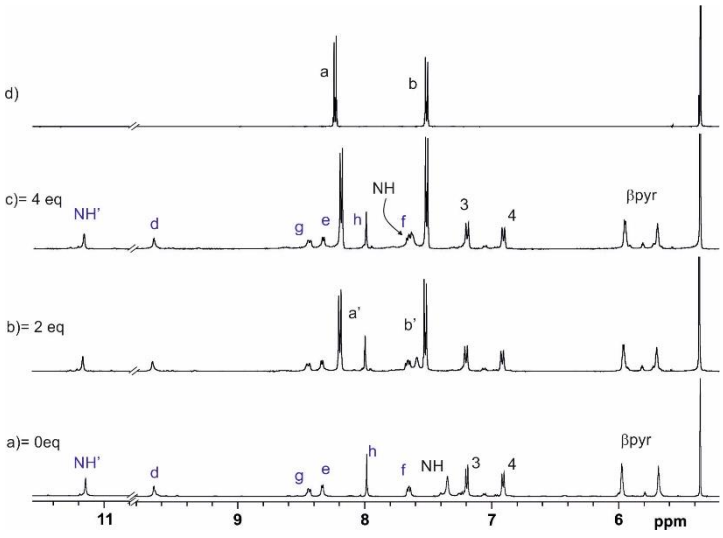

***Figure 20**: Selected regions of the ^{1}H NMR spectra (400 MHz, CH_2Cl_2, 298 K) of: (a) **2Pt$_2$•3-(TfO)$_2$** (4mM) and incremental amounts of bis pyridine-N,N'-oxide **6** b) 2 equiv.; c) 4 equiv; d) free **6**.*

We concluded that the restriction in conformational flexibility imposed by the clip **3** increased the steric hindrance caused by the triethyl phosphine ligands coordinated to the platinum metal. For this reason, the second polar binding site of the macrocycle's cavity that is defined by the *cis*-bis-carboxamide pyridine unit was inaccessible for binding (only 1:1 **5⊂2Pt$_2$•3-(TfO)$_2$** complex formed) or producing a ditopically bound complex (**6⊂2Pt$_2$•3-(TfO)$_2$**).

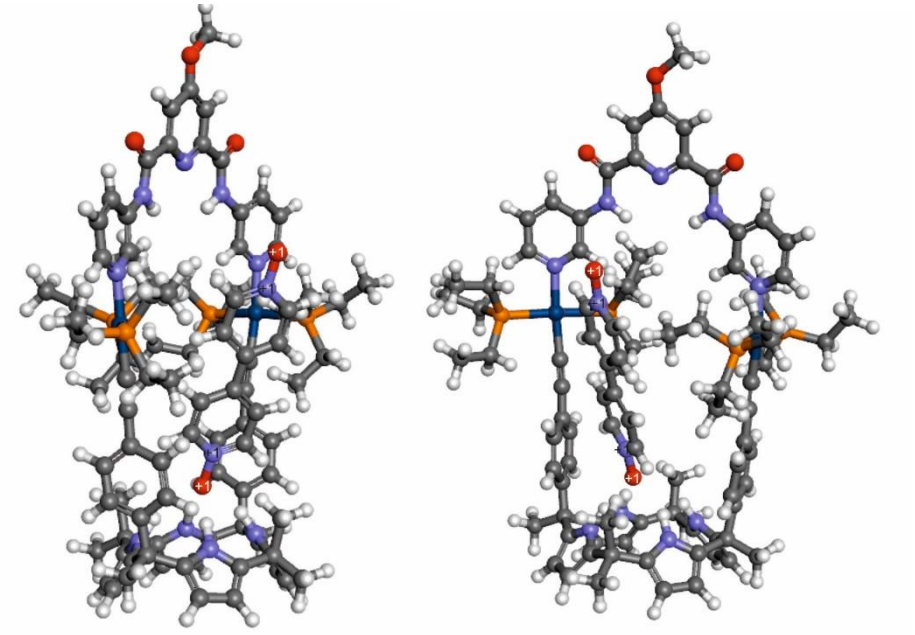

Figure 21**: Two different view of the energy minimized structure (MM3) **6⊂2Pt$_2$•3-(TfO)$_2$,

3.3 Conclusions

We reported the synthesis of two unprecedent *p*,*p*'-diethynyl "two wall" calix[4]pyrrole diplatinum(II) organo-metallic complexes (***2*Pt$_2$•*I*$_2$** and ***2*Pt$_2$•(TfO)$_2$**). We also describe the self-assembly of two metallo-macroccycles (***2*Pt$_2$•*3*-(TfO)$_2$** and ***2*Pt$_2$•*4*-(TfO)$_2$**) formed *via* ditopic coordination of the bis-triflate C[4]P ***2*Pt$_2$•(TfO)$_2$** with two bis-pyridine ligands (**3**- **4**, ***Figure 5***) having in common a 2,6-di-carboxamide pyridyl spacer.

We characterized the binding properties of the metallo-macrocycle ***2*Pt$_2$•*3*-(TfO)$_2$** and its synthetic C[4]P precursor ***2*Pt$_2$•I$_2$** using ^{1}H NMR titration experiments. We used pyridine N-oxide (**5**) and bis pyridine bis N,N'-oxide (**6**) as polar neutral guests in our binding studies.

The C[4]P receptor ***2*Pt$_2$•I$_2$** showed almost identical binding affinity toward both guests (K_a(**5**⊂***2*Pt$_2$•I$_2$**) = 63 ± 12 M^{-1}, K(**6**⊂***2*Pt$_2$•I$_2$**) = 2 × 10^2 ± 50 M^{-1}). On the other hand, the metallo-macrocycle ***2*Pt$_2$•*3*-(TfO)$_2$** showed a slight reduction in binding affinity for **5** compared to the C[4]P precursor ***2*Pt$_2$•I$_2$** (K_a(**5**⊂***2*Pt$_2$•3-(TfO)$_2$**) = 40 ± 8 M^{-1}). In contrast, the affinity of the metallo-macrocycle ***2*Pt$_2$•*3*-(TfO)$_2$** for the bis-pyridine bis-N,N'-oxide **6** was significantly reduced.

Most likely, the selectivity displayed by the metalo-macrocyle ***2*Pt$_2$•*3*-(TfO)$_2$** in the binding of the pyridine-N-oxide derivatives **5** and **6** is due to steric effects caused by of the ethyl substituents of the phosphine ligands and the reduction in conformational flexibility imposed by the ditopically bound pyridyl ligand (clip 3). Indeed, as showed in ***Figure 21***, molecular modelling studies revealed that the bis pyridine bis N,N'-oxide (**6**) can only be partially accommodated in the cavity of the metallo-macrocycle ***2*Pt$_2$•*3*-(TfO)$_2$**. Steric effects are also responsible for the lack of interaction between the bis-amide binding site of the metallo-macrocyle and the N-oxide group. Nonetheless and as showed in **Figure 18**, the shorter pyridine N-oxide (**5**) can uneventfully bind the C[4]P site of the metallo-macrocycle forming the **5**⊂***2*Pt$_2$•3-(TfO)$_2$** complex. The second polar binding site of metallo-macrocycle ***2*Pt$_2$•*3*-(TfO)$_2$** is also inaccessible to the pyridine-N-oxide **5** resulting in the exclusive formation of a 1:1 complex. Notably, the binding constant value of the latter 1:1 complex is almost identical than that formed with the C[4]P precursor **5**⊂***2*Pt$_2$-(TfO)$_2$**. The reduced size of **5** did not induce steric clashes with the ethyl substituents of the phosphine ligands when included into the metallo-macrocycle's cavity.

3.4 Experimental section

3.4.1 General methods and instrumentation.

Reagents and solvents used in the synthesis were obtained from commercial suppliers and were used without further purification unless otherwise stated. Pyrrole was distilled under vacuum and stored in the freezer for further use. Toluene was dried under distillation from sodium/benzophenone under argon atmosphere. Triethylamine (Et_3N) and diethylamine were distilled from CaH_2 under argon atmosphere and used immediately. Flash column chromatography was performed with silica gel, technical grade, pore size 60 Å, and 230–400 mesh particle size.

Automatic column chromatography purifications were done with a Combi-flash® RF^+. Routine ^1H, ^{31}P and ^{13}C NMR spectra were recorded on a Bruker Avance 400 (400 MHz for ^1H-NMR), Bruker Avance 500 (500 MHz for ^1H-NMR) ultrashield spectrometer. Deuterated solvents were purchased from Aldrich.

3.4.2 Synthesis and characterization data

Trans-$(PEt_3)_2PtI_2$

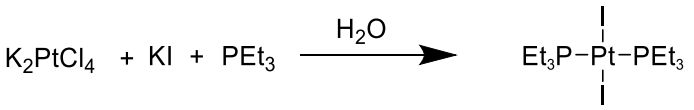

***Scheme S 1**: Scheme of the synthesis of t-$(PEt_3)_2PtI_2$.*

K_2PtCl_4 (250 mg, 0.6 mmol) was dissolved in deoxygenated distilled water (4.3 mL) in a two-neck round-bottom flask, with argon flow, and vigorously stirred (red solution). To this solution, 0.5 mL of a solution of KI (400 mg, 2.4 mmol, 4 equiv.) in deoxygenated water (1 mL) was added (the color of the solution turned dark), immediately followed by the addition of PEt_3 1 M in THF (1.2 mL, 1.2 mmol, 2 eq) (the solution change color to yellow/orange). The reaction mixture was vigorously stirred at room temperature under argon atmosphere until the solution became colorless and a yellow precipitate was formed (after ∼1 h). The resulting yellow precipitate was filtered off, washed with distilled water, and air-dried.

Right yellow needle-shaped crystals were obtained upon recrystallization from hot ethanol (300mg suspended in 3.5 ml of EtOH, final amount of ethanol 4.5 ml). 278 mg of crystals gained from the first crystallization.

The spectral data agreed with those published in literature for trans-*$(PEt_3)_2PtI_2$*[42].
^{1}H NMR (400 MHz, $CDCl_3$, 298 K), δ (ppm) 2.27(m, 12H,H^1), 1.09(quint, 18H, H^2).
^{31}P NMR (161 MHz, $CDCl_3$, 298 K), δ (ppm), P (t, 3.41 ppm, $J^{P\text{-}Pt}$ = 1132 Hz)

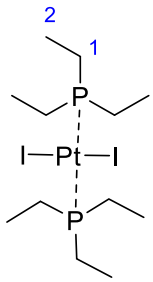

Figure S 1: Structure of trans-$(PEt_3)_2PtI_2$ and its proton assignment.

[42] Šembera, F.; Plutnar, J.; Higelin, A.; Janoušek, Z.; Císařová, I.; Michl, J., Metal Complexes with Very Large Dipole Moments: the Anionic Carborane Nitriles 12-NC–CB11X11– (X = H, F, CH3) as Ligands on Pt(II) and Pd(II). *Inorg. Chem.* **2016,** *55*, 3797-3806.

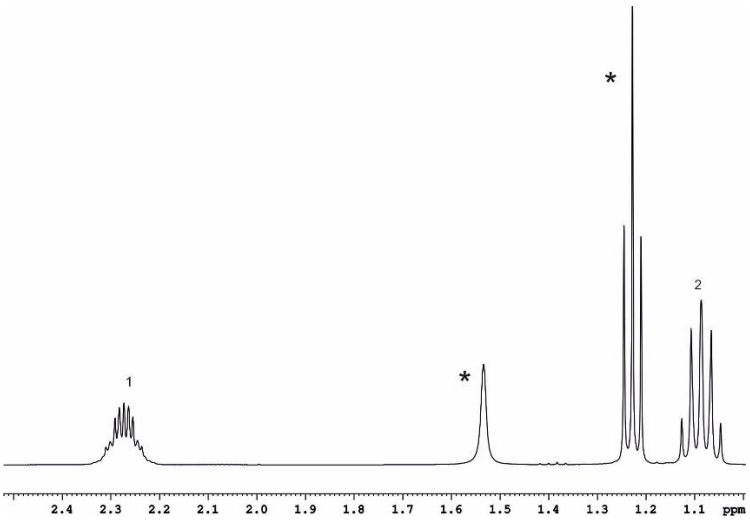

Figure S 2: *^{1}H NMR spectrum of trans-$(PEt_3)_2PtI_2$ in $CDCl_3$ solution (* impurities). See figure S1 for proton assignment.*

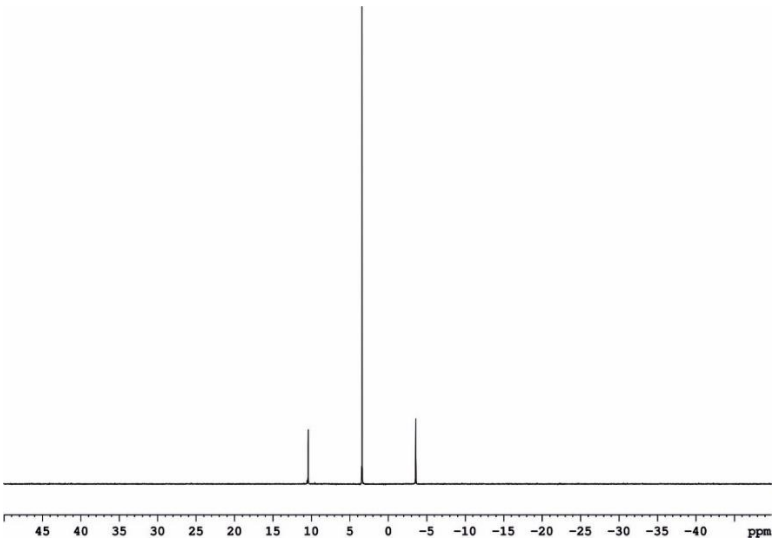

Figure S 3: *^{31}P NMR spectrum (161 MHz, $CDCl_3$, 298 K) of trans-$(PEt_3)_2PtI_2$.*

Trans- Di alkynyl calix[4]pyrrole two walls $[(PEt_3)_2PtI]_2$ (*2*Pt_2•I_2)

Self-assembly of Metallocycles based on a p,p'-diethynyl "two wall" Calix[4]pyrrole diplatinum(II) complex.

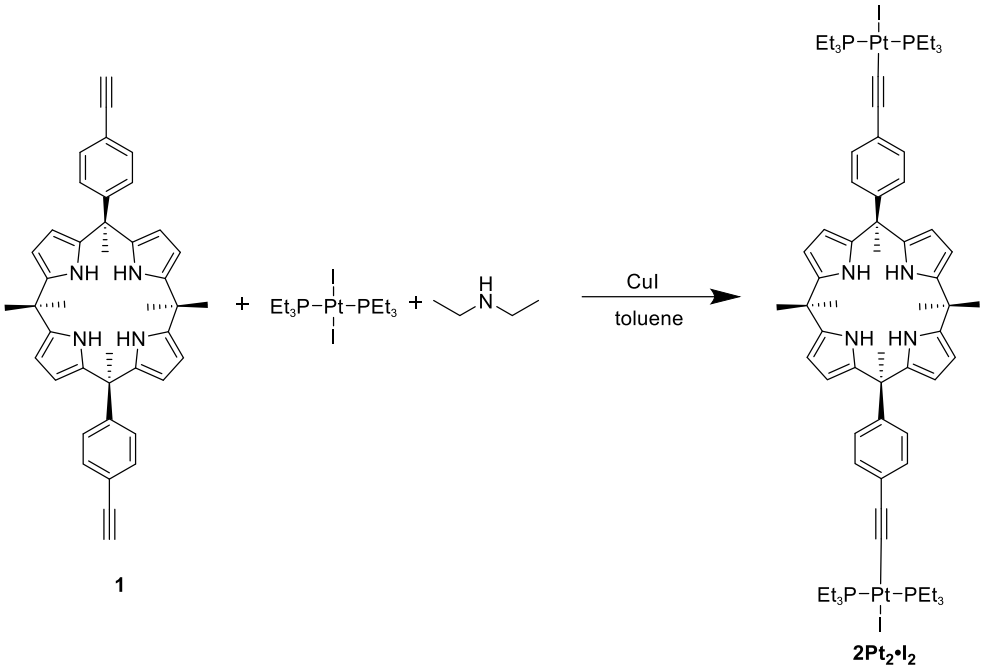

Scheme S 2: *Scheme of the synthesis of* ***2Pt₂•I₂****.*

1 (1 equiv, 100 mg, 166 µmol) and trans-$(PEt_3)_2PtI_2$ (2.63 equiv, 300 mg, 438 µmol) were added to a 10 mL round-bottom Schlenk under Ar. 4 mL of anhydrous toluene and 1.72 mL of diethylamine (16.6 mmol, 100 equiv) were added. The mixture was stirred for 15 min at room temperature, and 3 mg of CuI (0.12 equiv. 19 µmol) were added in one portion to the reaction flask. After 4.5 h the solvent is removed under reduced pressure. The crude was purified by column chromatography (silica gel) using dichloromethane/hexane (7:3) as eluent.

Self-assembly of Metallocycles based on a p,p'-diethynyl "two wall" Calix[4]pyrrole diplatinum(II) complex.

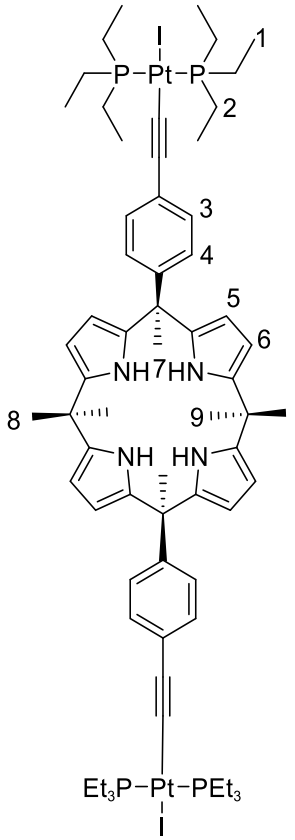

Figure S 4: Structure of ***2*Pt$_2$•*I*$_2$** for the assignments.

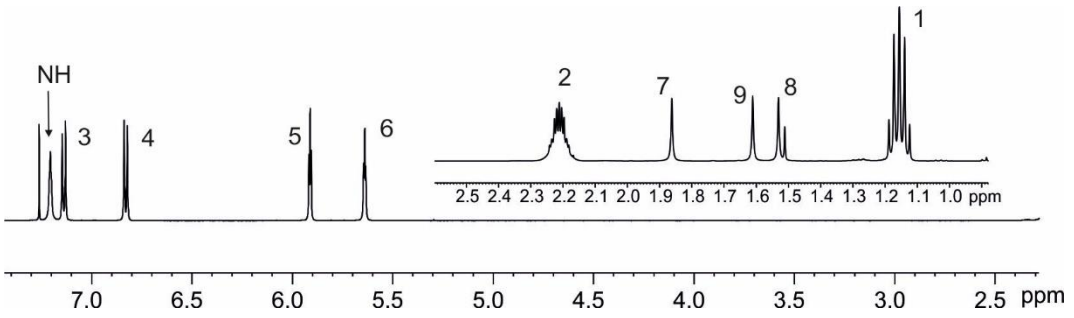

Figure S 5: ^{1}H NMR (500 MHz, $CDCl_3$, 298 K) of ***2*Pt$_2$•*I*$_2$**.

^{1}H NMR (500 MHz, $CDCl_3$, 298 K), δ (ppm) 7.20 (br,4H, NH), 7.14 (d, 4H, H^3, J^{3-4}= 8.42 Hz), 6.83(d, 4H, H^4, J^{3-4}= 8.42 Hz), 5.91 (dd, 4H, H^5, $J^{\beta1-\beta2}$=3.03 Hz), 5.63 (dd, 4H, H^6, $J^{\beta1-\beta2}$=3.03 Hz), 2.21 (m, 12H, H^2), 1.68 (s, 6H, H^7), 1.61 (s, 6H, H^9), 1.53 (s, 6H, H^8), 1.27 (m, 18H, H^1). ^{13}C (125 MHz, $CDCl_3$, 298 K) δ (ppm) 145.24, 138.55, 136.65, 130.03, 127.27, 126.72, 106.08, 103.28, 99.99, 89.01, 44.67, 35.27, 30.22, 28.10, 27.84, 16.77 (t, J^{C-P} = 17.91 Hz), 8.44.
^{31}P NMR (202 MHz, $CDCl_3$, 298 K), δ (ppm), P (t, 11.50 ppm, J^{P-Pt} = 1165 Hz).
HRMS (MALDI/ TOF) m/z: $[M+Na]^+$-= $[C66H98I2N4P4Pt2+Na]^+$ Calcd. 1737.4018; Found 1737.4021.

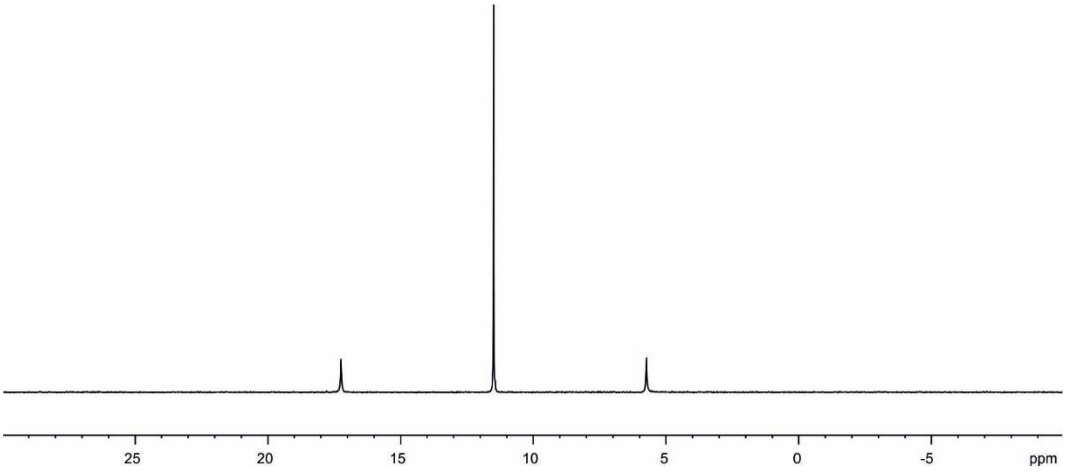

Figure S 6: ^{31}P NMR (161 MHz, $CDCl_3$, 298 K) of ***2*Pt$_2$•*I*$_2$.**

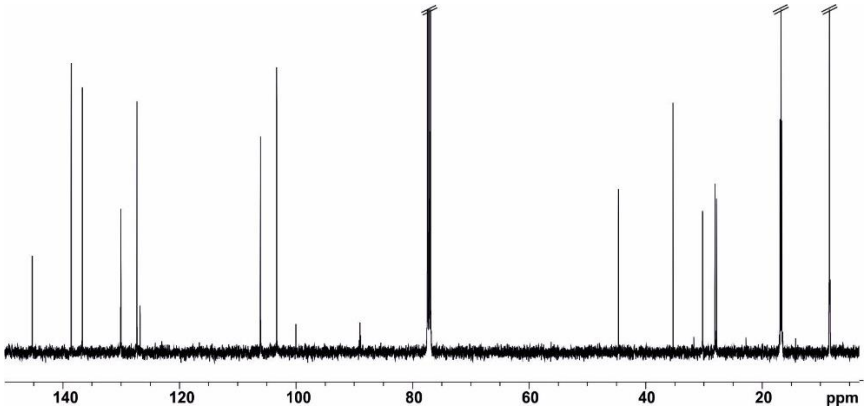

Figure S 7: ^{13}C NMR (125 MHz, $CDCl_3$, 298 K) of ***2*Pt$_2$•*I*$_2$**.

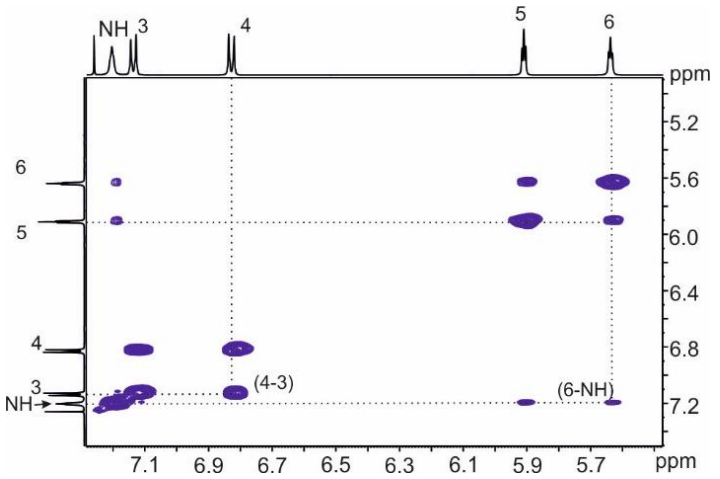

Figure S 8: COSY experiment of ***2*Pt$_2$•*I*$_2$** in $CDCl_3$, with assignments (aromatic region).

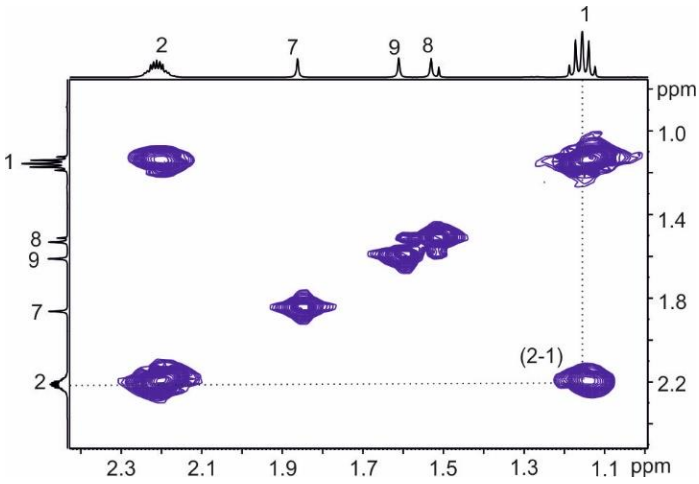

Figure S 9: COSY experiment of ***2*Pt$_2$•*I*$_2$** in $CDCl_3$, with assignments (aromatic region).

Di alkynyl calix[4]pyrrole two walls t-[(PEt3)2PtTOf]$_2$ (*2*Pt$_2$•(TfO)$_2$)

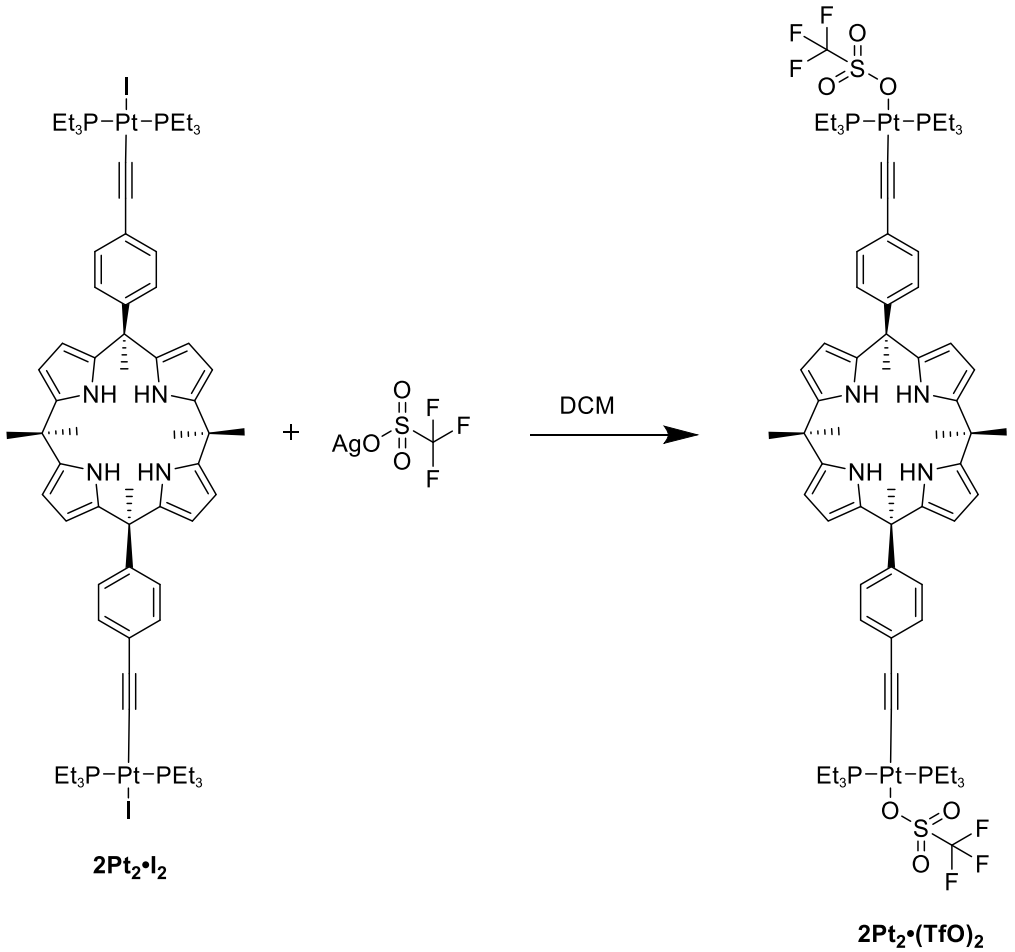

Scheme S 3: *Scheme of the synthesis of* ***2Pt$_2$•(TfO)$_2$****.*

To AgTfO (16 mg, 61 μmol, 2 eq) in a 5 ml amber rounded bottom schlenk under Ar were added 1.3 ml of a ***2*Pt$_2$•*I*$_2$** (50 mg, 29 μmol, 1 eq) previously solubilized in a 5 ml round bottom schlenk with 2.9 ml of dry DCM under Ar, giving at first a white suspension. After 10 minutes, the suspension is filtrate under Ar, using canula filtration with Celite. The solution is dried under Ar atmosphere.

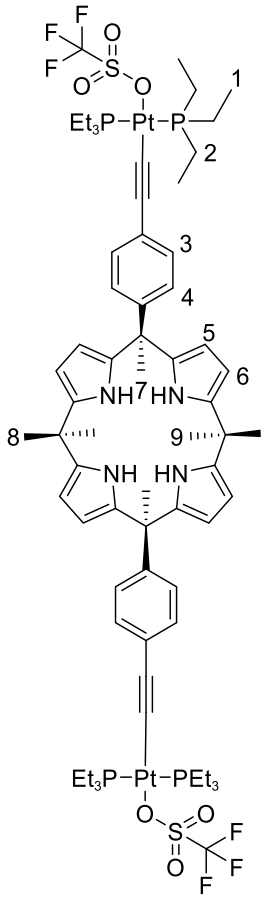

Figure S 10: *Structure of* ***2Pt$_2$•(TfO)$_2$*** *for the assignments.*

^{1}H NMR (500 MHz, CD_2Cl_2, 298 K), δ (ppm) 7.31 (br, 4H, NH), 7.11 (d, 4H, H^3, J^{3-4}= 8.44 Hz), 6.86(d,4H, H^4, $J^{3-4=}$ 8.44 Hz), 5.95(br t, 4H, H^6), 5.67(br t, 4H, H^5), 2.08(m, 12H, H^2), 1.88 (s, 6H, H^7), 1.66(s, 6H, H^9), 1.56 (s, H^8), 1.25 (quin, 18H,H^1). ^{13}C (125 MHz, $CDCl_3$, 298 K) δ (ppm) 145.97, 138.55, 136.31, 130.10, 127.06, 125.68, 120.19, 117.66, 150.87, 103.07, 44.45, 34.95, 30.04, 29.67, 27.18, 26.78, 14.74 (t, J^{C-P}= 17.24 Hz), 7.75.

^{31}P NMR (161 MHz, CD_2Cl_2, 298 K), δ (ppm), P (t, 25.15 ppm, J^{P-Pt} = 1186.17 Hz).

HRMS (MALDI/ TOF) m/z: $[M\text{-}TfO]^+$-= $[C67H98F3N4O3P4Pt2S]^+$ Calcd 1609.555; Found 1609.670.

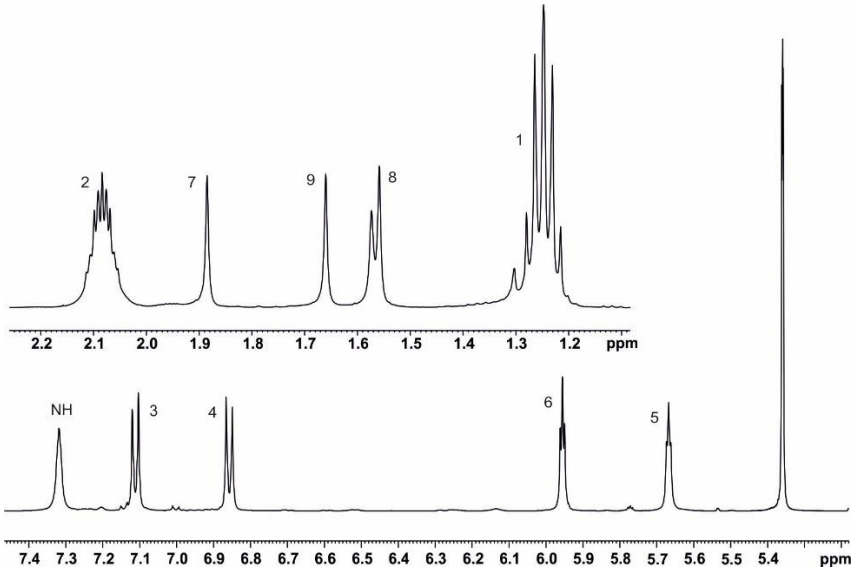

Figure S 11: *^{1}H NMR (500 MHz, CD_2Cl_2, 298 K) for **$2Pt_2$•(TfO)$_2$**, with the assignments.*

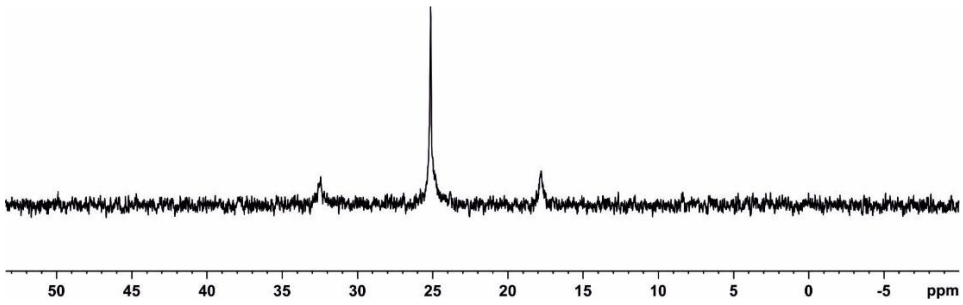

Figure S 12: *^{31}P NMR (161 MHz, CD_2Cl_2, 298 K) of **$2Pt_2$•(TfO)$_2$**.*

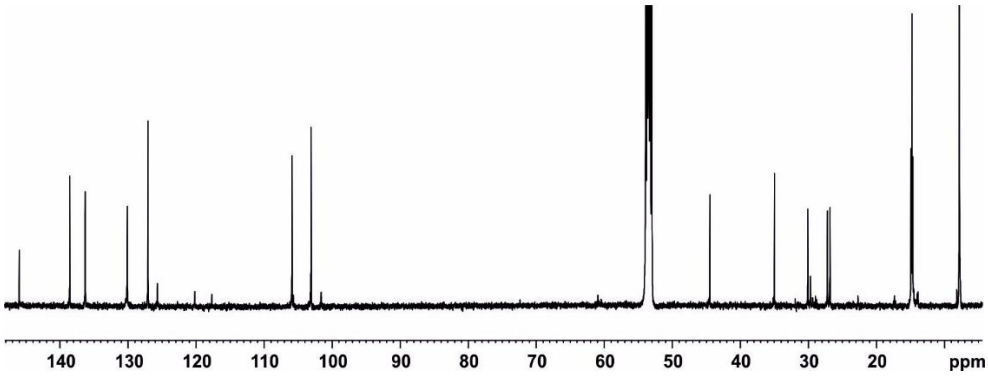

Figure S 13: *^{13}C NMR (125 MHz, $CDCl_3$, 298 K) of* ***$2Pt_2$•$(TfO)_2$****.*

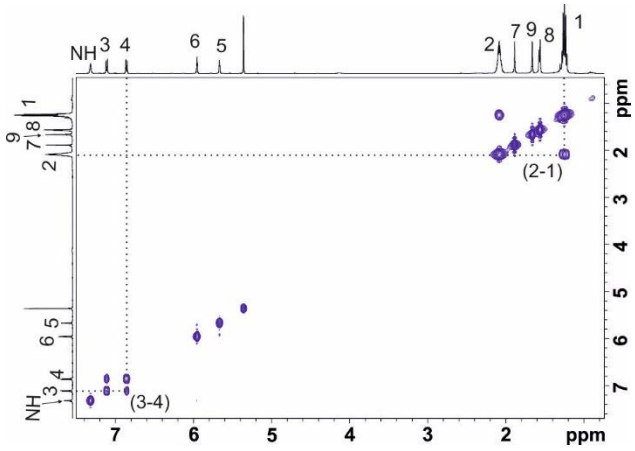

Figure S 14: *COSY NMR (500 MHz, CD_2Cl_2, 298 K) of* ***$2Pt_2$•$(TfO)_2$****, with the assignments.*

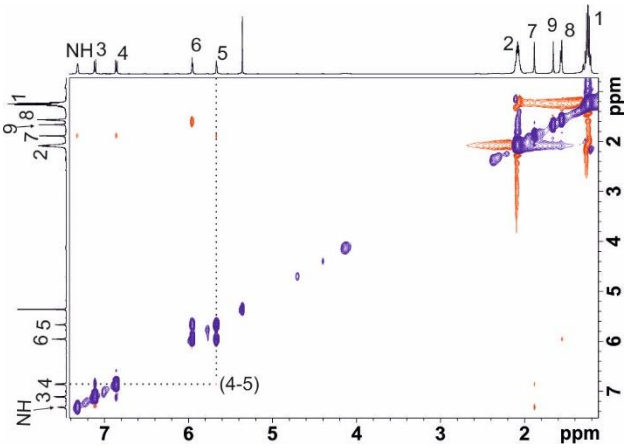

Figure S 15: *ROESY NMR (500 MHz, CD_2Cl_2, 298 K) of* ***$2Pt_2\bullet(TfO)_2$****, with the assignments.*

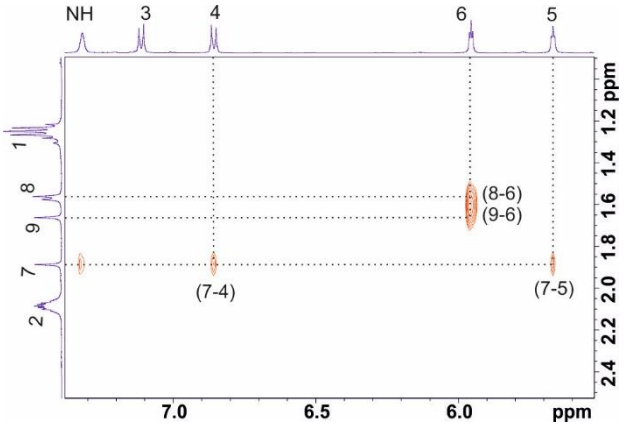

Figure S 16*: ROESY NMR (500 MHz, CD_2Cl_2, 298 K) of* ***$2Pt_2\bullet(TfO)_2$****, with the assignments, zoom.*

Diethyl 4-hydroxypyridine-2,6-dicarboxylate

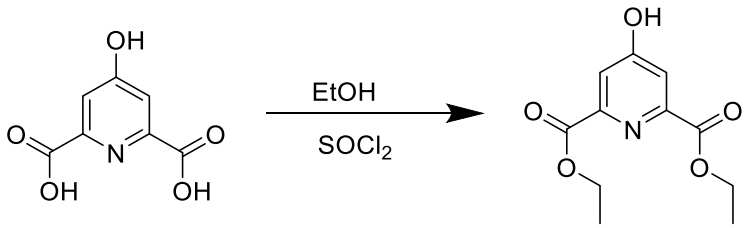

***Scheme S 4**: Scheme of the synthesis of diethyl 4-hydroxypyridine-2,6-dicarboxylate.*

First, 12.6 mL (173 mmol) thionyl chloride was added to 50 mL of anhydrous ethanol in a round-bottom flask under argon flow cooled in an ice bath. Then, 5.03 g (27 mmol) chelidamic acid was added in small portions, and the mixture was stirred for 5 min at 0 ◦C. The mixture was stirred for 20 h at room temperature, followed by 2 h at reflux. The solvent was removed under reduced pressure. The flask with the solid crude product was placed in an ice bath, and 50 mL water were added. The mixture was neutralized with 5 mL of 10% aqueous Na_2CO_3 and 5 mL of 50% aqueous ethanol. The precipitate was filtered and dried under reduced pressure. The product was obtained as a white solid (2.4 g, 90% yield).

^{1}H NMR (300 MHz, d_6-DMSO, 298 K), δ (ppm) H^1(s, 2H, 7.58), H^2(q, 4H, 4.35, J^{2-3}= 7.07 Hz), H^3(t, 3H, 1.33, J^{3-2}= 7.07 Hz).

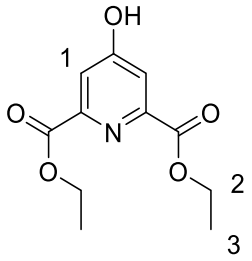

Figure S 17: Structure of diethyl 4-hydroxypyridine-2,6-dicarboxylate for the assignments.

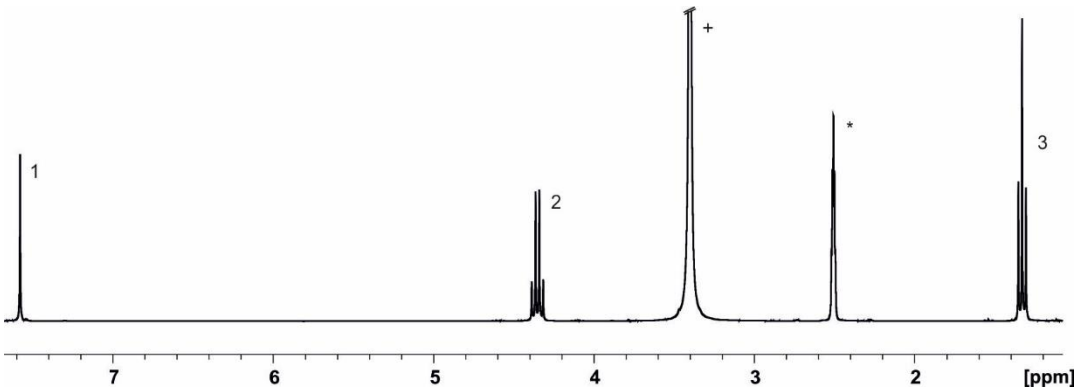

Figure S 18: ^{1}H NMR (300 MHz, d_6-DMSO, 298 K) for diethyl 4-hydroxypyridine-2,6-dicarboxylate, with the assignments.

Diethyl 4-(hexyloxy)pyridine-2,6-dicarboxylate

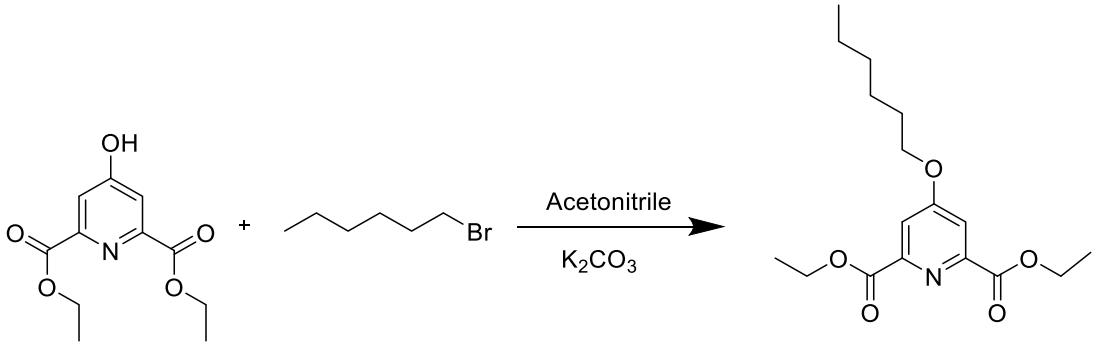

***Figure S 19**: Scheme of the synthesis of diethyl 4-(hexyloxy)pyridine-2,6-dicarboxylate*.

A mixture of 1-bromohexane (386 mL, 2.8 mmol, 1.1 equiv.), diethyl 5-hydroxyisophthalate (600 mg, 2.5 mmol, 1 equiv.), and K_2CO_3 (1.75 g, 12.5 mmol, 5 equiv.) in CH_3CN (25mL) was heated under reflux for 16 h; after cooling down the solution mixture to room temperature, the solvent was evaporated under reduced pressure. The residue was partitioned between CH_2Cl_2 (40 mL) and water (40 mL) and then the organic phase was dried ($MgSO_4$), filtered and concentrated. The residue was purified chromatographically (SiO_2; CH_2Cl_2) to afford a yellow oil (400 mg, 49.3% yield).

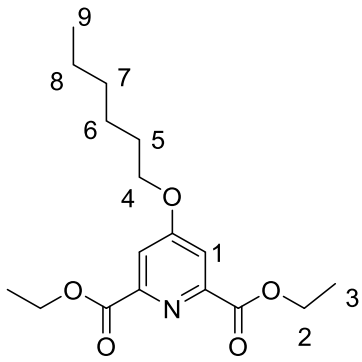

Figure S 20: *Structure of diethyl 4-(hexyloxy)pyridine-2,6-dicarboxylate for the assignments.*

^{1}H NMR (300 MHz, $CDCl_3$, 298 K), δ (ppm) 7.78 (s, 2H, H^1), 4.48 (q, 2H, H^2, J^{2-3}= 7. 17 Hz), 4.14 (t, 2H, H^4, J^{4-5}= 6,46 Hz), 1.85 (m, 2H, H^5), 1.48 (m, 2H, H^6), 1.46 (t, 3H, H^3, J^{3-2}= 7.17 Hz), 1.36 (m, 4H, $H^{7;8}$), 0.92 (t, 3H, H^9).

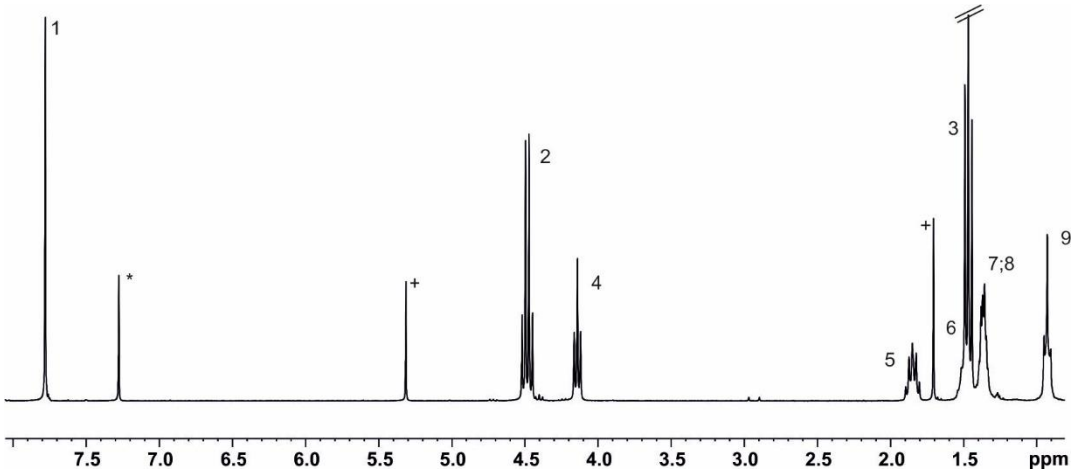

Figure S 21: ^{1}H NMR (300 MHz, $CDCl_3$, 298 K) for diethyl 4-(hexyloxy)pyridine-2,6-dicarboxylate, with the assignments.

4-(hexyloxy)pyridine-2,6-dicarboxylic acid

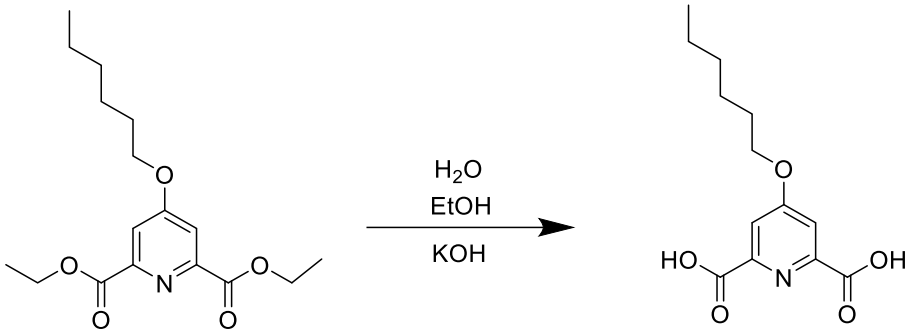

Figure S 22: *Scheme of the synthesis of 4-(hexyloxy)pyridine-2,6-dicarboxylic acid.*

4-(hexyloxy)pyridine-2,6-dicarboxylate 7 (5.7 g, 17.6 mmol) was dissolved in ethanol (200 mL) in an ice bath. A solution of potassium hydroxide (2.4 g, 44 mmol) in ethanol:water (90:10 mL) was added to the cooled solution and the resulting suspension was stirred at room temperature for 2 h. After completion of reaction, ethanol was evaporated and water (30 mL) added to the white residue and pH adjusted to 1.0 with aq. 10% HCl. The resulting precipitate was filtered, washed with water (2×10 mL) and dried to give 4-(hexyloxy)pyridine-2,6-dicarboxylic acid (8, 4.46 g, 16.68 mmol, yield 95%)

The NMR spectroscopy of the compound agrees with the literature[43]

[43] Mirzakhani, M.; Nozary, H.; Naseri, S.; Besnard, C.; Guénée, L.; Piguet, C., Bottom-Up Approach for the Rational Loading of Linear Oligomers and Polymers with Lanthanides. *Inorg. Chem.* **2021,** *60*, 15529-15542.

Hexyloxy -N2,N6-di(pyridin-3-yl)pyridine-2,6-dicarboxamide (3)

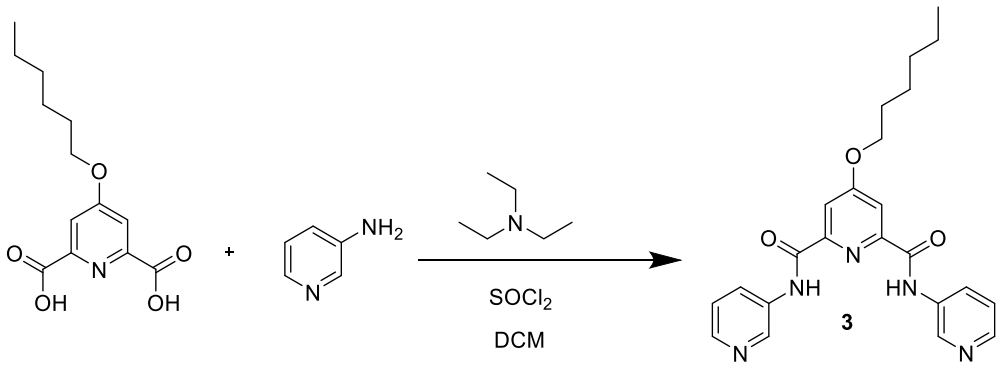

Scheme S 5: *Scheme of the synthesis of 4- Hexyloxy -N2,N6-di(pyridin-3-yl)pyridine-2,6-dicarboxamide.*

A mixture of 4-(hexyloxy)pyridine-2,6-dicarboxylic acid (175 mg, 655 μmol, 1 equiv.) and thionyl chloride (4.6 mL, 63 mmol, 95 equiv.) was heated at reflux under Ar atmosphere. After cooling the mixture, the excess of the $SOCl_2$ was removed under reduced pressure to give the product. The product is washed three times with Dry DCM.

To a solution of 4-(hexyloxy)pyridine-2,6-dicarbonyl dichloride (200 mg, 658 μmol, 1 equiv) in dry CH_2Cl_2 (2.19 mL) at 0 °C was added a solution of 3-aminopyridine (1.27 mL, 1.35 mmol, 2.05 eq) and triethylamine (347 μL, 2.63 mmol, 4 equiv.) in CH_2Cl_2 (1.35 mL). The mixture was stirred at ambient temperature for 1 h and subsequently heated at reflux for 3 h. After the mixture was cooled to room temperature, the suspension was poured in a beaker with saturated aqueous $NaHCO_3$. Then the suspension was filtered and washed with water, giving the crude ligand as a brown solid. The crude was purified by column chromatography (90%DCM 10% IPA 1% TEA) the first fraction taken from the column was a the desired compound, while the second fraction was a mixture of the desired compound. The compound had low solubility in cold DCM, so is possible precipitate it and filter a white compound (62mg, 22% yield).

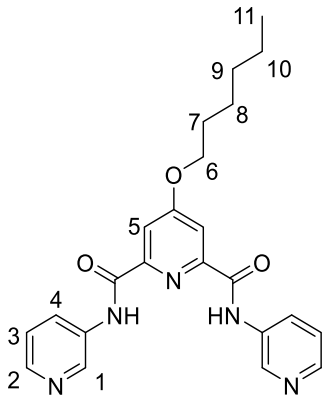

Figure S 23: Structure of 4- Hexyloxy -N2,N6-di(pyridin-3-yl)pyridine-2,6-dicarboxamide.

^{1}H NMR (400 MHz, $CDCl_3$, 298 K), δ (ppm) 10.28 (br, 2H,), 8.80(d br, 2H, H^{1}), 8.30 (br d, 4H, $H^{2,4}$), 7.90(s, 2H, H^{5}), 7.25(dd, 2H, H^{3}), 4.14 (t, 2H, H^{6}, J^{6-7}= 6.63 Hz), 1.85 (m, 2H, H^{7}), 1.48 (m, 2H, H^{8}), 1.37(m, 4H, $H^{9,10}$), 0.93 (t, 2H, H^{11}). ^{13}C (100 MHz, $CDCl_3$, 298 K) δ (ppm) 168.24, 162.283, 150.536, 145.481, 142.096, 134.419, 128.148, 123.798, 112.161, 69.354, 31.422, 28.676, 25.487, 22.541, 13.997.

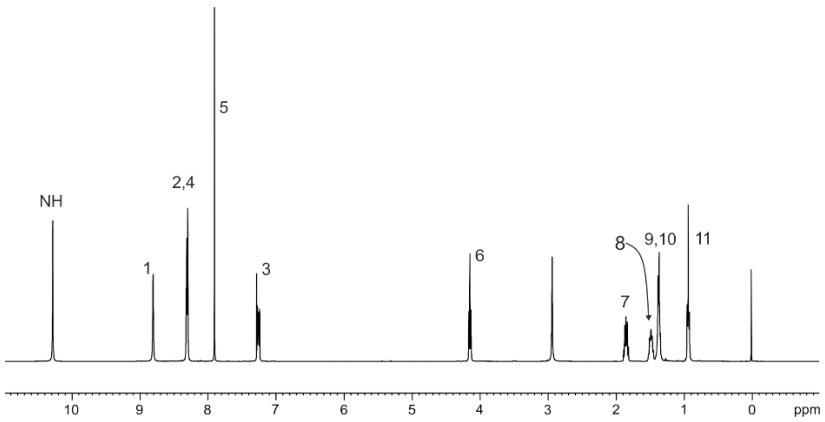

Figure S 24: *^{1}H NMR (400 MHz, $CDCl_3$, 298 K) for 4- Hexyloxy -N2,N6-di(pyridin-3-yl)pyridine-2,6-dicarboxamide, with the assignments.*

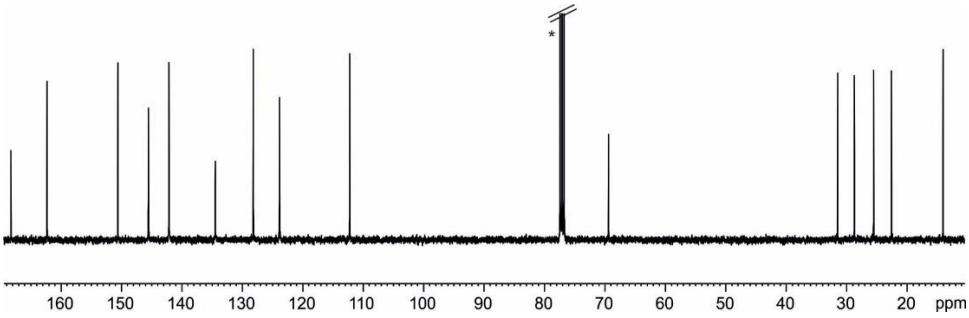

Figure S 25: *^{13}C NMR (100 MHz, $CDCl_3$, 298 K) for 4- Hexyloxy -N2,N6-di(pyridin-3-yl)pyridine-2,6-dicarboxamide.*

4-Hexyloxy-N2,N6-di(pyridin-3-yl)pyridine-2,6-dicarboxamide (4)

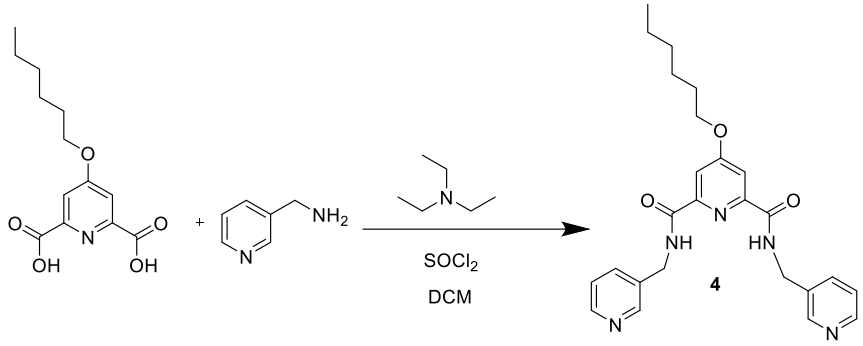

***Scheme S 6*:** Scheme of the synthesis of 4-Hexyloxy-N2,N6-di(pyridin-3-yl)pyridine-2,6-dicarboxamide.

A mixture of 2,6 -dicarboxilic acid (277 mg, 1.04 μmol) and thionyl chloride (4.6 mL, 63 mmol, 60.6 equiv.) was heated at reflux under Ar atmosphere. After cooling the mixture, the excess of the $SOCl_2$ was removed under reduced pressure to give the product. The product is washed 3 times with dry DCM.

To a solution of pyridine-2,6-dicarbonyl dichloride (317 mg, 1.04 μmol, 1 equiv) in dry CH_2Cl_2 (3.47 mL) was added a solution of 3-aminopyridine (212 ml, 2.08 mmol, 2 equiv.) and triethylamine (549 μl, 4.17 mmol, 4 eq) in CH_2Cl_2 (2.53 mL). The mixture was stirred at reflux for 3 h. After the mixture was cooled to room temperature, the suspension was poured in a beaker with saturated aqueous $NaHCO_3$. Then 20 ml of CH_2Cl_2 were added to the suspension and the mixture was washed with water three times (volume30 mL). The organic fractions were

collected, dried over MgSO4, filtered and the solvent was removed under reduced pressure to yield a brown oil.
The crude was purified by column chromatography (95% DCM 5%IPA 1%TEA) the second fraction was a mixture with the desired compound hat was purified a second time by column (Acetone 80%, DCM 20%, TEA 2.5%). The 4-Hexyloxy-N2,N6-di(pyridin-3-yl)pyridine-2,6-dicarboxamide ligand was collected in two fractions, the second one was pure compound (250 mg, 56% yield).

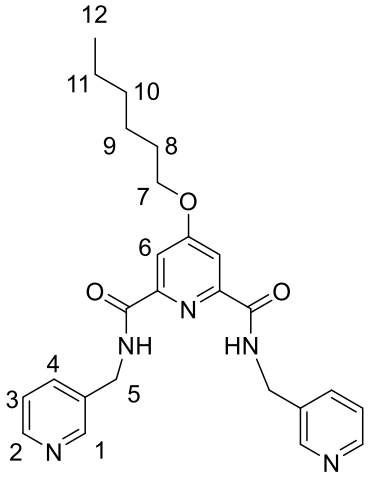

***Figure S 26*:** Structure of 4-Hexyloxy-N2,N6-di(pyridin-3-yl)pyridine-2,6-dicarboxamide.

^{1}H NMR (400 MHz, $CDCl_3$, 298 K), δ (ppm) 9.00 (br t, 2H, NH, J^{NH-5}= 6.36 Hz), 8.39(dd, 2H, H^2, J^{2-3}= 4.86 Hz, J^{2-1}= 1.72 Hz), 8.30 (s, 2H, H^1, J^{1-2}= 1.72 Hz), 7.85 (s, 2H, H^6), 7.58(br dd, 2H, H^4, J^{2-3}= 7.78 Hz), 7.18 (dd, 2H, H^3, , J^{3-4}= 7.78 Hz, J^{3-2}= 4.86 Hz), 4.46 (d, 4H, H^5, J^{5-NH}= 6.36 Hz), 4.16 (t, 2H, H^7, J^{7-8}= 6.63 Hz), 1.85 (quin, 2H, H^8), 1.50 (m, 2H, H^9), 1.38 (m, 4H, $H^{10,11}$), 0.94 (t, 3H, H^{12}). ^{13}C (100 MHz, CDCl3, 298 K) δ (ppm) 168.018, 163.848, 150.655, 148.846, 148.447, 135.625, 134.401, 123.548, 111.216, 69.163, 40.609, 31.427, 28.707, 25.455, 22.553, 13.761.

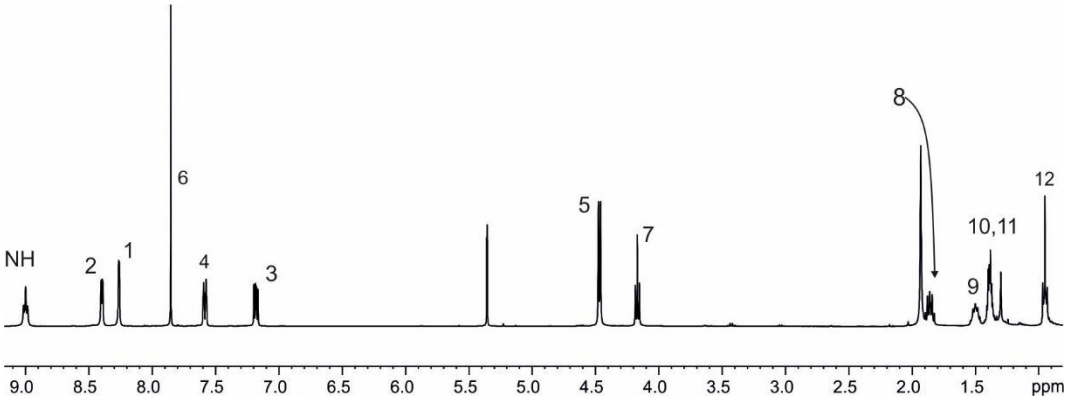

Figure S 27: ^{1}H NMR (400 MHz, $CDCl_3$, 298 K) for 4-Hexyloxy-N2,N6-di(pyridin-3-yl)pyridine-2,6-dicarboxamide, with the assignments.

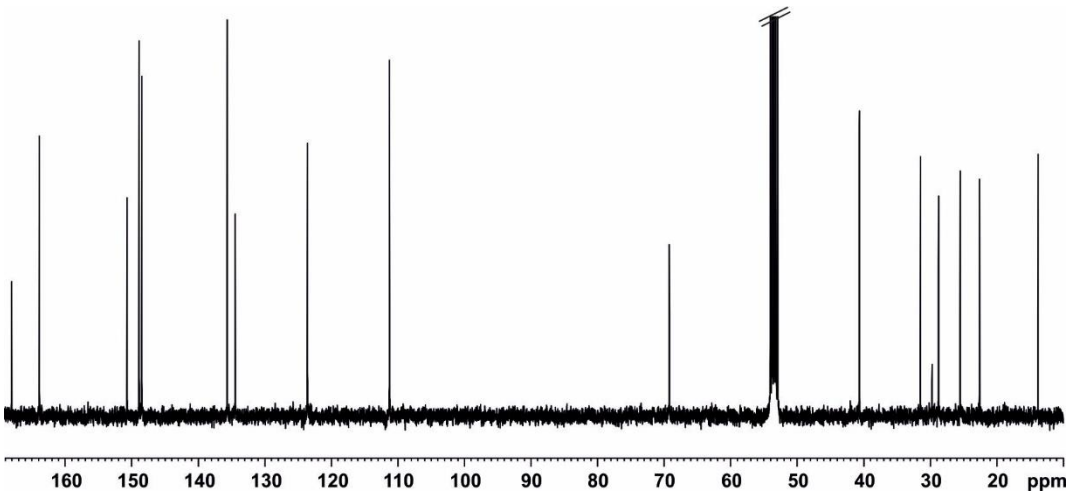

***Figure S 28*:** ^{13}C NMR (100 MHz, $CDCl_3$, 298 K) for 4-Hexyloxy-N2,N6-di(pyridin-3-yl)pyridine-2,6-dicarboxamide.

Self-assembly of Metallocycles based on a p,p'-diethynyl "two wall" Calix[4]pyrrole diplatinum(II) complex.

2Pt$_2$•3-(TfO)$_2$

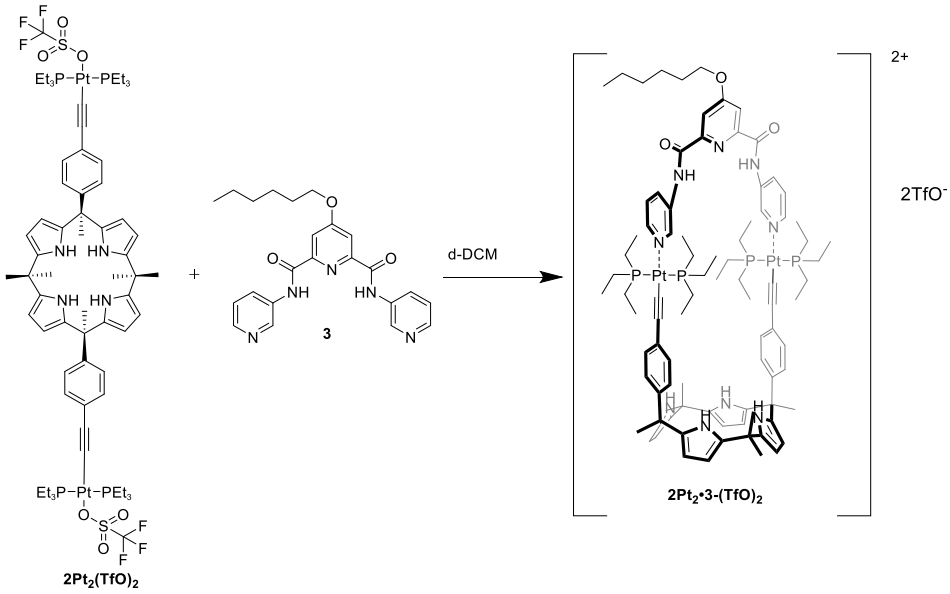

Scheme S 7: *Scheme of the assembly of the* ***2Pt$_2$•3-(TfO)$_2$****.*

The self-assembly of the metallacycle ***2*Pt$_2$•*3*-(TfO)$_2$** was achieved by titration of a 4.3 mM solution of ***2*Pt$_2$•(TfO)$_2$** in CD_2Cl_2, with a solution 0.04 M of **3** in CD_2Cl_2.

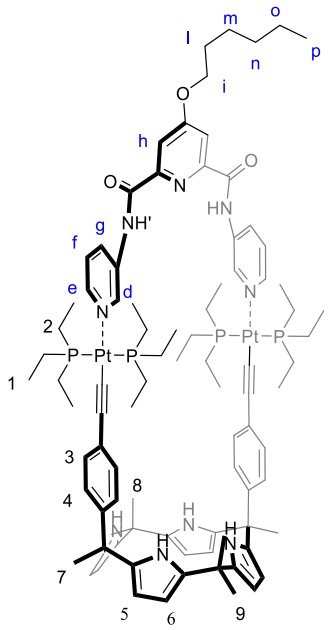

***Figure S 29**: Structure of **2Pt₂•3-(TfO)₂** for the assignments.*

^{1}H NMR (500 MHz, CD_2Cl_2, 298 K), δ (ppm) 11.14 (br, 2H, NH'), 9.66 (s, 2H, H^d), 8.43 (d, 2H, H^g), 8.33 (d, 2H, H^e), 7.98 (s, 2H, H^h), 7.65 (q, 2H, H^f), 7.34 (br, 4H, NH), 7.19 (d, 4H, H^3, J^{3-4}= 8.26 Hz), 6.90(d, 4H, H^4, J^{3-4}= 8.26 Hz), 5.97 (br t, 4H, H^6), 5.68(br t, 4H, H^5), 4.26 (t, 2H, H^i, J^{i-l}= 6.39 Hz), 1.90(s, 6H, H^7), 1.89 (m, 2H, H^l), 1.98 (m, 12H, H^2), 1.67 (s, 6H, H^9), 1.50 (s, 6H, H^8),1.55 (m br, 2H, H^m), 1.41 (m br, 4H, H^{n-o}), 1.22 (m, 18H, H^1), 0.96 (t, 3H, H^p). ^{31}P NMR (161 MHz, CD_2Cl_2, 298 K), δ(ppm), P (t, 18.802 ppm, J^{P-Pt} = 1168.37 Hz). Nominal mass (MALDI/ TOF) m/z: $[M\text{-}TfO]^+$-= $[C90H123F3N9O6P4Pt2S]^+$ Found 2029.8.

Self-assembly of Metallocycles based on a p,p'-diethynyl "two wall" Calix[4]pyrrole diplatinum(II) complex.

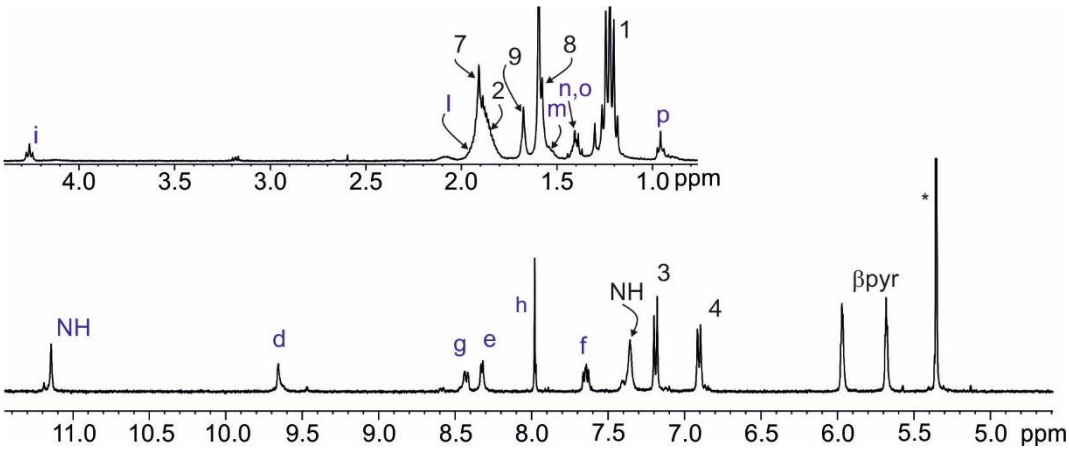

Figure S 30: ^{1}H NMR for the **2*Pt$_2$*•3-*(TfO)$_2$*** in CD_2Cl_2, with the assignments.

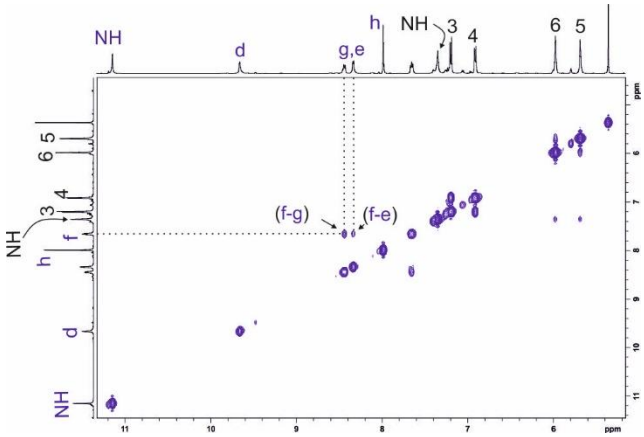

Figure S 31: COSY NMR (500 MHz, CD_2Cl_2, 298 K) spectrum of **2*Pt$_2$*•3-*(TfO)$_2$*** (aromatic region).

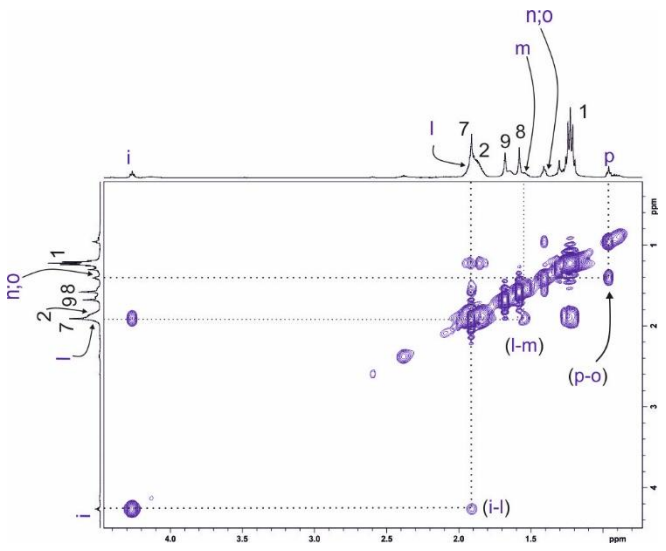

Figure S 32: COSY NMR (500 MHz, CD_2Cl_2, 298 K) spectrum of **2*Pt₂*•3-*(TfO)₂*** (aliphatic region).

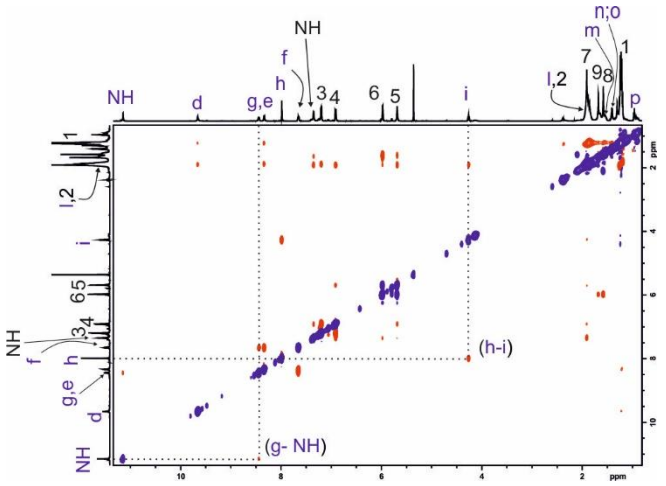

Figure S 33: ROESY NMR (500 MHz, CD_2Cl_2, 298 K) spectrum of **2*Pt₂*•3-*(TfO)₂***.

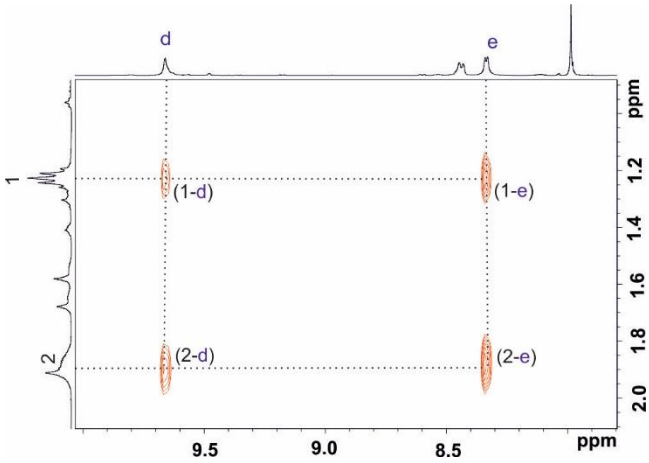

Figure S 34: ROESY NMR (500 MHz, CD_2Cl_2, 298 K) spectrum of **2*Pt₂*•3-*(TfO)₂***, zoom.

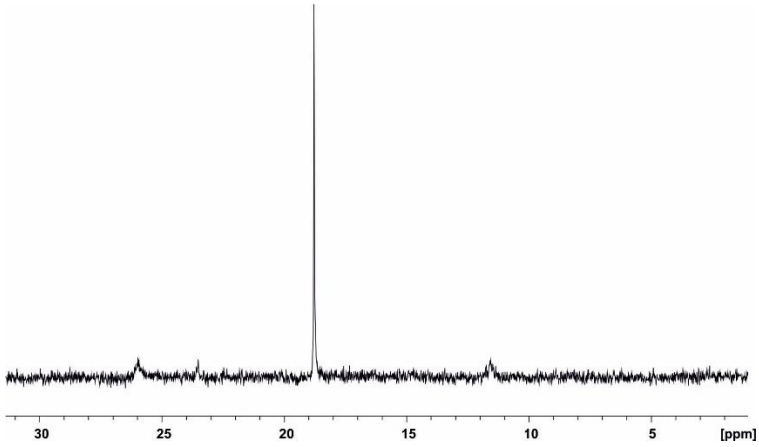

Figure S 35: ^{31}P NMR (161 MHz, CD_2Cl_2, 298 K) spectrum of **2*Pt₂*•3-*(TfO)₂***.

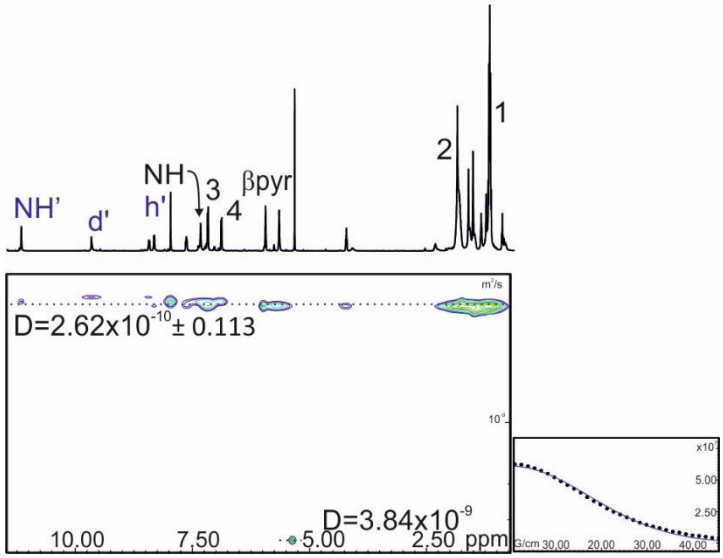

Figure S 36: DOSY experiment (500 MHz, CD_2Cl_2, 298 K) for **$2Pt_2$•3-*(TfO)*$_2$**, with the assignments.

2Pt₂•4-(TfO)₂

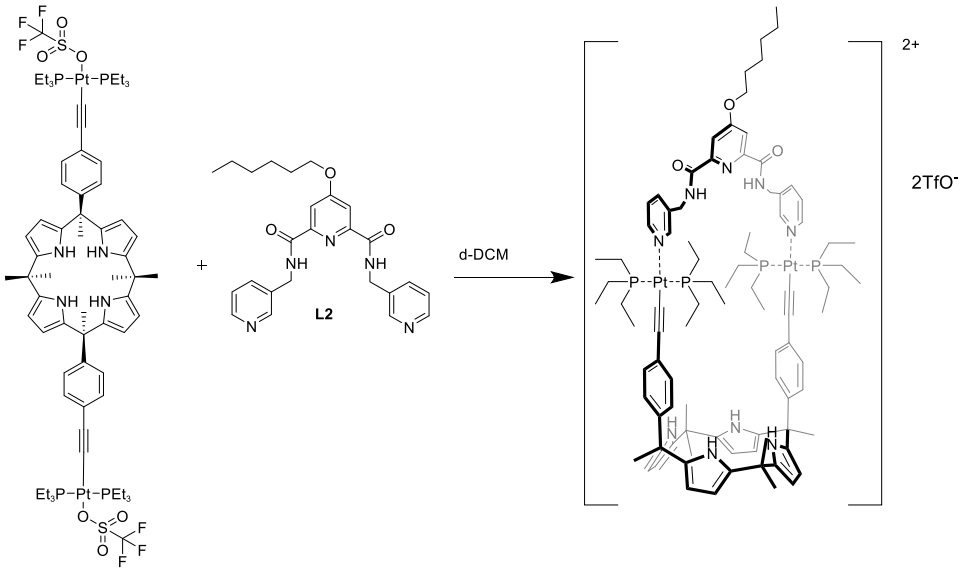

Scheme S 8: *Scheme of the assembly of the* ***2Pt₂•4-(TfO)₂****.*

The self-assembly of the metallacycle ***2*Pt₂•*4*-(TfO)₂** was achieved by titration of a 4.3 mM solution of ***2*Pt₂•(TfO)₂** in CD_2Cl_2, with a solution 0.04 M of **4** in CD_2Cl_2.

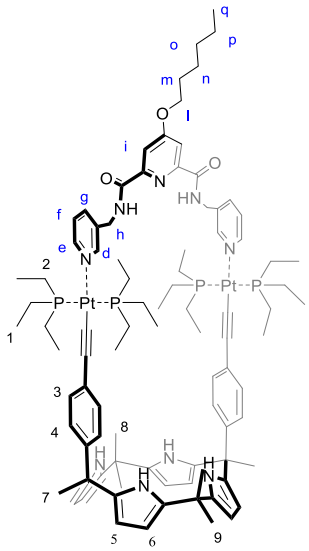

Figure S 37: *Structure of* ***2Pt$_2$•4-(TfO)$_2$*** *for the assignments.*

^{1}H NMR (500 MHz, CD_2Cl_2, 298 K), δ (ppm) 9.91 (br, 2H, NH, $J^{NH'-h}$= 6.04 Hz), 8.76 (s, 2H, H^d), 8.41 (d, 2H, H^e, J^{e-f}= 5.30 Hz), 8.20 (d, 2H, H^g, J^{g-f}= 8.09 Hz), 7.74 (s, 2H, H^i), 7.59 (br q, 2H, H^f), 7.39 (br, 4H, NH), 7.16 (d, 2H, H^3, J^{3-4}= 8.19 Hz), 6.89(d, 2H, H^4, J^{4-3}= 8.19 Hz), 5.96 (br t, 4H, H^6), 5.67 (br t, 4H, H^5), 4.75 (d,, 4H, H^h, $J^{h-NH'}$= 6.04 Hz), 4.14 (t, 2H, H^l, J^{l-m}= 6.37 Hz), 1.89 (s,6H, H^7), 1.78 (m, 3H, H^m), 1.78 (m, 12H, H^2), 1.66 (s, 6H, H^9), 1.56 (s, 6H, H^8), 1.48 (m br, 2H, H^n), 1.36 (m br, 4H, H^{o-p} ppm), 1.13(m, 18H, H^1), 0.92(t, 3H, H^q). ^{31}P NMR (161 MHz, CD_2Cl_2, 298 K), δ (ppm), P (t, 18.90 ppm, J^{P-Pt} = 1163.89 Hz). HRMS (ESI/ TOF) m/z: $[M-TfO]^+$-= $[C92H127F3N9O6P4Pt2S]^+$ Calcd 256.7822; Found 2056.7832.

Self-assembly of Metallocycles based on a p,p'-diethynyl "two wall" Calix[4]pyrrole diplatinum(II) complex.

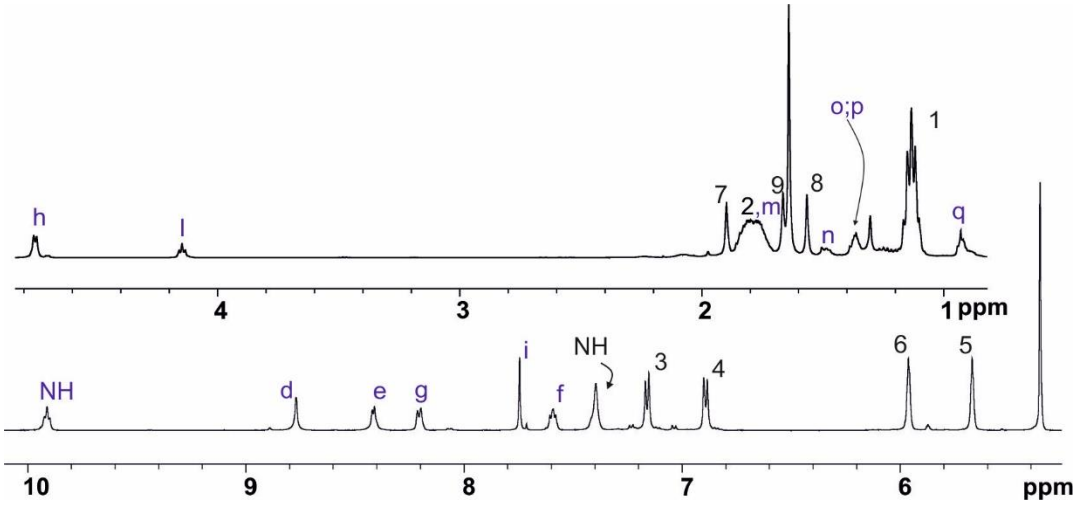

***Figure S 38**: ^{1}H NMR for the **$2Pt_2$•4-$(TfO)_2$** in CD_2Cl_2, with the assignments.*

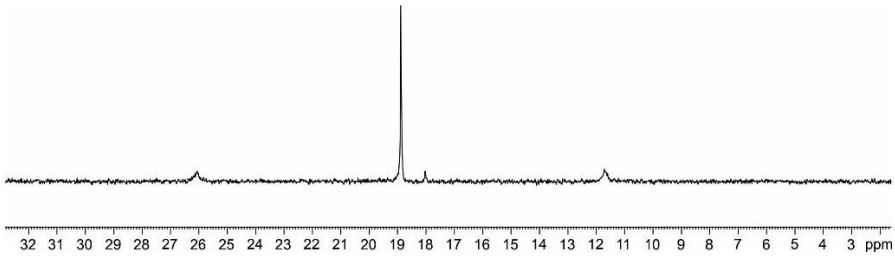

***Figure S 39**: ^{31}P NMR (161 MHz, CD_2Cl_2, 298 K) spectrum of **$2Pt_2$•4-$(TfO)_2$**.*

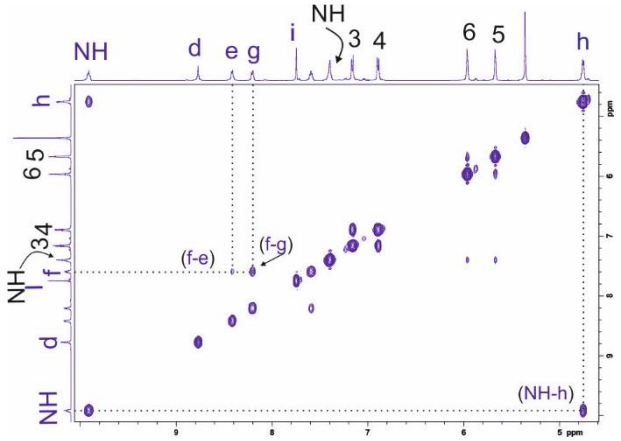

***Figure S 40**: COSY NMR (500 MHz, CD_2Cl_2, 298 K) spectrum of **$2Pt_2$•4-$(TfO)_2$** (aromatic region).*

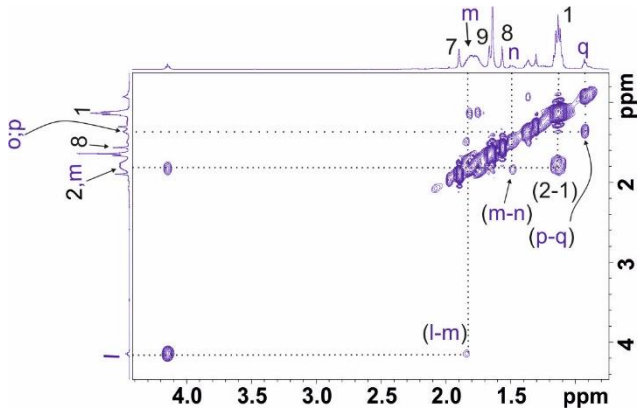

***Figure S 41:** COSY NMR (500 MHz, CD_2Cl_2, 298 K) spectrum of **$2Pt_2$•4-$(TfO)_2$** (alifatic region).*

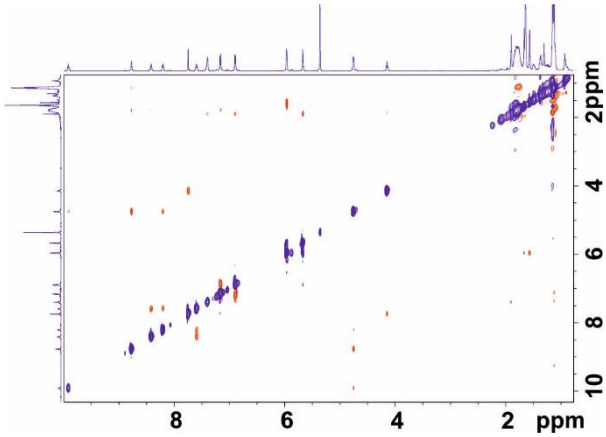

Figure S 42: *ROESY NMR (500 MHz, CD_2Cl_2, 298 K) spectrum of* ***2Pt₂•4-(TfO)₂.***

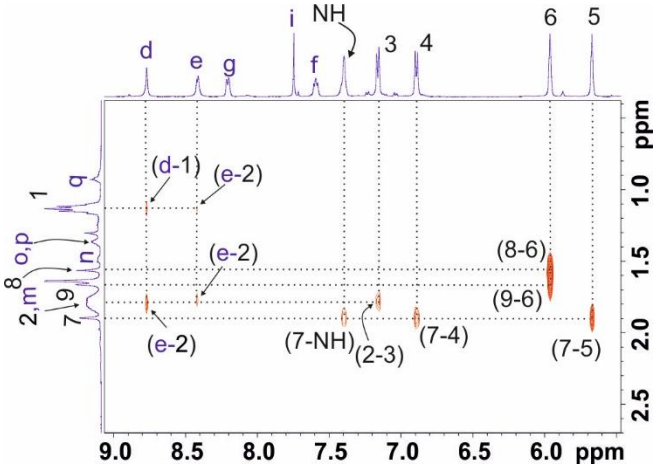

Figure S 43: *ROESY NMR (500 MHz, CD_2Cl_2, 298 K) spectrum of* ***2Pt₂•4-(TfO)₂*** *(zoom).*

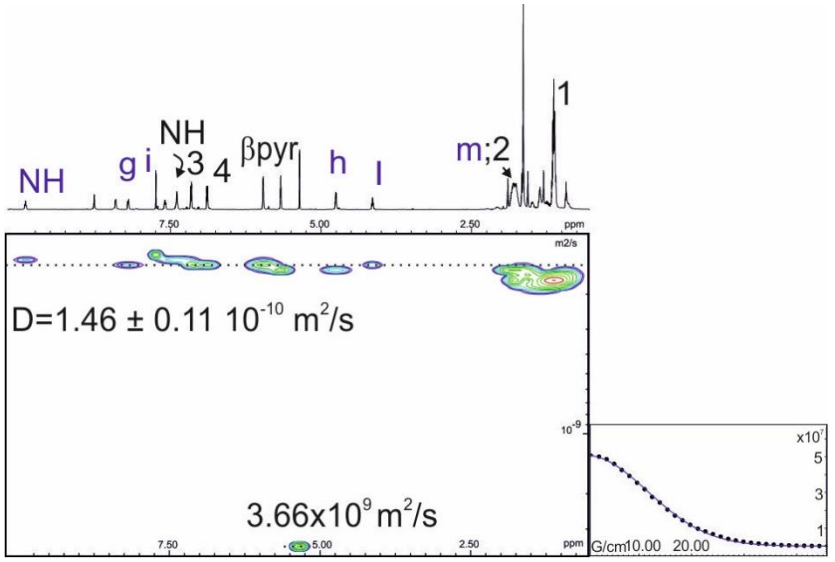

Figure S 44: *DOSY experiment (500 MHz, CD_2Cl_2, 298 K) for* ***2Pt₂•4-(TfO)₂****, with the assignments.*

3.4.3 ^{1}H NMR binding studies

A ~4 mM solution of **2Pt₂•I₂**, ***2*Pt₂•*3*-(TfO)₂** or **6** was prepared in dichloromethane-d_2. Subsequently, 0.5 mL of the solution were transferred to an NMR tube. The remaining solution of the host was used to prepare the titrant's solution, which contained guest **5** at 50-fold higher concentration ([**5**] = 225 mM and [H] = 4.6 mM). In the case of the reverse titration the remaining solution of the **6** was used to prepare the titrant's solution, which contained **2Pt₂•I₂** at 12-fold higher concentration ([**2Pt₂•I₂**] = 52 mM and [**6**] = 4 mM). In this manner, the concentration of the host was maintained constant throughout the titration. Regarding the titration of ***2*Pt₂•*3*-(TfO)₂** the guest was solubilized in the same solvent containing **5** or **6** at 50-fold higher concentration ([**G**] = 225 mM and [H] = 4.6 mM). Immediately, the 0.5 mL of the host solution was titrated by manually injecting incremental amounts of the titrant's solution using a micro syringe. A ^{1}H NMR spectrum of the mixture was acquired after each injection and vigorous hand shaking of the NMR tube for few seconds. The apparent binding constants were derived from the fit of

the chemical shift changes of the titration data to a 1:1 theoretical binding model and using the HypNMR2008[44,45] software.

$2Pt_2 \bullet I_2$ vs 5

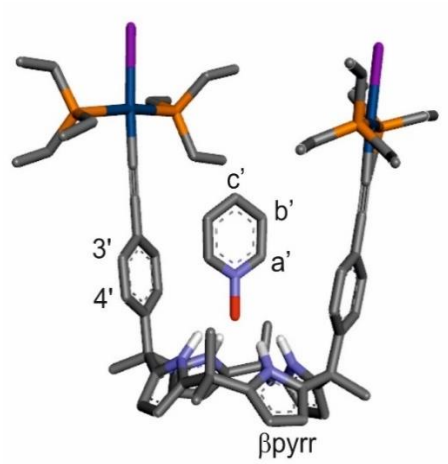

[44] Frassineti, C.; Alderighi, L.; Gans, P.; Sabatini, A.; Vacca, A.; Ghelli, S., Determination of protonation constants of some fluorinated polyamines by means of 13C NMR data processed by the new computer program HypNMR2000. Protonation sequence in polyamines. *Anal. Bioanal. Chem.* **2003,** *376*, 1041-1052.

[45] Frassineti, C.; Ghelli, S.; Gans, P.; Sabatini, A.; Moruzzi, M. S.; Vacca, A., Nuclear Magnetic Resonance as a Tool for Determining Protonation Constants of Natural Polyprotic Bases in Solution. *Anal. Biochem.* **1995,** *231*, 374-382.

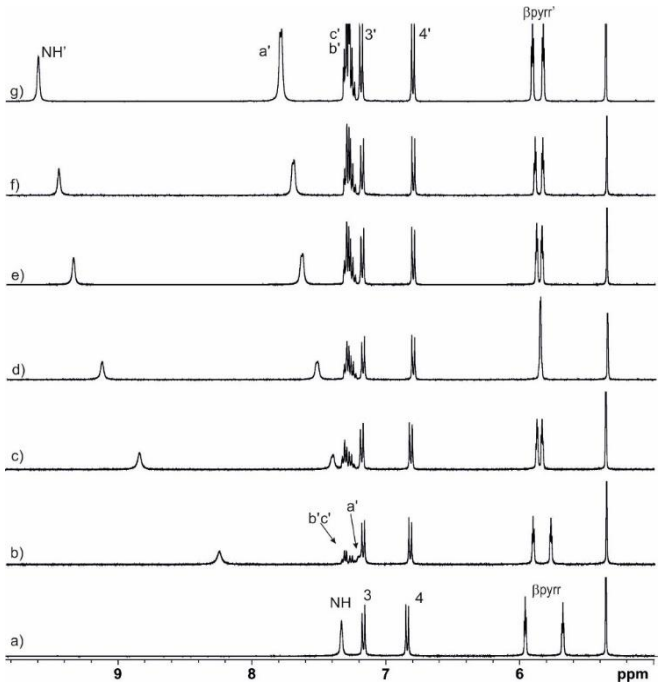

***Figure S 45**: Selected regions of the ^{1}H NMR spectra (400 MHz, CH_2Cl_2, 298 K) of **$2Pt_2•I_2$** (4.6 mM) with incremental amounts of pyridine N-oxide **5:** a) 0 equiv. b) 1 equiv.; c) 2 equiv.; d) 3 equiv.; e) 4 equiv.; f) 5 equiv. and g) 6 equiv. See above for proton assignment.*

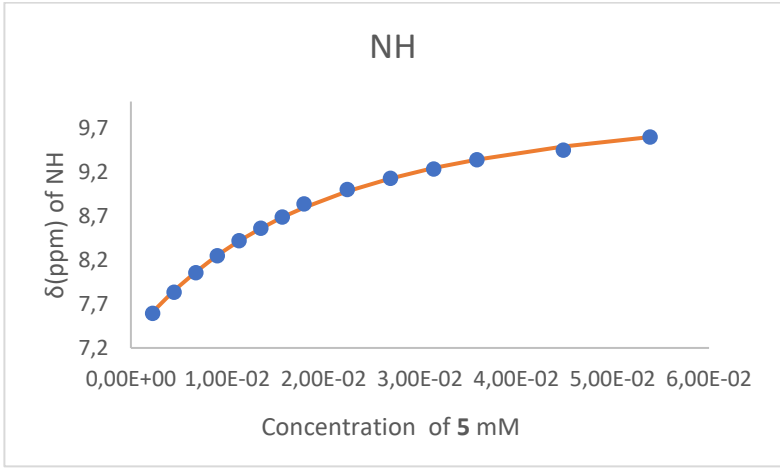

***Figure S 46:** Chemical shifts changes of NH pyrrole protons of **$2Pt_2•I_2$** upon incremental amounts of **5** and fit of the data to a theoretical 1:1 binding model*

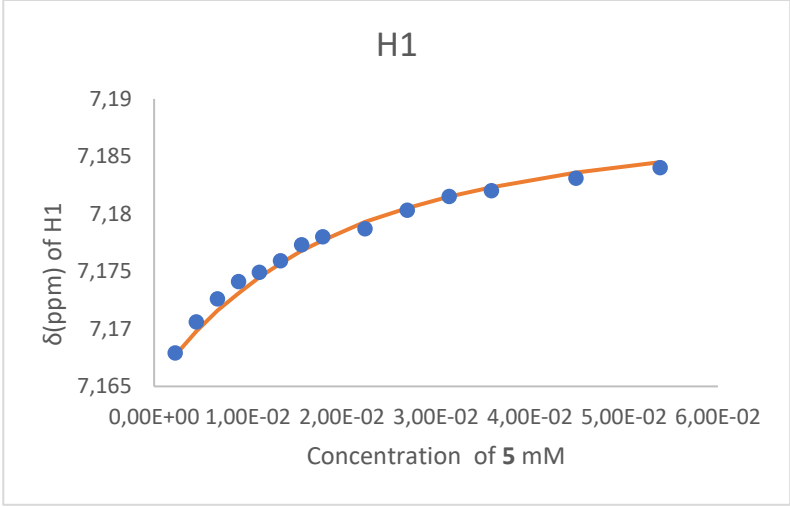

Figure S 47: *Chemical shifts changes of aromatic protons H1 of* ***2Pt$_2$•I$_2$*** *upon incremental amounts of* ***5*** *and fit of the data to a theoretical 1:1 binding model*

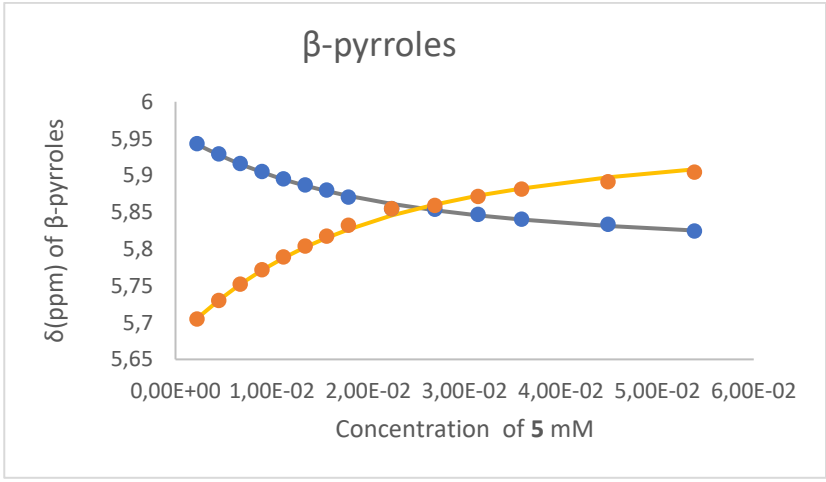

Figure S 48: *Chemical shifts changed of the β-pyrroles protons of* ***2Pt$_2$•I$_2$*** *upon incremental amounts of* ***5*** *and fit of the data to a theoretical 1:1 binding model.*

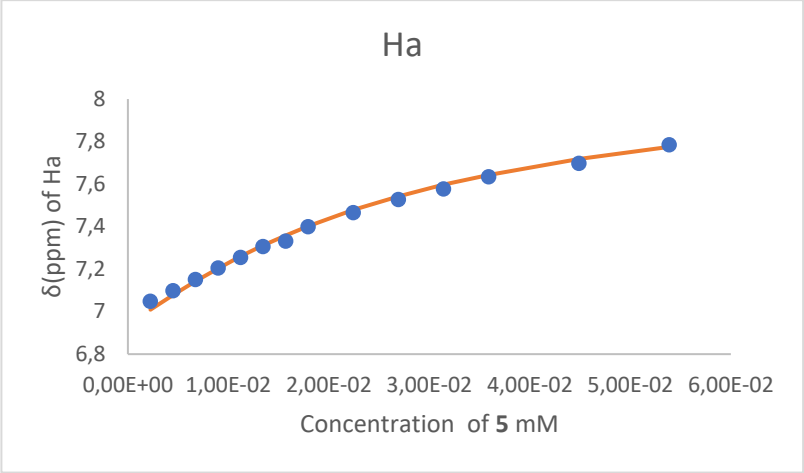

Figure S 49: *Chemical shifts changes of Ha protons of guest **5** upon incremental amounts of **5** to a mM solution of $2Pt_2 \bullet I_2$ and fit of the experimental data to a theoretical 1:1 binding model.*

Table S 1: *Table of chemical induced shifts (CIS) of several protons during the titration of **2Pt2•I2** with **5**.*

	NH	**H1**	**β-pyrroles**	**β-pyrroles**	**Ha**
δ_{free} (ppm)	7.33	7.16	5.96	5.79	8.17
δ_{bound} (ppm)	10.23	7.19	5.68	5.97	5.12
Δδ (ppm)	+2.9	+0.03	-0.28	+0.18	-3.05

Self-assembly of Metallocycles based on a p,p'-diethynyl "two wall" Calix[4]pyrrole diplatinum(II) complex.

$2Pt_2 \bullet I_2$ vs 6

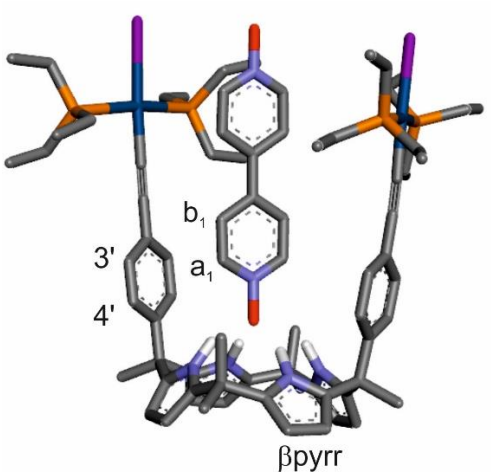

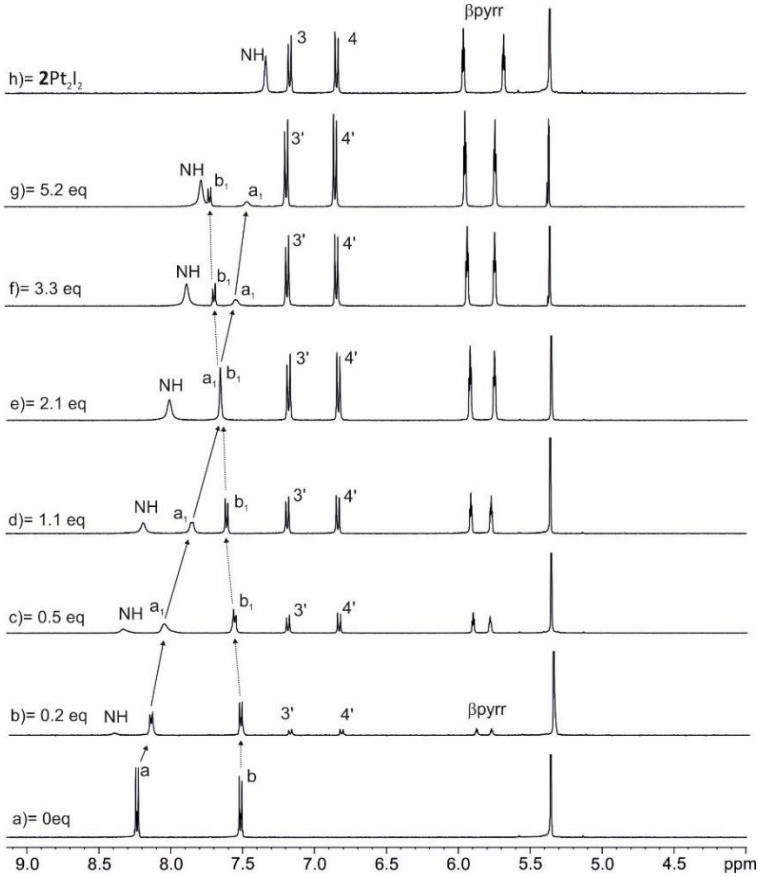

Figure S 50: *Selected region of the ^{1}H NMR spectra acquired during the titration of the **6** (4 mM) (a) with incremental amounts of **2 Pt_2•I_2** (h) in CD_2Cl_2 solution: a) 0 equiv; b) 0.2 equiv; c) 0.5 equiv; d) 1.1 equiv; e) 2.1 equiv; f) 3.3 equiv and g) 5.2 equiv.*

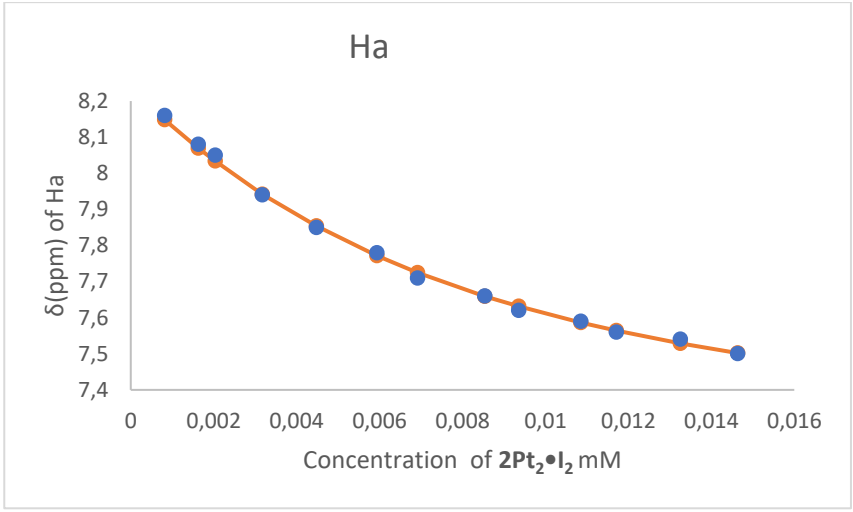

Figure S 51: *Chemical shifts of aromatic protons Ha of* ***6*** *upon incremental amounts of* ***2Pt$_2$•I$_2$*** *and fit of the NMR titration data to a theoretical 1:1 binding model*

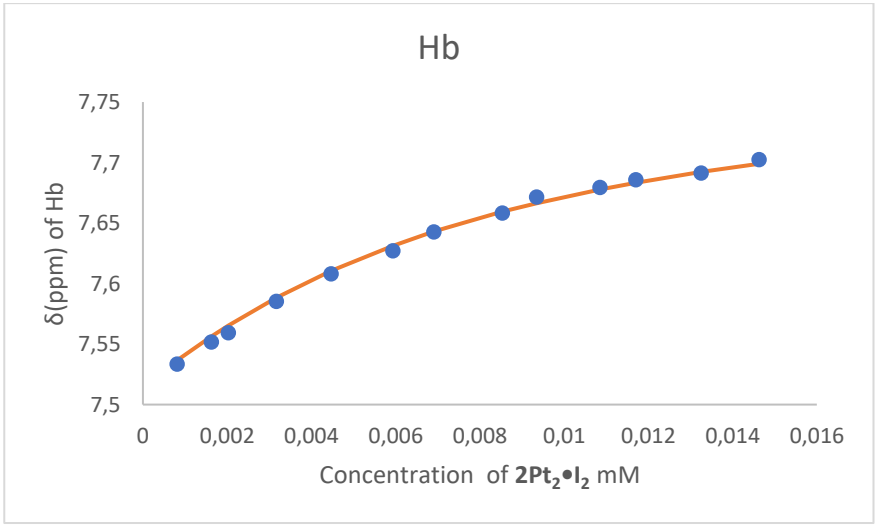

Figure S 52: *Chemical shifts of aromatic protons Hb of* ***6*** *upon incremental amounts of* ***2Pt$_2$•I$_2$*** *and fit of the NMR titration data to a theoretical 1:1 binding model*

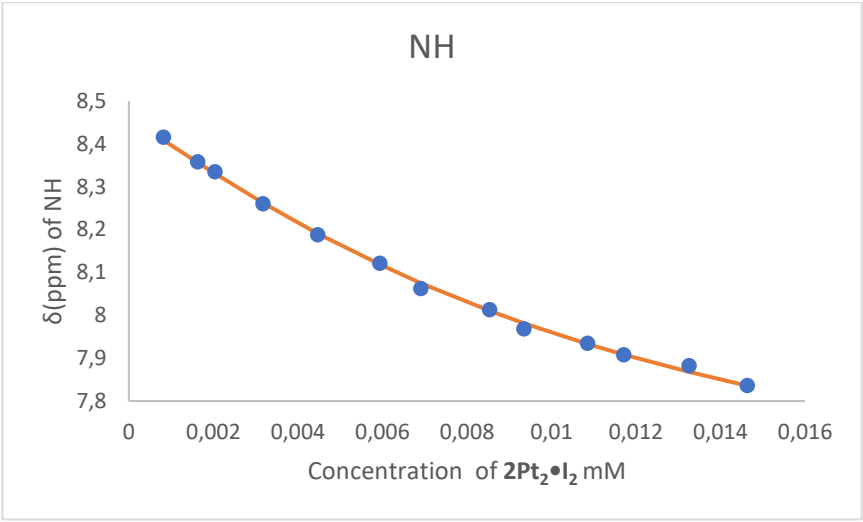

Figure S 53: *Chemical shifts of the NH protons of* ***2Pt₂•I₂*** *upon incremental amounts of* ***2Pt₂•I₂*** *and fit of the NMR titration data to a theoretical 1:1 binding model.*

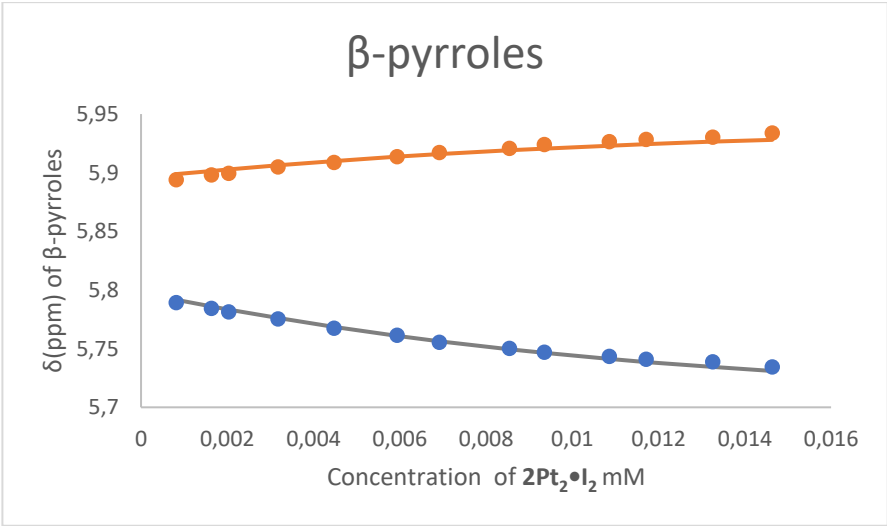

Figure S 54: Chemical shifts of the β-pyrroles protons of ***2Pt₂•I₂*** *upon incremental amounts of* ***2Pt₂•I₂*** *and fit of the NMR titration data to a theoretical 1:1 binding model.*

Table S 2: *Table of chemical induced shifts (CIS) of several protons during the titration of* ***6*** *with* ***2Pt2•I2****.*

	NH	**β-pyrroles**	**β-pyrroles**	**Ha**	**Hb**
δ_{free} (ppm)	7.33	5.96	5.68	8.23	7.51
δ_{bound} (ppm)	9.98	5.81	5.96	7.16	7.78
Δδ (ppm)	+2.65	-0.15	+0.28	-1.08	-0.27

Self-assembly of Metallocycles based on a-p,p'-diethynyl "two wall" Calix[4]pyrrole diplatinum(II) complex.

2Pt_2•3-$(TfO)_2$ vs 5

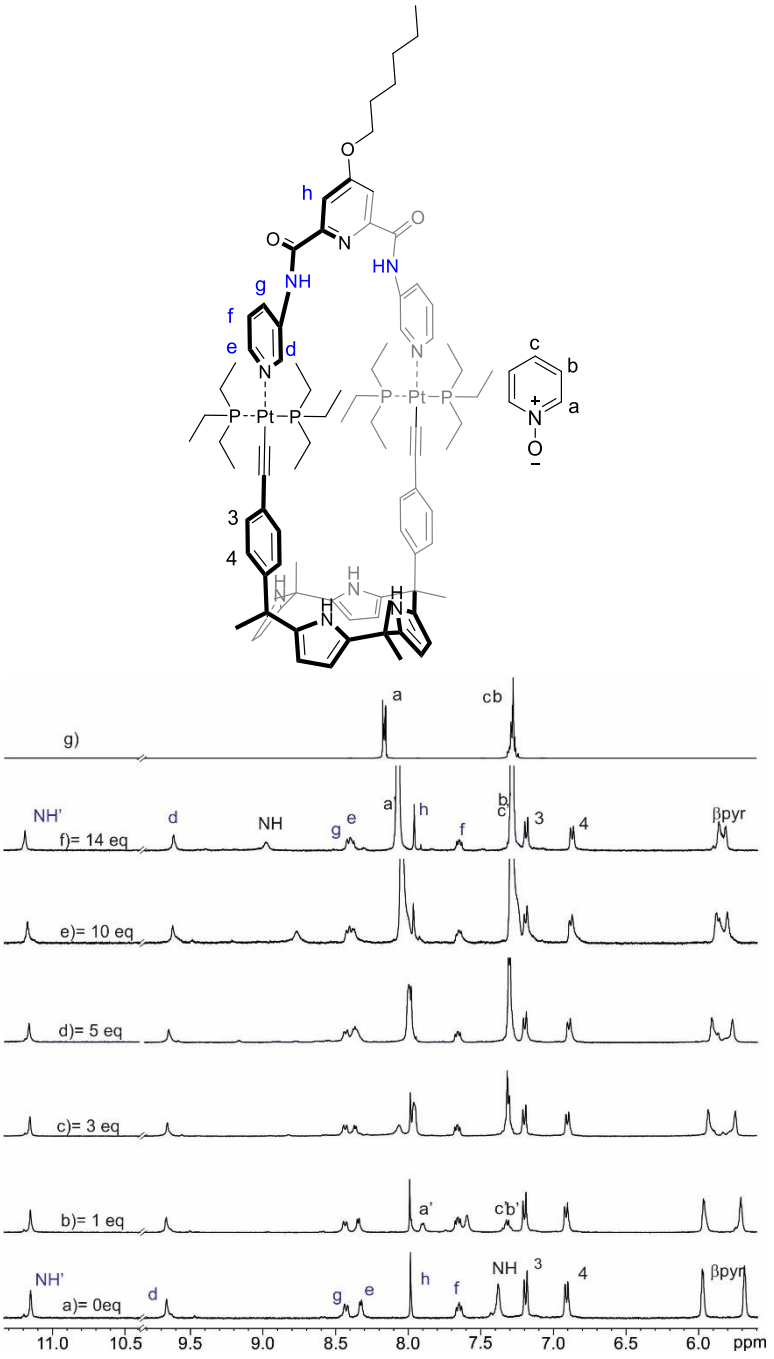

Figure S 55: *Selected regions of the ^{1}H NMR spectra (400 MHz, CH_2Cl_2, 298 K) of* ***2Pt$_2$•3-(TfO)$_2$*** *(4.6 mM) (a) with incremental amounts of Pyridine N-oxide* ***5*** *(g) b) 1 equiv.; c) 3 equiv.; d) 5 equiv.; e) 10 equiv. f) 14 equiv. and g) free pyridine N-oxide. See top panel for proton assignment.*

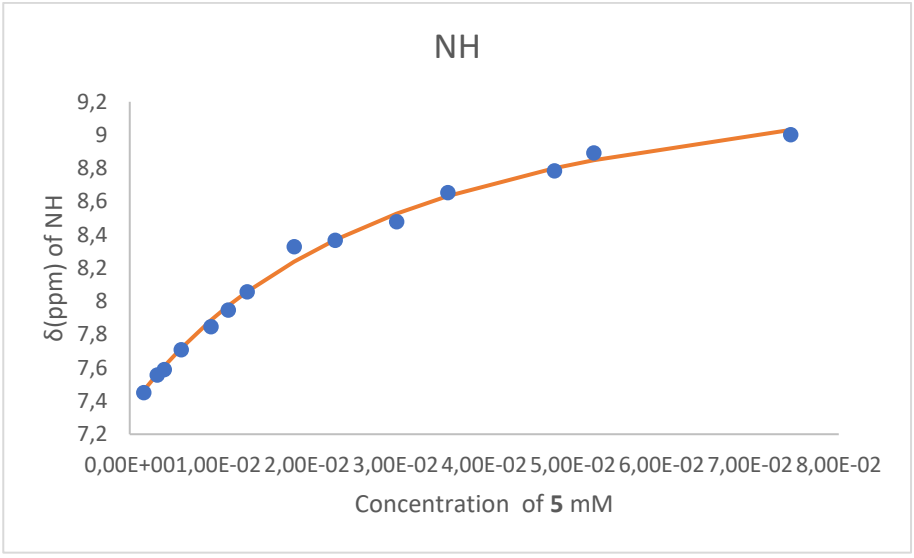

Figure S 56: *Chemical shifts of the NH protons of* ***2Pt$_2$•3-(TfO)$_2$*** *upon incremental amounts of* ***5*** *and fit of the NMR titration data to a theoretical 1:1 binding model.*

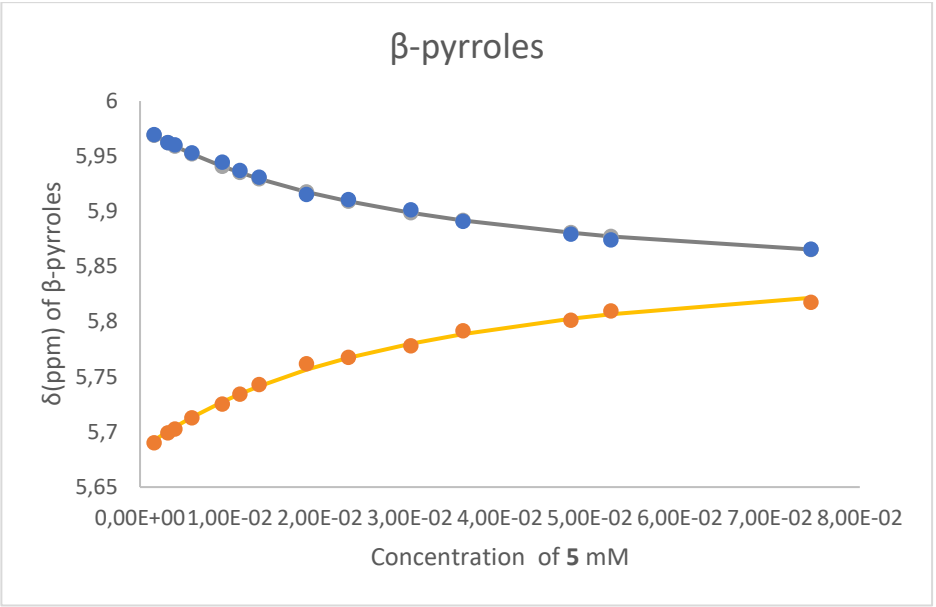

Figure S 57: *Chemical shifts of the β-pyrroles protons of* ***2Pt$_2$•3-(TfO)$_2$*** *upon incremental amounts of* ***5*** *and fit of the NMR titration data to a theoretical 1:1 binding model.*

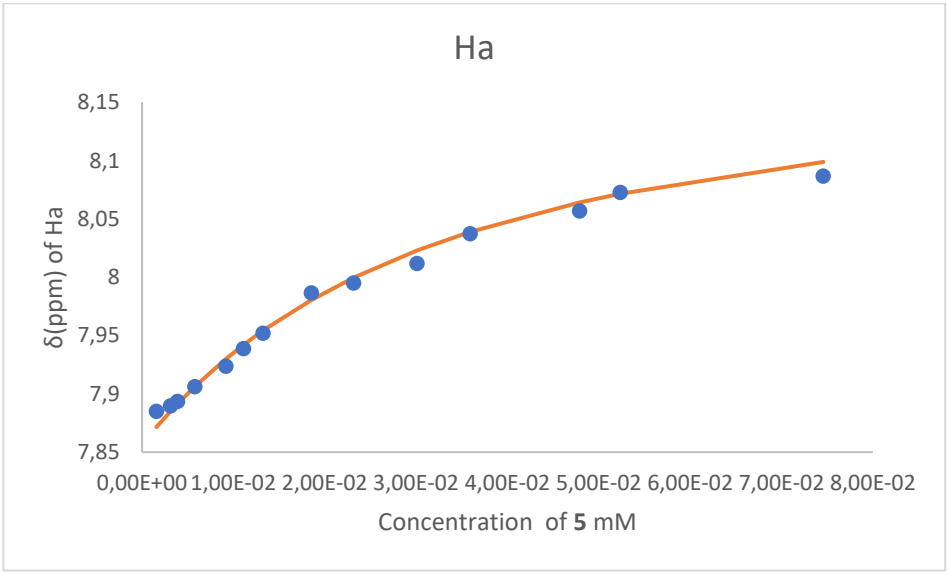

Figure S 58*: Chemical shifts of the Ha protons α to the nitrogen of* ***5*** *upon incremental amounts of* ***5*** *and fit of the NMR titration data to a theoretical 1:1 binding model.*

Table S 3: *Table of chemical induced shifts (CIS) of several protons during the titration of* ***2Pt$_2$•3-(TfO)$_2$*** *with* ***5.***

	NH	**β-pyrroles**	**β-pyrroles**	**Ha**
δ_{free}(ppm)	7.35	5.97	5.68	8.17
δ_{bound}(ppm)	9.66	5.82	5.87	6.00
Δδ(ppm)	+2.31	-0.15	+0.19	-2.20

UNIVERSITAT ROVIRA I VIRGILI
ARYL-EXTENDED CALIX[4]PYRROLE RECEPTORS WITH METAL CENTERS: ORGANOMETALLIC RECEPTORS AND METALLO-MACROCYCLES BASED ON COORDINATION BONDS
Andrea Rivoli

Chapter 4

Attempt to quantify chloride-π interactions using a supra-molecular conformational balance based on a "two wall" mono-alkynyl Au(I) *α,β* calix[4]pyrrole

4.1 Introduction

In the last decades, all the fascinating applications of supramolecular chemistry (e.g., sensing, separation, catalytic systems, and the field of biomedical technologies), made it one of the most thriving fields of chemistry[1,2,3]. Molecular recognition processes are at the heart of the majority of these applications, as well as in many biological processes. Molecular recognition is determined by multiple factors[4,5], i.e. size, shape and functional complementarity. Non-covalent interactions are involved in achieving host-guest function complementarity [6,7].The knowledge and understanding of these kind of interactions, as well as their energy quantification are fundamental to develop new supramolecular systems and materials and to gain further insight into biochemical systems[8].

Molecular torsion balances (MTB) are cleverly designed synthetic molecules used as tools in physical organic chemistry studies. They allow a detailed study and quantification of the strength of weak intermolecular interactions. These molecular balances are associated with the study of a rotation (molecular torsion) of one part of the molecule with respect to another around a covalent bond. The results of the study provide insights into the energy landscape (thermodynamics) of the molecule or the dynamics (kinetics) of the molecular rotation. MTB possess two conformations or states: folded and unfolded. In the folded state the molecular

[1] Biedermann, F.; Schneider, H.-J., Experimental Binding Energies in Supramolecular Complexes. *Chem. Rev.* **2016,** *116*, 5216-5300.
[2] Banerjee, R.; Chakraborty, D.; Mukherjee, P. S., Molecular Barrels as Potential Hosts: From Synthesis to Applications. *J. Am. Chem. Soc.* **2023,** *145*, 7692-7711.
[3] Pearcy, A. C.; Crowley, J. D., The Biologically Inspired Abilities of Metallosupramolecular Architectures. *Chem. Eur. J.* **2023,** *29*, e202203752.
[4] Meyer, E. A.; Castellano, R. K.; Diederich, F., Interactions with Aromatic Rings in Chemical and Biological Recognition. *Angew. Chem. Int. Ed.* **2003,** *42*, 1210-1250.
[5] Persch, E.; Dumele, O.; Diederich, F., Molecular Recognition in Chemical and Biological Systems. *Angew. Chem. Int. Ed.* **2015,** *54*, 3290-3327.
[6] Walker, M. G.; Mendez, C. G.; Ho, P. S., Non-classical Non-covalent σ-Hole Interactions in Protein Structure and Function: Concepts for Potential Protein Engineering Applications. *Chem. Asian J.* **2023,** *18*, e202300026.
[7] Krueger, A. T.; Kool, E. T., Model systems for understanding DNA base pairing. *Curr. Opin. Chem. Biol.* **2007,** *11*, 588-594.
[8] Kim, E.-i.; Paliwal, S.; Wilcox, C. S., Measurements of Molecular Electrostatic Field Effects in Edge-to-Face Aromatic Interactions and CH-π Interactions with Implications for Protein Folding and Molecular Recognition. *J. Am. Chem. Soc.* **1998,** *120*, 11192-11193.

adopts a compact state and certain regions of the molecule interact with each other through non-covalent forces. In contrast, the unfolded conformation refers to a more extended form of the molecule with a reduced number of intramolecular interactions. The results extracted from the studies of molecular torsion balances are important to gain further understanding of molecular interactions in synthetic and biomolecular systems. However, owing to the rigidity of the molecular balance scaffolds the strength of the interaction under study is highly dependent on the distance/angle provided by the balance scaffold. Examples of molecular balances not relying on rotation through a single bond but on the relative energies of 1,4/1,6 isomers of substituted cycloaoctatetraene scaffold are also known.

Supramolecular conformational balances refer to the equilibrium between different molecular conformations of supramolecular host-guest systems. The energy difference, as well as the energy barrier, between different conformations in these systems can be influenced by the strength and directionality of non-covalent interactions[9]. The use of MTBs overcome some of the challenges encountered in the quantification of intermolecular interactions using supramolecular host-guest systems, however it has its own limitations [10]. The complexation free energy ΔG of a host-guest complex is influenced by various factors. Firstly, there is an implicit entropic cost associated with bringing the binding partners together. Consequently, the intermolecular complex formation may occur to a reduced extent if the sum of the intermolecular forces involved in their stabilization is reduced (weak overall interaction). Secondly, the non-covalent interactions established between solvent molecules and host and guest in the free state and the complex affect complex formation (solvation/desolvation processes).[11] As mentioned above, the strength of the interactions stabilizing the complex are key for its thermodynamic stability. Supramolecular complexes represent a thermodynamically stable binding geometry. For this reason, measuring repulsive interactions using host-guest complexes as model systems is not trivial.[1]

Unimolecular approaches to measure weak interactions provide enhanced control over the geometry of the intramolecular interaction under study, thus offering a

[9] Schneider, H.-J., Binding Mechanisms in Supramolecular Complexes. *Angew. Chem. Int. Ed.* **2009,** *48*, 3924-3977.
[10] Mati, I. K.; Cockroft, S. L., Molecular balances for quantifying non-covalent interactions. *Chem. Soc. Rev.* **2010,** *39*, 4195-4205.
[11] Cockroft, S. L.; Hunter, C. A., Desolvation and substituent effects in edge-to-face aromatic interactions. *Chem. Commun.* **2009**, 3961-3963.

significant advantage. This is also a crucial point because even slight modifications in the interaction geometry can exert a substantial influence on the measured strength. The control of the intramolecular binding geometry offered by unimolecular constructs allows a more precise investigation and manipulation of the desired interaction[1,10]. Molecular torsion balances are unimolecular physical organic tools to quantify non-covalent interactions. Since the first report in literature multiple molecular scaffolds have been applied in the design of MTBs.[12]. By investigating non-covalent interactions within the framework of unimolecular constructs, we can gain a detailed understanding of their nature and characteristics (***Figure 1***).

The strength of non-covalent interactions in MTB is typically determined by studying the *fold-unfold* equilibria between the two possible conformers of the balance. Commonly, ^{1}H NMR spectroscopy[13], X-ray crystallography[14] and theoretical calculation[15]are combined in the study of the MTB. [16]. Among the large number of non-covalent interactions present in supramolecular and unimolecular systems, it is

[12] Paliwal, S.; Geib, S.; Wilcox, C. S., Molecular Torsion Balance for Weak Molecular Recognition Forces. Effects of "Tilted-T" Edge-to-Face Aromatic Interactions on Conformational Selection and Solid-State Structure. *J. Am. Chem. Soc.* **1994,** *116*, 4497-4498.

[13] Carroll, W. R.; Pellechia, P.; Shimizu, K. D., A Rigid Molecular Balance for Measuring Face-to-Face Arene−Arene Interactions. *Org. Lett.* **2008,** *10*, 3547-3550.

[14] Hof, F.; Scofield, D. M.; Schweizer, W. B.; Diederich, F., A Weak Attractive Interaction between Organic Fluorine and an Amide Group. *Angew. Chem. Int. Ed.* **2004,** *43*, 5056-5059.

[15] Bhayana, B.; Dickie, D. A., Intramolecular Nitro-Aromatic Interactions Within a Molecular Torsion Balance: A Quantitative Assessment. *Cryst. Growth Des.* **2018,** *18*, 6404-6410.

[16] Bravin, C.; Piękoś, J. A.; Licini, G.; Hunter, C. A.; Zonta, C., Dissection of the Polar and Non-Polar Contributions to Aromatic Stacking Interactions in Solution. *Angew. Chem.* **2021,** *133*, 24064-24070.

worth citing here, ion ···π, CH···π[8,17], OH···π[18,19], NH···π[19], CH···O[20,21], π ···π[22,8,23] and M ···π[24] among others(few example reported in ***Figure 1***).

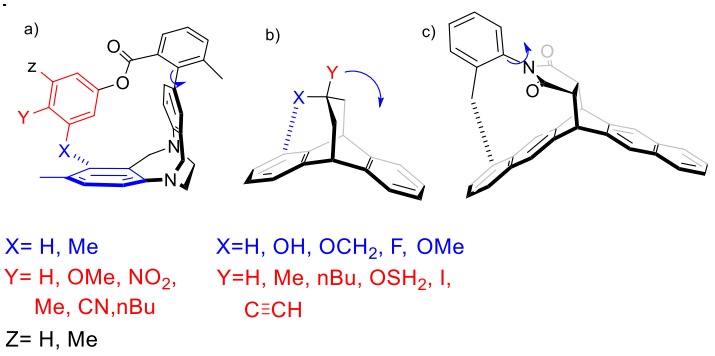

Figure 1: *Examples of the molecular scaffolds used in the design of unimolecular balances: a) Wilcoxs' torsion balance[18]; b) Motherwell et al.'s conformational balance[18,19]; c) Bicyclic N-arilamide torsion balance.*

For example, Shimizu[24] et al., designed a series of molecular torsion balances for the assessment of the strength of Ag(I)−π interactions in solution. To this end, they

[17] Carroll, W. R.; Zhao, C.; Smith, M. D.; Pellechia, P. J.; Shimizu, K. D., A Molecular Balance for Measuring Aliphatic CH−π Interactions. *Org. Lett.* **2011,** *13*, 4320-4323.
[18] Motherwell, W. B.; Moïse, J.; Aliev, A. E.; Nič, M.; Coles, S. J.; Horton, P. N.; Hursthouse, M. B.; Chessari, G.; Hunter, C. A.; Vinter, J. G., Noncovalent Functional-Group–Arene Interactions. *Angew. Chem. Int. Ed.* **2007,** *46*, 7823-7826.
[19] Aliev, A. E.; Moïse, J.; Motherwell, W. B.; Nič, M.; Courtier-Murias, D.; Tocher, D. A., Probing weak non-covalent interactions in solution and solid states with designed molecules. *Phys. Chem. Chem. Phys.* **2009,** *11*, 97-100.
[20] Li, P.; Vik, E. C.; Maier, J. M.; Karki, I.; Strickland, S. M. S.; Umana, J. M.; Smith, M. D.; Pellechia, P. J.; Shimizu, K. D., Electrostatically Driven CO−π Aromatic Interactions. *J. Am. Chem. Soc.* **2019,** *141*, 12513-12517.
[21] Ōki, M., Unusually High Barriers to Rotation Involving the Tetrahedral Carbon Atom. *Angew. Chem. Int. Ed.* **1976,** *15*, 87-93.
[22] Carroll, W. R.; Pellechia, P.; Shimizu, K. D., A Rigid Molecular Balance for Measuring Face-to-Face Arene−Arene Interactions. *Org. Lett.* **2008,** *10*, 3547-3550.
[23] Mathew, S. M.; Engle, J. T.; Ziegler, C. J.; Hartley, C. S., The Role of Arene–Arene Interactions in the Folding of ortho-Phenylenes. *J. Am. Chem. Soc.* **2013,** *135*, 6714-6722.

[24] Maier, J. M.; Li, P.; Hwang, J.; Smith, M. D.; Shimizu, K. D., Measurement of Silver−π Interactions in Solution Using Molecular Torsion Balances. *J. Am. Chem. Soc.* **2015,** *137*, 8014-8017.

coordinated a Ag(I) cation to a pyridine nitrogen atom. The molecular rotor's scaffold of balances **1** and **2** and control balance **3** are depicted in **Figure 2**. The nitrogen atom of the pyridine unit of the N-aryl imides **1**, **2** and **3** can coordinate to a Ag(I) cation. In the folded conformers of **1** and **2**, the Ag(I) ion is positioned over the benzene shelf forming an intramolecular Ag-π interactions. The relative strength of the interaction could be measured by monitoring the change of the folded-unfolded equilibria in the presence and absence of Ag(I) with balances **1** and **2**. The ability of the balances **1** and **2** to form Ag(I)-π interactions was established in the solid-state using X-ray crystallography. Next, the authors characterized the Ag(I)-π interactions in solution using ^{1}H NMR spectroscopy. As mentioned above, the strength of the interaction was quantitatively measured by its influence on the folded-unfolded equilibria. The folding energies (ΔG) where measured by integration of the peaks corresponding to the two conformers that were involved in a slow chemical exchange on the chemical shift timescale at r.t.. The folded-unfolded ratios for balances **1** and **2** changed from < 1 (0.25 and 0.064) in the absence of Ag(I) to > 1 (1.72 and 3.83) in the presence of 1 equiv of $AgBF_4$. Not surprising, balance **3** showed a small change in the folded-unfolded ratio. In short, the Ag(I)-π interactions in these systems are stronger than the corresponding CHπ interactions. Based on previous results, the authors assigned a strength larger than 1 kcal/mol for the Ag(I)-π interaction. In addition, the absolute value of the Ag-π interaction could also be extracted from the comparison of the folding energies of **1** and **2** with balance **3**, lacking the benzene-π shelf. A more accurate estimate of the Ag^{+} ···π interaction was obtained using a double mutant cycle (DMC) analysis.[25] combining the folding energies of **1**, **1**•Ag and **2**, **2**•Ag with the those of the control balance **3** and **3**•Ag. The Ag(I)-π interactions measured using the DMC were -1.34 and -2.63 kcal/mol for **1**•Ag and **2**•Ag, respectively.

[25]Fischer, F. R.; Schweizer, W. B.; Diederich, F., Molecular Torsion Balances: Evidence for Favorable Orthogonal Dipolar Interactions Between Organic Fluorine and Amide Groups. *Angew. Chem. Int. Ed.* **2007,** *46*, 8270-8273.

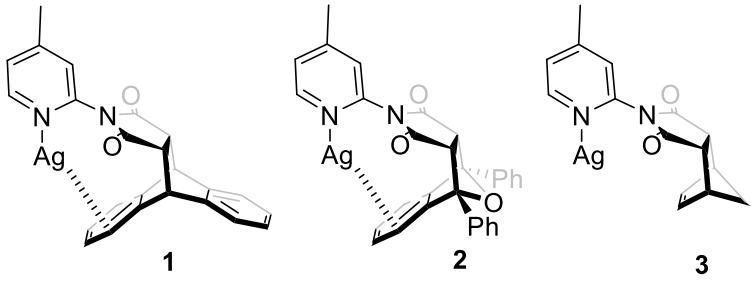

***Figure 2**: N-pyridyl succinyl imide based molecular torsion balances used by the Shimizu group to investigate and determine the strength of Ag–π.*

Recently, the group of Chen[26] reported the synthesis of a series of *o,o*'- disubstituted ("two-armed") pyridiniums salts. The conformations adopted by the organic molecules (molecular torsion/conformational balances) were used to "weigh" the importance of London dispersion forces against cation-π interactions in the absence of solvents. The authors begun with the unsubstituted molecular torsion balance and set-up the complexity by systematically adding alkyl groups (tert-butyl) as dispersion energy donors. Based on the experimentally observed structures, and the reasonable value of the reference cation-π interaction, they concluded, that the pairwise interaction between two tert-butyl groups was, in the best case, modest (**Figure 3**) [10,1].

[26] Gorbachev, V.; Tsybizova, A.; Miloglyadova, L.; Chen, P., Increasing Complexity in a Conformer Space Step-by-Step: Weighing London Dispersion against Cation−π Interactions. *J. Am. Chem. Soc.* **2022,** *144*, 9007-9022.

Attempt to quantify chloride-π interactions using a supra-molecular conformational balance based on a "two wall" mono-alkynyl Au(I) α,β calix[4]pyrrole

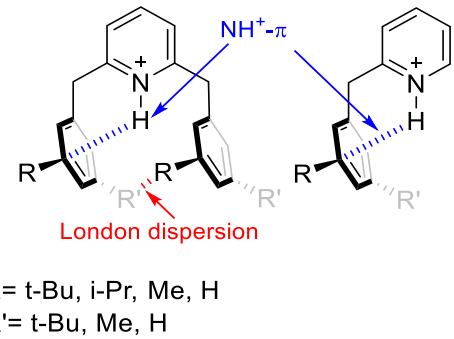

Figure 3: *Two-armed pyridinium salts used by Chen et al. to evaluate the importance of London dispersion forces in moderately large organic molecules*

To the best of our knowledge, the intuitive repulsive force assigned to the interaction between anions and aromatic systems (anion-π interaction) has not been evaluated using molecular torsion/conformational balances. The incorporation of anions, such as halides, in the scaffolds or constructs of molecular torsion/conformational balances is not trivial. We decided to enter this uncharted "field" using the α,β-isomer of a non-symmetrically substituted "two wall" calix[4]pyrrole as molecular conformational balance. The all-α isomers of "two and four wall" calix[4]pyrroles form thermodynamically stable 1:1 complexes with anions, such as chloride, establishing four simultaneous hydrogen bonding interactions with the pyrrole NHs and locking the calix[4]pyrrole core in cone conformation.[27]In addition, the *meso*-aromatic walls of the complex adopt an axial orientation and become involved in direct anion-π interactions.

[27] Molina-Muriel, R.; Romero, J. R.; Li, Y.; Aragay, G.; Ballester, P., The effect of solvent on the binding of anions and ion-pairs with a neutral [2]rotaxane. *Org. Biomol. Chem.* **2021,** *19*, 9986-9995.

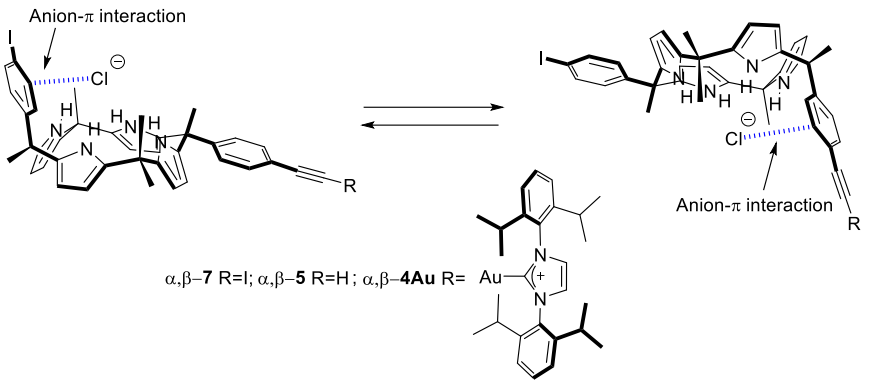

***Scheme 1**: Scheme of the dynamic equilibria of the two conformers of α,β –**2** and α,β –**1Au**.*

We reasoned that a chloride complex of a non-symmetrically substituted "two wall" α,β calix[4]pyrrole in cone conformation should locate one of its *meso*-phenyl substituent in axial orientation while the other remained in equatorial direction. This produces the existence of two different cone conformers for the complex, which are in equilibrium. Notably, in both of them only one *meso*-phenyl substituent, the axially oriented one, can establish anion-π interactions with the bound chloride. We considered that the putative existence of different attractive/repulsive chloride-π interactions in the two conformers of the complex could modify their (folded-unfolded) equilibrium ratio. We will refer to the folded conformer as the one placing the *meso*-phenyl substituent having the less negative molecular electrostatic potential value at the center of the ring in axial orientation. We studied the binding of chloride to symmetrically and non-symmetrically substituted "two wall" α,β calix[4]pyrroles in different solvents using ^{1}H NMR spectroscopic titrations, variable temperature NMR experiments (VT-NMR) and isothermal titration calorimetry (ITC) experiments. We used alkylammonium salts such as tetra-butyl ammonium chloride (TBACl) and methyl trioctyl ammonium chloride (MTOACl) as chloride precursors. Moreover, we performed theoretical calculations to validate and further support our experimental findings.

4.2 Results and Discussion

4.2.1 Synthesis

10α-(4-Iodophenyl)-20β-(1,3-bis(2,6-di*iso*propylphenyl)-2,3-dihydro-1H-imidazol-2-yl) (4-ethynylphenyl) gold(I) hexamethyl calix[4]pyrrole *α,β*-**4Au** (**Scheme 3**) was prepared in three synthetic steps from the corresponding *α,β*-bis(4-iodophenyl-

Attempt to quantify chloride-π interactions using a supra-molecular conformational balance based on a "two wall" mono-alkynyl Au(I) α,β calix[4]pyrrole

calix[4]pyrrole *α,β* -**7** (**Scheme 2**). The Sonogashira reaction of *α,β* -**7** with 1 equiv of 2-methyl-3-butyn-2-ol (5 equiv.), at r.t in dry toluene and using triethylamine amine as base, produced a statistical mixture of products that allowed the isolation of the non-symmetrically-substituted iodo-ethynyl protected calix[4]pyrrole α,β-*α,β* **6** in 42% yield, following column chromatography separation.

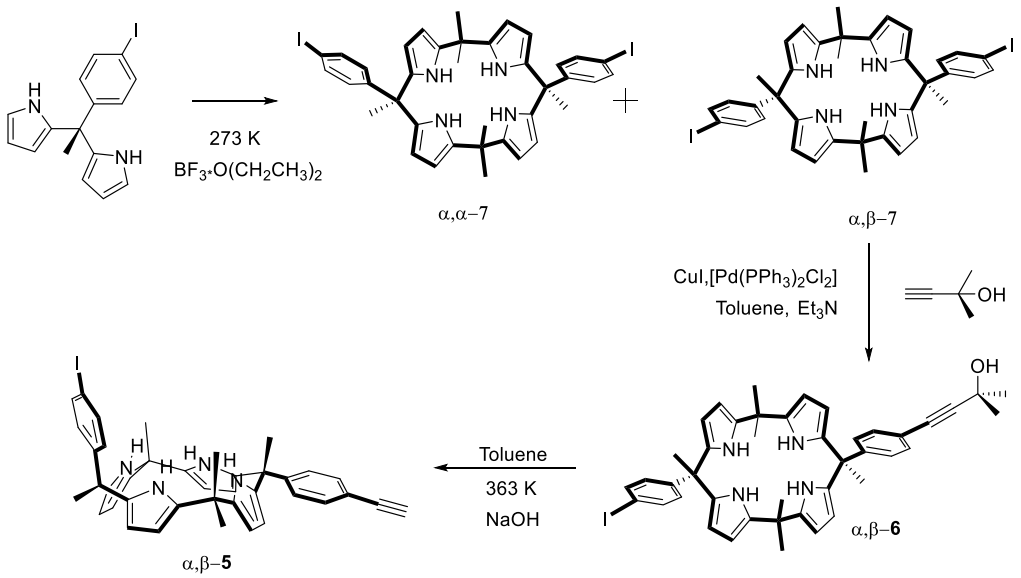

Scheme 2**: Synthetic scheme for the preparation of the mono-iodo-mono-ethynyl α,β- **5.

The subsequent treatment of the mono-protected *α,β*-**6** with sodium hydroxide in refluxing toluene for 12 h afforded the mono-iodo-mono-ethynyl calix[4]pyrrole α,β-**5** in 73% yield after column chromatography purification of the reaction crude using silica gel. Compound *α,β* -**5** was treated with (1,3-bis(2,6-diisopropylphenyl)-2,3-dihydro-1H-imidazol-2-yl)(2-oxopropyl)gold(I) (**Au(IPr)(CH_2COCH_3)**) in chloroform at 333 K for 24h, affording the organometallic Au(I)-acetylide N-heterocyclic carbene (NHC) complex *α,β*-**4Au** after trituration of the obtained reaction crude with DCM/pentane.

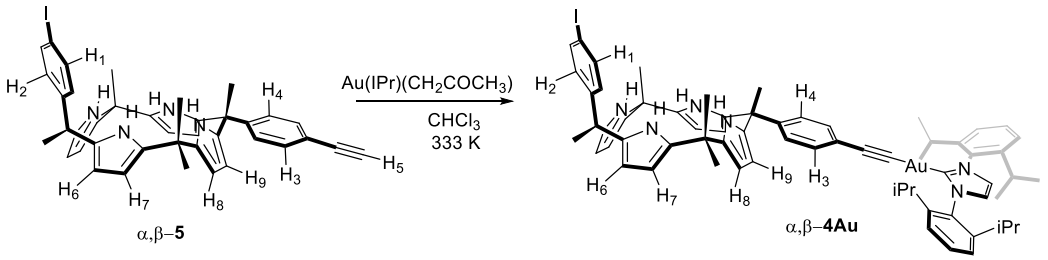

Scheme 3: *Synthetic schemefor the preparation of the Au(I)-acetylide NHC complex α,β-**4Au***

4.2.2 Binding Studies and Variable Temperature Experiments

The use of the chloride complex of the α,β-**4Au** calix[4]pyrrole, **Cl⁻●** α,β -**4Au**, as a "supramolecular" conformational balance to evaluate chloride-π interactions required performing VT-NMR experiments at low-temperature. This is due to the fact that the equilibrium between its two conformers shows fast exchange dynamics on the ^{1}H NMR chemical shift time scale. That is, at r.t. we observed just a single set of four aromatic proton signals for the bound receptor. This made the determination of the isomers ratio at equilibrium not viable at this temperature. Initially, we investigated the binding properties of the symmetrically substituted di-iodo calix[4]pyrrole α,β-**7** with chloride. We observed that a low temperature the two aromatic signals of the meso-phenyl substituents of the 1:1 **Cl⁻●*α,β*-7** complex split into four separate signals (**Figure 4**).

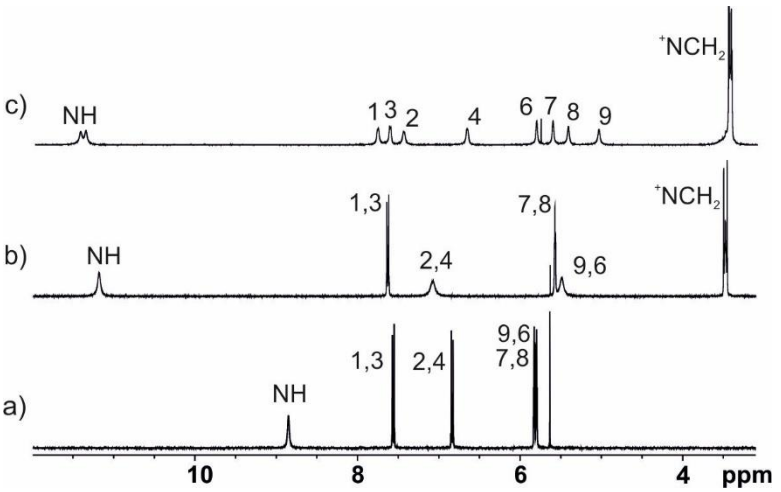

Figure 4: *Selected regions of the ^{1}H NMR spectra (400 MHz, acetone- d_6, 298 K) of α,β-**7** (6 mM) at: a) room temperature; b) room temperature with 1 equiv. of TBACl; c) at 213 K with 1 equiv. of TBACl.*

This observation indicated that at low temperature the conformational exchange process experienced between the two identical and energetically degenerated **Cl⁻●**α,β-**7** anionic complexes was slow on the ^{1}H NMR chemical shit timescale. The aromatic protons of its *meso*-phenyl groups, axially and equatorially oriented, resonated as four separate signals. For the same token, the freezing of the analogous conformational equilibrium taking place for a 1.1 chloride complex of a non-symmetrically substituted α,β-C[4]P, i.e. **Cl⁻●**α,β -**4Au**, was expected to produce up to eight separate signals for the aromatic protons of the *meso*-phenyl substituents. That is, four different signals for the aromatic protons of each one of the two conformers. Owing to the non-symmetric *para*-substitution of the *meso*-phenyl substituents the two conformers are not identical (chemically equivalent). The integral values of the respective signals were expected to be used for the determination of their isomeric ratio. We used tetrabutylammonium chloride (TBACl) as chloride precursor in the VT experiments conducted in deuterated acetone. We also performed ^{1}H NMR spectroscopic titrations of the *α,β* -**4Au** C[4]P receptor with chloride to gain some insights in the binding properties and geometry of the resulting anionic complex **Cl⁻●** *α,β* -**4Au**. Finally, we complemented the results of the binding studies in deuterated acetone with analogous experiments conducted in dichloromethane, a non-polar solvent. In these latter experiments, we used methyltrioctylammonium chloride[28] (MTOACl) as chloride source due to the known hetero-ditopic nature of C[4]P receptors in the biding of ion-pairs in non-polar solvent. Additionally, we employed the non-symmetrically substituted *α,β*-**5** C[4]P receptor, the synthetic precursor of *α,β*-**4Au**, as a model compound in analogous binding and VT experiments. We aimed to compare and increase our understanding of the results obtained with the latter.

[28] Adriaenssens, L.; Gil-Ramírez, G.; Frontera, A.; Quiñonero, D.; Escudero-Adán, E. C.; Ballester, P., Thermodynamic Characterization of Halide−π Interactions in Solution Using "Two-Wall" Aryl Extended Calix[4]pyrroles as Model System. *J. Am. Chem. Soc.* **2014,** *136*, 3208-3218.

Experiments in acetone solution

We monitored the interaction of the organometallic C[4]P receptor *α,β* **-4Au** with chloride using ^{1}H NMR spectroscopic titrations and TBACl as chloride precursor. The TBA^+ cation is known to be well-solvated in acetone while the chloride anions experiences a reduced solvation. This phenomenon leads to the dissociation of the ion-pair and an increase in the affinity of the C[4]P receptor for chloride, compared to that in non-polar chlorinated solvents. Thus, the formation of an anionic complex with 1:1 stoichiometry between chloride and the *α,β*-**4Au** C[4]P receptor is favored in acetone. The conformational preference exhibited by the formed $Cl^-\subset$*α,β* **-4Au** was expected to be used in the assessment of the relative strength of the established chloride-π interactions (***Scheme 4)***. The ^{1}H NMR spectra acquired during the titration of the *α,β* **-4Au** C[4]P receptor with incremental amounts of TBACl in acetone-d_6 solution are depicted in **Figure 5**. In agreement with C_s symmetry, the ^{1}H NMR spectrum of *α,β*-**4Au** displays two broad singlets for the pyrrole NHs, four doublets for the aromatic protons and four overlapping double doublets for the β-pyrrole (H_6, H_7, H_8, H_9) protons. (**Figure 5a**). The pyrrole NHs resonated at δ = 8.75 and δ = 8.62 ppm. The incremental addition of TBACl produced chemical shift changes in all the signals of the protons of *α,β* **-4Au**. This behaviour indicated that the binding equilibrium displayed fast exchange dynamics on the chemical shift timescale between the free and the bound receptor.

Attempt to quantify chloride-π interactions using a supra-molecular conformational balance based on a "two wall" mono-alkynyl Au(I) α,β calix[4]pyrrole

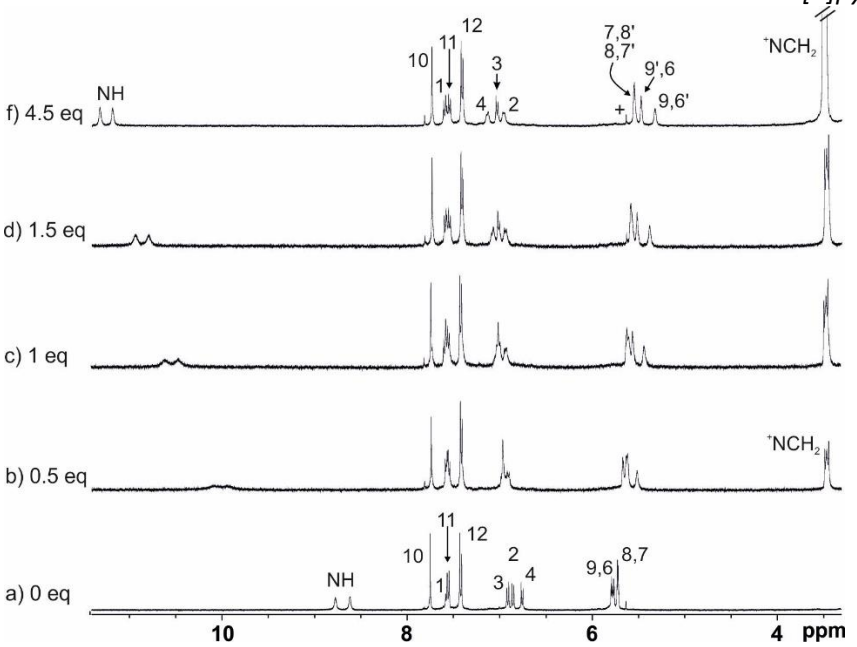

Figure 5: *Selected regions of the ^{1}H NMR spectra (400 MHz, acetone- d_6, 298 K) of α,β-**4Au** (3.4 mM) with incremental amounts of **TBACl :** a) 0 equiv. b) 0.5 equiv.; c) 1 equiv.; d) 1.5 equiv.; e) 4.5 equiv.; See scheme 3 for proton assignment.*

In more detail, the (H_1, H_2, H_3, H_4) doublets of the aromatic protons experienced reduced chemical shift changes. This observation hinted to the establishment of weak chloride–π interactions[29,30]. Chloride-π interactions tend to produce noticeable upfield shifts of the aromatic protons. In addition, the doublets assigned to the β-pyrrole protons (H_6, H_7, H_8, H_9) moved upfield. This is the expected result for the conformational change experienced by the bound receptor, that is locked in the cone conformation due to the formation of four convergent hydrogen bonding interactions between its pyrrole NHs and the bound chloride. C[4]Ps tend to adopt alternate 1,3 or 1,2 conformations in the free state and switch to the cone conformation upon binding suitable anionic guests (e.g. Cl^-). In the presence of 4.5 equiv. of TBACl, the pyrrole NHs resonated as two broadened and downfield shifted

[29]Adriaenssens, L.; Gil-Ramírez, G.; Frontera, A.; Quiñonero, D.; Escudero-Adán, E. C.; Ballester, P., Thermodynamic Characterization of Halide–π Interactions in Solution Using "Two-Wall" Aryl Extended Calix[4]pyrroles as Model System. *J. Am. Chem. Soc.* **2014,** *136*, 3208-3218.

[30] Rivoli, A.; Aragay, G.; Gimeno, M. C.; Ballester, P., Chloride Binding Properties of a Macrocyclic Receptor Equipped with an Acetylide Gold(I) Complex: Synthesis, Characterization, Reactivity, and Cytotoxicity Studies. *Inorganics* **2022,** *10*, 95.

singlets centered at δ = 11.32 ppm and δ = 11.18 ppm, respectively. The downfield shift experienced by the NHs protons supports the formation of hydrogen bonding interactions with the chloride. With the exception of the signals assigned to protons H1 and H3, the rest of the signals assigned to the bound α,β -**4Au** C[4]P showed broadening, even in the presence of a large excess of TBACl (4.5 equiv.). The excess of the salt assured the quantitative formation of the $Cl^-\subset\alpha,\beta$-**4Au** complex. The observation of broadened signals suggested that the anionic 1:1 complex $Cl^-\subset\alpha,\beta$-**4Au** was involved in an additional dynamic process than the one produced by host-guest binding. We surmised that the dynamics of the equilibrium between the two possible conformers of the $Cl^-\subset\alpha,\beta$-**4Au** complex could be responsible for the observed broadening. Because after the addition of slightly more than 1 equiv of TBACl the signals of the bound receptor did not suffer significant changes, we estimated that the binding constant of the $Cl^-\bullet\ \alpha,\beta$ -**4Au** was in the order of 10^3-10^4 M^{-1}. Remarkably, the signal of the methylene protons *alpha* to the nitrogen atom of the TBA^+ cation did not experience noticeable chemical shift changes throughout the titration. This behavior supported the non-involvement of the TBA^+ cation in the formation of the complex. That is, the species mainly formed in acetone solution was the anionic 1:1 complex $Cl^-\bullet\ \alpha,\beta$ -**4Au**.

We performed analogous titration experiments using the mono-iodo mono-ethynyl calix[4]pyrrole *α,β* -**5**, the synthetic precursor of the Au(I) acetylide *α,β*-**4Au** (**Figure 6**). In this case, we observed that the signal of the methylene alpha to the nitrogen atom of the TBA^+ cation and the alkynyl proton H_5 displayed reduced non-monotonic chemical shift changes. Most likely, the $Cl^-\bullet\ \alpha,\beta$-**5** showed a greater tendency to form an ion-paired complex than the $Cl^-\bullet\ \alpha,\beta$ -**4Au** counterpart. The rest of observations were very similar for both titrations suggesting that the anionic complexes exhibited binding constants of the same order of magnitude.

Attempt to quantify chloride-π interactions using a supra-molecular conformational balance based on a "two wall" mono-alkynyl Au(I) α,β calix[4]pyrrole

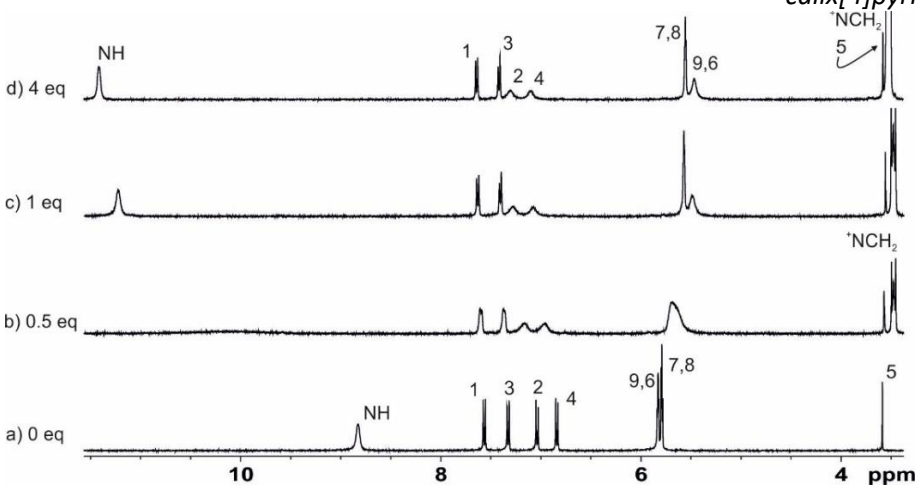

Figure 6: *Selected regions of the ^{1}H NMR spectra (400 MHz, acetone-d_6, 298 K) of α,β-**5**(6.2 mM) with incremental amounts of **TBACl :** a) 0 equiv. b) 0.5 equiv.; c) 1 equiv.; d) 4 equiv.; See scheme 3 for proton assignment*

In order to obtain more accurate values of the binding constants in acetone solution, we performed ITC experiments. The binding isotherms obtained from the plot of the normalized integrations of the heat peaks *vs* molar ratio showed single sigmoidal curves with inflexion points centered at molar ratios [TBACl]/[*α,β* **-4Au**] and [TBACl]/[*α,β* **-5**] close to 1. These results confirmed the formation of mainly 1:1 anionic complexes in acetone solution (see SI section **3.6.5** for more details). The fit of the titration data to the one set of sites model implemented in the Microcal ITC Data Analysis software (version 7.0, Northampton, MA, USA) was good. The fitting procedure returned the values of the binding constant and the enthalpy of binding for the formation of the Cl^{-}● *α, β* **-4Au** and Cl^{-}● *α, β* **-5** complexes (see SI and **Table 1**).

Table 1: *Binding constant values (K_a, M^{-1}) and thermodynamic constants (kcal mol^{-1}) for the binding equilibria of receptors α,β-**5**, and α,β-**4Au** with TBACl in acetone solution at 288 K determined using ITC experiments.*

Receptor	**K_a (10^4 M^{-1}) Acetone [a]**	**ΔH kcal/mol**	**ΔG kcal/mol**	**-TΔS kcal/mol**
α, *β* **-5**	4.18 ±0.65	-2.50±0.19	-6.09±0.09	-3.59±0.21
α, *β* **-4Au**	1.55±0.10	-2.21±0.42	-5.49±0.04	-3.29±0.42

Based on the results of the ITC experiments, we concluded that the incorporation of a gold(I) carbene moiety in the scaffold of *α*,*β*-**5** C[4]P receptor leaded to a reduced decrease in the free energy of binding for chloride of 0.6-0.5 kcal/mol (**5** vs. **4Au**). We ascribed this difference in binding affinity to an increase in the repulsive chloride-π interactions present in the Cl^-● *α*,*β* **-4Au** compared to those in the Cl^-● *α*, *β* **-5** analog. In doing so, we also assumed that the binding energy provided by the hydrogen bonding interactions was almost identical in both complexes.

DFT calculations of the electrostatic surface potentials (ESPs) of model systems for the *meso*-substituents in the C[4]P receptors

We performed DFT calculations to estimate the ESP values of the *meso*-phenyl walls in the C[4]P receptors *α*,*β*-**5** and *α*,*β*-**4Au** (ESP1, center of the aromatic ring andESP2 center of the *p*-susbtituent). To this end, we used *p*-iodotoluene, *p*-ethynyltoluene and *p*-gold(I)acetylide-NHC-toluene as model systems (**Figure 7**). The introduction of the gold(I) NHC carbene moiety, produced a significant change in the ESP values of the model systems used for the *meso*-phenyl walls of *α*,*β*-**4Au** and *α*,*β* **-5** (i.e. −34.8; −45.3 kcal/mol and −14.8; −18.7 kcal/mol, respectively). In contrast, the ESPs of the *p*-iodo and *p*-ethynyl *meso*-phenyl walls showed almost identical values (i.e. −13.1; −13.7 kcal/mol and −14.8; −18.7 kcal/mol respectively).

Taken together, the result of the theoretical calculations suggested that the decrease in binding affinity measured for chloride with the *α*,*β*-**4Au** C[4]P receptor could be due to the existence of stronger repulsive chloride-π interactions in one of

the conformers of the anionic Cl^-●*α,β*-**4Au** complex. This effect may also be expected to shift the conformers equilibrium towards the one featuring the *p*-iodophenyl substituent in axial orientation and involved in chloride-π interatcions.

On the other hand, the *α,β*-**5** C[4}P receptor used as model compound bears aromatic walls featuring almost identical and considerable less negative ESP values. For this reason, the Cl^-● *α,β* **-5** complex was expected to be thermodynamically more stable and displaying a ratio close to 1 for its two conformers: *p*-iodophenyl and p-ethynyl phenyl *meso*-substituents in axial orientation.

The experimental verification of our hypotheses required freezing the conformational exchange processes between the two conformers of the Cl^-● *α,β* **-4Au** and Cl^-● *α,β* **-5** complexes that putatively occurred in acetone solution.

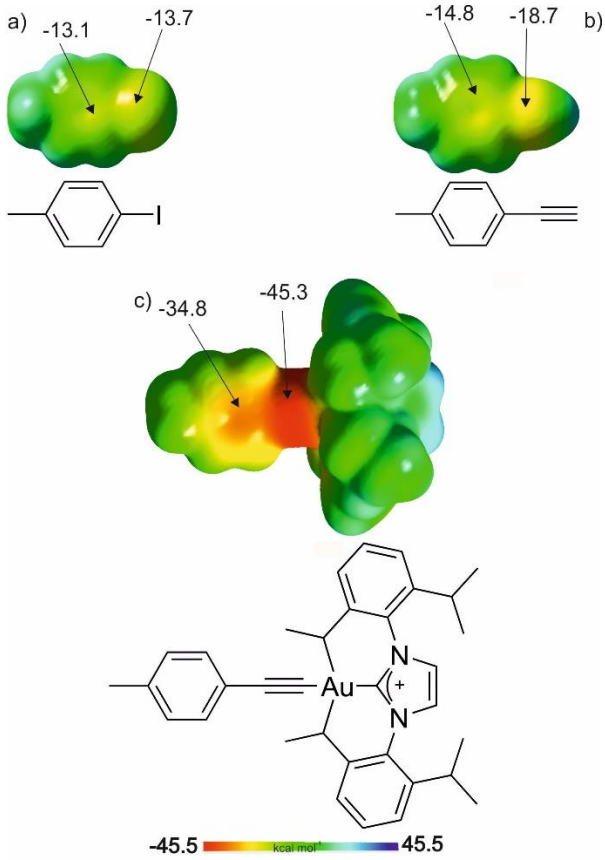

Figure 7: *Calculated ESPs of the model systems used for the meso-phenyl substituents of α,β-**5** and α,β-**4Au** a)* p*-iodotoluene, b) p-ethynyltoluene and c) p-gold(I)acetylidetoluene.*

Attempt to quantify chloride-π interactions using a supra-molecular conformational balance based on a "two wall" mono-alkynyl Au(I) α,β calix[4]pyrrole

4.2.3 Variable temperature ^{1}H NMR experiments in acetone solution.

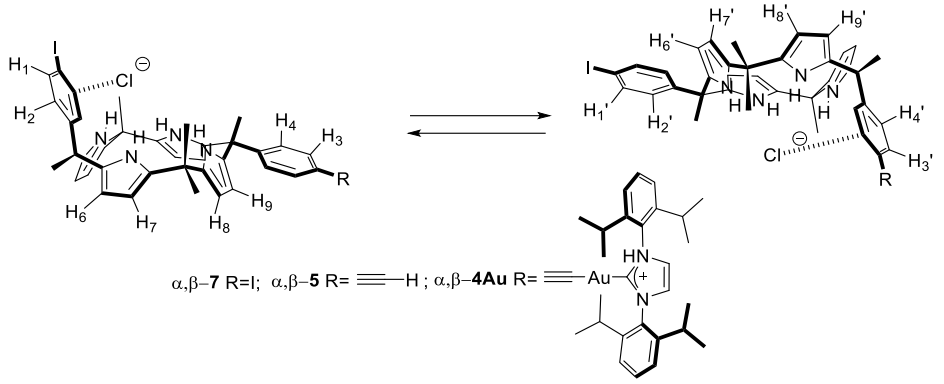

Scheme 5: *Scheme of the dynamic equilibrium between the two conformers of chloride complexes with α,β-C[4]Ps. The proton assignment is also shown. In the case of the α,β-**7** the two conformers become indistinguishable owing to the presence of identical p-substituents. of the molecule.*

As depicted in panels f and d of **Figure 5** and **Figure 6** , respectively, the quantitate formation of the chloride 1:1 complexes of C[4]P receptors *α,β*-**5** and *α,β*-**4Au** showed broadening in some of their proton signals. We hypothesized above that the observed broadening was caused by the existence of a dynamic exchange equilibrium between the two possible conformers of the anionic complexes (**Cl^-●** *α,β*-**5**, **Cl^-●** *α,β*-**4Au**). At r.t. the dynamics of the exchange process were fast to intermediate on the ^{1}H NMR chemical shift timescale. In order to determine the presence and ratio of the two conformers in equilibrium we performed variable temperature ^{1}H NMR experiments. Lowering the temperature of an acetone solution of the reference Cl^-● *α,β* **-5** anionic complex at 198 K, revealed a complex ^{1}H NMR spectrum displaying multiple sharp and well-defined proton signals. The careful analysis of the spectrum revealed the presence of two set of signals for the C[4]P receptor that were assigned to the two conformers of the Cl^-● *α,β* **-5** complex **Figure 8**a. We observed six doublets for the aromatic protons, four signals for the β-pyrrole protons and two singlets for the terminal alkyne protons. The proton assignment was performed by means of two-dimensional ^{1}H_NMR experiments (COSY and ROESY, see **Figure 9 and Figure 10**), and assuming that the most downfield shifted aromatic signal corresponded to the proton *ortho* to the iodine atom of the iodophenyl group in axial orientation (H1). Similarly, the most upfield shifted signal was assigned to the *meta*-proton with respect to the iodine atom of the iodophenyl group in equatorial orientation (H2'). The results of COSY and ROESY

experiments (see **Figure 9 and Figure 10**) evidenced the overlap of multiple proton signals, as well as the existence of cross peaks due to chemical exchange, respectively.

For example, four of the eight aromatic protons displayed identical chemical shifts in the two conformers (H_1'-H_4' and H_3'-H_2). The four β-pyrrole protons (H_6-H_9', H_7-H_8', H_8-H_7', H_9-H_6') overlapped in the two conformers (**Figure 8**, **Figure 9 and Figure 10**). The existence of cross-peaks due to chemical exchange indicated that although the exchange process between conformers was slow on the ^{1}H NMR chemical shift times scale, it was fast of the ROESY timescale. Finally, the integral values of the signals assigned to terminal alkynyl protons and selected aromatic protons were used to determine that the ratio of the concentrations of the conformers was close to 1. This result was in complete agreement with our expectations based on the ESP values of the meso-phenyl walls of *α,β* **-5**. It is worth mentioning here that the chemical exchange between the two conformers of the free *α,β*-**5** receptor cannot be frozen at 198 K or even lower temperatures. This finding indicated that the binding of the chloride anion produced a significant increase in the energy barrier of the conformational interconversion process.

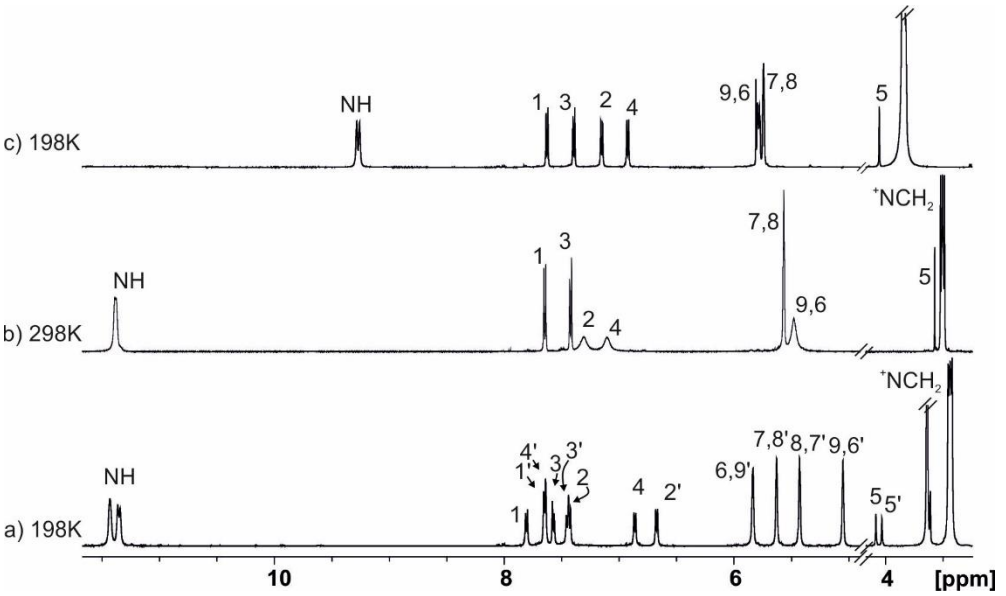

Figure 8: *Selected ^{1}H NMR spectra (400 MHz, acetone d_6) of α,β-**5** (6.2 mM) with 1 equiv. of **TBACl** at a) 198 K, b) 298 K, c) α,β-**5** at 198 K **.** See **Scheme 4** for proton assignment.*

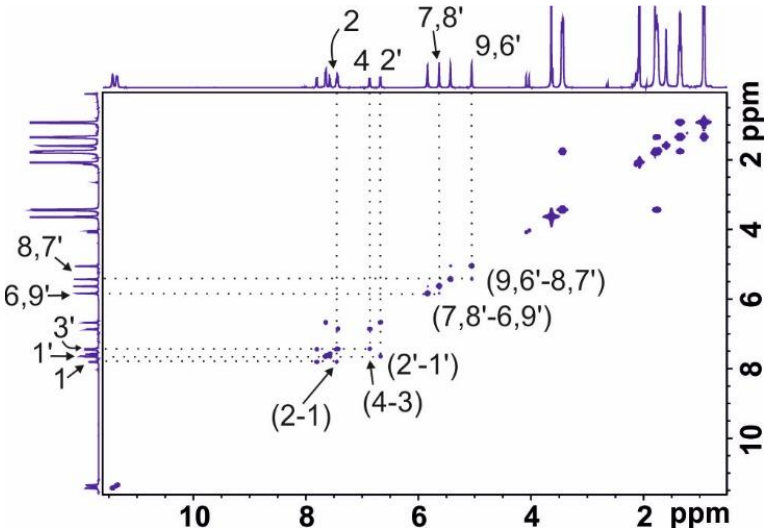

Figure 9: *COSY experiment of Cl^-● α,β **-5** complex in acetone-d_6-at 198 K (aromatic region). See **Scheme 4** for proton assignment.*

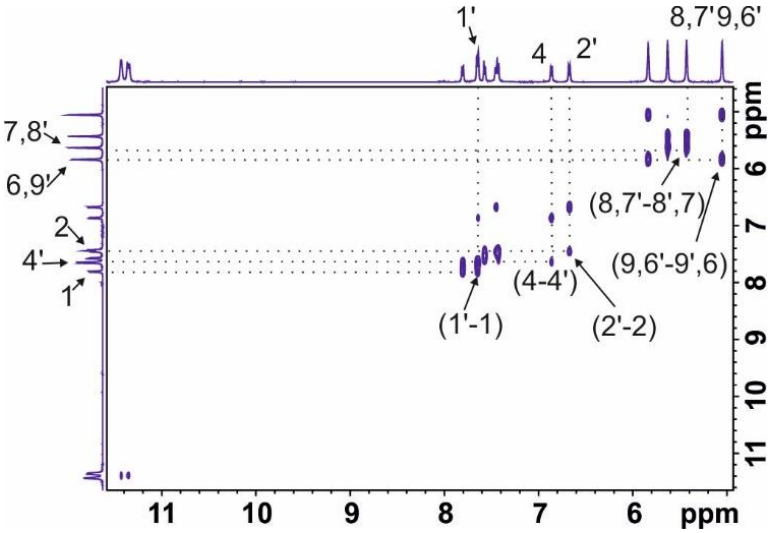

Figure 10: *Aromatic region of the ROESY experiment of the Cl^-● α,β **-5** complex in acetone-d_6 at 198 K.. See **Scheme 4** for proton assignment.*

Next, we also undertook variable temperature ^{1}H NMR experiments using the **Cl⁻●** α,β -**4Au** complex. As mentioned in the previous paragraph, the aromatic walls of the α,β -**4Au** C[4]P receptor exhibit a significant difference in ESP values. **Figure 11**a and **10**b depict selected regions of the ^{1}H NMR spectra of the Cl⁻● α,β -**4Au** complex acquired at 298 K and 198 K, respectively. To our surprise, at 198 K we observed only four intense signals for the protons of the aromatic walls. Likewise, the β-pyrrole protons produced only four signals. This observation can be attributed to an overlap of all the signals of the protons in the two conformers. The overlap of the β-pyrrole protons is precedented in the ^{1}HNMR spectrum of the two conformers of the Cl⁻● *α,β* **-5** complex at 198 K. However, in the case at hand we observed an additional set of signals of low intensity, both in the aromatic and β-pyrrole regions of the spectrum, that could correspond to the second conformer of the **Cl⁻●** α,β -**4Au** or an unidentified impurity. Notably, the putative complete overlap of the signals for the two conformers provided a pattern of exchange cross-peaks observed in the ROESY of the **Cl⁻●** α,β -**4Au** at 198K that was very different to that obtained for the **Cl⁻●**α,β -**5** counterpart. Unfortunately, all the available experimental evidence was not sufficient to support the undisputable presence of the two conformers of the **Cl⁻●** α,β -**4Au** complex in a ratio different than 1.

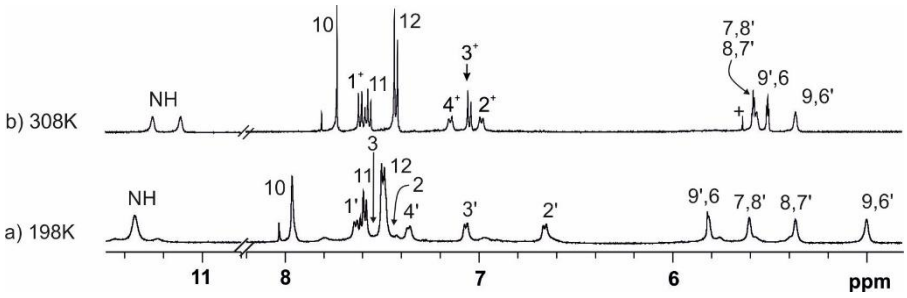

Figure 11: *Selected regions of the ^{1}H NMR spectra (400 MHz, -acetone d_6) of α,β-* ***4Au*** *(3.4 mM) with 1 equiv. of* ***TBACl*** *at a) 198 K and b) 308 K. See* ***Scheme 4*** *for proton assignment.*

Attempt to quantify chloride-π interactions using a supra-molecular conformational balance based on a "two wall" mono-alkynyl Au(I) α,β calix[4]pyrrole

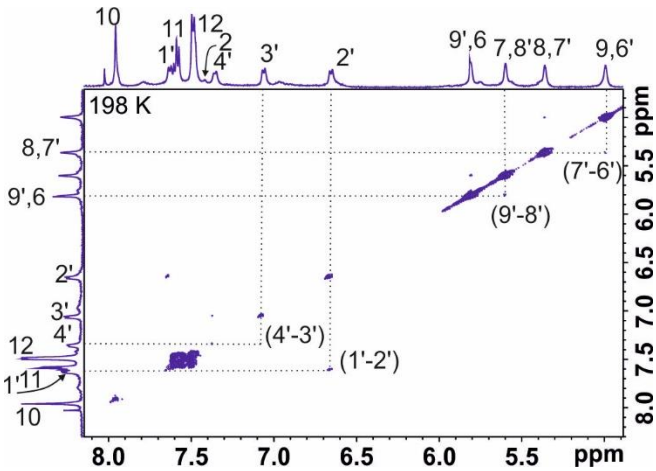

Figure 12: *COSY experiment of an acetone-d_6 solution of α,β-**4Au** with 1 equiv. of **TBACl** at 198 K (aromatic region). See **Scheme 4** for proton assignment.*

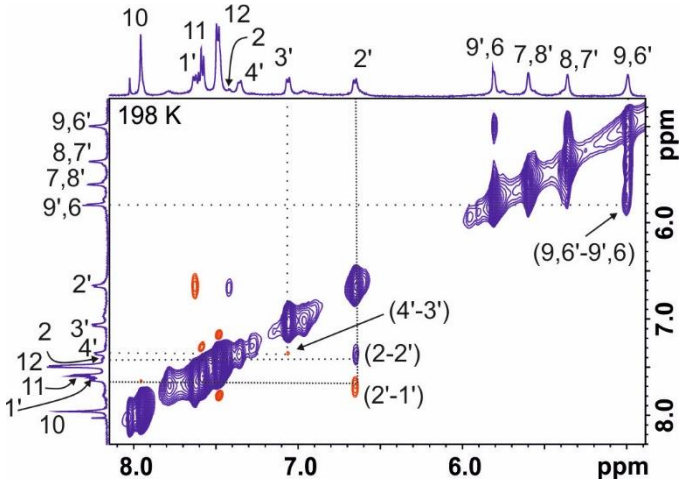

Figure 13: *ROESY experiment of an acetone-d_6 solution of α,β-**4Au** with 1 equiv. of **TBACl** at 198 K(aromatic region). See **Scheme 4** for proton assignment.*

4.2.4 Binding Studies of the α,β-4Au and α,β-5 C[4]P receptors in dichloromethane solution with MTOACl

In order to corroborate the obtained results in acetone solution and investigate potential changes in the conformers' ratio caused by the modification of the solvent[31] and the ion-paired nature of the complex, we conducted additional binding studies of the C[4]P receptors α,β -**4Au** and α,β -**5** in dichloromethane solution. It is well-known that *α,α*-"two walls" C[4]P receptors exhibit lower binding affinity towards TBACl in dichloromethane ($<10^3$ M^{-1})[29] than in acetone. This is mainly due to the heteroditopic nature of the C[4]P receptors in the binding of ion-pair in non-polar solvents. In these solvents, the quantitative formation of the C[4]P complexes with only 1 equivalent of the salt requires the use of the anions as methyl-trialkylammonium salts. The methyl group is a perfect fit for the shallow an electron rich cavity defined by the pyrrole rings in cone conformation. In this manner, the cation is located opposite to the bound anion producing a ion-paired ternary complex that is highly stable kinetically and thermodynamically.[32]. Therefore, we used methyltrioctylammonium chloride (MTOACl) as chloride precursor in the binding experiments performed in dichloromethane solution.

[31]Cockroft, S. L.; Hunter, C. A., Desolvation tips the balance: solvent effects on aromatic interactions. *Chem. Commun.* **2006**, 3806-3808.

[32] Sun, Q.; Aragay, G.; Pinto, A.; Aguiló, E.; Rodríguez, L.; Ballester, P., Influence of the Attachment of a Gold(I) Phosphine Moiety at the Upper Rim of a Calix[4]pyrrole on the Binding of Tetraalkylammonium Chloride Salts. *Chem. Eur. J.* **2020,** *26*, 3348-3357.

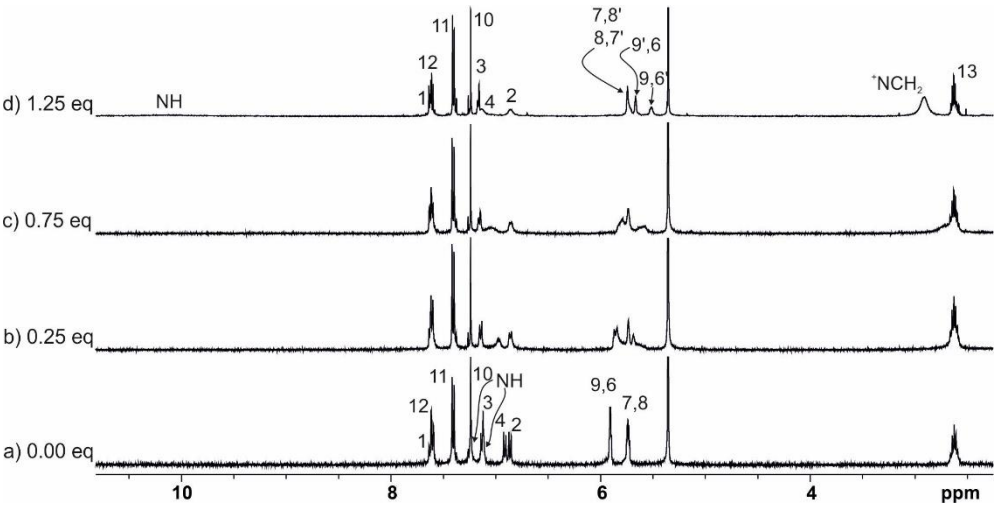

***Figure 14**: Selected regions of the ^{1}H NMR spectra (400 MHz, CD_2Cl_2, 298 K) of α,β-**4Au**(3 mM) with incremental amounts of **MTOACl :** a) 0.00 equiv. b) 0.25 equiv.; c) 0.75 equiv.; d) 1.25 equiv.; See **Scheme 3** for proton assignment.*

The incremental addition of MTOACl to a mM dichloromethane solution of *α,β* **-4Au** produced broadening and chemical shift changes to the proton signals of the C[4]P. **Figure 14**. This result is in agreement with the observations made in acetone-d_6 solution. Moreover, the quantitative formation of the Cl^-● *α,β* **-4Au**●$MTOA^+$ complex (1.25 equiv. of MTOACl added) did not induce the sharpening of some of the receptor's signals. These observations suggested the existence of a dynamic process between the two possible conformers of the Cl^-● *α,β* **-4Au**●$MTOA^+$complex for which we estimated a binding constant value larger than 10^4 M^{-1}. Notably, the significant upfield shift experienced by the methylene protons alpha to the nitrogen atom of the $MTOA^+$ cation in the initial phase of the titration is attributed to the formation of an ion-paired complex.

We also carried out analogous ^{1}H NMR titration experiments of *α,β* **-5** in dichloromethane-d_2 solution with MTOACl. We obtained similar results to those described above for *α,β* **-4Au**.

4.2.5 Variable temperature ^{1}H NMR experiments in dichloromethane solution of the ion-paired complexes Cl^-● ***α,β*** -4Au●**MTOA**$^+$ and Cl^-● ***α,β*** -5●**MTOA**$^+$

The ^{1}H NMR spectrum of the Cl^-● *α,β* **-5**●$MTOA^+$**complex** at 183 K in DCM-d_2 solution displayed sharp and well resolved proton signals. (**Figure 15**) We detected eight signals for the protons of the aromatic walls of the C[4]P receptor, which was diagnostic of its presence as an equilibrium of two conformers displaying slow chemical exchange on the ^{1}H NMR chemical shift timescale. Because all aromatic signals had the same intensity we assigned the ratio between the conformers to be equal to 1. The complex ^{1}H NMR spectra registered for the Cl^-● *α,β*-**5**●$MTOA^+$ ion-paired complex resembled the one obtained in acetone-d_6 for the anionic counterpart. While the aromatic protons assigned to the two conformers of the ion-paired complex Cl^-● *α,β*-**5**●$MTOA^+$ resonated as eight separate signals, their β-pyrrole protons produced only four signals, as previously observed for the anionic counterpart.

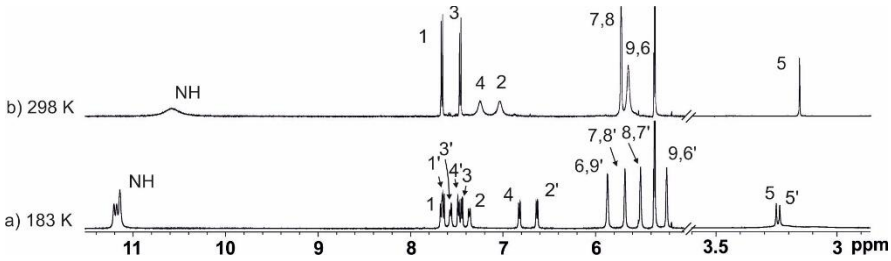

***Figure 15**: Selected ^{1}H NMR spectra (400 MHz, CD_2Cl_2) at a) 183 K and b) 298 K of α,β-**5**(5.6 mM) with 1 equiv. of **MTOACl.** See **Scheme 4** for proton assignment.*

Similarly to the results obtained in acetone-d_6, at 183 K the ^{1}H NMR spectrum of the ion-paired Cl^-● *α,β* **-4Au**●$MTOA^+$ (**Figure 16**) complex in dichloromethane-d_2 displayed only four signals for the aromatic protons. (H_1'-H_2'-H_3'-H_4'). Some of them even overlapped with those of the NHC unit. (H_{12}-H_1', H_{11}-H_2-H_3'-H_{10}). The β-pyrrole protons of the Cl^-● *α,β* **-Au**●$MTOA^+$ also resonated as four separate signals (H_6, H_7, H_8, H_9). In the case at hand, it was impossible to differentiate the proton signals of the two conformers and determine their ratio. Either all the proton signals of the two conformers overlap or one conformer is more favourably formed in solution at low temperature.

In summary, the results of the 1D and 2D ^{1}H NMR experiments performed at 198 K in deuterated dichloromethane solution for the ion-paired complexes Cl^-● *α,β* -**4Au**●$MTOA^+$ and *Cl^-● α,β* ***-5●MTOA***$^+$ are consistent with those obtained for the

corresponding anionic complexes in deuterated acetone. We observe the presence of two conformers in a 1:1 ratio for the Cl^-● *α,β* **-5**●$MTOA^+$ complex. However, in the case of the Cl^-● *α,β* **-4Au**●$MTOA^+$ complex, we cannot determine the ratio of the isomers owing to the possible overlap of their proton signals.

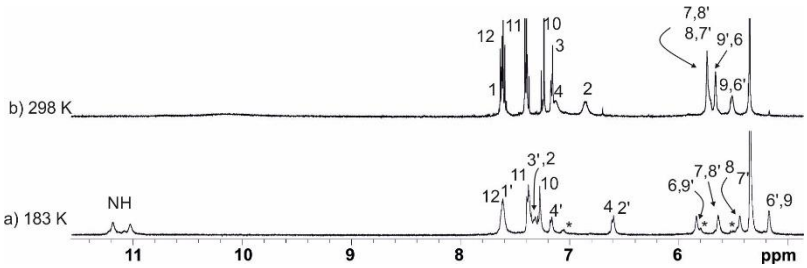

***Figure 16**: Selected ^1H NMR spectra (400 MHz, CD_2Cl_2) at a) 183 K and b) 298 K of α,β-**4Au**(3 mM) with 1 equiv. of **MTOACl.** See **Scheme 4** for proton assignment.*

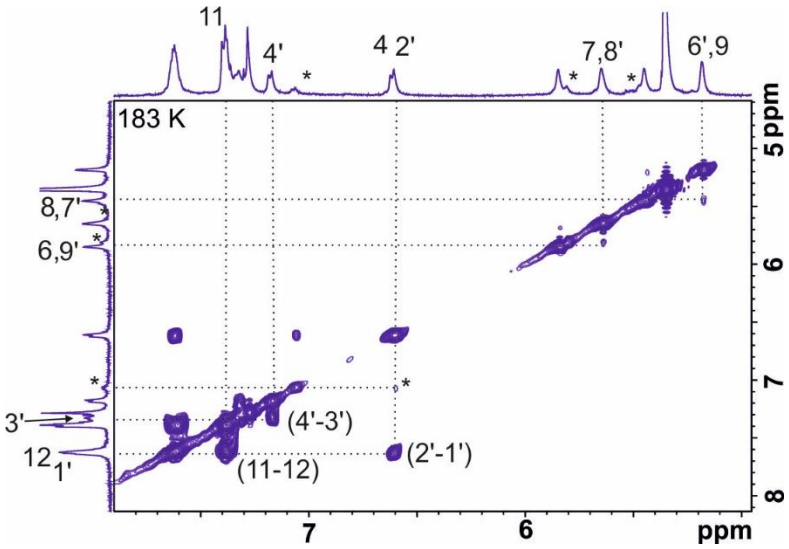

***Figure 17**: COSY experiment of α,β-**4Au** with 1 equiv. of **MTOACl** in CD_2Cl_2 at 183 K with assignments (aromatic region). See **Scheme 4** for proton assignment.*

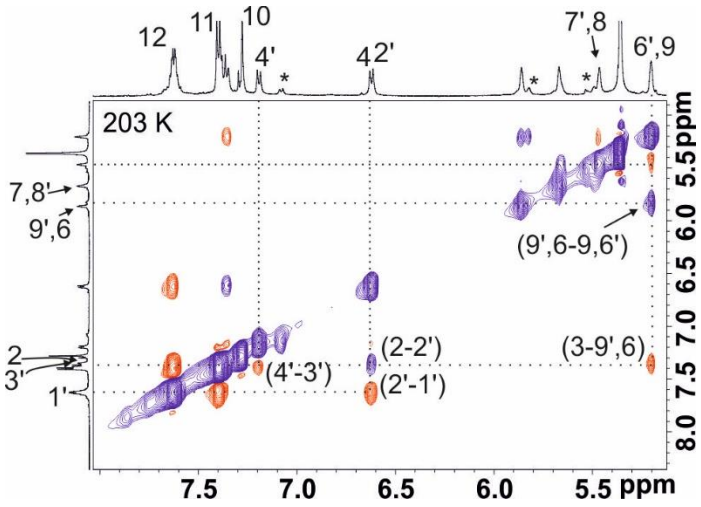

***Figure 18:** ROESY experiment of α,β-**4Au** with 1 equiv. of **MTOACl** in CD_2Cl_2 at 183 K with assignments (aromatic region). See **Scheme 4** for proton assignment.*

It is noteworthy that in the 1D and 2D ^{1}H NMR experiments of the Cl^-● *α,β* -**4Au**●$MTOA^+$ complex performed in deuterated dichloromethane (**Figure 17**, **Figure 18**) we detected a set of signals with lower intensity (signals marked with *). These signals may correspond to one of the two conformers, suggesting that they are present in solution and at lower temperature in a ratio that is significantly different than 1. However, we cannot propose a reliable and undisputable assignment of the

signals of low intensity to the protons of one of the conformers. They might be assigned to other complexes or impurities present in solution.

4.3 Theoretical Calculations

Finally, we decided to perform theoretical calculations to shed some light on the energy difference between the two conformers of the chloride complexes of the "two wall" calix[4]pyrrole *α,β* **-4Au** and *α,β-**5***. At the same time, the results of the theoretical calculations are expected to provide some insights on their binding geometries. The theoretical calculations were performed by Prof. Dr. A. Frontera (Universitat de les Illes Balears) using Turbomole 7.0 and at the RI[33,34,35]BP86[36]- def2-TZVP[37] (C, H, N, P, O, Au) (def2-ECP(Au)) level of theory and employing a continuum solvent model.

[33] Eichkorn, K.; Treutler, O.; Öhm, H.; Häser, M.; Ahlrichs, R., Auxiliary basis sets to approximate Coulomb potentials (VOL 240, PG 283, 1995). *Chem. Phys. Lett.* **1995,** *242*, 652-660.
[34] Eichkorn, K.; Weigend, F.; Treutler, O.; Ahlrichs, R., Auxiliary basis sets for main row atoms and transition metals and their use to approximate Coulomb potentials. *Theor. Chem. Acc.* **1997,** *97*, 119-124.
[35] Sierka, M.; Hogekamp, A.; Ahlrichs, R., Fast evaluation of the Coulomb potential for electron densities using multipole accelerated resolution of identity approximation. *J. Chem. Phys.* **2003,** *118*, 9136-9148.
[36] Perdew, J. P., Density-functional approximation for the correlation energy of the inhomogeneous electron gas. *Phys. Rev. B* **1986,** *33*, 8822-8824.
[37] Weigend, F.; Ahlrichs, R., Balanced basis sets of split valence, triple zeta valence and quadruple zeta valence quality for H to Rn: Design and assessment of accuracy. *Phys. Chem. Chem. Phys.* **2005,** *7*, 3297-3305.

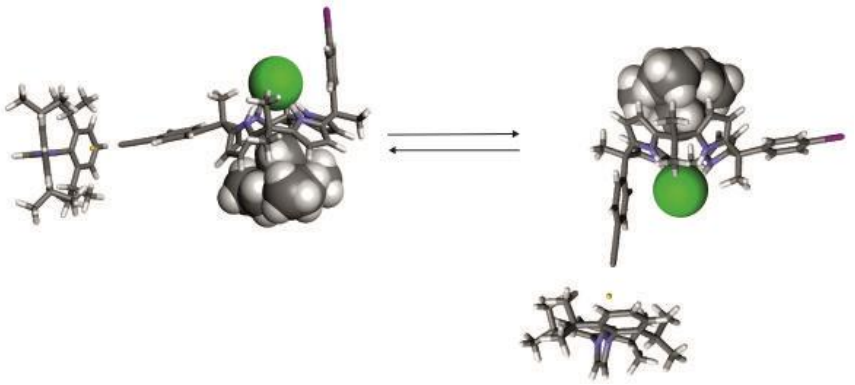

***Figure 19**: Conformation equilbrium and molecular structures of the two conformers of the ion-paired complex Cl^-● α,β -**4Au**●TMA^+. The receptor is displayed in stick representation. The chloride and the TMA^+ cation are shown as CPK models. The $MTOA^+$ cation used experimentally was prunned to TMA^+ to ease the calculations-*

In order to simulate the experimental conditions, the geometry optimization and energy calculation of the conformers was performed using continuum solvent models of acetone and dichloromethane. As shown in **Table 2** in both solvents the calculated electronic energies, ΔΔE, between the two conformers is of the order of 0.7 kcal/mol. This value although small with respect to the typical error of DFT calculations is considered to be appropriate to estimate that the two conformers of the Cl^-● *α,β* **-4Au**●TMA^+ and Cl^-● *α,β* **-4Au** complexes should be present in solution in a ratio close to 80:20 favoring the axial orientation of the iodo-phenyl substituent (folded state). The calculated ΔΔE value of the two conformers is not solvent dependent.

Attempt to quantify chloride-π interactions using a supra-molecular conformational balance based on a "two wall" mono-alkynyl Au(I) α,β calix[4]pyrrole

***Table 2**: Energy of the conformers (E_h/mol) in acetone and dichloromethane and the energy difference (Kcal/mol) in the two conformers, * calculation for* Cl^-● *α,β* **-5** *using the same level of theory of the gold complexes and in gas phase.*

	ΔG E_h/mol	**ΔΔG kcal/mol**
Unfolded-Cl^-● *α,β* **-4Au**	-3821.901385	0.7
Folded-Cl^-● *α,β* **-4Au**	-3821.902543	
Unfolded-Cl^-● *α,β* **-4Au**●$MTOA^+$	-4154.215760	0.7
Folded-Cl^-● *α,β* **-4Au**●$MTOA^+$	-4154.216881	
Folded-Cl^-● *α,β* **-5**●*	-2525,87199236	0.1
Unfolded-Cl^-● *α,β* **-5**●*	-2525,871704918	

We also performed DFT calculations for the conformers of the anionic complex of the *α,β*-**5** C[4]P receptor in the gas phase. In these, case the energy difference decreased to 0.1 kcal/mol supporting their formation in an almost identical extent (54:46) as we observed experimentally.

Based on the results of the VT ^{1}H NMR experiments and the computational study, it is sensible to consider that in solution the folded conformer (*p*-iodophenyl in axial orientation) of the anionic and ion-paired Cl^-complexes of the organometallic C[4]P receptor *α,β* -**4Au** is energetically slightly favored. The large difference in the ESP values of its two aromatic walls (*meso*-phenyl substituents) might be responsible for the observed conformational preference. The *p*-iodophenyl substituent will exhibit

a reduced repulsive chloride-π interaction compared to the *p*-Au-acetylide substitutet counterpart.

4.4 Conclusions

We described the synthesis of unprecedented "two-wall" *α,β* -C[4]Ps non-symmetrically substituted *α,β*-**4Au** and *α,β*-**5**. We investigated the binding properties of the two C[4]P receptors in dichloromethane and acetone solution by means of ^{1}H NMR spectroscopic titration experiments and used tetraalkylammonium salts (TBACl, MTOACl) as chloride precursor. Both receptors formed thermodynamically stable ($K_{as} > 10^3$ M-1) anionic 1:1 complexes in acetone and the corresponding ion-paired analogues in dichloromethane. We performed ITC experiments to accurately determine the binding affinity of the receptors for chloride in acetone solution (TBACl). The obtained data revealed that the **Cl$^-$●***α,β*-**5** complex was slightly energetically favoured (0.5 kcal/mol) than the **Cl$^-$●***α,β*-**4Au** counterpart. We used the formed complexes as supramolecular conformational balances to investigate the relative strength of the chloride-π interactions present in them. The results of low-temperature ^{1}H NMR experiments carried out with the anionic and ion-paired complexes of the *α,β*-**5** receptor evidenced their existence in solution as an equilibrium between two conformational isomers in a ratio close to 1. Remarkably, similar VT experiments with the complexes of the Au-acetylide receptor, *α,β*-**4Au**, did not provide clear experimental evidence to determine the composition of the conformers in the analogous equilibrium. The problem arised due to the lack of observation of separate proton signals for the two conformers. This limitation might be caused by the coincidentally complete overlap of the proton signals or by their presence of the two conformers to very different extent in the equilibrium. We undertook DFT calculations to determine the relative energies of the two conformers of the anionic and ion-paired complexes of *α,β*-**4Au** using a continuum model of the solvents-. The calculated differences between the energies of the two conformers was ΔΔE = 0.7 kcal/mol independently of the solvent used. This result can be translated to an 80:20 ratio of conformers at equilibrium in favour of the conformer displaying the p-iodophenyl substituent in axial orientation (folded conformer) supporting the preferential formation of one conformer hinted by the experimental results. In contrast, we calculated an energy difference ΔΔE of 0.1 kcal/mol for the two conformers of the Cl−● *α,β*-**5** complex supporting its existence

in solution in almost identical extent (46:54) in agreement with experiment. The use of the Cl−●*α*,*β*-**4Au** complexes (anionic and ion-paired) as supramolecular conformational balances for the assessment of the relative strength of chloride-π interactions produced interesting results. However, they are not clear cut owing to the lack of detection of separate signals for the two conformers in the ^{1}H NMR spectra acquired at low temperatures.

4.5 Experimental section

4.5.1 General methods and instrumentation

Reagents were obtained from commercial suppliers and used without further purification unless otherwise stated. Dry solvents were taken from a solvent system MB SPS 800. Et_3N was dried, distilled and degassed by three freeze-pump-thaw cycles before used in the cross-coupling reactions. Flash column chromatography was performed with silica gel (technical grade, pore size 60 Å, 230-400 mesh particle size). Routine ^{1}H NMR and ^{13}C(^{1}H) NMR spectra were recorded on a Bruker Avance 300 (300 MHz for ^{1}HNMR and 75 MHz for ^{13}C NMR), Bruker Avance 400 (400 MHz for ^{1}H NMR and 100 MHz for ^{13}C NMR), Bruker Avance 500 (500 MHz for ^{1}H NMR and 125 MHz for ^{13}C NMR), or Bruker Avance 500 with cryoprobe (500 MHz for ^{1}H NMR and 125 MHz for ^{13}C NMR). Deuterated solvents used are indicated in the characterization and chemical shifts are given in ppm. Residual solvent peaks were used as reference. All NMR J values are given in Hz. COSY, NOESY, HMQC, and HMBC experiments were recorded to help with the assignment of ^{1}H and ^{13}C signals. High Resolution Mass Spectra (HRMS) were obtained on a Bruker HPLC-TOF (MicroTOF Focus), Bruker Corporation, Bremen, Germany, with ESI as ionization mode and Bruker HPLC-QqTOF (MaXis Impact), Bruker Corporation, Bremen, Germany with ESI as ionization mode. Nominal mass spectra were obtained by direct injection on an Agilent 1200 and as detection unit an Agilent 6130 quadrupole. Melting points were measured on a MP70 Melting Point System Mettler Toledo. Column chromatography was performed with silica gel technical grade (Sigma-Aldrich, Merck Life Science S. L. U., Madrid, Spain), pore size 60 Å, 230–400 mesh particle size, 40–63 µm particle size and Thin Layer Chromatography (TLC) analysis on silica gel 60 F254.

4.5.2 Synthesis and characterization data

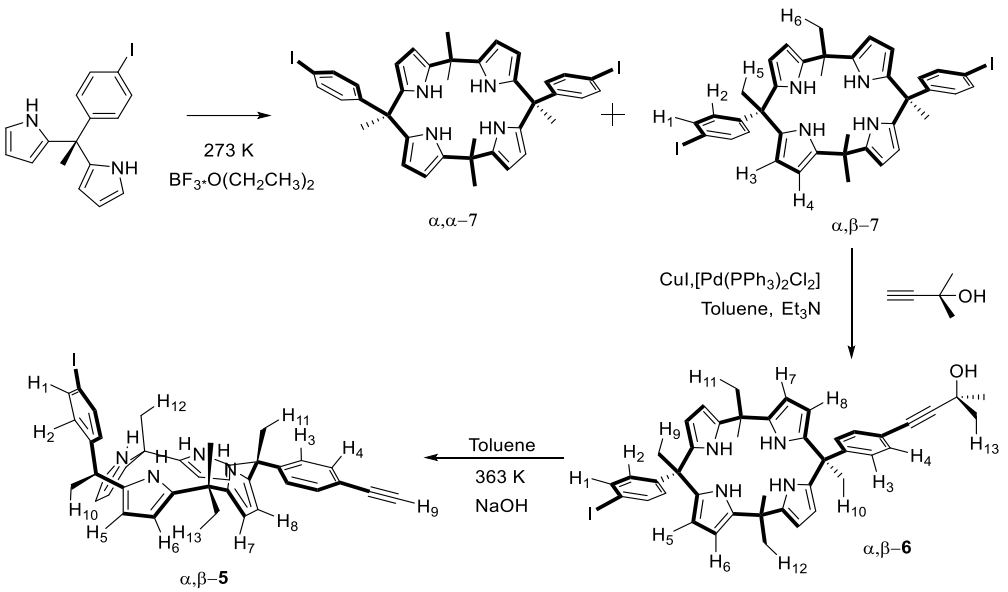

Scheme S 1: *Synthetic scheme for the preparation of the α,β-"two wall" calix[4]pyrroles whose X-ray single crystal structures are investigated in this work: α,β-**7**, α,β-**6** and α,β-**5***

10α,20β-Bis(4-iodophenyl)-hexamethyl calix[4]pyrrole (α,β-**7**)

To a solution of 4-iodophenyl, methyl-*meso*-dipyrromethane[38] (8 g, 23 mmol, 1 equiv.) in 600 mL of acetone, BF_3•OEt_2 (3 mL, 23 mmol assuming 99.9% purity, 1 equiv.) was added dropwise over a period of 30 min at 0 ºC. The reaction mixture was stirred at room temperature for 12 hours. 100 mL of distilled water were then added. The acetone was removed under reduced pressure to obtain a residual solution (~100 mL) that was neutralized (KOH 2M ~20 mL to pH = 7). Next,100 mL of distilled water were added. The water phase was extracted with DCM (3 × 100 mL). The collected organic layers were dried over anhydrous Na_2SO_4 and concentrated under reduced pressure. The final product was purified by combi-flash chromatography on a silica gel column (120g SiO_2, ethyl acetate/hexane 5:95). The

[38] Valderrey, V.; Escudero-Adán, E. C.; Ballester, P., Polyatomic Anion Assistance in the Assembly of [2]Pseudorotaxanes. *J. Am. Chem. Soc.* **2012,** *134* (26), 10733-10736.

combined tubes containing the first eluting compound yielded, after solvent evaporation in vacuo, 1.5 g of α,β-**7** as a white solid (16.5 % yield).

^{1}H NMR (400 MHz, acetone-d_6, 298 K) δ(ppm): 8.85 (br s, 4H, NHs), 7.56 (d, 4H, $J^{1\text{-}2}$= 8.55 Hz, H^1), 6.83 (d, $J^{2\text{-}1}$= 8.55, 4H, H^2), 5.82 (dd, $J^{3\text{-}4}$=3.6 Hz, $J^{3\text{-}NH}$=3 Hz, 4H, H^3), 5.80 (dd, $J^{4\text{-}3}$= 3.6 Hz, $J^{4\text{-}NH}$=3 Hz 4H, H^4), 1.83 (br s, 6H, H^5), 1.53 (s, 12 H, H^{6,7}). ^{13}C (125 MHz, acetone-d_6, 298 K) δ(ppm) 149.08, 139.09, 136.63, 135.91, 129.82, 105.28, 102.87, 90.92, 44.49, 35.42, 29.89, 29.51. HRMS (ESI/ TOF) m/z: [M +Na]$^{+\cdot}$= [$C_{38}H_{38}I_2N_4Na$]$^+$ Calcd 827.1078; Found 827.1041.

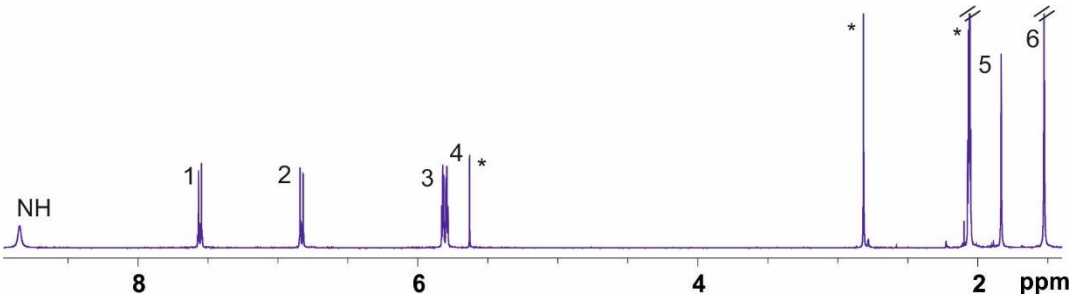

***Figure S 1**: ^{1}H NMR (500 MHz, d_6-Acetone, 298 K) spectrum of α,β-**7**. See scheme S1 for proton assignment. *Solvent residual peak.*

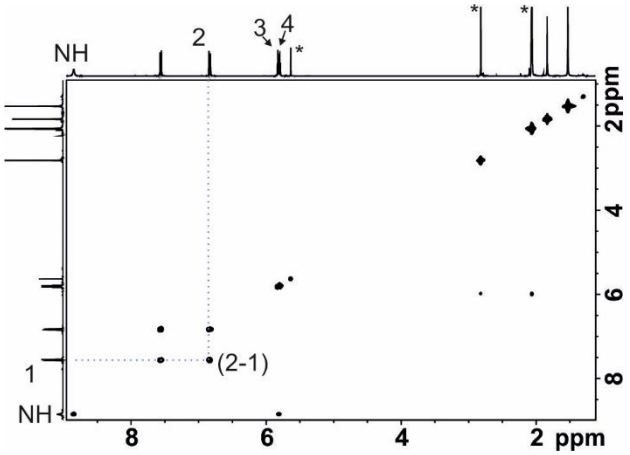

***Figure S 2:** 2D ^{1}H-^{1}H COSY NMR (400 MHz, d_6-Acetone, 298 K) spectrum of α,β-**7**. Some selected COSY cross-peaks are indicated. See scheme S1 for proton assignment. *Solvent residual peak.*

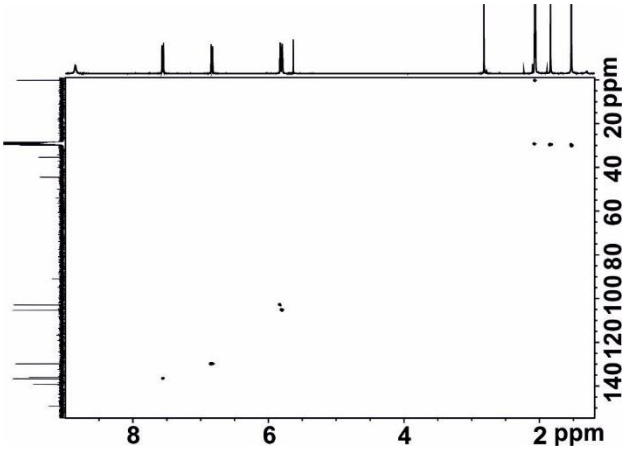

Figure S 3: *2D ^{1}H-^{13}C HSQC NMR (d_6-Acetone, 298 K) spectrum of α,β-**7**.*

10α-(4-Iodophenyl)-20β(4-[(3-methyl-3-hydroxybut-1-yn-1-yl)phenyl]-hexamethyl-calix[4]pyrrole (**4**) **and 10α,20 β-bis(4-[(3-methyl-3-hydroxybut-1-yn-1-yl)phenyl]-hexamethyl calix[4]pyrrole** (*α,β*-**6**)

10α,20β-bis(4-iodophenyl) hexamethyl calix[4]pyrrole (α,β-**4**) (300 mg, 0.373 mmol, 1 equiv.), $Pd(PPh_3)_2Cl_2$ (13.1 mg, 18.6 µmol, 0.05 equiv.) and CuI (3.55 mg, 18.6 µmol, 0.05 equiv.) were placed in a Schlenk flask. The flask was purged with argon and later 21 mL of dry toluene were added. The reaction mixture was left stirring under Ar for 15 min producing a yellow suspension. 4.91 mL of freshly distilled triethylamine (100 equiv.) and 2-methyl-3-butyn-2-ol (181 µL, 1.86 mmol, 5 equiv) were added and the mixture was stirred at RT under Ar during 2 h. After this time has elapsed, DCM (60 mL) was added to the reaction mixture. The resulting organic layer was washed with 0.5 M HCl (60 mL × 1) and water (60 mL ×2). The organic layer was dried over sodium sulfate, filtered and concentrated under vacuum to obtain a brown solid. The solid was purified using silica column chromatography and different eluents (CH_2Cl_2/hexane, CH_2Cl_2 and CH_2Cl_2/ethyl acetate (9:1)). The unreacted compound α,β-**4** eluted with the front of the solvent. Using CH_2Cl_2 as eluent allowed the isolation of compound α,β-**6** as the second fraction (105 mg, 42% yield).

^{1}H NMR (400 MHz, d_6-Acetone, 298 K) δ(ppm): 8.85, 8.75 (two br s, 4H,NHs), 7.56 (d, 2H, J^{1-2}= 8.6 Hz, H^1), 7.22 (d, 2H, J^{4-3}= 8.49 Hz, H^4), 7.01 (d, 2H , J^{4-3}= 8.49 Hz, H^3), 6.84 (d, 2H, J^{2-1}= 8.6, H^2), 5.82 (dd, 4H, $J^{5.8-6.7}$=3.2 Hz, $J^{5,8-NH}$=3.5 Hz, $H^{5,8}$), 5.77 (dd, 4H, $J^{6,7-5,8}$=3.2 Hz, $J^{6,7-NH}$=7.63 Hz ,$H^{6,7}$), 4.32 (s, 1H, OH), 1.84 (s, 3H, H^9), 1.83 (s, 3H, H^{10}), 1.53 (s, 12H, $H^{11,12}$), 1.52 (s, 6H, H^{13}). ^{13}C (125 MHz, d_6-Acetone, 298 K) δ(ppm) 149.05, 139.05, 138.98, 133.64, 136.15,135.86, 130.62, 129.82, 127.48, 121, 105.3 ,105.27, 102.89, 102.82, 94.96, 90.97, 64.23, 44.61, 44.49, 35.37, 31.17, 29.81,

29.71. M.P. =268.2 ºC HRMS (ESI/ TOF) m/z: $[M+Na]^{+\cdot}$= $[C_{43}H_{45}IN_4ONa]^+$ Calcd 783.2530; Found 783.2520.

10α-(4-iodophenyl)-20β(4-[(3-methyl-3-hydroxybut-1-yn-1-yl)phenyl]-hexamethyl calix[4]pyrrole *(α,β-**6**)*

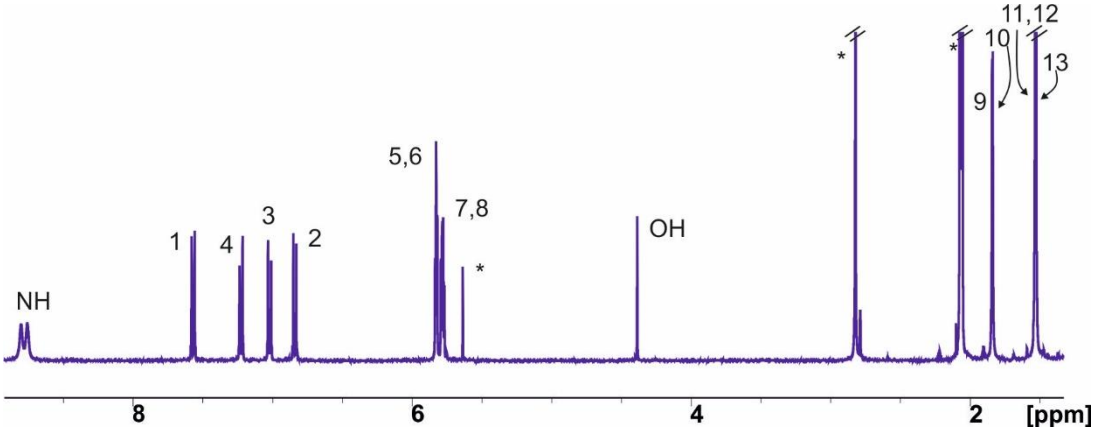

Figure S 4: *^{1}H NMR (500 MHz, d_6-Acetone, 298 K) spectrum of α,β-**6**. See scheme S1 for proton assignment. *Solvent residual peak.*

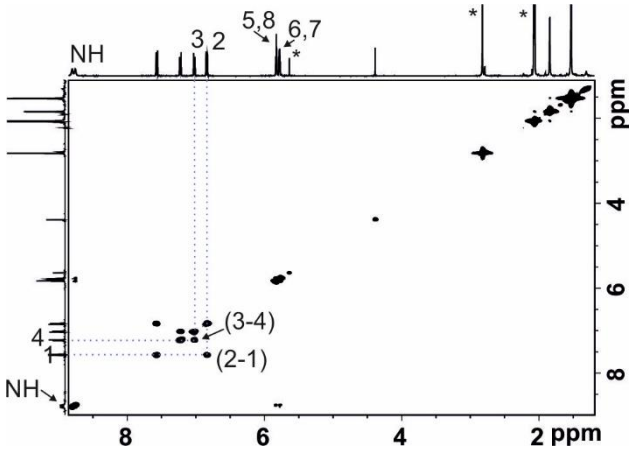

Figure S 5: *2D ^{1}H-^{1}H COSY NMR (400 MHz, d_6-Acetone, 298 K) spectrum of α,β-**6**. Some selected COSY cross-peaks are indicated. See scheme S2 for proton assignment. *Solvent residual peak.*

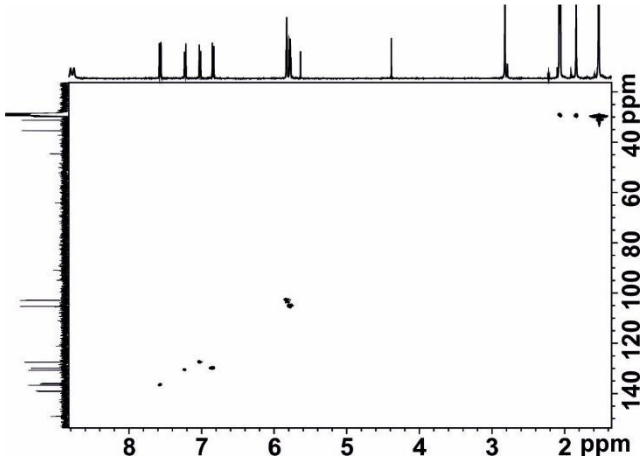

Figure S 6: *2D ^{1}H-^{13}C HSQC NMR (d_6-Acetone, 298 K) spectrum of α,β-**6**.*

10α-(4-Iodophenyl)-20β-(4-ethynylphenyl) hexamethyl calix[4]pyrrole (*α,β*-**5**)

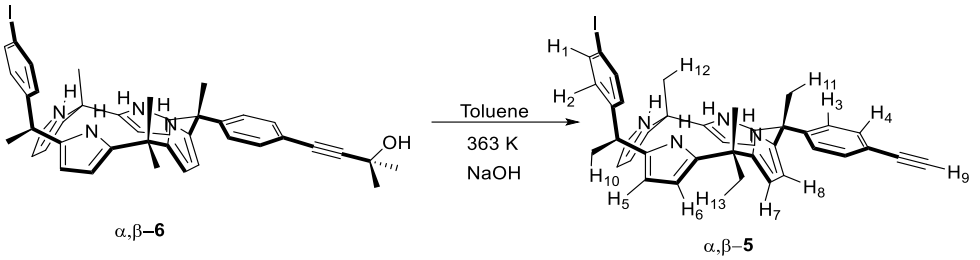

***Scheme S 2**: Synthesis of compound α,β-**5**.*

A solution of 10α-(4-iodophenyl)-20β-(4-[(3-Methyl-3-hydroxybut-1-yn-1-yl)phenyl] hexamethyl calix[4]pyrrole (*α,β*-**6**) (250 mg, 0.329 mmol, 1 equiv.) in toluene (25 mL) was treated with powdered NaOH (418 mg, 10.5 mmol, 20 equiv.) and refluxed for 12 h under Ar atmosphere. The reaction mixture was concentrated in vacuum. The residue was triturated with DCM (30 mL × 2). The combined organic extracts were washed with 0.5 M HCl (30 mL × 1) and water (30 mL × 2), dried over anhydrous Na_2SO_4, filtered and concentrated under vacuum to give a brown solid. The solid was purified using column chromatography (CH_2Cl_2/hexane 9:1). The tubes containing the major collected fraction were combined and the solvent removed under vacuum yielding *α,β*-**5** as a white brownish solid (170 mg, 73% yield). NMR (400 MHz, d_6-Acetone, 298 K) δ(ppm): 8.83 (br s, 4H, NHs), 7.56 (d, 2H, J^{1-2}= 8.64 Hz, H^1), 7.32 (d, 2H, J^{4-3}= 8.57 Hz, H^4), H^3 (d, 7.04 ppm, J^{4-3}= 8.57 Hz, 2H), 6.84 (d, 2H, J^{2-1}= 8.64, H^2), $H^{5,8}$ (m, 5.83 ppm, 4H), 5.79 (dd, 4H , $J^{6,7-5,8}$ =2.89 Hz, $J^{6,7-NH}$=3.5 Hz, $H^{6,7}$), 3.59 (s, 1H, H^9), 1.85 (s, 3 H, H^{10}), 1.84 (s, 3 H, H^{11}), 1.53 (s, 12H, $H^{12,13}$). ^{13}C (125 MHz, d_6-Acetone, 298 K) δ(ppm) 149.86, 149.02, 139.16, 139.07, 136.64, 136.03, 135.92 ,131.20, 129.81, 127.57, 119.93 105.3, 102.87, 102.84, 90.5, 83.29, 77.83, 44.68, 44.49, 35.4, 29.83, 29.43. M.P. =271.6 ºC HRMS (ESI/ TOF) m/z: $[M+Na]^{+\cdot}$= $[C_{40}H_{39}I_1N_4Na]^+$ Calcd 725.2111; Found 725.2099.

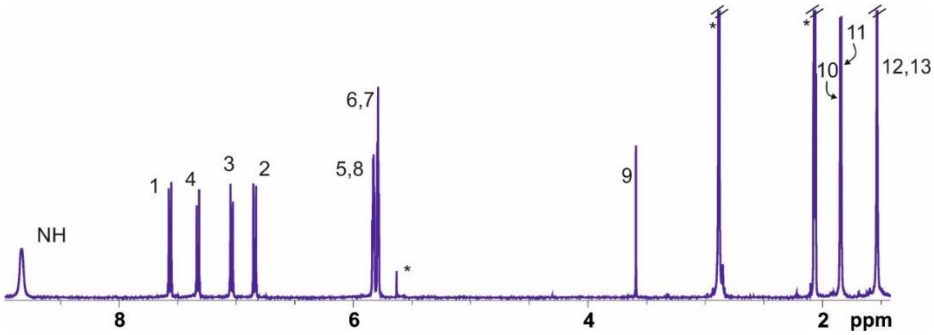

***Figure S 7**: ^{1}H NMR (500 MHz, d_6-Acetone, 298 K) spectrum of α,β-**5** See scheme S2 for proton assignment. *Solvent residual peak.*

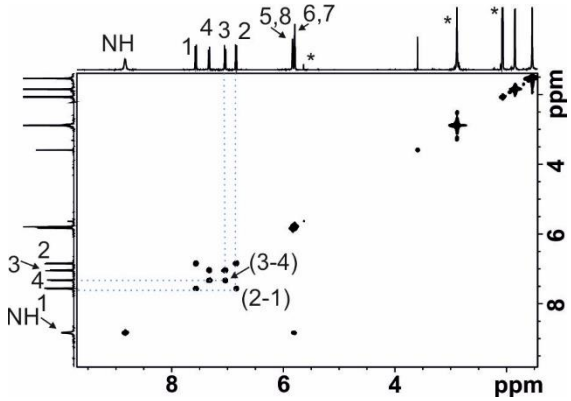

***Figure S 8:** 2D ^{1}H-^{1}H COSY NMR (400 MHz, d_6-Acetone, 298 K) spectrum of α,β-**5**. Some selected COSY cross-peaks are indicated. See scheme S2 for proton assignment. *Solvent residual peak.*

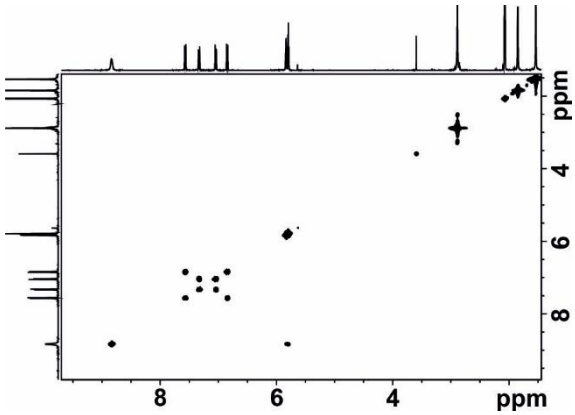

Figure S 9: *2D ^{1}H-^{13}C HSQC NMR (d_6-Acetone, 298 K) spectrum of α,β-**5**.*

10α-(4-Iodophenyl)-20β-(1,3-bis(2,6-di*iso*propylphenyl)-2,3-dihydro-1H-imidazol-2-yl) (4-ethynylphenyl) gold hexamethyl calix[4]pyrrole (*α,β*-**4Au**)

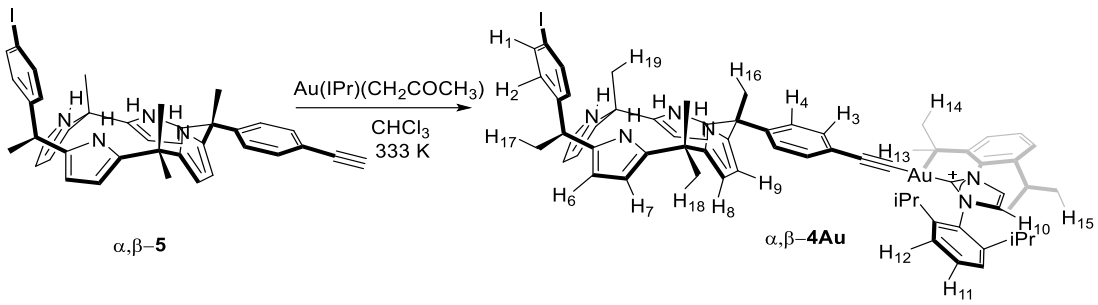

Scheme S 3**: Synthesis of compound α,β- **4Au

[Au(IPr)(CH2COCH3)] (1 equiv, 41.24 mg, 58.7µmol) and α,β-**5** (1 equiv, 36.5 mg, 56.8 µmol) were dissolved in CDCl3 (1.5mL) and stirred at 60°C for 24h. The solvent was removed under vacuum and the resulting solid dissolved in CH2Cl2 (2-3 mL). The solution was concentrated (ca. 1 mL) and the product precipitated by addition of pentane (ca. 5 mL). The precipitate was collected by centrifugation, washed with pentane (3 x 5 mL) and dried under vacuum affording the corresponding *α,β*- **4Au** in 65% yield (49.1 mg, 38.15 µmol). NMR (400 MHz, d_6-Acetone, 298 K) δ(ppm): 8.78 (br s, 2H, NHs), 8.62 (br s, 2H, NHs), 7.75 (s, 2H, H^{10}), 7.56 (t, 2H, $J^{11\text{-}13}$= 7.83 Hz, H^{11}), 7.55 ppm (d, $J^{1\text{-}2}$= 8.6 Hz, 2H, H^1), 7.42 (d, 2H, $J^{12\text{-}11}$= 7.8 Hz, H^{12}), 6.9 ppm (d, 2H, $J^{3\text{-}4}$= 8.6 Hz, H^3), 6.86 (d, 2H , $J^{4\text{-}3}$ =8.6 Hz, H^4), 6.77 (4, 2H , $J^{2\text{-}1}$ =8.6 Hz Hz, H^2), 5.79, 5.77 (t,t, 4H, $J^{9,6\text{-}7,8}$= 3 Hz, $H^{9,6}$), 5.73, 5.72 (t,t, 4H, $J^{7,8\text{-}9.6}$= 3 Hz, $H^{9,6}$), 5.72 (qui, 4 H, $J^{13\text{-}14,15}$=6.9 Hz , H^{13}), 1.83 (s, 3H, H^{16}), 1.75 (s, 3H, H^{17}), 1.4 (s, 6H, H^{19}), 1.48 (s, 6H, H^{18}), 1.38 (d, $J^{14\text{-}13}$=6.9 Hz,12H, H^{14}), 1.25 (d, $J^{15\text{-}13}$=6.9 Hz ,12H, H^{15}). ^{13}C (125 MHz, d_6-Acetone, 298 K) δ(ppm) 190.5, 148.8, 145.7, 139.1, 138.7,163.6, 136.5, 136.9, 134.7, 130.7, 130.3, 129.8, 126.7, 124.1, 124, 105.3, 104.9, 102.8, 102.6, 90.9, 44.5, 44.3, 35.3, 23.9, 23.2. HRMS (ESI/ TOF) m/z: $[M+H]^{+\cdot}$= $[C_{67}H_{74}AuIN_6H]^+$ Calcd 1287.4758; Found 1287.4758.

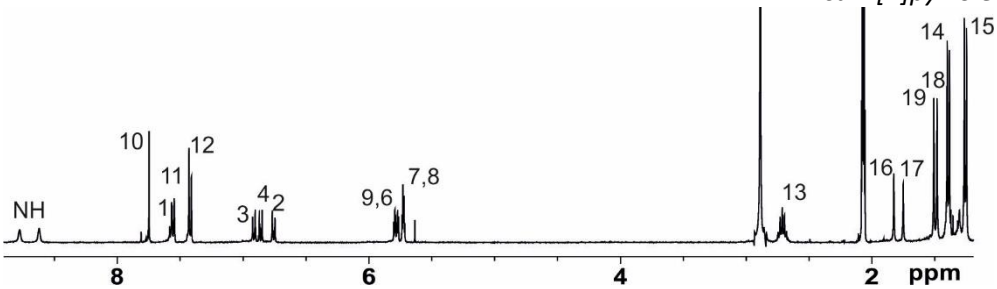

***Figure S 10**: ^{1}H NMR (500 MHz, d_6-Acetone, 298 K) spectrum of α,β-**4Au** See scheme S2 for proton assignment.*

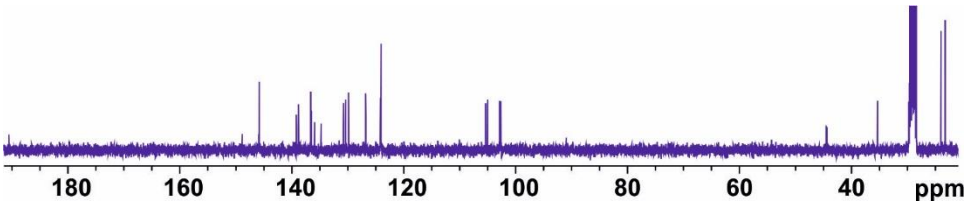

***Figure S 11**: ^{13}C NMR (125 MHz, d_6-Acetone, 298 K) spectrum of α,β-**4Au** See scheme S2 for proton assignment. *Solvent residual peak.*

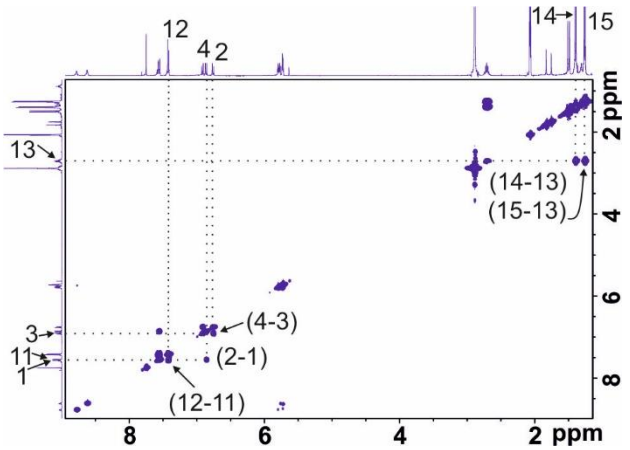

***Figure S 12**: 2D ^{1}H-^{1}H COSY NMR (400 MHz, d_6-Acetone, 298 K) spectrum of α,β-**4Au**. Some selected COSY cross-peaks are indicated. See scheme S4 for proton assignment.*

Au(IPr)(CH_2COCH_3)

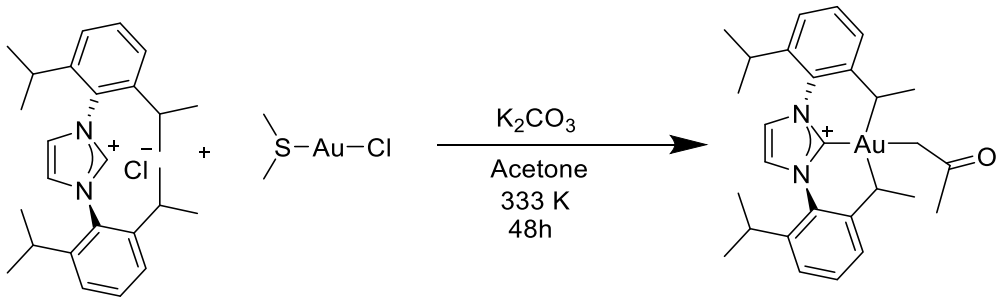

Scheme S 4:** Synthesis of **Au(IPr)(CH_2COCH_3)

IPr·HCl (369.6 mg, 0.87 mmol, 1 equiv), [Au(SMe2)(Cl)] (255.4 mg,0.87 mmol, 1 equiv), K_2CO_3 (755.8 mg, 5.47 mmol, 6 equiv) in acetone (3 mL). The reaction mixture was stirred for 48 h at 60ºC. The solution was then filtered through a pad of Celite, the solvent was removed under vacuum. The resulting solid was dissolved in the minimum amount of CH_2Cl_2 (2–3 mL) and precipitated by addition of n-pentane (ca. 10 mL). The precipitate was collected by filtration, washed with n-pentane (3-5 mL), and dried under vacuum, affording the corresponding [Au(IPr)(CH_2COCH_3)] in 80% yield (450 mg, 0.87 mmol)

The NMR spectroscopy of the compound agrees with the literature[39]

4.5.3 ^{1}H NMR binding studies

A solution of host (3-6 mM), *α,β*-**5** or *α,β*-**4Au**, was prepared in dichloromethane-d_2 or acetone-d6. Subsequently, 0.5-0.4 mL of the solution were transferred to an NMR tube. The remaining solution of the host was used to prepare the titrant's solution, which contained TBACl or MTOA at 20-30 fold higher concentration ([TBACl] = 120 mM, [MTOACl] = 100 mM and [H] = 3-6 mM). In this manner, the concentration of the host was maintained constant throughout the titration. Immediately, the 0.5 mL of the host solution was titrated by manually injecting incremental amounts of the titrant's solution using a micro syringe. A ^{1}H NMR spectrum of the mixture was acquired after each injection and vigorous hand shaking of the NMR tube for few seconds. The apparent binding constants were derived from the fit of the chemical shift changes of the titration data to a 1:1 theoretical binding model and using the HypNMR2008[40,41] software.

[39] Gasperini, D.; Collado, A.; Goméz-Suárez, A.; Cordes, D. B.; Slawin, A. M. Z.; Nolan, S. P., Gold–Acetonyl Complexes: From Side-Products to Valuable Synthons. *Chem. Eur. J.* **2015,** *21*, 5403-5412.

.

[40] Frassineti, C.; Ghelli, S.; Gans, P.; Sabatini, A.; Moruzzi, M. S.; Vacca, A., Nuclear Magnetic Resonance as a Tool for Determining Protonation Constants of Natural Polyprotic Bases in Solution. *Anal. Biochem.* **1995,** *231*, 374-382.

[41] Frassineti, C.; Alderighi, L.; Gans, P.; Sabatini, A.; Vacca, A.; Ghelli, S., Determination of protonation constants of some fluorinated polyamines by means of 13C NMR data processed by the new computer program HypNMR2000. Protonation sequence in polyamines. *Anal Bioanal Chem* **2003,** *376*, 1041-1052.

Acetone

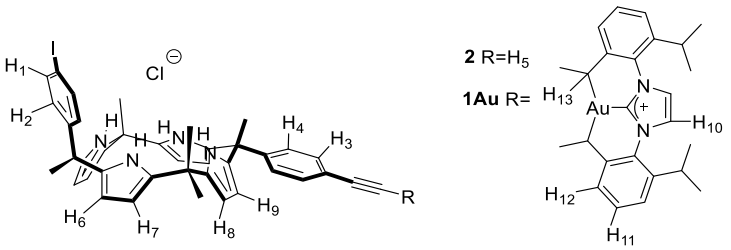

Scheme S 5: *General structure for the Cl⁻● α,β-C[4]P complex with assignment.*

α,β-5 vs TBACl

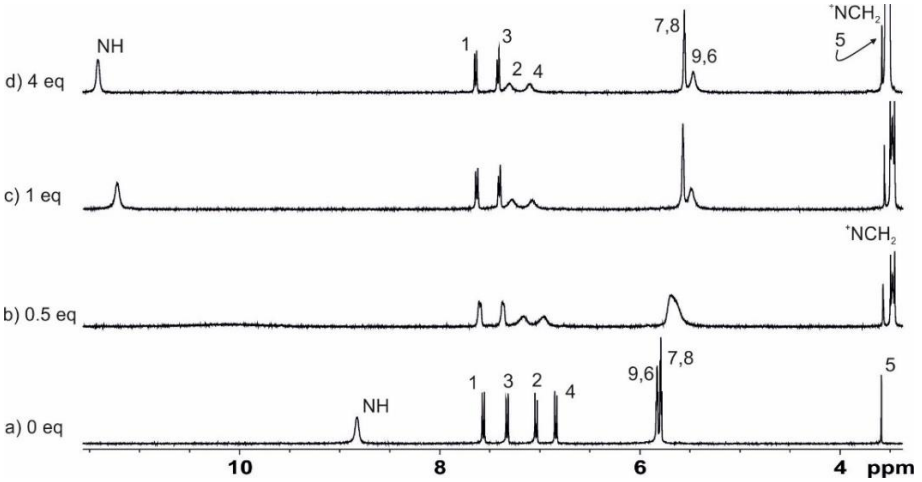

Figure S 13: *Selected regions of the ^{1}H NMR spectra (400 MHz, d_6-Acetone, 298 K) of α,β-**5**(6.2 mM) with incremental amounts of **TBACl** : a) 0 equiv. b) 0.5 equiv.; c) 1 equiv.; d) 4 equiv.; See scheme S5 for proton assignment.*

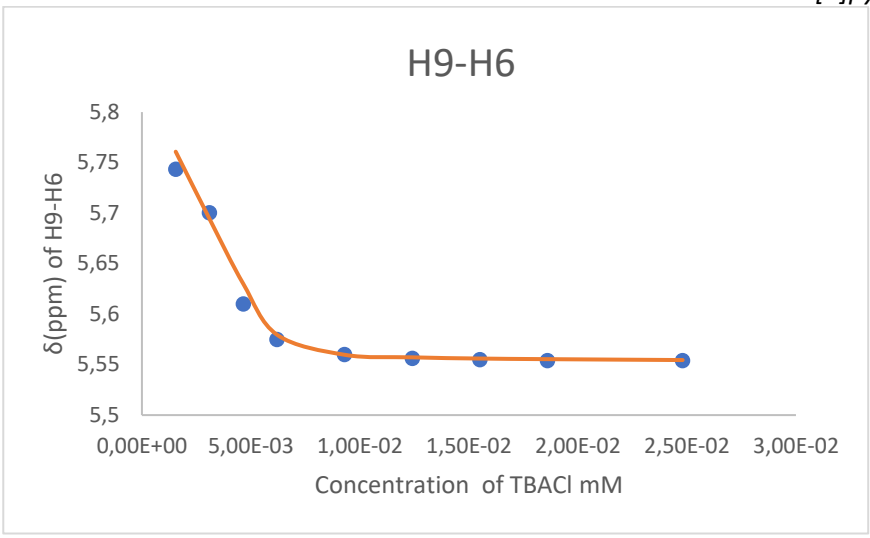

Figure S 14: *Chemical shifts of the β-pyrroles (H6-H9) protons of α,β-**5** upon incremental amounts of TBACl and fit of the NMR titration data to a theoretical 1:1 binding model.*

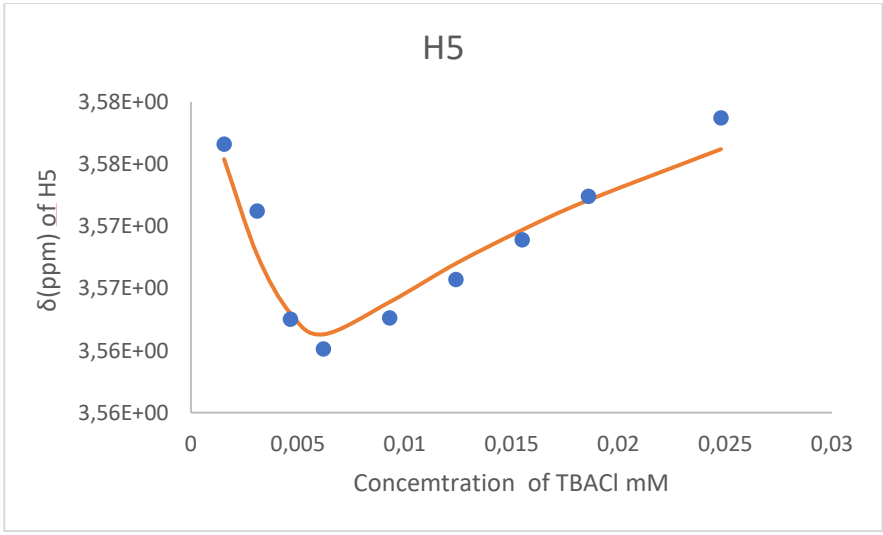

Figure S 15: *Chemical shifts of th alkyne proton H5 of α,β-**5** upon incremental amounts of TBACl and fit of the NMR titration data to a theoretical 1:1 binding model*

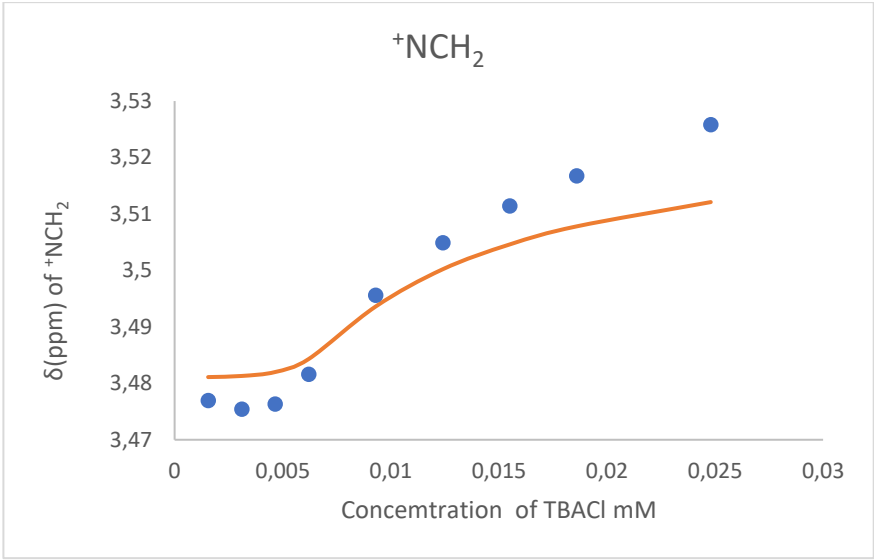

Figure S 16: *Chemical shifts of the CH_2 protons α to the nitrogen of TBA^+ cation upon incremental amounts of TBACl and fit of the NMR titration data to a theoretical 1:1 binding model.*

α,β-4Au vs TBACl

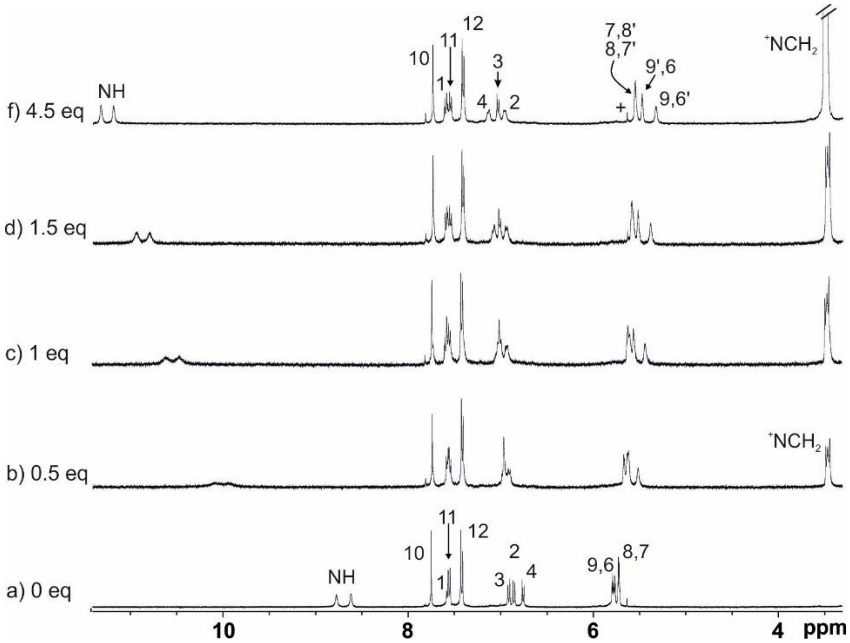

Figure S 17: *Selected regions of the ^{1}H NMR spectra (400 MHz, d_6-Acetone, 298 K) of α,β-**4Au** (3.4 mM) with incremental amounts of **TBACl :** a) 0 equiv. b) 0.5 equiv.; c) 1 equiv.; d) 1.5 equiv.; e) 4.5 equiv.; See scheme S5 for proton assignment*

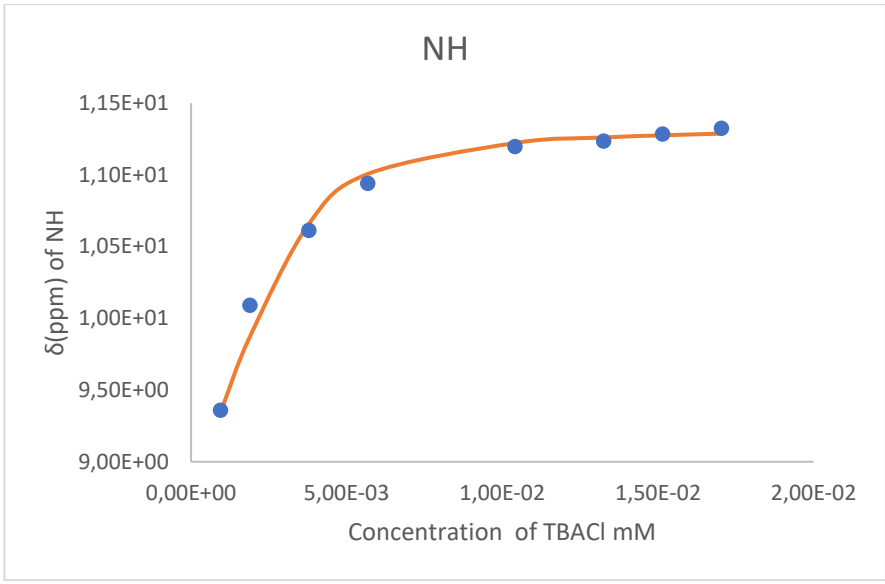

Figure S 18: *Chemical shifts of the alkyne proton NH of α,β-**4Au** upon incremental amounts of TBACl and fit of the NMR titration data to a theoretical 1:1 binding model*

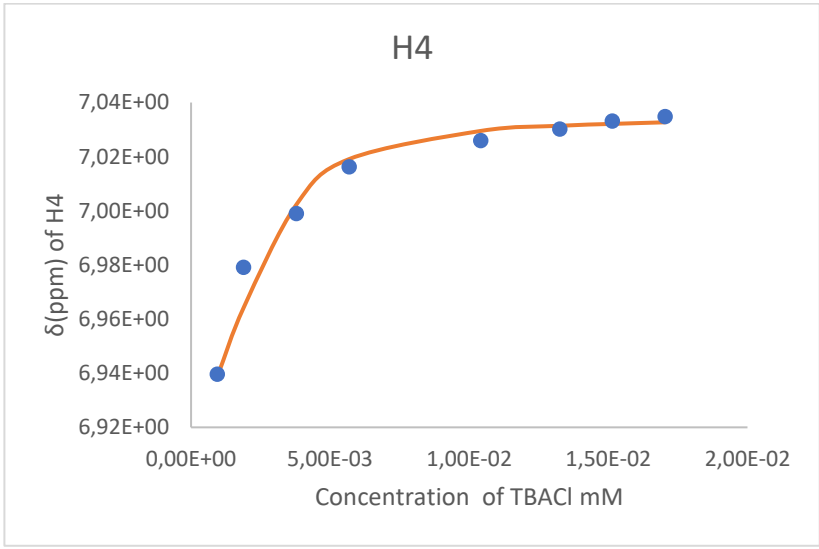

Figure S 19: *Chemical shifts of the aromatic H4 of **4Au** upon incremental amounts of TBACl and fit of the NMR titration data to a theoretical 1:1 binding model*

DCM

***α,β*-5 vs MTOACl**

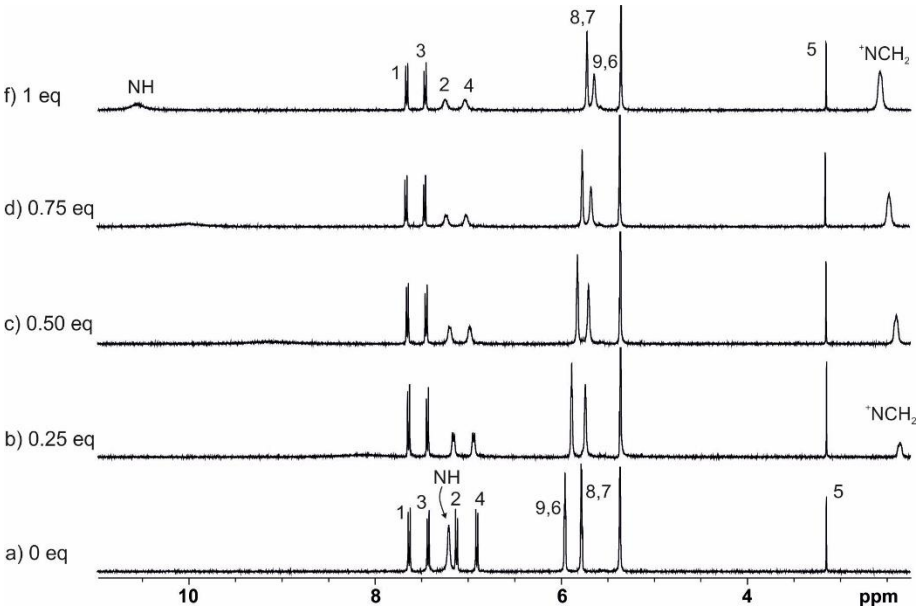

Figure S 20: *Selected regions of the ^{1}H NMR spectra (400 MHz, CD_2Cl_2, 298 K) of α,β-**5**(5.6 mM) with incremental amounts of **MTOACl** : a) 0 equiv. b) 0.25 equiv.; c) 0.5 equiv.; d) 0.75 equiv. and f) 1 equiv.; See scheme S5 for proton assignment.*

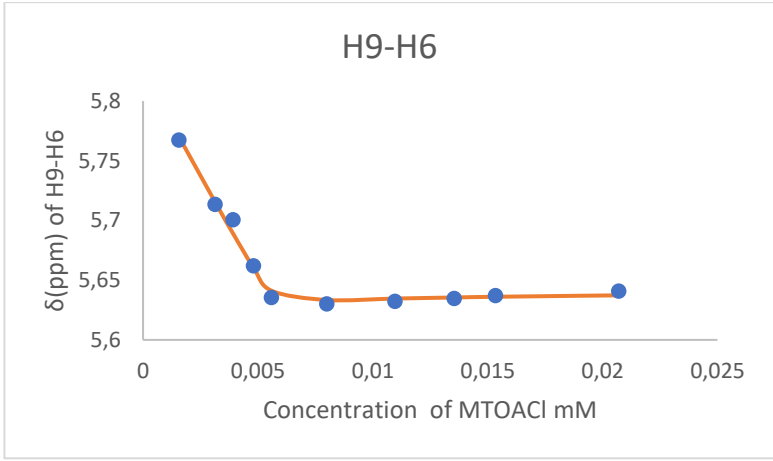

Figure S 21: *Chemical shifts of the β-pyrroles (H6-H9) protons of α,β-**5** upon incremental amounts of MTOACl and fit of the NMR titration data to a theoretical 1:1 binding model.*

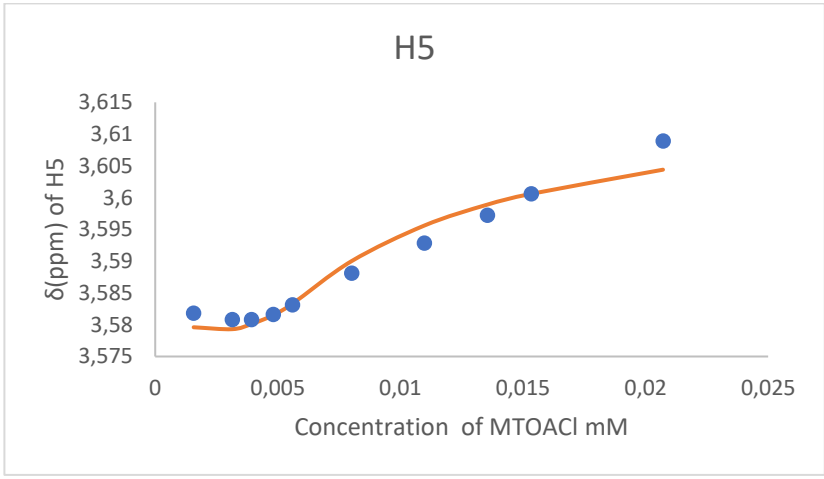

Figure S 22: *Chemical shifts of the alkyne proton H5 protons of α,β-**5** upon incremental amounts of MTOACl and fit of the NMR titration data to a theoretical 1:1 binding model.*

Attempt to quantify chloride-π interactions using a supra-molecular conformational balance based on a "two wall" mono-alkynyl Au(I) α,β calix[4]pyrrole

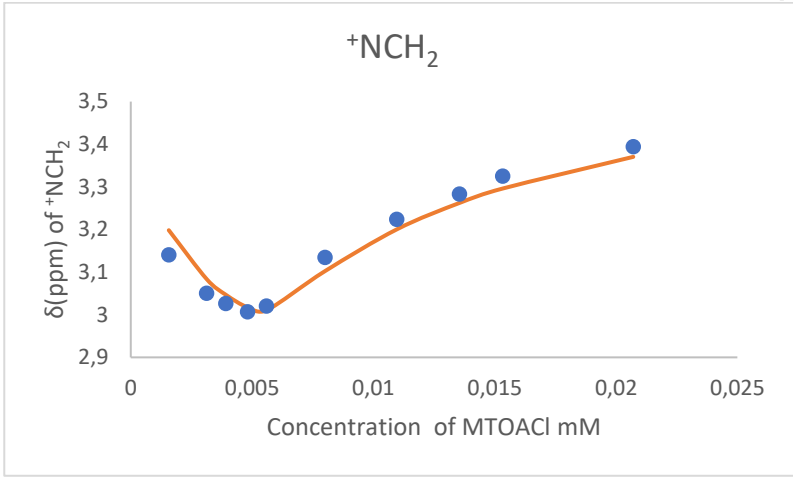

Figure S 23: *Chemical shifts of the CH_2 protons α to the nitrogen of $MTOA^+$ cation upon incremental amounts of MTOACl and fit of the NMR titration data to a theoretical 1:1 binding model.*

α,β-4Au vs MTOACl

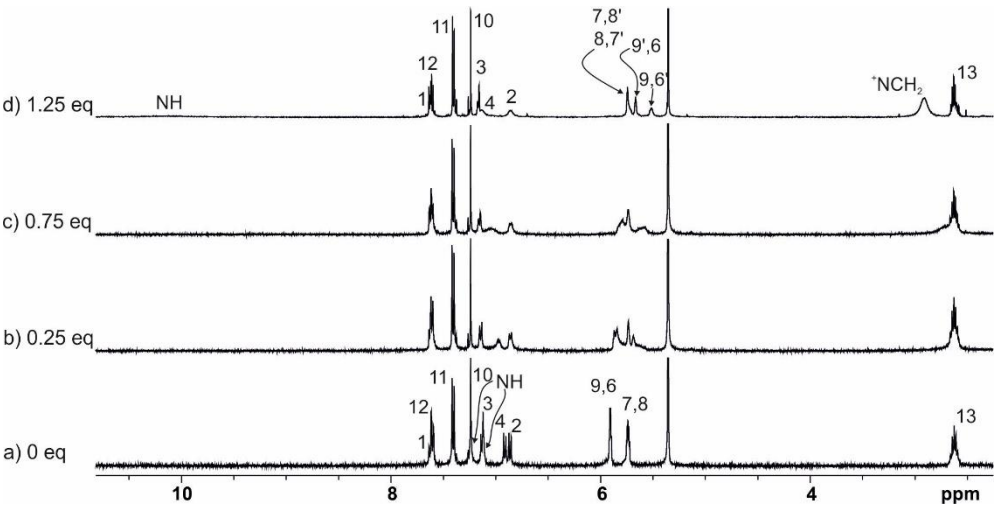

Figure S 24**:** Selected regions of the ^1H NMR spectra (400 MHz, CD_2Cl_2, 298 K) of α,β-**4Au** (3 mM) with incremental amounts of MTOACl : a) 0 equiv. b) 0.25 equiv.; c) 0.75 equiv.; d) 1.25 equiv.; See scheme 2 for proton assignment.

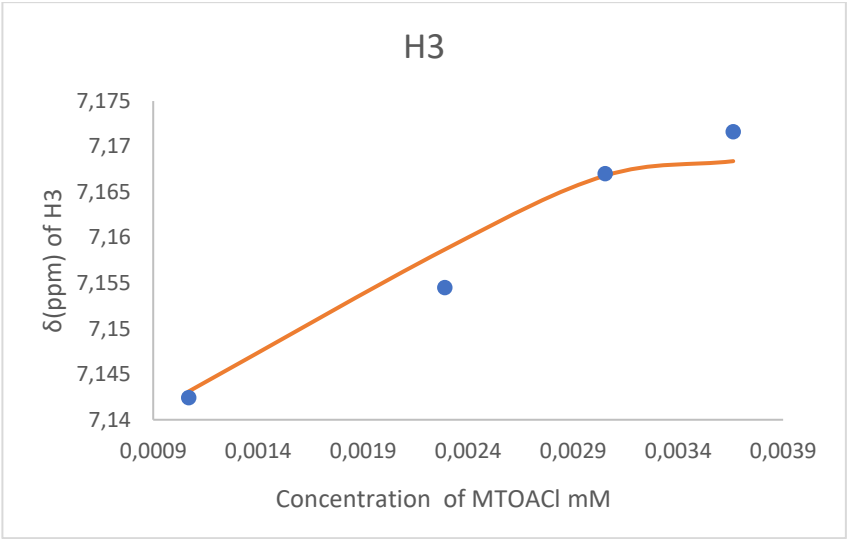

Figure S 25: *Chemical shifts of the aromatic proton H2 protons of α,β-**4Au** upon incremental amounts of MTOACl and fit of the NMR titration data to a theoretical 1:1 binding model.*

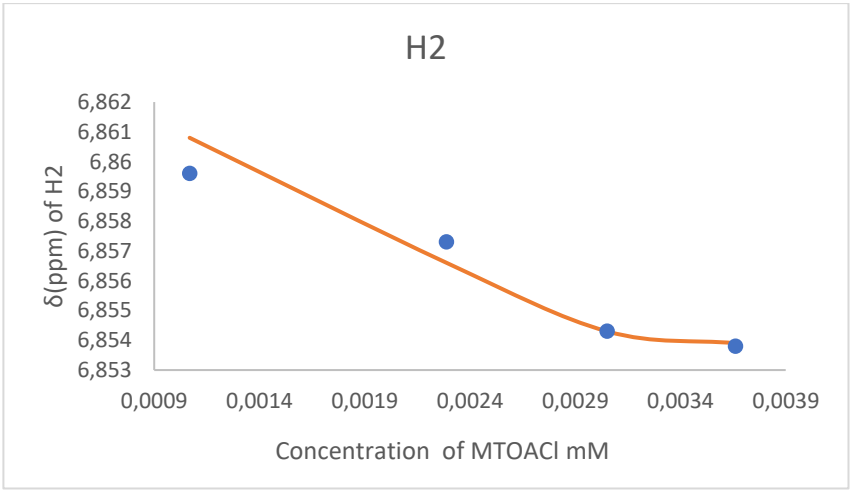

Figure S 26: *Chemical shifts of the aromatic proton H2 protons of α,β-**4Au** upon incremental amounts of MTOACl and fit of the NMR titration data to a theoretical 1:1 binding model.*

4.5.4 Variable temperatura ^{1}H NMR

Acetone

Variable temperature experiment performed on the 1:1 solution of C[4]Ps *α,β*-**5** and *α,β*-**4Au** with TBACl in Acetone, increasing the temperature from 198K to 308 or 298K.

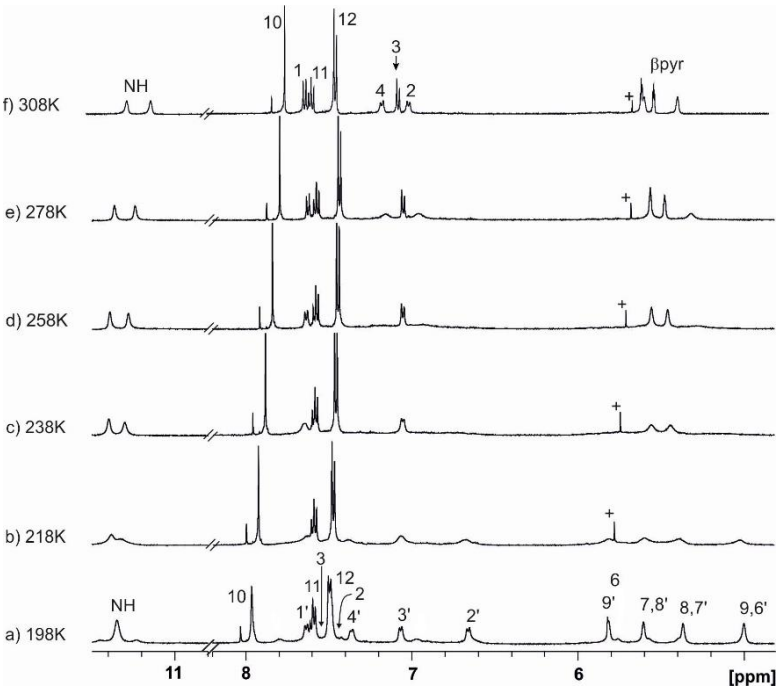

Figure S 27: Selected ^{1}H NMR spectra (400 MHz, d_6-Acetone) of the variable temperature experiments of α,β-**4Au** (4.6 mM) with 1 equiv. of **TBACl.**

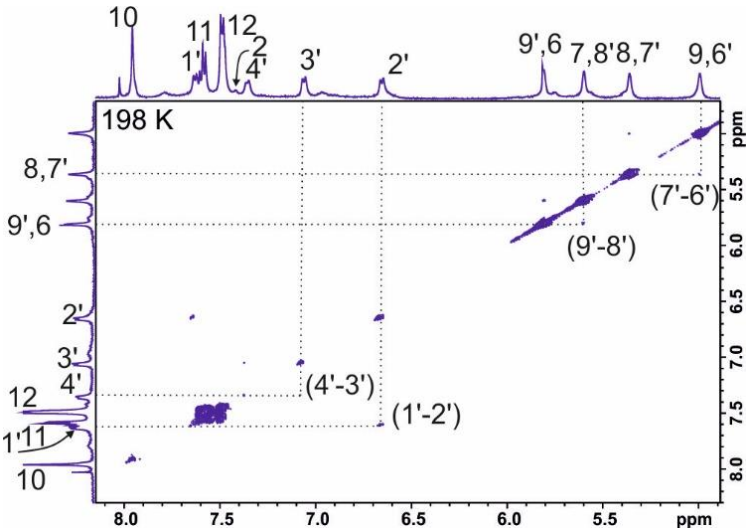

Figure S 28: *COSY experiment of α,β-**4Au** with 1 equiv. of **TBACl** in d_6-Acetone at 198 K with assignments (aromatic region).*

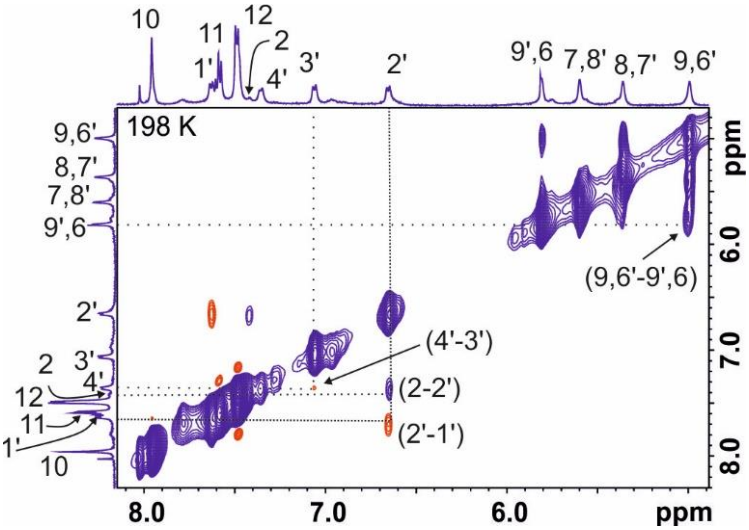

Figure S 29: *ROESY experiment of α,β-**4Au** with 1 equiv. of **TBACl** in d_6-Acetone at 198 K with assignments (aromatic region).*

Attempt to quantify chloride-π interactions using a supra-molecular conformational balance based on a "two wall" mono-alkynyl Au(I) α,β calix[4]pyrrole

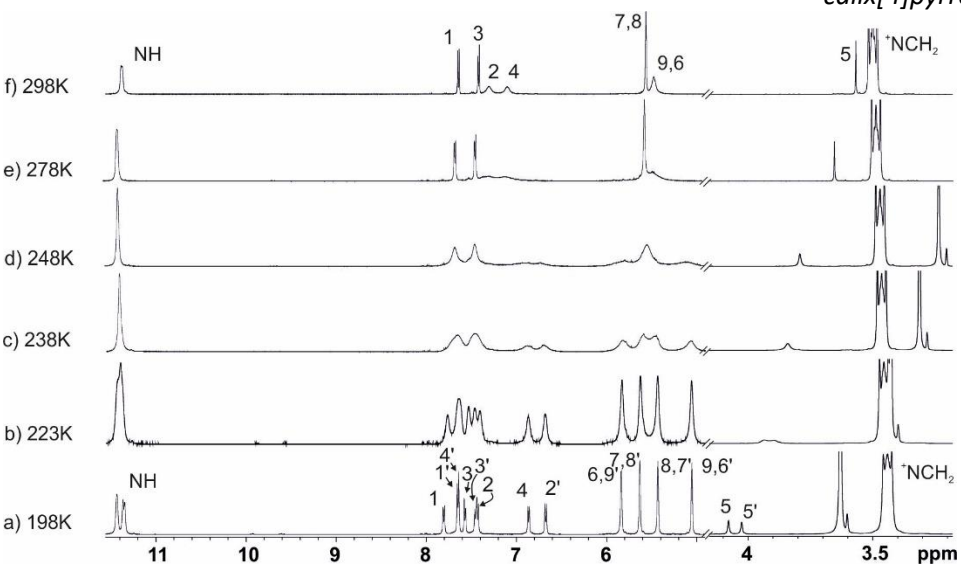

Figure S 30: *Selected ^{1}H NMR spectra (400 MHz, d_6-Acetone) of the variable temperature experiments of α,β-**5**(4.6 mM) with 1 equiv. of **TBACl**.*

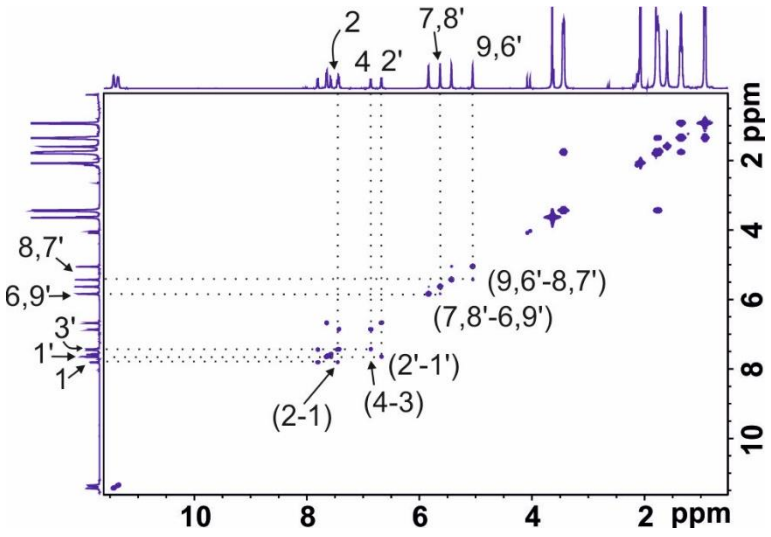

Figure S 31: *COSY experiment of α,β-**5** with 1 equiv. of **TBACl** in d_6-Acetone at 198 K with assignments.*

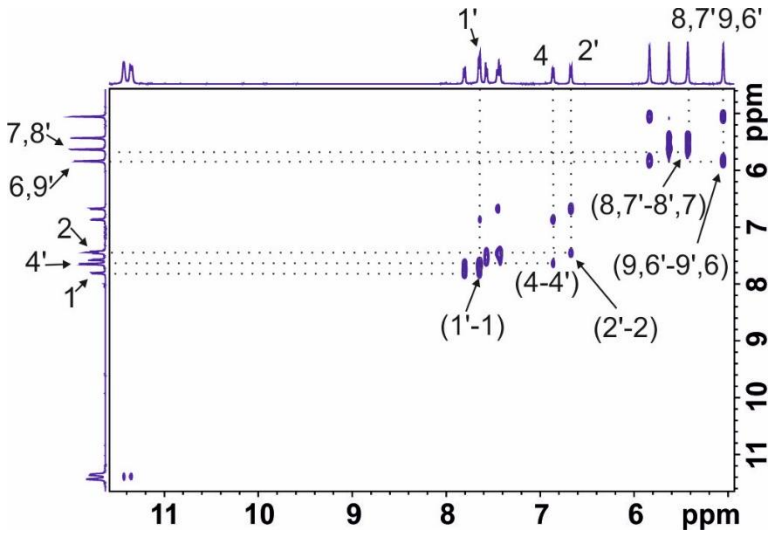

Figure S 32: ROESY *experiment of α,β-***5** *with 1 equiv. of* ***TBACl*** *in d_6-Acetone at 198 K with assignments (aromatic region).*

Dichloromethane

Variable temperature experiment performed on the 1:1 solution of C[4]Ps *α,β*-**5** and α,β-**4Au** with **MTOACl** in deuterated dichloromethane, increasing the temperature from 183K to 298 K.

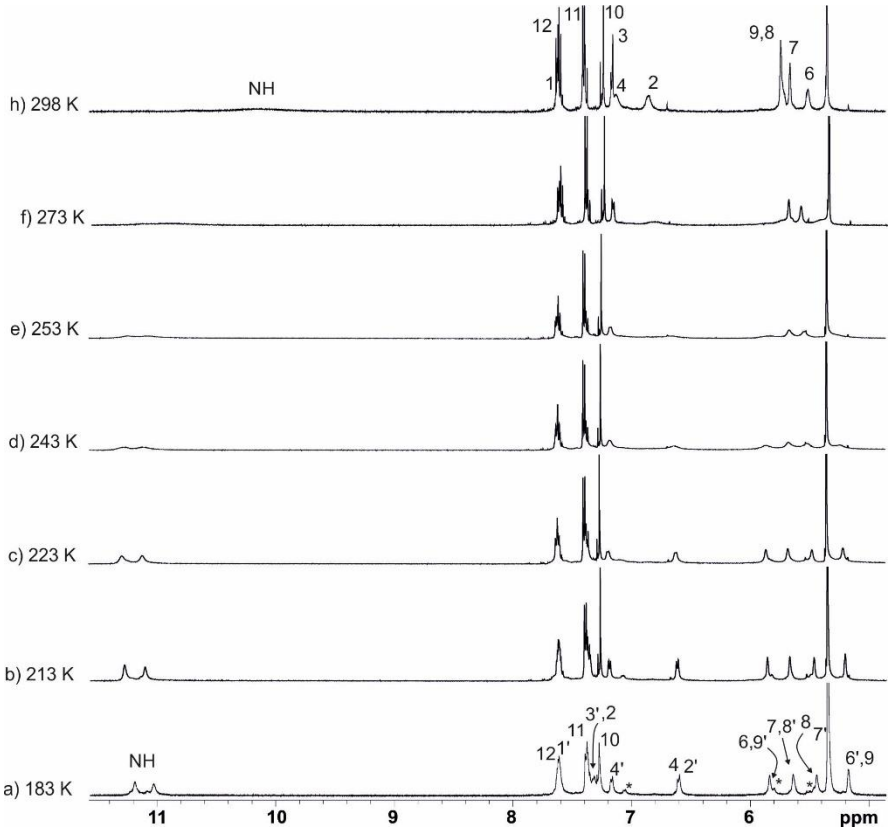

Figure S 33: *Selected ^{1}H NMR spectra (400 MHz, CD_2Cl_2) of the variable temperature experiments of α,β-**4Au** (4.6 mM) with 1 equiv. of **MTOACl.***

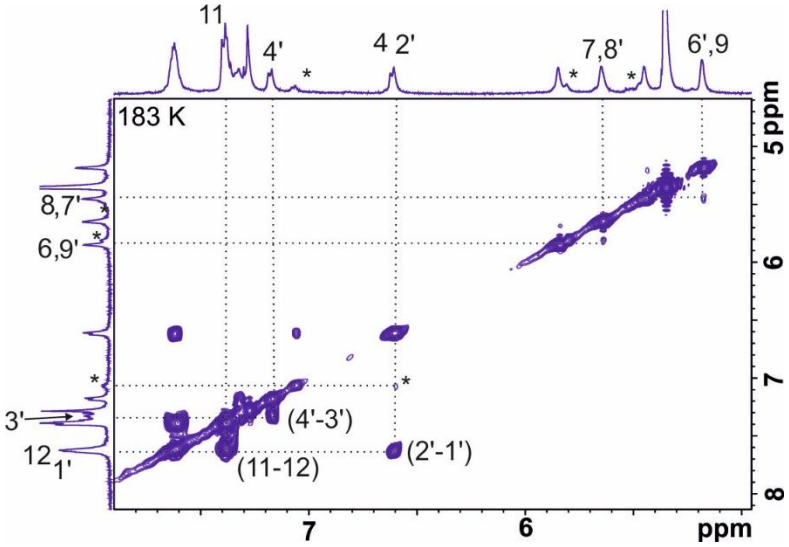

Figure S 34: *COSY experiment of α,β-**4Au** with 1 equiv. of **MTOACl** in CD_2Cl_2 at 183 K with assignments (aromatic region).*

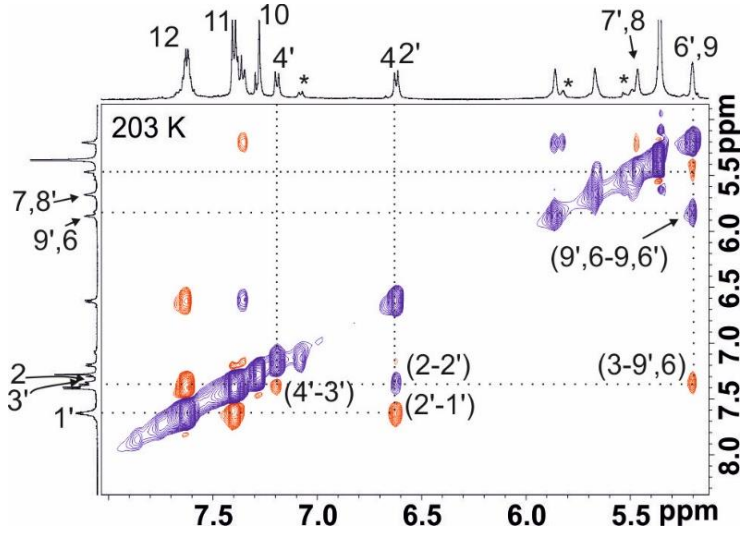

Figure S 35: *ROESY experiment of α,β-**4Au** with 1 equiv. of **MTOACl** in CD_2Cl_2 at 183 K with assignments (aromatic region).*

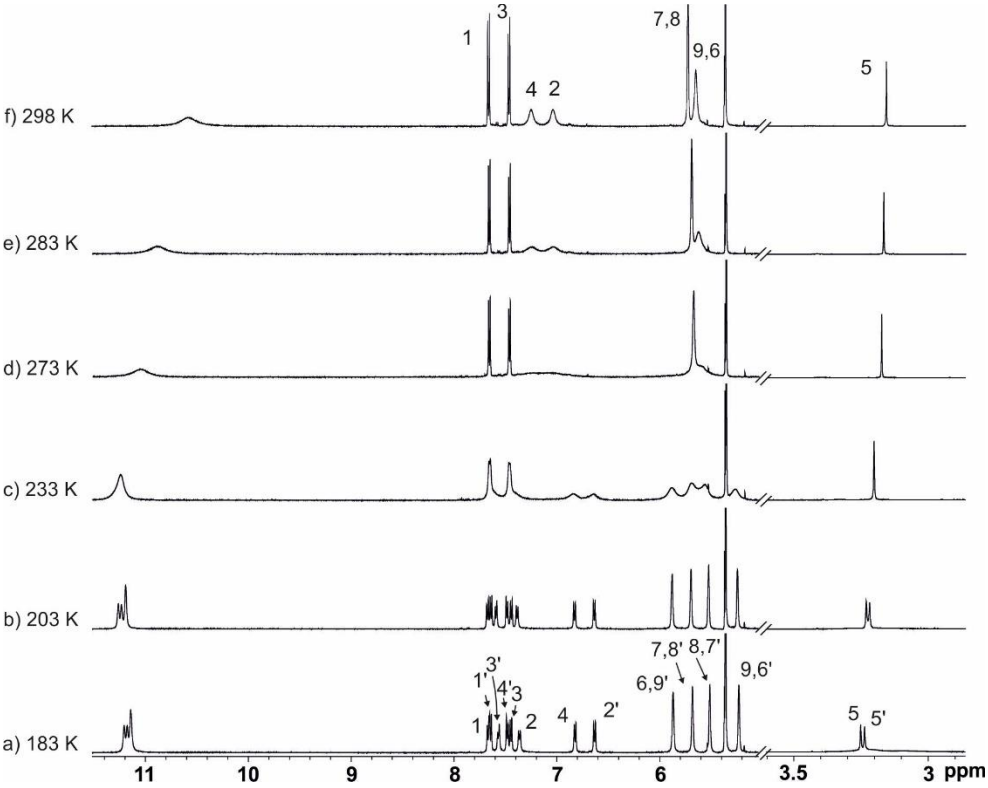

Figure S 36: *Selected ^1H NMR spectra (400 MHz, CD_2Cl_2) of the variable temperature experiments of α,β-**5**(4.6 mM) with 1 equiv. of **MTOACl.***

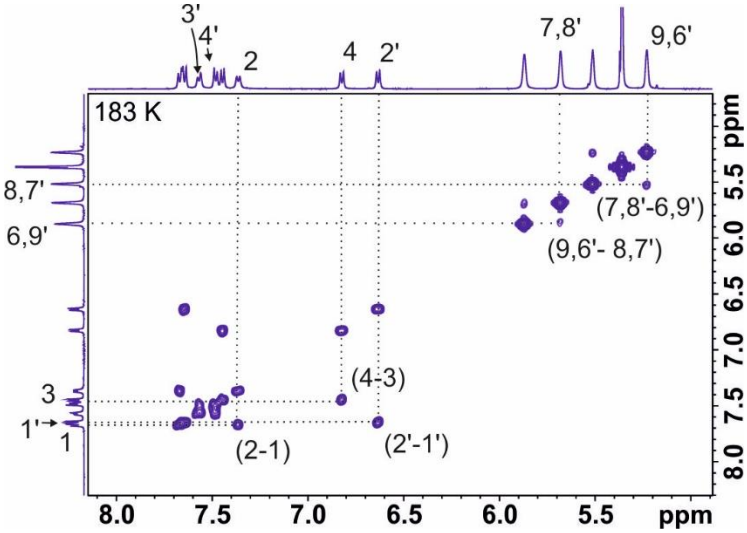

Figure S 37: *COSY experiment of α,β-**5** with 1 equiv. of **MTOACl** in CD_2Cl_2 at 183 K with assignments (aromatic region).*

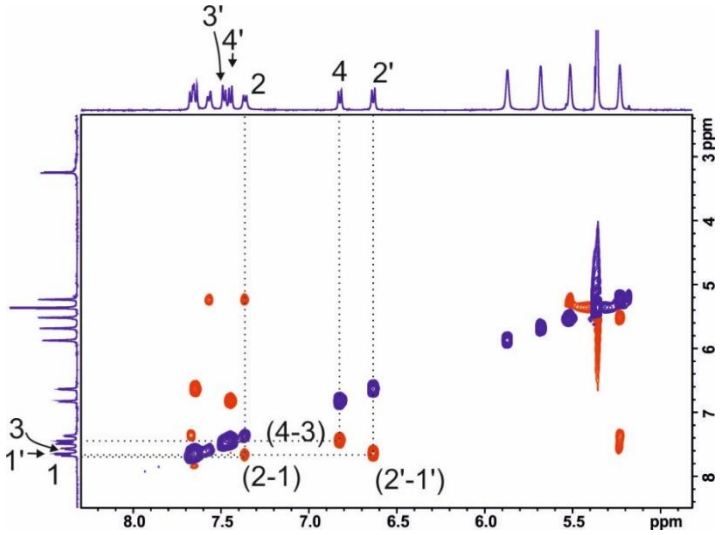

Figure S 38: *ROESY experiment of α,β- **5** with 1 equiv. of **MTOACl** in CD_2Cl_2 at 183 K with assignments (aromatic region).*

4.5.5 ITC experiments

ITC Titration experiments of receptors α,β-5 and α,β-4Au with TBACl

ITC experiments were performed in a MicroCal VP-ITC Micro Calorimeter with the VP Viewer 2000 software. The, titrations were carried out by adding small aliquots (10- 20 μL) of a chloroform solution of the guest into a solution of the host in the same solvent. The concentration of the solution in the syringe was approximately seven to ten times more concentrated than the cell solution. The association constants and the thermodynamic parameters were obtained from the fit of the titration data to the "one set of sites" binding model implemented in the Microcal ITC Data Analysis module. The enthalpy of binding for each injection is plotted against the molar ratio of guest/host in the cell. The continuous line represents the least-squares-fit of the data to a single-site binding model. The reduced heat release of the binding process displayed for some calix[4]pyrrole cavitands limits the titrations at lower concentrations.

Table S 1: *Binding constants (K_a, M^{-1}) and thermodynamic constants (Kcal mol^{-1}) of the binding equilibria of receptors α,β-**5**, and α,β-**4Au** with TBACl salt in acetone solution at 288 K determined by ITC experiments*

Receptor	**K_a ×10^4 Acetone [a]**	**ΔH kcal/mol**	**ΔG kcal/mol**	**-TΔS kcal/mol**
α,β-**5**	4.18 ±0.65	-2.50±0.19	-6.09±0.09	-3.59±0.21
α,β-**4Au**	1.55±0.1	-2.21±0.42	-5.49±0.04	-3.29±0.42

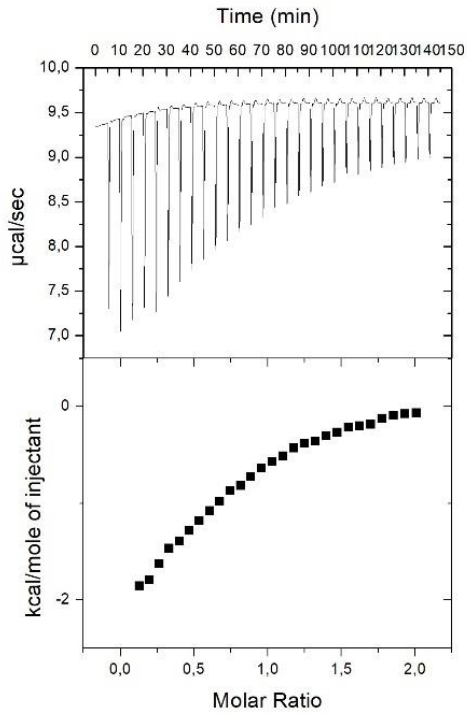

Figure S 39: On top the raw data for the titration of **TBACl**⊂ α,β-**4Au** in chloroform are shown. The titration was performed at 288 K. The binding isotherm of the calorimetric titration is shown at the bottom. [α,β-**4Au**] = 3.0 mM over [**TBACl**] = 0.29 mM. Derived thermodynamic parameters: K_a = (1.5 ± 0.1) × 10^4 M^{-1}; ΔH = -2.21± 0.1 kJ mol^{-1}.

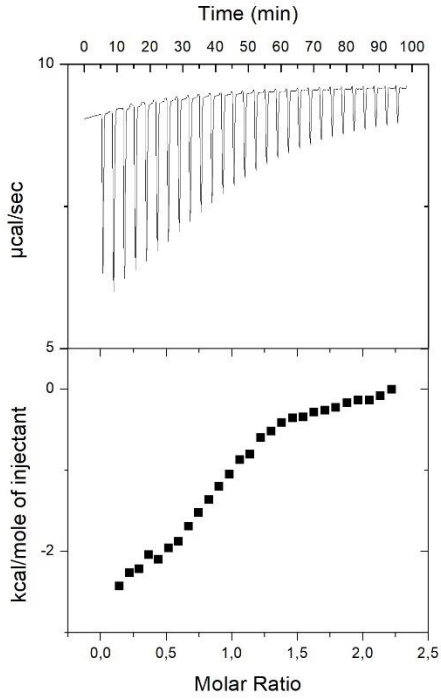

Figure S 40:On top the raw data for the titration of **TBACl**⊂ *α,β*-**5** in chloroform are shown. The titration was performed at 288 K. The binding isotherm of the calorimetric titration is shown at the bottom. [*α,β*-**5**] = 3.0 mM over [**TBACl**] = 0.29 mM. Derived thermodynamic parameters: K_a = (4.18 ± 0.65) × 10^4 M^{-1}; ΔH = -2.50± 0.19 kJ mol^{-1}.

UNIVERSITAT ROVIRA I VIRGILI
ARYL-EXTENDED CALIX[4]PYRROLE RECEPTORS WITH METAL CENTERS: ORGANOMETALLIC RECEPTORS AND METALLO-MACROCYCLES BASED ON COORDINATION BONDS
Andrea Rivoli

Chapter 5

Interchangeability and Disorder in the Solid State Structures of "Two Wall" Calix[4]pyrroles equipped with Iodine and Ethynyl *para*-Substituents

Chapter 5

5.1 Introduction

The investigation of noncovalent interactions (NCIs) is an ongoing endeavor owing to their fundamental role across various disciplines.[1,2,3,4] In recent years, there has been a significant scientific focus on the understanding and utilization of σ-hole interactions.[5,6] This class of NCIs has found successful applications in the fields of supramolecular chemistry[7], crystal engineering[8], catalysis[9], transport[10,11],etc. Among the σ-hole interactions, halogen bonding, involving elements from group 17, is very successful in the field of crystal engineering owing to its high directionality[12]. Iodine derivatives are frequently chosen to construct robust synthons to be used in crystal growth due to the large polarizability of iodine, leading to stronger halogen bonds[13].

More than two decades ago, Philp and co-workers demonstrated the interchangeability of the ethynyl substituent with halogens in the solid state. They

[1] Scheiner, S., *Noncovalent forces*. Springer: 2015; Vol. 19.

[2] de la Roza, A. O.; DiLabio, G. A., *Non-covalent interactions in quantum chemistry and physics: theory and applications*. Elsevier: 2017.

[3] Maharramov, A. M.; Mahmudov, K. T.; Kopylovich, M. N.; Pombeiro, A. J., *Non-covalent interactions in the synthesis and design of new compounds*. John Wiley & Sons: 2016.

[4] P. Hobza, K. Müller-Dethlefs, *Non-Covalent Interactions: Theory, Experiment. Theoretical, Computational Chemistry Series.* RSC, 2009

[5] Alkorta, I.; Elguero, J.; Frontera, A., Not Only Hydrogen Bonds: Other Noncovalent Interactions. *Crystals* **2020,** *10*, 180.

[6] Bauzá, A.; Mooibroek, T. J.; Frontera, A., The Bright Future of Unconventional σ/π-Hole Interactions. *ChemPhysChem* **2015,** *16*, 2496-2517.

[7] Navarro-García, E.; Galmés, B.; Velasco, M. D.; Frontera, A.; Caballero, A., Anion Recognition by Neutral Chalcogen Bonding Receptors: Experimental and Theoretical Investigation. *Chem. Eur. J.* **2020,** *26*, 4644-4644.

[8] Frontera, A.; Bauzá, A., On the Importance of σ–Hole Interactions in Crystal Structures. *Crystals* **2021,** *11*, 1205.

[9] Benz, S.; Poblador-Bahamonde, A. I.; Low-Ders, N.; Matile, S., Catalysis with Pnictogen, Chalcogen, and Halogen Bonds. *Angew. Chem. Int. Ed.* **2018,** *57*, 5408-5412.

[10] Bickerton, L. E.; Docker, A.; Sterling, A. J.; Kuhn, H.; Duarte, F.; Beer, P. D.; Langton, M. J., Highly Active Halogen Bonding and Chalcogen Bonding Chloride Transporters with Non-Protonophoric Activity. *Chem. Eur. J.* **2021,** *27*, 11738-11745.

[11] Humeniuk, H. V.; Gini, A.; Hao, X.; Coelho, F.; Sakai, N.; Matile, S., Pnictogen-Bonding Catalysis and Transport Combined: Polyether Transporters Made In Situ. *JACS Au* **2021,** *1*, 1588-1593.

[12] Cavallo, G.; Metrangolo, P.; Milani, R.; Pilati, T.; Priimagi, A.; Resnati, G.; Terraneo, G., The Halogen Bond. *Chem. Rev.* **2016,** *116*, 2478-2601.

[13] Metrangolo, P.; Resnati, G., Halogen Bonding: Where We Are and Where We Are Going. *Cryst. Growth Des.* **2012,** *12*, 5835-5838.

examined a series of crystal structures involving di- and tri-substituted benzenes to demonstrate this phenomenon[14]. They also showed that the crystal structures of di- and tri-substituted halogen-benzenes were comparable to the crystal structures of di- and tri-substituted ethynylbenzenes. Moreover, they synthesized and characterized the crystal structures of 1,3-dibromo-5-ethynylbenzene and 1-bromo-3,5-diethynylbenzene using single crystal X-ray diffraction data (see **Figure 1**). In both compounds, one molecule with orientational disorder of the arene was present within the asymmetric unit.

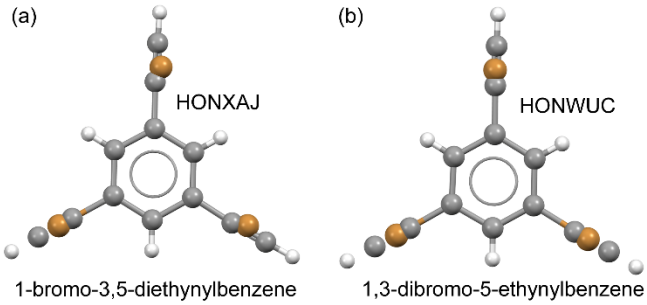

***Figure 1**: X-ray structures of HONXAJ[14] (a) and HONWUC[14] (b), showing orientational disorder.*

Precisely, in the $C_8H_4Br_2$ crystal structure (**Figure 1a**), the molecules adopt three orientations, representing disorder of the bromine and ethynyl substituents among three sites corresponding to the 1, 3 and 5 positions on the benzene ring. The crystal structure of $C_{10}H_5Br$ is isomorphous with the structure of $C_8H_4Br_2$, also with orientational disorder corresponding to the bromine and ethynyl substituents in the 1, 3 and 5 positions on the benzene ring. Interestingly, for both compounds, the positions of the carbon atoms within the benzene ring are indistinguishable across the three molecular orientations.

It is worth mentioning that the study of Philp and co-workers[14] was limited to the interchange of halogen and ethynyl- substituents in bromo-, chloro and fluoro-substituted ethynyl benzenes. An earlier study by Weiss *et al.*[15] reported the analogous interchange of the iodine and ethynyl substituents for 1,4-disusbtitued

[14]M. A. Robinson, J.; M. Kariuki, B.; D. M. Harris, K.; Philp, D., Interchangeability of halogen and ethynyl substituents in the solid state structures of di- and tri-substituted benzenes†. *J. Chem. Soc. Perkin Trans. 2* **1998**, 2459-2470.

[15] Weiss, H.-C.; Boese, R.; Weiss, H.-C.; L. Smith, H.; M. Haley, M., □CH···π versus □CH···Halogen interactions—the crystal structures of the 4-halogenoethynylbenzenes. *Chem. Commun.* **1997**, 2403-2404.

benzene. These studies provided evidence for the interchange of substituents by observing orientational disorder in the X-ray crystal structures of the non-symmetrically substituted derivatives. On the other hand, the symmetrically substituted counterparts did not undergo significant changes in their average solid-state structures as a result of the interchange of ethynyl substituents with halogens. Those pioneering works were fundamental for understanding the opportunities of the interchange of halogens and ethynyl substituents in crystal structures and its possible applications in crystal engineering. Unfortunately, the topic was not further explored and these works have been overlooked for many years.

Our efforts in the preparation of unprecedented "two wall" aryl-extended calix[4]pyrrole receptors, led us to the isolation and structural characterization of the α,β-isomer of 10,20-(4-ethynylphenyl)(4-iodophenyl)-hexamethyl-calix[4]pyrrole **1** (Chapter 3 of the thesis and ***Figure 2***).Compound **1** was synthesized by means of a Sonogashira reaction using the symmetrically-substituted α,β-di-iodo derivative **2** as starting material. In turn, the double Sonogashira reaction of **1** produced the doubly protected synthetic precursor of the α,β-di-ethynyl derivative **3**. In this chapter, we report the X-ray crystal structures of the three α,β-calix[4]pyrroles: **1**, **2** and **3**. We show that the three of them crystallize in the 1,3-alternate conformation as acetonitrile solvates. The calix[4]pyrrole units form infinite one-dimensional (1D) polymeric rods that are stabilized by antiparallel, offset π-stacking interactions between the meso-aryl groups of adjacent units. These interactions are further influenced by the participation of the para-substituents. In addition, the *para*-substituents pointing towards a pyrrole ring of the adjacent calix[4]pyrrole unit are engaged in σ-hole-π interactions (I-) and CH-π interactions (C≡CH), respectively. We also describe the structure of a co-crystal formed by the symmetrically substituted calix[4]pyrroles **2** and **3**. The obtention of the co-crystal **2•3** and the observation of orientational disorder of the substituents in the crystal structure of **1** evidenced the interchangeability of the iodo and ethynyl groups. In addition, the similarity of the unit cell metrics measured for all the X-ray structures reported in this work (**1**, **2**, **3**, and **2•3**) provides additional support to this notion. Unfortunately, the exact nature of the disorder (ordered domains or statistically disorder domains) observed in the average crystal structures of **1** and **2•3** cannot be determined unambiguously from the diffraction data alone The type of disorder observed in crystal structures has significant implications for the interactional complementarities within the crystal structures. In fact, the energies of the different antiparallel offset π-stacked interactions, which are stablished

between the 4-substituted-*meso*-aryl groups of adjacent calix[4]pyrrole units and reinforced with σ-hole-π (I-) and CH-π interactions (C≡CH), should be considered when attempting to rationalize the packing of the molecules in the two crystals. We use DFT calculations to investigate this issue and also to analyse which halogen atom (Br or I) is more similar to the ethynyl group in terms of size and anisotropy of the electron density.

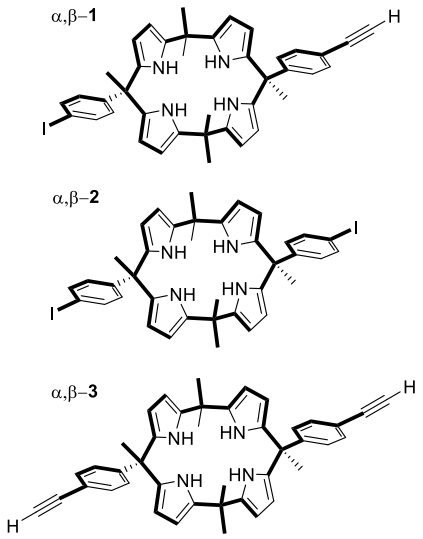

Figure 2: *Line drawing structures of the non-symmetrically substituted **1** and symmetrically substituted, **2** and **3**, α,β-"two wall" calix[4]pyrroles whose X-ray single crystal structures are investigated in this work.*

5.2.1 Preliminary MEP analysis of model compounds

In the first instance, we computed the molecular electrostatic potential (MEP) surfaces of the model compounds **6–14** (see **Scheme 1**) and compared the electronic anisotropy, in terms of energetic and geometric features, of the bromine and iodine atoms in the haloarenes to that of the corresponding ethynyl arenes. Electron-withdrawing (cyano) and donating (dimethylamino) substituents in *para* position were introduced to investigate if the MEP around the halogen and ethynyl substituents behave in the same way. The MEP surfaces of the three unsubstituted arenes are shown in **Figure 3** and the values of all compounds are displayed in **Table 1**, along with the cone angles as a measure of the size of the σ-holes. It is clear, from

the geometric features represented in **Figure 3**, that the iodo substituent exhibits similarities to the ethynyl counterpart in terms of cone angle and σ-hole distances. However, the ethynyl substituent exhibits a larger electron anisotropy with a difference between the MEP minimum and maximum values close to 50 kcal/mol. Moreover, the data of **Table 1** shows that the ethynyl is stronger electron acceptor and π-donor than the bromine or iodine atoms.

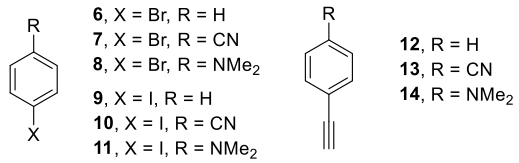

Scheme 1: *Line drawing structures of the model compounds 6-14 studied in this work.*

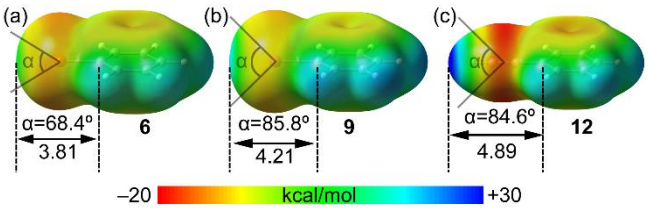

Figure 3*: MEP surfaces of compounds **6** (a), **9** (b) and **12** (c). The σ-hole cone angles (α) are indicated. The distance between the aromatic C_{ipso}-atom and the σ-hole maximum is also indicated in Å. The MEP values at the σ-hole are listed in Table 1.*

In Figure 3, the σ-hole cone angles are represented for compounds **6**, **9** and **12** and their associated values (see alsoTable 1 for the rest of compounds). The cone angle value is useful as a measure of the extension of the σ-hole and to know in each case the maximum deviation from linearity allowed for a given contact to be considered as a halogen bond (or H-bond in case of ethynyl). For the ethynyl, the angle is measured from the middle of the C≡C bond.

The effects exerted by the electron-withdrawing (EW) and donating (ED) groups on the MEP values of the *para*-substituents (Cl, I and C≡CH) are comparable. That is, for the EW cyano group, the maximum positive MEP values of the substituents increase around 8-9 kcal/mol, while their negative minimum decrease to a similar extent in comparison to those of the mono-substituted benzene (**6**, **9** and **12**; R = H). The opposite effect is observed for the ED dimethylamino group. Notably, the induced changes in the MEP values are smaller for the ED dimethylamino group (5-6

kcal/mol). The *para*-substituents also influence the size of the σ-hole (see cone angles in **Table 1**), generating an increase in the cone angle for the EW cyano group and a decrease for the ED dimethylamino group. It is noteworthy that the cone angles for the iodo-arenes (**9**, **10** and **11**) are very similar to those of the ethynyl-arenes counterparts (**12**, **13** and **14**). Based on this preliminary study, which considers both energetic (MEP values) and geometric features, it is suggested that iodine is likely to be more interchangeable with ethynyl than bromine in general. However, there are exceptions in X-ray structures where the crystal packing is predominantly influenced by interactions with ethynyl as a π-electron donor. In such cases, bromine would be a more suitable substitute than iodine to assume the π-donor role of ethynyl.

Table 1: *Cone angle of the σ-hole (α, °) and MEP values at the σ-hole and the negative belt for compounds **6**-**14** at the PBE0-D3/def2-TZVP.*

Compound	α (angle)	σ-hole	belt
6; X= Br, R=H	68.4	+9.4	–12.1
7; X= Br, R=CN	112.2	+18.6	–3.1
8; X= Br, R=N(Me)$_2$	43.6	+3.7	–17.6
9; X= I, R=H	85.8	+16.9	–10.7
10; X= I, R=CN	129.4	+26.2	–2.6
11; X= I, R=N(Me)$_2$	58.2	+11.3	–16.3
12; -C≡CH, R=H	84.6	+29.5	–18.7
13; -C≡CH, R=CN	123.6	+37.4	–8.8
14; -C≡CH, R=N(Me)$_2$	71.2	+23.7	–25.0

Experimental confirmation of the almost equivalent size and similar electronic features of iodine and ethynyl substituents were obtained from the comparison of the X-ray structures of 1-bromo-4-ethynylbenzene (NECNEO) and 1-iodo-4-ethynylbenzene (NECNIS)[15]. In the case of NECNEO, the presence of head-tail disorder between the bromo and ethynyl substituents (as shown in **Figure 4b**) at the 1 and 4 positions of the phenyl ring affected the positions of its carbon atoms. These

carbon atom positions were found to be different in the two orientations of the molecule. That is, in the asymmetric unit of the crystal, one molecule is translated along the bromine-ethynyl direction with respect to the other. In sharp contrast, the positions of the phenyl carbon atoms are equivalent for the two molecular orientations in NECNIS (iodine). This agrees well with the fact that the size of the ethynyl is more comparable to iodine than bromine.

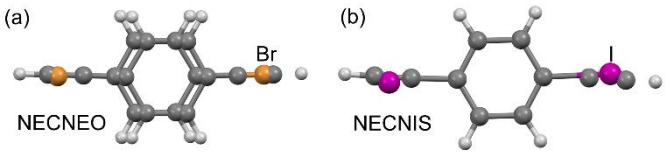

Figure 4: *Comparison of the orientational disorder in the X-ray solid state structures of 1-bromo-4-ethynylbenzene NECNEO (a) 1-iodo-4-ethynylbenzene and NECNIS (b)[15].*

5.2.2 Synthesis

Meso-hexamethyl-α10,β20-(4-ethynylphenyl)(4-iodophenyl)-calix[4]pyrrole **1** was prepared in two synthetic steps from the corresponding α,β-bis(4-iodophenyl-calix[4]pyrrole **2** (**Scheme 2**). The statistical Sonogashira reaction of **2** with 2-methyl-3-butyn-2-ol (5 equiv.), at r.t in dry toluene and using triethylamine amine as base, allowed the isolation of the mono-substituted iodo-ethynyl protected calix[4]pyrrole **4** and the disubstituted derivative **5** in 42% and 30% yield, respectively, after column chromatography purification of the reaction crude. The subsequent treatment of **4** with sodium hydroxide in refluxing toluene for 12 h afforded the mono-iodo-mono-ethynyl calix[4]pyrrole **1** in 73% yield after purification of the reaction crude using column chromatography. Likewise, the disubstituted derivative **5** was treated under identical conditions producing the bis-(4-ethynylphel)calix[4]pyrrole **3** in 75% following column chromatography purification. In turn, α,β-bis(4-iodophenyl-calix[4]pyrrole **2** was isolated in 8% yield from the column chromatography purification of the reaction crude obtained in the

acid-mediated cyclocondensation of the 4-iodo-phenyl,methyl-meso-substituted dipyrromethane using acetone as solvent[16].

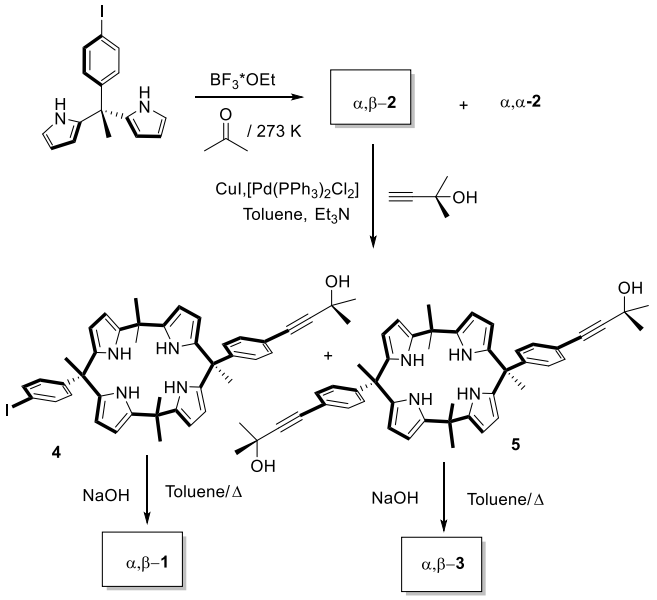

***Scheme 2**: Synthetic scheme for the preparation of the α,β-"two wall" calix[4]pyrroles whose X-ray single crystal structures are investigated in this work: α,β-1, α,β-2 and α,β-3 (see Figure 2 for their structures).*

5.2.3 Description of the crystal structure

Single crystal grew from slow evaporation of separate acetonitrile solutions of the calix[4]pyrroles **1**, **2** and **3**. In addition, suitable crystals for X-ray analysis were also obtained from an acetonitrile solution containing an equimolar mixture of the symmetrically substituted calix[4]pyrroles **2** and **3**.

The asymmetric unit of the P1 space group structure of **1** contains one molecule in 1,3-alternate conformation. The molecule features orientational and conformational disorder between two potions with 65:35 relative occupancies (see **Figure 5**). Because the 1,3-alternate conformation of **1** is intrinsically chiral[17] this

[16] Szumna, A., Inherently chiral concave molecules—from synthesis to applications. *Chem. Soc. Rev.* **2010,** *39*, 4274-4285.

[17] Valderrey, V.; Escudero-Adán, E. C.; Ballester, P., Polyatomic Anion Assistance in the Assembly of [2]Pseudorotaxanes. *J. Am. Chem. Soc.* **2012,** *134*, 10733-10736.

disorder implies the presence of two conformational enantiomers in the packing of the lattice. The two enantiomers display a head-to-tail disorder between their iodo and ethynyl substituents (I-C[4]P-C≡CH and HC≡C-C[4]P-I) and have identical positions of their carbon and nitrogen atoms. The packing of the lattice shows that 1 forms infinite 1D assemblies involving the ethynyl/iodine groups, as depicted in **Figure 5**.

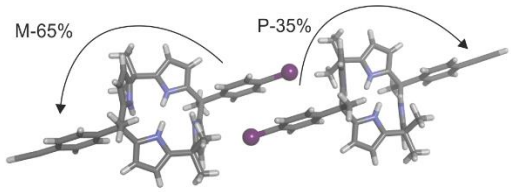

Figure 5: *Stick representation of two adjacent molecules (enantiomers) of **1** involved in an antiparallel π-staking and double I σ-hole-π interaction and displaying the two orientations ((M)-HC≡C-C[4]P-I•(P)-I-C[4]P-C≡CH) that may be found in a domain of the crystal. The absolute M/P configuration is assigned based on the screw-sense defined by the superimposition of the iodo over the alkynyl passing through the bisecting axial methyl group facing the viewer. Acetonitrile molecules were removed for clarity.*

The reported crystal structure determination provides an average structure for compound **1**. This average takes into account all the unit cells within the crystals. As a result, the precise nature of the molecular disorder (enantiomers) cannot be definitively determined. For an average crystal structure showing head-to-tail disorder of one molecule between two different orientations (i.e. **1**, I-C[4]P-C≡CH and HC≡C-C[4]P-I) having distinct occupancies (i.e. 65% and 35%) it is not possible to conclude whether the crystal structure contains 65% of *ordered domains* comprising one orientation i.e. I-C[4]P-C≡CH and 35% *ordered domains* with the other orientation (HC≡C-C[4]P-I) or that in each region of the crystals the molecule experiences a *statistical disorder* with a possibility of 65% of being in one orientation and 35% in the opposite one. In a disorder with *ordered domains*, the intermolecular interactions remain identical for all neighboring molecules. Furthermore, the local structure within the domains should be identical to that of a fully ordered crystal. On the contrary, in domains exhibiting statistical disorder, multiple orientations of the molecule coexist and depending on the orientation of one molecule and the set of orientations of its neighbors the intermolecular interactions may vary. For example, the second molecules in the array of **Figure 6b** displays a different orientation and experiences dissimilar interactions with its neighbors that the first or third ones. *Statistical disorder, a.k.a.* disorder at the molecular level, may be ruled out if some molecular interactions that, on a statistical basis, are predicted to exist

between neighbors are highly unfavorable. In short, in a crystal of **1** showing *statistical disorder*, three types of intermolecular antiparallel offset π-staking and their corresponding σ-hole-π interactions exist in the 1D rods: HC≡C-C[4]P-I•HC≡C-C[4]P-I, I-C[4]P-C≡CH•HC≡C-C[4]P-I and HC≡C-C[4]P-I•I-C[4]P-C≡CH (**Figure 6b**) . On the contrary, for a crystal of **1** showing disorder through *ordered domains* only one type of intermolecular antiparallel offset π-staking and their corresponding σ-hole-π interactions will be present: HC≡C-C[4]P-I•HC≡C-C[4]P-I (**Figure 6a**).

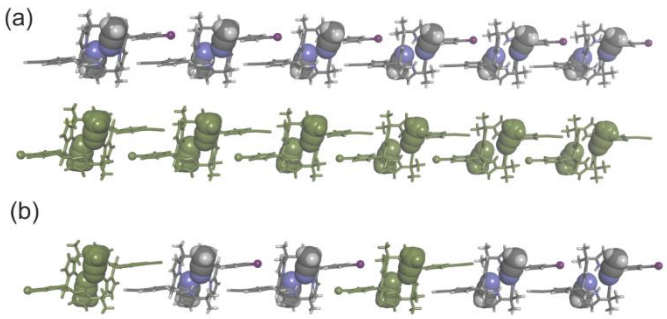

Figure 6: (*a)* Disorder in ordered domains: *example of two ordered sections domains of the crystal structure of **1** showing the unidirectional orientation of the molecules. First row shows the packing of the M-isomer with 65% occupancy and the second corresponds to the P-isomer with 35% occupancy. Please, note that in both cases the offset π-staked interactions exclusively involve different* meso*-4-phenyl substituted groups 5 × HC≡C-C[4]P-I•HC≡C-C[4]P-I. (b)* Statistical disorder in domains*: example of a statistically ordered lineal domain of the crystal of **1** containing the two orientations. Each enantiomer is unidirectionally oriented as in (a), however, different and identical* meso*-4-phenyl substituted groups are involved in the offset π-staked interactions driving the packing: 2 × HC≡C-C[4]P-I•HC≡C-C[4]P-I, 2 × I-C[4]P-C≡CH•HC≡C-C[4]P-I and 1 × HC≡C-C[4]P-I•I-C[4]P-C≡CH The depicted statistical disorder corresponds to 67:33 occupancy.*

The crystal structures of symmetrically substituted calix[4]pyrroles **2** and **3** were determined using single X-ray diffraction data. In both cases, the asymmetric unit contains half of the calix[4]pyrrole molecule along with one acetonitrile molecule that is hydrogen bonded. The corresponding other half of the calix[4]pyrrole molecule was generated by the inversion center of the *P*-1 space group of the crystal. The packing of the crystals of **2** and **3** shows 1D rods formed by symmetrically substituted calix[4]pyrroles experiencing intermolecular antiparallel offset π-staking and their corresponding σ-hole-π interactions between identical adjacent units. The metrics and volumes of the two unit cells are highly similar, and the overall packing arrangements of the molecules exhibit a remarkable similarity. Moreover, the crystal structure of the di-iodo calix[4]pyrrole **2** is isomorphous with that of the non-symmetrically substituted counterpart **1**.

To our delight, an acetonitrile solution containing an equimolar mixture of the symmetrically substituted calix[4]pyrroles **2** and **3** also produced single crystals suitable for X-ray diffraction analysis. The solution of the diffracted data in the *P*-1 space group revealed the formation of a co-crystal supporting the interchangeability of the iodo- and ethynyl substituents (**Figure 7**). The asymmetric unit showed half of each calix[4]pyrrole molecules with an occupancy disorder of 63:37%, being the di-alkynyl derivative **3** present in a larger extent that the putatively expected 50:50 ratio. Remarkably, the positions of all carbon and nitrogen atoms of the bi-aryl-calix[4]pyrrole scaffolds of **2** and **3** and the corresponding hydrogen bonded acetonitrile molecules are identical with respect to one another. The structure of the co-crystal **2•3** is isomorphous with those of the symmetrically substituted di-iodo **2** and non-symmetrically-substituted derivative **1** (see **Table S 1**).

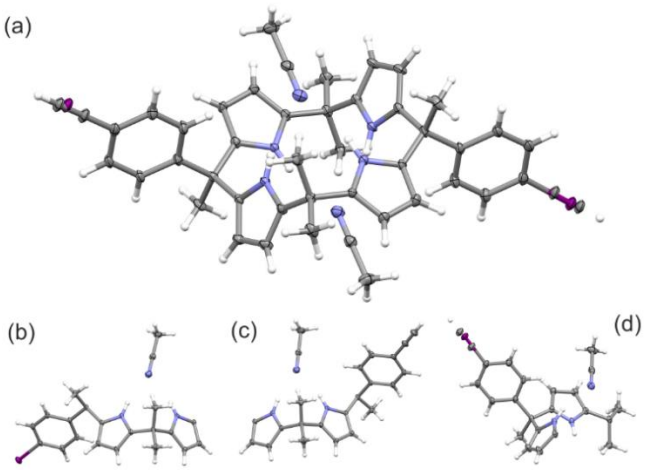

Figure 7: *Asymmetric units of the X-ray structures of: (a)* ***1*** *; (b)* ***2****; (c)* ***3*** *and (d) co-crystal* ***2•3*** *reported in this work displaying the modelled disorder of the atoms in the para-substituents.*

Notably, the observed disorder in the **2•3** co-crystal raised the issue about its possible nature owing to the average characteristics of the reported X-ray structure: disorder in *ordered domains* or *statistical disorder* in domains (*vide supra*). The **2•3** co-crystal packing also showed 1D rods featuring antiparallel offset π-stacking interactions between adjacent *meso*-4-substituted aryl groups. To us, the existence of a 67:33 occupancy of the two symmetrically substituted calix[4]pyrroles, **2** and **3**, was surprising. Even more, when it is almost coincident with the orientational disorder observed for the single crystal of the non-symmetrically substituted counterpart **1**. Owing to the symmetrical substitution of **2** and **3**, the packing of the

2•3 co-crystal assuming *disordered domains* will necessary imply the existence of antiparallel offset π-stacking interactions exclusively involving identical groups: H-C≡C-C[4]P-C≡CH•HC≡C-C[4]P-C≡CH and I-C[4]P-I•I-C[4]P-I, one interaction in each domain. In contrast, the 67:33 *statistical disorder* of the molecules in the domains of the **2•3** co-crystal will avoid having interactions between identical iodo-substituted groups and involve only offset π-staking interactions between identical ethynyl-substituted *meso*-phenyls (I-C[4]P-C≡CH•HC≡C-C[4]P-I) and between different iodo- and ethynyl counterparts (HC≡C-C[4]P-I•HC≡C-C[4]P-I) (**Figure 8**, **Figure 9**).

Figure 8: *Example of a statistically disordered lineal domain of the co-crystal of **2•3** showing the existence of offset π-staking interactions between differently substituted* meso*-4-phenyl groups and for identical alkynyl substituent: 3 × HC≡C-C[4]P-I•HC≡C-C[4]P-I, 2 × I-C[4]P-C≡CH•HC≡C-C[4]P-I. Please, note that offset π-staking interactions between identical iodo substituent are lacking 0 HC≡C-C[4]P-I•I-C[4]P-C≡CH. The depicted statistical disorder corresponds to 66:33 occupancy.*

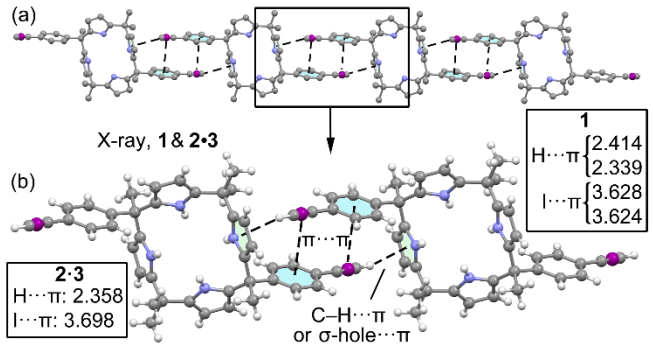

Figure 9: *(a) Partial view of the X-ray packing observed in the solid-state domains of compounds **1** and **2•3**, showing 1D supramolecular rods and not considering a specific disorder type. H-atoms omitted for clarity. (b) Detail of a dimer extracted from the infinite chain. Distances in Å*

In the following section, we assess the energies associated with three distinct types of offset π-stacking interactions observed within the domains of the crystals. Our objective is to comprehend the influence of the iodine and ethynyl groups in these π-stacking interactions, aiming to provide a computational perspective and rationalize the experimental observations. Through this analysis, we aim to shed

light on the plausible disorder present in the crystal structures of compound **1** and the co-crystal **2•3**.

5.2.4 DFT study of compounds 1 and 2•3

First, the lattice energies of compound **1** and co-crystal **2•3** were computed by creating a supercell that includes four calix[4]pyrrole molecules and eight acetonitrile solvent molecules by means of the Dmol3 program[18] as implemented in Materials Studio[19]. These calculations were performed using periodic boundary conditions, the PBE0[20] functional and the DNP basis set,[18] that is a compromise between the size of the system (~390 atoms) and the accuracy of the results. The numerical basis sets like DNP (double zeta plus polarization) are more efficient than Gaussian basis sets and present negligible basis set superposition error[21]. The lattice energies are included in **Table 2:** Lattice energies (LE, kcal/mol) obtained for ordered domains of the two orientations of **1** and the two components of the co-crystal **2•3**, using two different methods to evaluate dispersion and without dispersion correction.**Table 2**, and were computed without and with the dispersion correction (using both Grimme's[22] and Tkatchenko-Scheffler[23] methodologies to estimate the dispersion correction). The examination of the energies suggests that the dispersion correction provides an overestimation of the lattice energies, since such large values (see **Table 2**) are typical of ionic salts. In fact, the utilization of M06-L functional[24]

[18] Delley, B., From molecules to solids with the DMol 3 approach. *J. Chem. Phys.* **2000,** *113*, 7756-7764.
[19] BIOVIA Materials Studio. Available from https://www.3ds.com/
[20] Adamo, C.; Barone, V., Toward reliable density functional methods without adjustable parameters: The PBE0 model. *J. Chem. Phys.* **1999,** *110*, 6158-6170.
[21] Inada, Y.; Orita, H., Efficiency of numerical basis sets for predicting the binding energies of hydrogen bonded complexes: Evidence of small basis set superposition error compared to Gaussian basis sets. *J. Comput. Chem.* **2008,** *29*, 225-232.
[22] Grimme, S., Semiempirical GGA-type density functional constructed with a long-range dispersion correction. *J. Comput. Chem.* **2006,** *27*, 1787-1799.
[23] Tkatchenko, A.; Scheffler, M., Accurate Molecular Van Der Waals Interactions from Ground-State Electron Density and Free-Atom Reference Data. *Phys. Rev. Lett.* **2009,** *102*, 073005.
[24] Zhao, Y.; Truhlar, D. G., The M06 suite of density functionals for main group thermochemistry, thermochemical kinetics, noncovalent interactions, excited states, and transition elements: two new functionals and systematic testing of four M06-class functionals and 12 other functionals. *Theor. Chem. Acc.* **2008,** *120*, 215-241.

reduces significantly the LE values compared to PBE0-D values. In any case, the trends are in most cases similar.

Not surprisingly, for compound **1** the lattice energies for the domains of its two orientations, assuming disorder in *ordered domains*, are similar. The orientation of **1** having the larger occupancy produced a slightly higher lattice energy (1.1 kcal/mol) and within the accuracy of the method. The lattice energy difference between the two orientations is even smaller if the dispersion correction is used (≤ 0.7 kcal/mol), see **Table 2**. This small energy difference is due to the dissimilar positions refined for the ethynyl carbon atoms in the two orientations of **1**.

In case of the co-crystal **2•3**, due to symmetry restrictions (*P*-1 symmetry of the crystal), the lattice energies were exclusively computed considering 100% di-iodo or 100% of di-ethynyl calix[4]pyrroles in *ordered domains* of the X-ray structure. It is interesting to highlight that the ordered domain considering only iodo-substituted calix[4]pyrrole **2** exhibited a lattice energy that is slightly less favourable than those of the non-symmetrically substituted analogue **1**. In contrast, the ordered domain of the co-crystal involving exclusively the symmetrically substituted di-ethynyl **3** has the more favourable lattice energy (with and without the dispersion correction). These results indicate that antiparallel offset π-stacking interactions involving two ethynyl substituent perform better (form stronger interactions) than those between two iodo-substituted phenyl groups or one iodo-phenyl and one ethynyl-phenyl group. This finding is also in line with the aforementioned MEP surface analysis (see **Table 1**) evidencing the larger ability of ethynyl substituents to act as both electron donor (via the π-system) and acceptor (via the σ-hole) group.

Table 2: *Lattice energies (LE, kcal/mol) obtained for ordered domains of the two orientations of **1** and the two components of the co-crystal **2•3**, using two different methods to evaluate dispersion and without dispersion correction.*

Compound	LE(TS)	LE (Grimme)	LE (No Disp)
1 (major orientation)	-390.2	-323.9	-81.6
1 (minor orientation)	-389.5	-323.5	-80.7
2•3 (diiodo domain)	-374.8	-319.9	-78.9
2•3 (diethynyl domain)	-396.0	-325.5	-102.4

To further support the stronger electron acceptor ability of the terminal ethynyl CH (CH···π interaction) compared to the pole of the iodide atom (σ-hole···π interaction), we computed the MEP surface of the non-symmetrically substituted C[4]P-**1**. Figure 10 shows that the MEP value at the H-atom of the ethynyl is more positive (+24.0 kcal/mol) than the σ-hole at the iodine atom (+15.1 kcal/mol). It also shows that the MEP is negative at the π-system of the pyrrole rings (around –26 kcal/mol), thus disclosing the strong π-basicity of these heterocyclic rings. The high MEP value calculated for the pyrrole rings is likely due to the presence of H-bonded acetonitrile molecules donating electron density. This was corroborated by computing the MEP surface of **1** removing the acetonitrile molecules. In this case, we observed a diminution of the MEP value to –19.5 kcal/mol at the center of the pyrrole ring. Therefore, the presence of the solvent molecules strengthens the CH···π and σ-hole···π interactions.

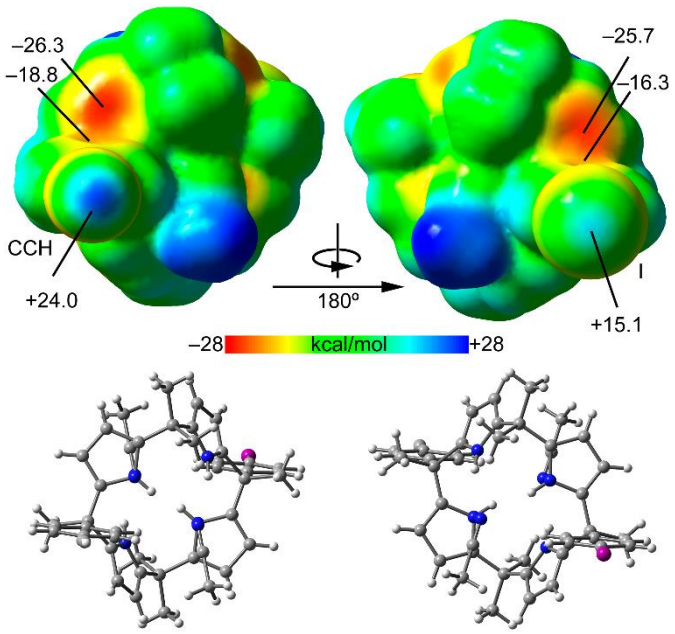

Figure 10: *Two opposite views of the MEP surface of **1** at the PBE0/def2-TZVP level of theory. The MEP values at selected points are indicated. The geometries of the calix[4]pyrrole in the same orientation used to build up the surfaces are given in the low part of the figure.*

It is noteworthy to mention that the MEP values over the center of the phenyl rings, which are *para*-substituted with ethynyl and iodo groups, exhibit significant negative values. (–18.8 and –16.3 kcal/mol, respectively, see **Figure 10**). Consequently, it would be expected that the interaction between the aromatic rings and either the π-system of ethynyl or the negative electron belt of iodine would be repulsive based solely on electrostatic forces.

Next, the energetics of three different orientational dimers of C4P-**1** were computed along with the quantum theory of "atoms-in-molecules" (QTAIM) analysis of critical points (CPs) and bond paths. The obtained results were summarized in **Figure 11**, revealing an identical distribution of CPs and bond paths interconnecting the interacting monomers in the different dimers. This result strongly supports the existence of interactional complementarity between the *meso*-phenyls *para*-substituent either with iodine or ethynyl groups in adjacent C[4]Ps. Three intermolecular bond CPs and bond paths connect the iodine/ethynyl groups of one C[4]P to the other one. One CP connects a C-atom of the phenyl ring to the substituent (either I or C). Another one connects an H-atom of the methyl group to the substituent (either I or C) and finally a third one connects a C-atom of the pyrrole ring to the *para*-substituent (either I or H).

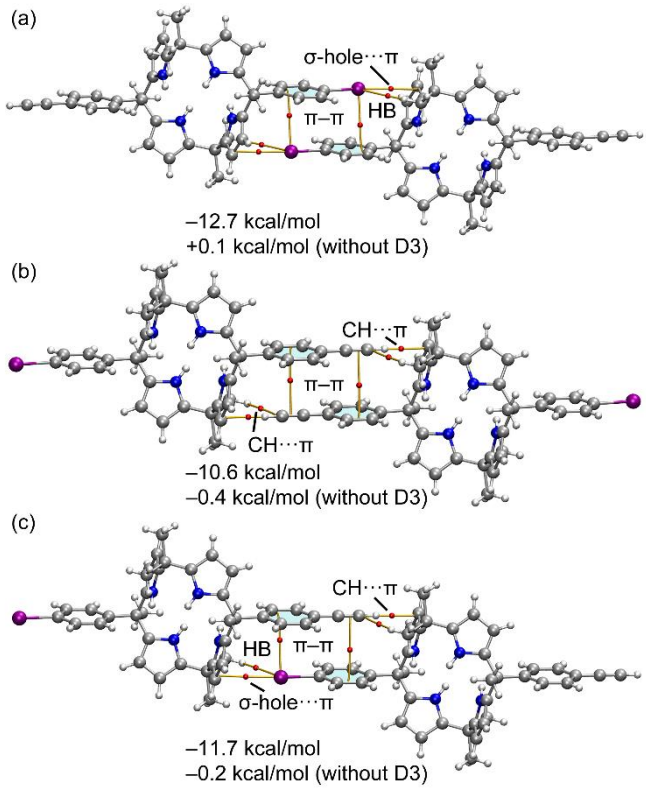

Figure 11: *Dimerization energies of the three possible dimers of compound **1**. Distribution of intermolecular bond critical points (small red spheres) and bond paths (orange lines) for each dimer is also represented.*

Regarding the calculated interaction/dimerization energies, all dimers present similar values, ranging from –10.6 to –12.7 kcal/mol. The less stable dimer is characterized by an antiparallel π-stacking interaction between the meso-phenyls, both of which are para-substituted with identical ethynyl groups (**Figure 11b**), while the most stable one features phenyls that are *para*-substituted with two iodo-atoms. It is interesting to compare this trend of energies with those obtained without dispersion, which are also indicated in **Figure 11**. The energies without D3 correction are very small, due to a compensating effect between the electrostatic attraction of the CH···π or σ-hole···π interaction and the electrostatic repulsion between the negative belts and the aromatic rings. Without D3 correction, the most stable dimer turned out to be the one involving the *para*-ethynyl substituents. The energies of the dimers without D3 correction are in agreement with the trend of computed energies for *ordered domains* in the lattice of the **2•3** co-crystal and the

performed MEP analysis. This finding might also serve to explain the major occupancy of the symmetrically *para*-substituted C[4]P **3** (65%) and favor the existence of *statistical disorder* in the domains of the **2•3** crystal structure. On the other hand, the results of the theoretical calculations suggest the presence of a preferential disorder in compound **1** within ordered domains, which effectively prevents the occurrence of antiparallel π-stacking interactions among meso-phenyls substituted with iodo groups. The energetic analysis further highlights the significant contribution of dispersion forces in stabilizing the dimers.

5.3 Conclusions

The experimental results reported in this chapter demonstrate for the first time the interchangeability of iodine and ethynyl substituents in the solid state by using a cocrystal of two symmetric "two wall" aryl-extended calix[4]pyrroles. Moreover, by using a non-symmetrically substituted "two wall" aryl-extended calix[4]pyrrole, orientational disorder is observed, as previously observed in 1-iodo-4-ethynylbenzene. DFT calculations demonstrate that iodine is more similar to ethynyl in terms of electron acceptor (via de σ-hole) and bromine is more similar to ethynyl in terms of electron donor (via the negative belt). The computed lattice energies confirm the small difference between both orientations of the ethynyl and iodine groups in **1** and reveal a larger stability for the ordered domain of the symmetric di-ethynyl derivative in **2•3**. This result is also substantiated by the DFT energy values of the dimers without D3 dispersion. Finally, this study is expected to inspire researchers working in different disciplines (supramolecular, crystal engineering, materials, theoretical chemistry) to further explore this interesting topic of interchanging halogens and ethynes.

5.4 Experimental section

5.4.1 General methods and instrumentation

All reagents were obtained from commercial suppliers and used without further purification unless otherwise stated. Dry solvents were taken from a solvent system MB SPS 800. Et_3N was dried, distilled and degassed by three freeze-pump-thaw cycles before used in the cross-coupling reactions. Flash column chromatography was performed with silica gel (technical grade, pore size 60 Å, 230-400 mesh particle size). Automatic column chromatography purifications were done with a Combi-flash® RF+. Routine ^{1}H NMR and $^{13}C(^{1}H)$ NMR spectra were recorded on a Bruker

Avance 300 (300 MHz for ^{1}HNMR and 75 MHz for ^{13}C NMR), Bruker Avance 400 (400 MHz for ^{1}H NMR and 100 MHz for ^{13}C NMR), Bruker Avance 500 (500 MHz for ^{1}H NMR and 125 MHz for ^{13}C NMR), or Bruker Avance 500 with cryoprobe (500 MHz for ^{1}H NMR and 125 MHz for ^{13}C NMR). Deuterated solvents used are indicated in the characterization and chemical shifts are given in ppm. Residual solvent peaks were used as reference. All NMR J values are given in Hz. COSY, NOESY, HMQC, and HMBC experiments were recorded to help with the assignment of ^{1}H and ^{13}C signals. High Resolution Mass Spectra (HRMS) were obtained on a Bruker HPLC-TOF (MicroTOF Focus), Bruker Corporation, Bremen, Germany, with ESI as ionization mode and Bruker HPLC-QqTOF (MaXis Impact), Bruker Corporation, Bremen, Germany with ESI as ionization mode. Nominal mass spectra were obtained by direct injection on an Agilent 1200 and as detection unit an Agilent 6130 quadrupole. IR spectra were recorded on a Bruker Optics FTIR Alpha spectrometer equipped with a DTGS detector, KBr beamsplitter at 4 cm^{-1} resolution using a one bounce ATR accessory with diamond windows. Melting points were measured on a MP70 Melting Point System Mettler Toledo. Column chromatography was performed with silica gel technical grade (Sigma-Aldrich, Merck Life Science S. L. U., Madrid, Spain), pore size 60 Å, 230–400 mesh particle size, 40–63 µm particle size and Thin Layer Chromatography (TLC) analysis on silica gel 60 F254.

5.4.2 X-ray analysis

Crystal preparation

Crystals of **1**, **2**, **3** and the co-crystal **2•3** were grown by slow evaporation of acetonitrile solutions. The measured crystals were prepared under inert conditions immersed in perfluoropolyether as protecting oil for manipulation.

Data collection

Crystal structure determinations of **1**, **3** and **2•3** were carried out using an Apex DUO Kappa 4-axis goniometer equipped with an APPEX 2 4K CCD area detector, a Microfocus Source E025 IuS using MoKα radiation (0.71073 Å), Quazar MX multilayer Optics as monochromator and a Oxford Cryosystems low temperature device Cryostream 700 plus (T = -173 °C). Full-sphere data collection was used with

□ and □ scans. Programs used: Data collection APEX-2[25], data reduction Bruker Saint[26] V/.60A and absorption correction SADABS[27,28]

Crystal structure determination for compound **2** was carried out using a Rigaku diffractometer equipped with a Pilatus 200K area detector, a Rigaku MicroMax-007HF microfocus rotating anode with MoK□ radiation, Confocal Max Flux optics and an Oxford Cryosystems low temperature device Cryostream 700 plus (T = -173 °C). Full-sphere data collection was used with □ and □ scans. Programs used: Data collection and reduction with CrysAlisPro V/.60A and absorption correction with Scale3 Abspack scaling algorithm[29].

Structure Solution and Refinement

Crystal structure solution was achieved using the computer program SHELXT.[30] Visualization was performed with the program SHELXle[31]. Missing atoms were subsequently located from difference Fourier synthesis and added to the atom list. Least-squares refinement on F2 using all measured intensities was carried out using the program SHELXL 2015[32]. All non-hydrogen atoms were refined including anisotropic displacement parameters.

Deposition Number(s) 2220964, 2220965, 2220966, 2220967 contain(s) the supplementary crystallographic data for this thesis chapter and the related paper[33]. These data are provided free of charge by the joint Cambridge Crystallographic Data Centre and Fachinformationszentrum Karlsruhe.

[25] Data collection with APEX II v2014.9-0. Bruker **2014**, Bruker AXS Inc., Madison, Wisconsin, USA.

[26] Data reduction with Bruker SAINT+ version V8.35 A. Bruker **2013**, Bruker AXS Inc., Madison, Wisconsin, USA.

[27] SADABS: V2014/5 Bruker **2001**, Bruker AXS Inc., Madison, Wisconsin, USA.

[28] Blessing, R. H., An empirical correction for absorption anisotropy. *Acta Crystallogr. Sect. A* **1995,** *51*, 33-38.

[29] CrysAlisPro 1.171.39.12b (Rigaku OD, **2015**).

[30] Sheldrick, G., SHELXT - Integrated space-group and crystal-structure determination. *Acta Crystallogr. Sect. A* **2015,** *71*, 3-8

[31] Hubschle, C. B.; Sheldrick, G. M.; Dittrich, B., ShelXle: a Qt graphical user interface for SHELXL. *J. Appl. Crystallogr.* **2011,** *44*, 1281-1284.

[32]. Sheldrick, G., Crystal structure refinement with SHELXL. *Acta Crystallogr. Sect. C* **2015,** *71*, 3-8.

[33] Rivoli, A., Gomila, R. M., Frontera, A., Ballester, P., Interchangeability and Disorder in the Solid-State Structures of "Two Wall" Calix[4]pyrroles Equipped with Iodine and Ethynyl *para*-Substituents *Chem. Asian J.* **2023**, *18*, e202201192.

5.4.3 DFT calculations

The DFT calculations included in the thesis were performed by Prof. Dr. Antonio Frontera and Dr. Rosa Gomila from the Universitat de les Illes Balears using Turbomole 7.0[34] at the PBE0[20]-D3[35]/def2-TZVP[36] level of theory. For iodine, the def2-TZVP basis set used in this work includes effective core potentials (ECP), and relativistic effects are used for the inner electrons[37]. This level of theory has been used before[37,38,39] to analyze similar interactions and it has been proved to provide results similar to high level ab initio methods[40]. The geometries of models **6**-**14** were fully optimized without symmetry constrains. The crystallographic coordinates have been used to evaluate the interactions in the solid state of compounds **1**-**3**, since we are interested to study the interactions as they stand in the solid state. The interaction energies were computed by calculating the difference between the energies of the isolated monomers and the corresponding dimers. The Bader's "Atoms in molecules" theory (QTAIM)[41] was used to study the interactions discussed herein using the Multiwfn program[42] and represented using the VMD visualization software[43]. The molecular electrostatic potential (MEP) surfaces were computed using the 0.001 a.u. isosurface as best estimation of the van der Waals surface at

[34] Ahlrichs, R.; Bär, M.; Häser, M.; Horn, H.; Kölmel, C., Electronic structure calculations on workstation computers: The program system turbomole. *Chem. Phys. Lett.* **1989,** *162*, 165-169.
[35] Grimme, S.; Antony, J.; Ehrlich, S.; Krieg, H., A consistent and accurate ab initio parametrization of density functional dispersion correction (DFT-D) for the 94 elements H-Pu. *J. Chem. Phys.* **2010,** *132*.
[36] Weigend, F., Accurate Coulomb-fitting basis sets for H to Rn. *Phys. Chem. Chem. Phys.* **2006,** *8*, 1057-1065.
[37] Daolio, A.; Pizzi, A.; Terraneo, G.; Frontera, A.; Resnati, G., Anion···Anion Interactions Involving σ-Holes of Perrhenate, Pertechnetate and Permanganate Anions. *ChemPhysChem* **2021,** *22*, 2281-2285.
[38] Daolio, A.; Pizzi, A.; Calabrese, M.; Terraneo, G.; Bordignon, S.; Frontera, A.; Resnati, G., Molecular Electrostatic Potential and Noncovalent Interactions in Derivatives of Group 8 Elements. *Angew. Chem. Int. Ed.* **2021,** *60*, 20723-20727.
[39] Daolio, A.; Pizzi, A.; Terraneo, G.; Ursini, M.; Frontera, A.; Resnati, G., Anion···Anion Coinage Bonds: The Case of Tetrachloridoaurate. *Angew. Chem. Int. Ed.* **2021,** *60*, 14385-14389.
[40]. Mallada, B.; Gallardo, A.; Lamanec, M.; de la Torre, B.; Špirko, V.; Hobza, P.; Jelinek, P., Real-space imaging of anisotropic charge of σ-hole by means of Kelvin probe force microscopy. *Science* **2021,** *374*, 863-867.
[41] Bader, R. F. W., A quantum theory of molecular structure and its applications. *Chem. Rev.* **1991,** *91*, 893-928.
[42] Lu, T.; Chen, F., Multiwfn: A multifunctional wavefunction analyzer. *J. Comput. Chem.* **2012,** *33*, 580-592.
[43] Humphrey, W.; Dalke, A.; Schulten, K., VMD: Visual molecular dynamics. *J. Mol. Graphics* **1996,** *14*, 33-38.

the same level of theory and represented using the GaussView program[44]. The σ-hole cone angles, like those represented in **Figure 3**, have been previously used to rationalize halogen bonding interactions for chloro-, bromo- and iodo-pentafluorobenzene[45].

5.4.4 Synthesis and characterization data

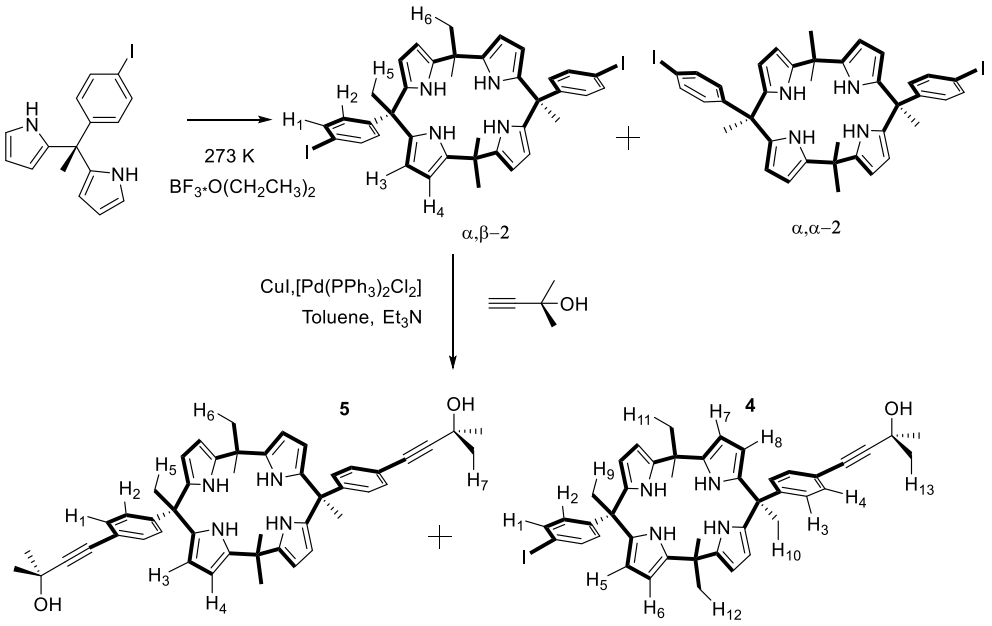

Scheme S 1: *Scheme of the synthesis of compounds **2, 4** and **5**.*

10α,20β-Bis(4-iodophenyl)-hexamethyl calix[4]pyrrole (α,β-**2**)

To a solution of 4-iodophenyl, methyl-*meso*-dipyrromethane[17] (8 g, 23 mmol, 1 equiv.) in 600 mL of acetone, $BF_3{\bullet}OEt_2$ (3 mL, 23 mmol assuming 99.9% purity, 1 equiv.) was added dropwise over a period of 30 min at 0 ºC. The reaction mixture was stirred at room temperature for 12 hours. 100 mL of distilled water were then added. The acetone was removed under reduced pressure to obtain a residual solution (~100 mL) that was neutralized (KOH 2M ~20 mL to pH = 7). Next,100 mL of distilled water were added. The water phase was extracted with DCM (3 × 100

[44] T. A. Keith, J. Millam, GaussView, Version 6.0.16, R. Dennington, Semichem Inc., Shawnee Mission, KS, **2019**.
[45] Benito, I.; Gomila, R. M.; Frontera, A., On the energetic stability of halogen bonds involving metals: implications in crystal engineering. *CrystEngComm* **2022,** *24*, 4440-4446.

mL). The collected organic layers were dried over anhydrous Na_2SO_4 and concentrated under reduced pressure. The final product was purified by combi-flash chromatography on a silica gel column (120g SiO_2, ethyl acetate/hexane 5:95). The combined tubes containing the first eluting compound yielded, after solvent evaporation in vacuo, 1.5 g of α,β-**2** as a white solid (16.5 % yield). ^{1}H NMR (400 MHz, acetone-d_6, 298 K) δ(ppm): 8.85 (br s, 4H, NHs), 7.56 (d, 4H, $J_{1\text{-}2}$= 8.55 Hz, H^1), 6.83 (d, $J_{2\text{-}1}$= 8.55, 4H, H^2), 5.82 (dd, $J_{3\text{-}4}$=3.6 Hz, $J_{3\text{-}NH}$=3 Hz, 4H, H^3), 5.80 (dd, $J_{4\text{-}3}$= 3.6 Hz, $J_{4\text{-}NH}$=3 Hz 4H, H^4), 1.83 (br s, 6H, H^5), 1.53 (s, 12 H, $H^{6,7}$). ^{13}C (125 MHz, acetone-d_6, 298 K) δ(ppm) 149.08, 139.09, 136.63, 135.91, 129.82, 105.28, 102.87, 90.92, 44.49, 35.42, 29.89, 29.51. HRMS (ESI/ TOF) m/z: $[M+Na]^{+\cdot}$= $[C_{38}H_{38}I_2N_4Na]^+$ Calcd 827.1078; Found 827.1041.

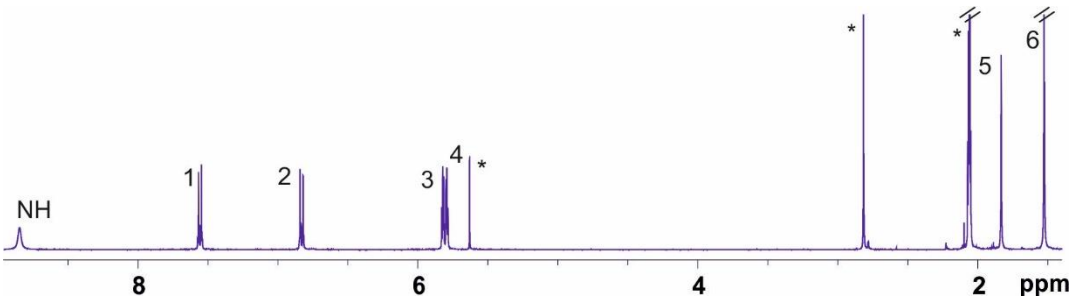

***Figure S 1**: ^{1}H NMR (500 MHz, d_6-Acetone, 298 K) spectrum of α,β-**2**. See scheme S1 for proton assignment. *Solvent residual peak.*

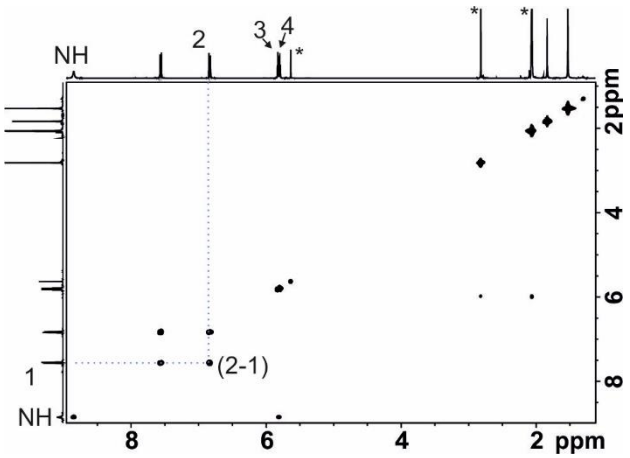

***Figure S 2:** 2D ^{1}H-^{1}H COSY NMR (400 MHz, d_6-Acetone, 298 K) spectrum of α,β-**2**. Some selected COSY cross-peaks are indicated. See scheme S1 for proton assignment. *Solvent residual peak.*

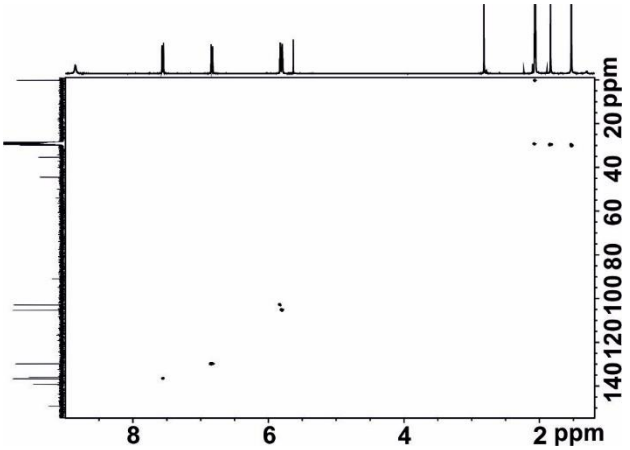

Figure S 3: *2D ^{1}H-^{13}C HSQC NMR (d_6-Acetone, 298 K) spectrum of α,β-**2**.*

10α-(4-Iodophenyl)-20β(4-[(3-methyl-3-hydroxybut-1-yn-1-yl)phenyl]-hexamethyl-calix[4]pyrrole (4) and 10α,20 β-bis(4-[(3-methyl-3-hydroxybut-1-yn-1-yl)phenyl]-hexamethyl calix[4]pyrrole (5)

10α,20β-bis(4-iodophenyl) hexamethyl calix[4]pyrrole (α,β-**2**) (300 mg, 0.373 mmol, 1 equiv.), $Pd(PPh_3)_2Cl_2$ (13.1 mg, 18.6 µmol, 0.05 equiv.) and CuI (3.55 mg, 18.6 µmol, 0.05 equiv.) were placed in a Schlenk flask. The flask was purged with argon and later 21 mL of dry toluene were added. The reaction mixture was left stirring under Ar for 15 min producing a yellow suspension. 4.91 mL of freshly distilled triethylamine (100 equiv.) and 2-methyl-3-butyn-2-ol (181 µL, 1.86 mmol, 5 equiv) were added and the mixture was stirred at RT under Ar during 2 h. After this time has elapsed, DCM (60 mL) was added to the reaction mixture. The resulting organic layer was washed with 0.5 M HCl (60 mL × 1) and water (60 mL ×2). The organic layer was dried over sodium sulfate, filtered and concentrated under vacuum to obtain a brown solid. The solid was purified using silica column chromatography and different eluents (CH_2Cl_2/hexane, CH_2Cl_2 and CH_2Cl_2/ethyl acetate (9:1)). The unreacted compound α,β-**2** eluted with the front of the solvent. Using CH_2Cl_2 as eluent allowed the isolation of compound **4** as the second fraction (105 mg, 42% yield). ^{1}H NMR (400 MHz, d_6-Acetone, 298 K) δ(ppm): 8.85, 8.75 (two br s, 4H,NHs), 7.56 (d, 2H, $J_{1\text{-}2}$= 8.6 Hz, H^{1}), 7.22 (d, 2H, $J_{4\text{-}3}$= 8.49 Hz, H^{4}), 7.01 (d, 2H , $J_{4\text{-}3}$= 8.49 Hz, H^{3}), 6.84 (d, 2H, $J_{2\text{-}1}$= 8.6, H^{2}), 5.82 (dd, 4H, $J_{5.8\text{-}6.7}$=3.2 Hz, $J_{5,8\text{-}NH}$=3.5 Hz, $H^{5,8}$), 5.77 (dd, 4H, $J_{6,7\text{-}5,8}$=3.2 Hz, $J_{6,7\text{-}NH}$=7.63 Hz ,$H^{6,7}$), 4.32 (s, 1H, OH), 1.84 (s, 3H, H^{9}), 1.83 (s, 3H, H^{10}), 1.53 (s, 12H, $H^{11,12}$), 1.52 (s, 6H, H^{13}). ^{13}C (125 MHz, d_6-Acetone, 298 K) δ(ppm) 149.05, 139.05, 138.98, 133.64, 136.15,135.86, 130.62, 129.82, 127.48, 121, 105.3 ,105.27, 102.89, 102.82, 94.96, 90.97, 64.23, 44.61, 44.49, 35.37, 31.17, 29.81, 29.71. M.P. =268.2 ºC HRMS (ESI/ TOF) m/z: $[M+Na]^{+}$= $[C_{43}H_{45}IN_4ONa]^{+}$ Calcd 783.2530; Found 783.2520.

After all **4** has eluted, the solvent mixture was change from CH_2Cl_2 to CH_2Cl_2/ethyl acetate (9:1) to isolated a third fraction containing compound **5**. (105 mg, 35% yield). ^{1}H NMR (400 MHz, d_6-Acetone, 298 K) (ppm): 8.71 (br s, 4H, NHs), 7.23 (d, 4H, $J_{1\text{-}2}$= 8.6 Hz, H^1), 7.02 (d, 4H, $J_{2\text{-}1}$= 8.6, H^2), 5.83 (dd, 4H, $J_{3\text{-}4}$=3.3 Hz, $J_{3\text{-}NH}$=3.56, H^3), 5.76 (dd, 4H, $J_{4\text{-}3}$= 3.3 Hz, $J_{3\text{-}NH}$=3.6 Hz, H^4), 4.32 (s, 2H, OH), 1.84 (br s, 6H, H^5), 1.53 (s, 12H, $H^{6,7}$), 1.53 (s, 12H, H^8). ^{13}C (125 MHz, d_6-Acetone, 298 K) (ppm) 149.9, 139.09, 136.14, 130.68, 127.49, 121.04, 105.21, 102.84, 94.94, 80.59, 64.2, 44.49, 35.33, 31.17, 29.89, 29.51. M.P. =269.4 ºC HRMS (ESI/TOF) m/z: $[M+Na]^{+\cdot}$= $[C_{48}H_{52}N_4O_2Na]^+$ Calcd 739.3982; Found 739.3941.

10α-(4-iodophenyl)-20β(4-[(3-methyl-3-hydroxybut-1-yn-1-yl)phenyl]-hexamethyl calix[4]pyrrole (4)

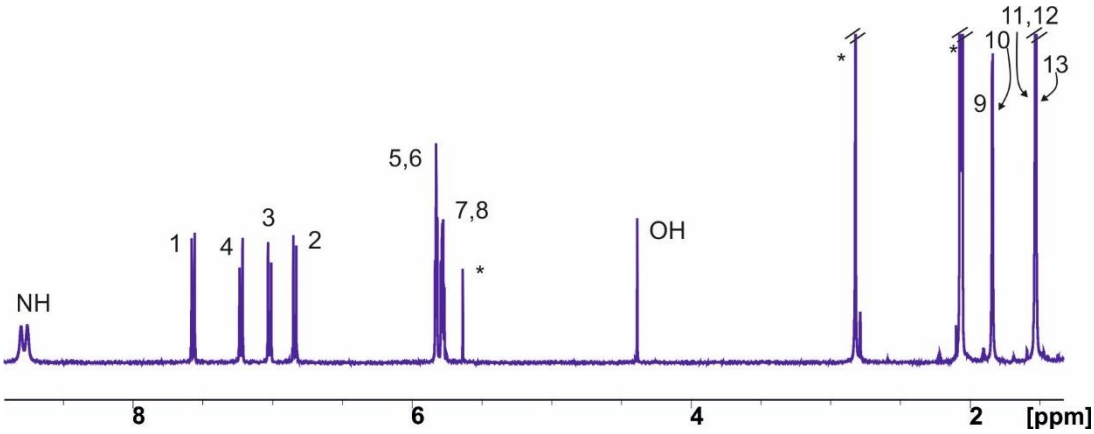

Figure S 4: *^{1}H NMR (500 MHz, d_6-Acetone, 298 K) spectrum of **4**. See scheme S1 for proton assignment. *Solvent residual peak.*

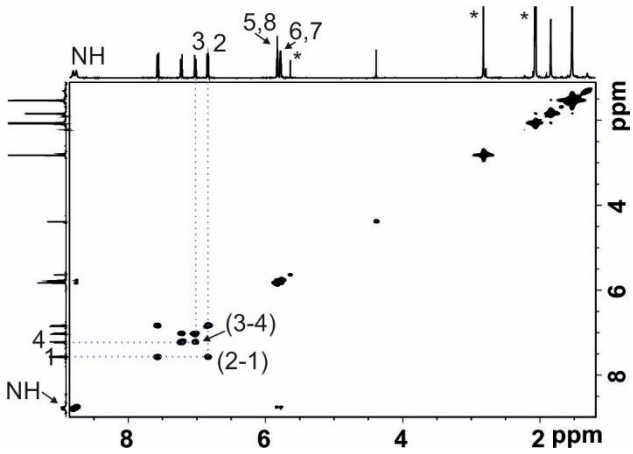

Figure S 5: *2D ^{1}H-^{1}H COSY NMR (400 MHz, d_6-Acetone, 298 K) spectrum of **4**. Some selected COSY cross-peaks are indicated. See scheme S2 for proton assignment. *Solvent residual peak.*

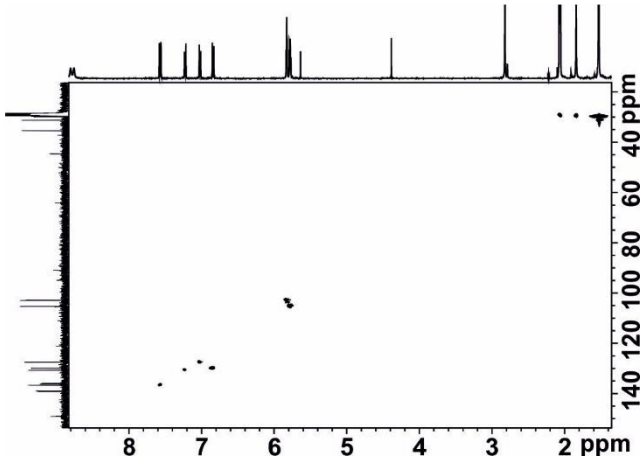

Figure S 6: *2D ^{1}H-^{13}C HSQC NMR (d_6-Acetone, 298 K) spectrum of **4**.*

Interchangeability and Disorder in the Solid State Structures of "Two Wall" Calix[4]pyrroles equipped with Iodine and Ethynyl para-Substituents

10α,20β-Bis(4-[(3-Methyl-3-hydroxybut-1-yn-1-yl)phenyl] hexamethyl calix[4]pyrrole (5)

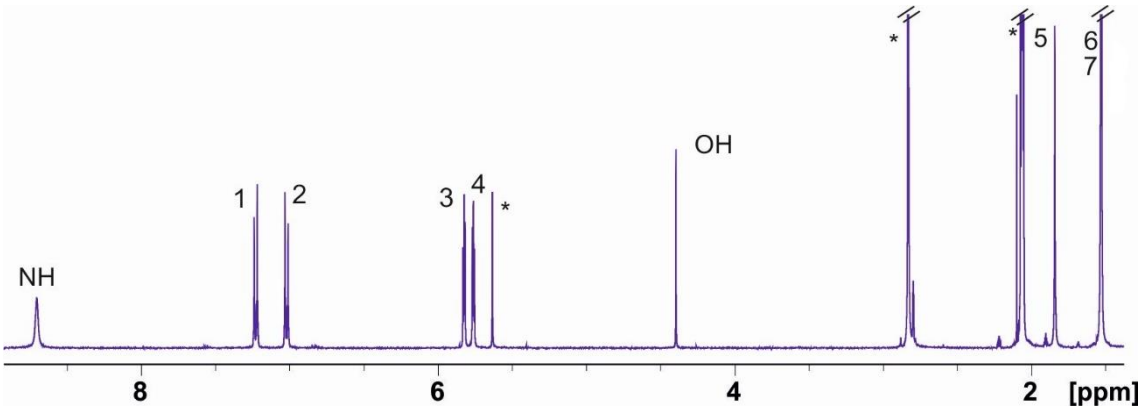

Figure S 7: *^{1}H NMR (500 MHz, d_6-Acetone, 298 K) spectrum of **5**. See scheme S1 for proton assignment. *Solvent residual peak.*

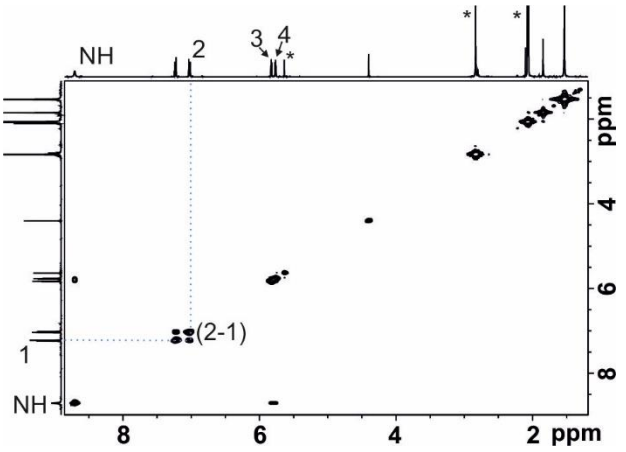

Figure S 8*: 2D ^{1}H-^{1}H COSY NMR (400 MHz, d_6-Acetone, 298 K) spectrum of **5**. Some selected COSY cross-peaks are indicated. See scheme S2 for proton assignment. *Solvent residual peak.*

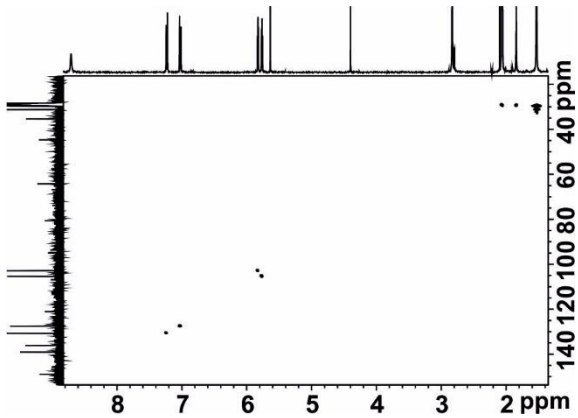

Figure S 9: *2D ^{1}H-^{13}C HSQC NMR (d_6-Acetone, 298 K) spectrum of* ***5.***

Interchangeability and Disorder in the Solid State Structures of "Two Wall" Calix[4]pyrroles equipped with Iodine and Ethynyl para-Substituents

10α-(4-Iodophenyl)-20β-(4-ethynylphenyl) hexamethyl calix[4]pyrrole (**1**)

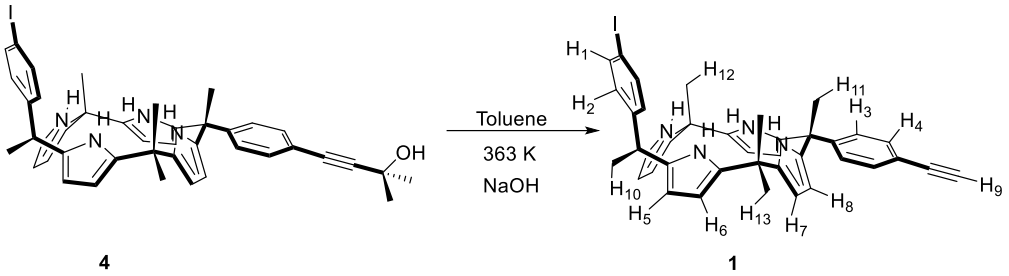

Scheme S 2**: Synthesis of compound **1.

A solution of 10α-(4-iodophenyl)-20β-(4-[(3-Methyl-3-hydroxybut-1-yn-1-yl)phenyl] hexamethyl calix[4]pyrrole (**4**) (250 mg, 0.329 mmol, 1 equiv.) in toluene (25 mL) was treated with powdered NaOH (418 mg, 10.5 mmol, 20 equiv.) and refluxed for 12 h under Ar atmosphere. The reaction mixture was concentrated in vacuum. The residue was triturated with DCM (30 mL × 2). The combined organic extracts were washed with 0.5 M HCl (30 mL × 1) and water (30 mL × 2), dried over anhydrous Na_2SO_4, filtered and concentrated under vacuum to give a brown solid. The solid was purified using column chromatography (CH_2Cl_2/hexane 9:1). The tubes containing the major collected fraction were combined and the solvent removed under vacuum yielding α,β-**1** as a white brownish solid (170 mg, 73% yield). NMR (400 MHz, d_6-Acetone, 298 K) δ(ppm): 8.83 (br s, 4H, NHs), 7.56 (d, 2H, $J_{1\text{-}2}$= 8.64 Hz, H^1), 7.32 (d, 2H, $J_{4\text{-}3}$= 8.57 Hz, H^4), H^3 (d, 7.04 ppm, $J_{4\text{-}3}$= 8.57 Hz, 2H), 6.84 (d, 2H, $J_{2\text{-}1}$= 8.64, H^2), $H^{5,8}$ (m, 5.83 ppm, 4H), 5.79 (dd, 4H , $J_{6,7\text{-}5,8}$ =2.89 Hz, $J_{6,7\text{-}NH}$=3.5 Hz, , $H^{6,7}$), 3.59 (s, 1H, H^9), 1.85 (s, 3 H, H^{10}), 1.84 (s, 3 H, H^{11}), 1.53 (s, 12H, $H^{12,13}$). ^{13}C (125 MHz, d_6-Acetone, 298 K) δ(ppm) 149.86, 149.02, 139.16, 139.07, 136.64, 136.03, 135.92 ,131.20, 129.81, 127.57, 119.93 105.3, 102.87, 102.84, 90.5, 83.29, 77.83, 44.68, 44.49, 35.4, 29.83, 29.43. M.P. =271.6 ºC HRMS (ESI/ TOF) m/z: $[M+Na]^{+}$= $[C_{40}H_{39}I_1N_4Na]^+$ Calcd 725.2111; Found 725.2099.

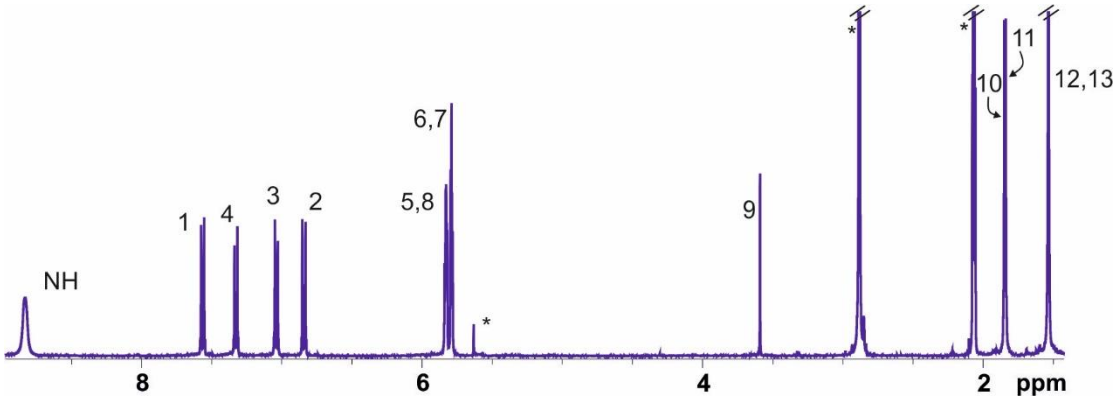

***Figure S 10**: ^{1}H NMR (500 MHz, d_6-Acetone, 298 K) spectrum of α,β-**1** See scheme S2 for proton assignment. *Solvent residual peak.*

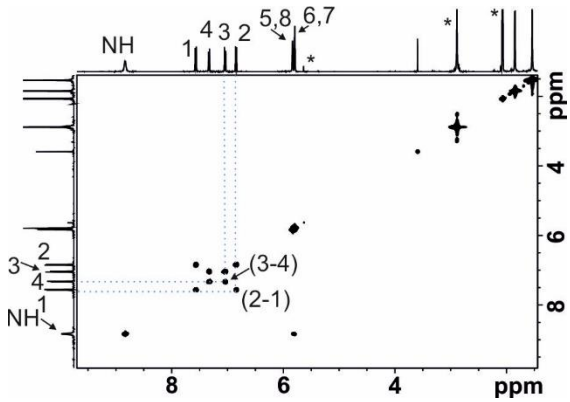

***Figure S 11:** 2D ^{1}H-^{1}H COSY NMR (400 MHz, d_6-Acetone, 298 K) spectrum of α,β-**1**. Some selected COSY cross-peaks are indicated. See scheme S2 for proton assignment. *Solvent residual peak.*

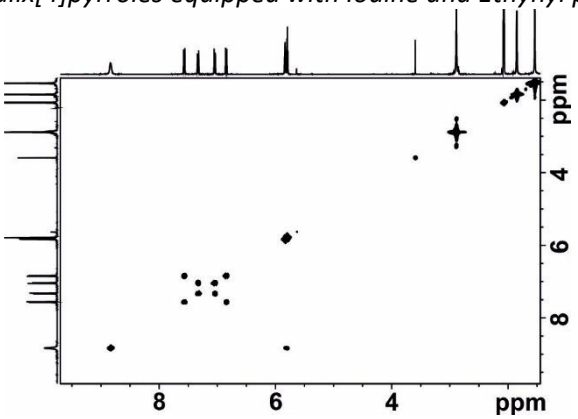

Figure S 12: *2D ^{1}H-^{13}C HSQC NMR (d_6-Acetone, 298 K) spectrum of α,β-**1**.*

10α,20β-Bis-(4-ethynylphenyl) hexamethyl calix[4]pyrrole (**3**)

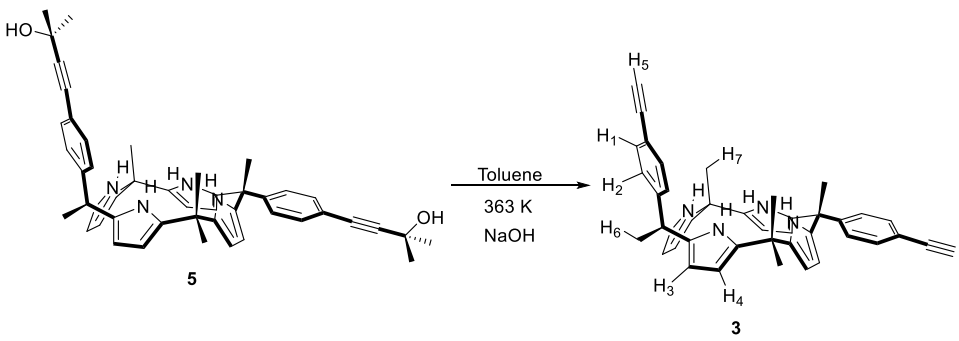

Scheme S 3**: Synthesis of compound **3.

A solution of 10α,20β-bis(4-[(3-methyl-3-hydroxybut-1-yn-1-yl)phenyl] hexamethyl calix[4]pyrrole (**5**) (250 mg, 0.349 mmol, 1 equiv.) in toluene (25 mL) was treated with powdered NaOH (418 mg, 10.5 mmol. 30 equiv.) and refluxed for 12 h under Ar atmosphere. The reaction mixture was concentrated and the solid residue triturated with DCM (30 mL × 2). The combined organic phases were washed with 0.5 M HCl (30 mL × 1) and water (30 mL × 2). The organic phase was dried over anhydrous Na_2SO_4, filtered and concentrated under vacuum to give a brown solid that was purified using column chromatography (CH_2Cl_2/hexane 9:1). The tubes containing the major fraction were combined and the solvent evaporated in vacuum to obtain α,β-**3** as a white brownish solid (175 mg, 75% yield). ^{1}H NMR (400 MHz, acetone-d_6, 298 K) δ(ppm): 8.79 (br s, 4H, NHs), 7.33 (d, 4H, $J_{1\text{-}2}$= 8.53 Hz, H^1), 7.04 (d, 4H, $J_{2\text{-}1}$= 8.53, H^2), 5.83 (dd, 4H, $J_{3\text{-}4}$=3.11 Hz, $J_{3\text{-}NH}$= *3.45* Hz, H^3), 5.78 (dd, 4H, $J_{4\text{-}3}$= 3.11 Hz, $J_{4\text{-}NH}$= *3.5* Hz, H^4), 3.58 (s, 2H, H^5), 1.85 (s, 6 H, H^6), 1.54 (br s, 12H, $H^{7,8}$). ^{13}C (125 MHz, d_6-Acetone, 298 K) δ(ppm) 149.87, 139.07, 35.97, 131.21, 127.58, 119.94, 105.33, 102.87, 83.27, 77.81, 44.69, 35.37, 29.78, 29.40. M.P. =273.5 ºC. HRMS (ESI/ TOF) m/z: $[M+Na]^{+\cdot}$= $[C_{42}H_{40}N_4Na]^+$ Calcd 623.3145; Found 623.3150.

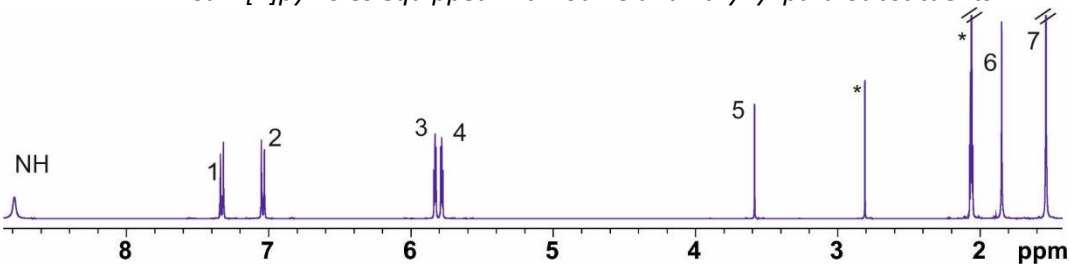

***Figure S 13**: ^{1}H NMR (500 MHz, d_6-Acetone, 298 K) spectrum of α,β- **3**. See scheme S3 for proton assignment. *Solvent residual peak.*

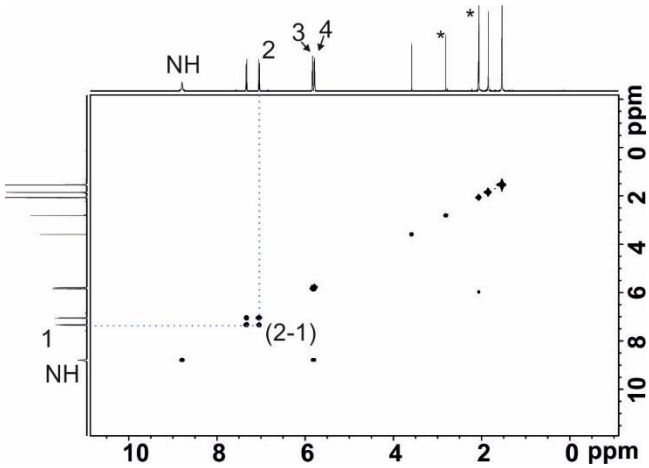

***Figure S 14:** 2D ^{1}H-^{1}H COSY NMR (400 MHz, d_6-Acetone, 298 K) spectrum of α,β-**3**. Some selected COSY cross-peaks are indicated. See scheme S3 for proton assignment. *Solvent residual peak.*

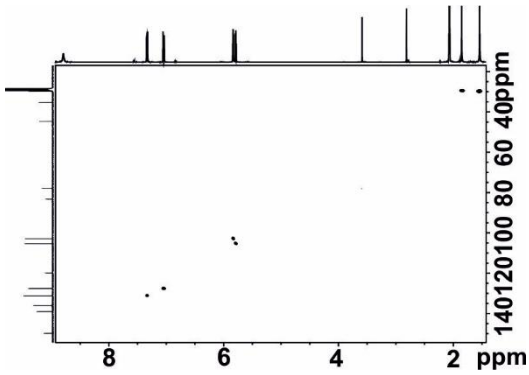

Figure S 15 :** 2D ^{1}H-^{13}C HSQC NMR (d_6-Acetone, 298 K) spectrum of α,β-**3.

5.4.5 Crystal data

Table S 1: *Crystal data and structure refinement for compounds 1-4.*

Identification code	**1**	**2**	**3**	**4[a]**
Empirical formula	$C_{44}H_{45}IN_6$	$C_{42}H_{44}I_2N_6$	$C_{45.92}H_{45.96}I_{0.04}N_6$	$C_{44.53}H_{45.26}I_{0.74}N_6$
Formula weight	784.76	886.63	687.20	757.81
Temperature	100(2)K	100(2)K	100(2)K	99(2)K
Wavelength	0.71073 Å	0.71073 Å	0.71073 Å	0.71073 Å
Crystal system	triclinic	triclinic	triclinic	triclinic
Space group	P1	P-1	P-1	P-1
Dimensions a b c	 7.4274(12)Å 11.5016(18)Å 11.597(2)Å	 7.3804(2)Å 11.5389(3)Å 11.5823(2)Å	 7.4411(8)Å 11.5183(12)Å 11.6024(12)Å	 7.4197(8)Å 11.4779(13)Å 11.5924(13)Å
α β γ	99.529(5)°. 105.418(4)°. 95.638(4)°.	100.306(2)°. 105.915(2)°. 96.200(2)°.	99.244(2)°. 92.705(3)°. 107.653(3)°.	99.343(3)°. 105.639(2)°. 95.263(3)°.
Volume	931.3(3) $Å^3$	920.31(4) $Å^3$	930.42(17) $Å^3$	928.49(18) $Å^3$
Z	1	1	1	1
Density (calculated)	1.399 Mg/m^3	1.600 Mg/m^3	1.226 Mg/m^3	1.355 Mg/m^3
Absorption coefficient	0.900 mm^{-1}	1.748 mm^{-1}	0.108 mm^{-1}	0.683 mm^{-1}
F(000)	404	444	366	393
Crystal size	0.100 x 0.050 x 0.020 mm^3	0.090 x 0.080 x 0.060 mm^3	0.200 x 0.100 x 0.100 mm^3	0.100 x 0.050 x 0.050 mm3
Theta range for data collection	1.816 to 35.039°.	3.506 to 31.918°.	1.888 to 33.912°.	1.817 to 30.543°.
Index ranges	-7≤h≤11 18≤k≤18 -18≤l≤18	-10≤h≤10 -17≤k≤16 -17≤l≤17	-11≤h≤11 -18≤k≤18 -11≤l≤18	-10≤h≤10 -16≤k≤11 -16≤l≤16
Reflections collected	20797	38635	21212	13198
Independent reflections	10723 [R(int) =0.0275]	6016 [R(int) =0.0310]	7138 [R(int) =0.0551]	5520 [R(int) =0.0242]

Completeness to theta =35.039°	90.2%	94.9%	94.6%	97.0%
Absorption correction	Multi-scan	Multi-scan	Multi-scan	Multi-scan
Max. and min. transmission	0.74 and 0.65	1.00 and 0.77	0.74 and 0.62	0.74 and 0.68
Refinement method	Full-matrix leastsquares on F^2	Full-matrix leastsquares on F^2	Full-matrix leastsquares on F^2	Full-matrix leastsquares on F^2
Data/restraints /parameters	10723/9/474	6016/0/230	7138/0/249	5520/0/243
Goodness-of-fit on F2	1.001	1.075	1.037	1.206
Final R indices [I>2sigma(I)]	R1 = 0.0354 wR2 = 0.0834	R1 = 0.0211 wR2 = 0.0580	R1 = 0.0476 wR2 = 0.1271	R1 = 0.0408 wR2 = 0.0894
R indices (all data)	R1 = 0.0380 wR2 = 0.0851	R1 = 0.0221 wR2 = 0.0584	R1 = 0.0568 wR2 = 0.1344	R1 = 0.0455 wR2 = 0.0911
Flack parameter	x =0.248(14)			
Largest diff. peak and hole	0.607 and -0.321 e.Å^{-3}	1.636 and -0.479 e.Å^{-3}	0.598 and -0.325 e.Å^{-3}	0.377 and -0.253 e.Å^{-3}

[a]Traces of iodine were detected in this structure, for this reason it was refined assuming a 98:2 occupancy disorder of **2** and **3**. It is worth mentioning that **2** is the synthetic precursor of **3**.

5.4.6 X-ray coordinates

6

C	-0.62704488	-1.20807885	0.00050272
C	0.76006152	-1.20004911	0.00091389
C	1.45593807	-0.00002275	0.00048473
C	0.76023932	1.19988666	-0.00056093
C	-0.62693534	1.20823337	-0.00109434
C	-1.30623806	0.00002170	-0.00042599
H	-1.17603188	-2.14128875	0.00096046
H	1.29661073	-2.14183751	0.00165738
H	2.53933694	-0.00013812	0.00099432
H	1.29687162	2.14169833	-0.00090225
H	-1.17580856	2.14136760	-0.00197171
Br	-3.19699842	0.00020691	-0.00055881

7

C	-0.96380058	-1.20891283	0.00034291
C	0.41880516	-1.20741473	0.00076307
C	1.11723605	-0.00003281	0.00031751
C	0.41893799	1.20730519	-0.00073979
C	-0.96367199	1.20904936	-0.00123775
C	-1.64467284	0.00004075	-0.00058315

H	-1.51090953	-2.14270589	0.00078530
H	0.96346773	-2.14341181	0.00150657
H	0.96368786	2.14331021	-0.00111498
H	-1.51068410	2.14282548	-0.00208602
C	2.54380901	-0.00011695	0.00107053
N	3.69552731	-0.00012012	0.00178015
Br	-3.52773155	0.00018310	-0.00080329

8

C	-2.15318465	-1.15968877	0.01293680
C	-0.77076148	-1.18665193	-0.02015583
C	-0.01869848	0.00044451	-0.04883301
C	-0.72833311	1.21350715	-0.02375318
C	-2.11088540	1.23536588	0.00929129
C	-2.82593192	0.05010039	0.02486657
H	-2.70781903	-2.08972889	0.03206338
H	-0.27769846	-2.14906818	-0.02394633
H	-0.20214941	2.15824359	-0.03039277
H	-2.63247742	2.18442410	0.02565398
N	1.35214312	-0.02414001	-0.10289322
C	2.09220544	1.20570549	-0.00846631
H	1.91311228	1.73314704	0.93848686

H	3.15692224	0.98999591	-0.07750859
H	1.84015462	1.88868811	-0.82685162
C	2.04789426	-1.27923414	-0.00366244
H	1.77419796	-1.95521574	-0.82098834
H	3.11981686	-1.10166819	-0.07037899
H	1.84805999	-1.79751298	0.94417181
Br	-4.71656846	0.08328615	0.07035888

9

C	-0.61110765	-1.20748194	0.00050219
C	0.77652316	-1.19970674	0.00091177
C	1.47243887	-0.00003863	0.00048526
C	0.77667292	1.19956016	-0.00055775
C	-0.61096741	1.20760682	-0.00109540
C	-1.29458346	0.00003228	-0.00043604
H	-1.15349739	-2.14479243	0.00096522
H	1.31332744	-2.14146179	0.00166109
H	2.55595257	-0.00014711	0.00100279
H	1.31359997	2.14132156	-0.00089113
H	-1.15329313	2.14487022	-0.00197965
I	-3.38506537	0.00023760	-0.00056834

10

C	-0.94901219	-1.20795079	0.00033973
C	0.43417459	-1.20714115	0.00076572
C	1.13266845	-0.00002963	0.00032227
C	0.43430847	1.20701520	-0.00073609
C	-0.94887990	1.20809155	-0.00123986
C	-1.63480738	0.00003810	-0.00059480
H	-1.48871107	-2.14627942	0.00078847
H	0.97851171	-2.14344144	0.00151027
H	0.97873766	2.14333720	-0.00110810
H	-1.48848088	2.14639372	-0.00209131
I	-3.71889578	0.00020955	-0.00081123
C	2.55933190	-0.00012065	0.00107476
N	3.71105443	-0.00012224	0.00178068

11

C	-2.14411138	-1.15910561	0.01197475
C	-0.76148500	-1.18683238	-0.01728610
C	-0.00880816	-0.00001376	-0.04458054
C	-0.71853380	1.21303407	-0.02065220
C	-2.10124273	1.23490020	0.00844461
C	-2.82148578	0.05043747	0.02145126
H	-2.69196806	-2.09343578	0.02999112

H	-0.26895169	-2.14965398	-0.01925464
H	-0.19207335	2.15774193	-0.02510311
H	-2.61531779	2.18830456	0.02355844
N	1.36119417	-0.02450937	-0.09598534
C	2.10205237	1.20553615	-0.00867004
H	1.92642479	1.73589400	0.93709512
H	3.16638710	0.98894179	-0.08053284
H	1.84738847	1.88572313	-0.82852647
C	2.05780363	-1.27977390	-0.00372752
H	1.78125930	-1.95295880	-0.82239383
H	3.12928014	-1.10123796	-0.07348261
H	1.86134552	-1.80092988	0.94306900
I	-4.90915776	0.08793762	0.06461201

12

C	-0.01358451	-1.20523505	0.00057363
C	1.37040344	-1.20105402	0.00091812
C	2.06627417	-0.00004022	0.00044345
C	1.37050028	1.20099052	-0.00057786
C	-0.01349296	1.20531602	-0.00099909
C	-0.72126912	0.00004604	-0.00030322
H	-0.56134752	-2.13971233	0.00101549

H 1.90883336 -2.14172320 0.00160129

13

H 3.14995086 -0.00009314 0.00087579

H 1.90900428 2.14163483 -0.00102449

H -0.56117025 2.13982240 -0.00184895

C -2.14487922 0.00007832 -0.00033709

C -3.34750701 0.00001482 -0.00020903

H -4.41171527 -0.00004445 -0.00012806

13

C -0.34646452 -1.20657705 0.00041858

C 1.03340538 -1.20859056 0.00077524

C 1.73149177 -0.00006509 0.00031274

C 1.03348052 1.20860909 -0.00073556

C -0.34638937 1.20660509 -0.00115043

C -1.05350512 0.00008731 -0.00045033

H -0.89286119 -2.14128505 0.00086679

H 1.58003331 -2.14347055 0.00146794

H 1.58017671 2.14339382 -0.00117266

H -0.89271355 2.14141099 -0.00198653

C -2.47516943 0.00006721 -0.00048896

C -3.67730615 0.00001693 -0.00037042

H	-4.74192187	-0.00003969	-0.00027253
C	3.15792133	-0.00007250	0.00104195
N	4.30982272	-0.00008996	0.00174364

14

C	-1.62747934	-1.16109003	0.00878963
C	-0.24934038	-1.19705556	-0.01344904
C	0.50752385	-0.01106404	-0.03936497
C	-0.19843459	1.20585948	-0.01627643
C	-1.57680056	1.22860617	0.00566802
C	-2.32589964	0.04910765	0.01337760
H	-2.18383778	-2.09103914	0.02498669
H	0.24242086	-2.16011211	-0.01156940
H	0.33404843	2.14707107	-0.01667967
H	-2.09278913	2.18156443	0.01958062
N	1.87572750	-0.03920568	-0.08741267
C	2.62111810	1.18913642	-0.00857585
H	2.44949428	1.72390707	0.93508107
H	3.68440506	0.96863355	-0.08194892
H	2.36619384	1.86587898	-0.83109668
C	2.57106905	-1.29630116	-0.00340102
H	2.29084588	-1.96539658	-0.82399459

H	3.64238204	-1.11852301	-0.07553582
H	2.37704092	-1.82013372	0.94203816
C	-3.74554885	0.07814308	0.02234398
C	-4.94932602	0.10042038	0.01947849
H	-6.01281459	0.12159223	0.01796028

UNIVERSITAT ROVIRA I VIRGILI
ARYL-EXTENDED CALIX[4]PYRROLE RECEPTORS WITH METAL CENTERS: ORGANOMETALLIC RECEPTORS AND METALLO-MACROCYCLES BASED ON COORDINATION BONDS
Andrea Rivoli

General Conclusions.

This doctoral thesis describes the results obtained in the design and synthesis of a series of *α,α*- and *α,β*- "two wall" metallo-acetylide calix[4]pyrrole receptors. Most examples relate to mono-nuclear derivatives. However, di-nuclear derivatives are also produced in the case of Pt(II) and used for the self-assembly of metallo-macrocycles by coordination with di-phosphine ligands. The influence of the incorporation of the metal in the binding properties of the calix[4]pyrrole receptors and the self-assembled macrocycles are also investigated.

From the different results obtained in the thesis we draw the following conclusions:

1) In dichloromethane solution, the symmetric bis-ethynyl-Pt(II) α,α-"two wall" calix[4]pyrrole receptor **$2Pt_2(TfO)_2$** forms 1:1 complexes with **pyridine *N*-oxide 5** and **bis-pyridine-*N,N'*-dioxide 6** featuring binding constant of 60 M^{-1} and 10^2 M^{-1}, respectively
2) The bis-ethynyl-Pt(II) α,α-"two wall" calix[4]pyrrole **$2Pt_2(TfO)_2$** self-assembles into thermodynamically and kinetically stable di-nuclear metallo-macrocycles **$2Pt_2$•3-$(TfO)_2$** by di-topic coordination with bis-pyridine ligands i.e **3**. The self-assembled metallo-macrocycle **$2Pt_2$•3-$(TfO)_2$** also forms a 1:1 complex with **pyridine-*N*-oxide 5** featuring a binding constant of 40 M^{-1}. Most likely, the fixed dimension of the aromatic cavity of the metallo-macrocyclic receptor **$2Pt_2$•3-$(TfO)_2$** imposed reduced constrains to the inclusion of **5**. In contrast, the hydrogen bonding interaction of the metallo-macroycle **$2Pt_2$•3-$(TfO)_2$** with the bis-*N*-oxide **6** was weaker. Most likely, the larger size of **6** does not allow for an ideal binding geometry with **$2Pt_2$•3-$(TfO)_2$** .
3) The non-symmetric mononuclear ethynyl-Au(I)-PTA α,α-"two wall" calix[4]pyrrole form 1:1 complexes with **TBACl** both in dichloromethane solution and in acetone solutions. The binding constant of the complex was two orders of magnitude larger in acetone owing to the dissociation of the salt and the reduced solvation of the chloride.
4) The addition of more that 1 equiv of TBACl to the mononuclear ethynyl-Au(I)-PTA α,α-"two wall" calix[4]pyrrole produced the decomposition of the receptor and the formation of anionic-bis(alkynyl)gold(I) dimers .
5) The cytotoxic activity of the mononuclear ethynyl-Au(I)-PTA α,α-"two wall" calix[4]pyrrole was comparable to that of a model compund containing only

the ethynyl-Au phosphine unit suggesting that the calix[4]pyrrole moiety had a reduced effect.

6) We demonstrated the interchangeability of iodine and ethynyl substituents in the solid state structures of symmetric and non-symmetric α,β-"two wall" calix[4]pyrroles. Moreover, DFT calculations showed that iodine is more similar to the ethynyl substituent in terms of electron acceptor (via the σ-hole), while bromine is more similar to the ethynyl in terms of electron donor (via the negative belt).
7) We synthesized a non-symmetric mononuclear alkynyl-Au(I)-carbene α,β-calix[4]pyrrole receptor (α,β-**4Au**) and showed that it formed 1:1 complexes with tetraalkylammonium chloride salts. In acetone solution and using **TBACl** as chloride precursor we estimated a binding constant of the order of 10^4 M^{-1}. Likewise, in dichloromethane solution, using **MTOACl** as anion precursor the complex binding constant was of the order of 10^4 M^{-1}.
8) The results of variable-temperature ^{1}H NMR experiments performed in dichloromethane and acetone solutions using the 1:1 chloride complex of the ethynyl-*α,β*-calix[4]pyrrole receptor (Cl^-● α,β-**5**) showed the presence of the two conformers in identical extent. Unfortunately, analogous experiments undertaken with the Cl^-● α,β-**4Au** counterpart did not provide unequivocal evidence to determine the exact population of the two conformers in equilibrium. Either both conformers exhibited identical chemical shifts or one of them was present in solution to a very large extent.
9) The DFT calculations performed in both solvents to determine the relative energies of the two conformers of the model system Cl^-● α,β-**5** assigned ΔΔE values of approximately 0.2 kcal/mol. This result supported that the two conformers were almost isoenergetic and was in agreement with the experiment. In contrast, the energy differences calculated for the conformers of Cl^-● α,β-**4Au** raised to 0.7 kcal/mol supporting the preferential population, in an 80:20 ratio, of the conformer locating the chloride towards the π-face of the *meso*-phenyl group having the *p*-iodo substituent.

List of Abbreviations.

1D	One-dimensional
A549 cells	Adenocarcinomic human alveolar basal epithelial
AgTfO	Silver trifluoromethanesulfonate
BCN	Dibenzobicyclo[3.2.2]nonane
°C	Celsius
C4P	Calix[4]pyrrole
COSY	Correlation spectroscopy
DCM	Dichloromethane
DFT	Density-functional theory
DMC	Double Mutant Cycle
DOSY	Diffusion ordered spectroscopy
DMSO	Dimethyl sulfoxide
ED	Electron-donating
ESI	Electrospray ionization
ESP	Electrostatic surface potential
EW	Electron-withdrawing
HeLa	Cervical cancer cell line
HPLC	High Performance Liquid Chromatography
ITC	Isothermal Titration Calorimetry
IUPAC	International Union of Pure and Applied Chemistry
LE	Lattice energies
LFER	Linear free-energy relationship

MCB	Molecular conformational balance
MEP	Molecular electrostatic potential
MIA PaCa-2	A human pancreatic cancer cell line
MHz	Megahertz
MM3	Molecular mechanics force field
MTB	Molecular torsion balances
MTOACl	Methyl trioctyl ammonium chloride
NECNEO	1-bromo-4-ethynylbenzene
NECNIS	1-iodo-4-ethynylbenzene
NCI	noncovalent interaction
NBA	2-(*N*,*N*-dimethylaminomethyl)phenylboronic acid
NHC	N-heterocyclic carbene
PTA	1,3,5-triaza-7-phosphaadamantane
ROESY Spectroscopy	Rotating-frame Overhauser Enhancement
TBACl	Tetrabutylammonium chloride
TLC	Thin Layer Chromatography
TOF	Time-of-flight
TS	Transition state
VT	Variable temperature

UNIVERSITAT ROVIRA I VIRGILI
ARYL-EXTENDED CALIX[4]PYRROLE RECEPTORS WITH METAL CENTERS: ORGANOMETALLIC RECEPTORS AND METALLO-MACROCYCLES BASED ON COORDINATION BONDS
Andrea Rivoli

UNIVERSITAT ROVIRA I VIRGILI
ARYL-EXTENDED CALIX[4]PYRROLE RECEPTORS WITH METAL CENTERS: ORGANOMETALLIC RECEPTORS AND METALLO-MACROCYCLES BASED ON COORDINATION BONDS
Andrea Rivoli

UNIVERSITAT ROVIRA I VIRGILI
ARYL-EXTENDED CALIX[4]PYRROLE RECEPTORS WITH METAL CENTERS: ORGANOMETALLIC RECEPTORS AND METALLO-MACROCYCLES BASED ON COORDINATION BONDS
Andrea Rivoli

UNIVERSITAT ROVIRA I VIRGILI
ARYL-EXTENDED CALIX[4]PYRROLE RECEPTORS WITH METAL CENTERS: ORGANOMETALLIC RECEPTORS AND METALLO-MACROCYCLES BASED ON COORDINATION BONDS
Andrea Rivoli

UNIVERSITAT
ROVIRA i VIRGILI

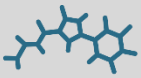

ICIQ

Institute
of Chemical
Research
of Catalonia